



UNIVERSITAT POLITÈCNICA DE CATALUNYA
BARCELONATECH

Group of Environmental Engineering
and Microbiology

Doctoral Degree in Environmental Engineering

Universitat Politècnica de Catalunya

PhD Thesis

NUMERICAL MODELLING OF MICROALGAE SYSTEMS FOR WASTEWATER TREATMENT

Alessandro Solimeno

2017

Univeristat Politècnica de Catalunya·Barcelona Tech
Department of Civil and Environmental Engineering

THESIS DISSERTATION OF THE PHD TITLE

NUMERICAL MODELLING OF MICROALGAE SYSTEMS FOR WASTEWATER TREATMENT

Author: Alessandro Solimeno

Graduated in Civil Engineering specialized in
Hydraulic Engineering

Supervisors: Dr. Joan García Serrano

PhD program: Environmental Engineering

Research Group: GEMMA- Environmental Engineering and
Microbiology Research Group, Department of
Civil and Environmental Engineering

Barcelona, May 2017



Acta de calificación de tesis doctoral

Curso académico:

Nombre y apellidos

Programa de doctorado

Unidad estructural responsable del programa

Resolución del Tribunal

Reunido el Tribunal designado a tal efecto, el doctorando / la doctoranda expone el tema de su tesis doctoral titulada

Acabada la lectura y después de dar respuesta a las cuestiones formuladas por los miembros titulares del tribunal, éste otorga la calificación:

NO APTO

APROBADO

NOTABLE

SOBRESALIENTE

(Nombre, apellidos y firma)		(Nombre, apellidos y firma)	
Presidente/a		Secretario/a	
(Nombre, apellidos y firma)	(Nombre, apellidos y firma)	(Nombre, apellidos y firma)	(Nombre, apellidos y firma)
Vocal	Vocal	Vocal	Vocal

_____, _____ de _____ de _____

El resultado del escrutinio de los votos emitidos por los miembros titulares del tribunal, efectuado por la Comisión Permanente de la Escuela de Doctorado, otorga la MENCIÓN

CUM LAUDE:

SÍ

NO

(Nombre, apellidos y firma)	(Nombre, apellidos y firma)
Presidente/a de la Comisión Permanente de la Escuela de Doctorado	Secretario/a de la Comisión Permanente de la Escuela de Doctorado

Barcelona, _____ de _____ de _____

Mención Internacional en el título de doctor o doctora

- Como secretario/a del tribunal hago constar que parte de la tesis doctoral, como mínimo el resumen y las conclusiones, se ha redactado y presentado en una de las lenguas habituales para la comunicación científica en su campo de conocimiento y diferente de las que son oficiales en España. Esta norma no se aplica si la estancia, los informes y los expertos provienen de un país de habla hispana.

(Nombre, apellidos y firma)
Secretario/a del Tribunal

A mia figlia, Sofia

Preface

The current thesis is framed within the context of two Spanish National Projects: DIBROBIO (2013-2016) “Production and digestion of algal biomass in wastewater treatment systems” (CTM-2012-37860) and FOTOBIOGAS (2015-2017) “Biogas production from microalgae-bacteria grown in closed photobioreactors for wastewater treatment” (CTQ2014-57293-C3-3-R) both granted by the Spanish Ministry of Economy and Competitiveness.

Alessandro Solimeno kindly acknowledges the FPU-AP2012-6062 scholarship provided by the Spanish Ministry of Education and Science.

Abstract

Reactions and processes that occur in microalgae and bacteria systems are difficult to understand because most of them take place simultaneously and depend on many parameters such as temperature, solar radiation, nutrients availability (e.g. carbon and nitrogen) as well on certain inhibitory conditions (e.g. excess of oxygen in the culture medium). In comparison with conventional wastewater treatment technologies, less is known about the physical, chemical and biochemical reactions and processes that occur in microalgae-bacteria treatment systems.

The main outcome of the present PhD thesis was to develop a new integrated mechanistic model, named BIO_ALGAE, which includes crucial physical and biokinetic processes to simulate microalgae growth in different type of cultures, and most particularly in wastewater. The model was used to advance the understanding the inherent complexity of microalgae and bacteria interactions that occur in high rate algal ponds (HRAP) and photobioreactors.

BIO_ALGAE model was mainly built by coupling the River Water Quality Model 1 (RWQM1) formulation and the modified ASM3 model, and was implemented in COMSOL MultiphysicsTM simulation platform. Inorganic carbon, as a limiting substrate for the growth of microalgae, is one of the major innovative features of BIO_ALGAE. Carbon is an essential resource for microalgae production. Moreover, temperature, photorespiration, pH dynamics, solar radiation, light attenuation and transfer of gases to the atmosphere are considered main limiting factors for microalgae growth.

In a pragmatic approach to reduce the model's complexity in the initial stages of its development, it was decided to start by studying physical, chemical and biokinetic processes of microalgae alone, hence neglecting bacterial processes. Once calibrated the most uncertain parameters of the model, bacteria processes were added, and this gave place to the integral model BIO_ALGAE. This model was calibrated and validated with high quality experimental data from pilot raceway ponds over short-time scale and for long-term operation.

The BIO_ALGAE model has proved to be an efficient tool to understand microalgae and bacteria interactions in wastewater treatment and to simulate the dynamics of different components in the ponds. The model was used to investigate the effect of environmental conditions and nutrients availability on microalgae growth and the different hydraulic retention time (HRT) operating strategies on the relative proportion of microalgae and bacteria and biomass production. Moreover, thanks to the model it was possible to optimize the performance of both HRAP and photobioreactor.

Resumen

Las reacciones y los procesos que ocurren en sistemas mixtos de microalgas y bacterias son difíciles de entender ya que la mayoría de ellos tienen lugar simultáneamente y dependen de muchos parámetros tales como temperatura, radiación solar, disponibilidad de nutrientes (e.g. carbono y nitrógeno) así como ciertas condiciones inhibitorias (e.g. exceso de oxígeno en el medio de cultivo). En comparación con las tecnologías convencionales de tratamiento de aguas residuales, actualmente hay poco conocimiento de las reacciones físicas, químicas y bioquímicas y de los procesos que se producen en los sistemas de tratamiento de microalgas y bacterias.

El objetivo principal de la presente tesis doctoral fue desarrollar un nuevo modelo mecanístico integrado, denominado BIO_ALGAE, que incluye procesos físicos y bioquímicos cruciales para simular el crecimiento de microalgas en diferentes tipos de cultivos, principalmente en aguas residuales. El modelo se utilizó para comprender de una mejor forma las interacciones que se llevan a cabo entre microalgas y bacterias en lagunas de alta carga (LAC) y fotobiorreactores.

El modelo BIO_ALGAE se construyó mediante el acoplamiento del River Water Quality Model 1 (RWQM1) y del modelo ASM3 modificado, y se implementó en la plataforma de simulación COMSOL Multiphysics™. El carbono inorgánico, utilizado como sustrato limitante para el crecimiento de microalgas, es una de las principales características innovadoras de BIO_ALGAE. Además, la temperatura, la fotorespiración, la dinámica del pH, la radiación solar, la atenuación de la luz y la transferencia de gases a la atmósfera se consideraron los principales factores limitantes del crecimiento de las microalgas.

Para reducir la complejidad del modelo en las etapas iniciales de su desarrollo, se decidió empezar por estudiar los procesos físicos, químicos y bioquímicos sólo de las microalgas, dejando de lado los procesos bacterianos. Una vez calibrados los parámetros más sensibles del modelo, se añadieron los procesos bacterianos, lo que dio lugar al modelo integral BIO_ALGAE. Este modelo fue calibrado y validado con datos

experimentales de alta calidad procedentes de LAC operadas a corto y largo plazo.

El modelo BIO_ALGAE ha demostrado ser una herramienta eficaz para entender las interacciones de microalgas y bacterias en el tratamiento de aguas residuales y simular la dinámica de diferentes componentes en las LAC. El modelo se utilizó para investigar el efecto de las condiciones ambientales y la disponibilidad de nutrientes en el crecimiento de microalgas. También se estudió el efecto del tiempo de retención hidráulica sobre la proporción relativa de microalgas-bacterias y la producción de biomasa.

Gracias al modelo fue posible optimizar el rendimiento tanto de las lagunas de alta carga como del fotobiorreactor.

Acronyms and Abbreviations

AM	Ante Meridiem
A.M.S.L	Above Mean Sea Level
ASM	Activated Sludge Model
ASM1	Activated Sludge Model No.1
ASM2	Activated Sludge Model No.2
ASM2d	Activated Sludge Model No.2d
ASM3	Activated Sludge Model No.3
ATP	Adenosine Triphosphate
BOD	Biochemical Oxygen Demand
C	Carbon
CFD	Computational Fluid Dynamics
CO ₂	Carbon dioxide
CO ₃	Carbonate
COD	Chemical Oxygen Demand
CWM1	Constructed Wetland Model No.1
Delft3D	Deltares' hydrodynamic and water quality modelling suite
Delft3D FLOW	Deltares' hydrodynamic model software
Delft3D WAQ	Deltares' water quality and suspended sediment model software
DNA	Deoxyribonucleic Acid
DO	Dissolved Oxygen
EES	Elementary Effects
EE.UU	United States
EIA	Energy Information Administration
FEM	Finite Elements Method
GEMMA	Group of Environmental Engineering and Microbiology
H	Height
HCO ₃	Bicarbonate
HRAP	High Rate Algal Pond
HRAP _{4d}	HRAP operating at 4-day HRT

HRAP _{8d}	HRAP operating at 8-day HRT
HRAP _{8-4-8d}	HRAP operating at 4-day HRT and at 8-day HRT
HRT	Hydraulic Retention Time
INRA	Institut National de la Recherche Agronomique
IWA	International Water Association
L	Length
LBE	Laboratory of Environmental Biotechnology
M1, M2, M3	Triplicate Middle ponds
N	Nitrogen
NH ₄ Cl	Ammonium chloride
OAT	One-At-a-Time
P	Phosphorous
P ₂ O ₅	Phosphorus pentoxide
PAR	Photosynthetically Active Radiation
PBR	Photobioreactor
Period I	July 21 st – October 14 th , 1993
Period II	November 10 th , 1993 – February 8 th , 1994
PFD	Photon Flux Density
PLC	Programmable Logic Controller
PM	Post Meridiem
PSF	Photosynthetic Factories
RMSNE	Root Mean Square Normalized Error
RNA	Ribonucleic acid
RWQM1	River Water Quality Model 1
SEE	Scaled Elementary Effect
TCD	Thermal Conductivity Detector
TN	Total Nitrogen
TSS	Total Suspended Solid
VSS	Volatile Suspended Solid
W	Width
WPCF	Water Pollution Control Federation
WSPs	Waste Stabilization Ponds

List of symbols

B^*	Trajectory matrix
B'	Random lower left triangle unit matrix
c	Chemical species in equilibrium
d	Depth (Chapter 7, 8)
d	Diameter of tube (Chapter 6)
D^*	Diagonal matrix
$D1$	Loop configuration domain
$D2$	Open-air tank or bubble column volume
D_T	Turbulent diffusion
E_f	Photosynthetic efficiency of solar radiation
f_{ALG}	Production of inert particulate organic matter in endogenous respiration of microalgae
F_{ij}	Finite distribution
f_L	Light factor
$f_{T,FS}$	Thermic photosynthetic factor
$f_{T,MB}$	Thermal factor for bacteria
f_{PR}	Photorespiration factor
f_{XI}	Production of inert particulate organic matter in endogenous respiration of heterotrophic bacteria
g	Dissolved gas species
i	Number of components (Chapters 4, 6, 7)
i	Input parameter (Chapter 5)
I	Light intensity / irradiance
I_{av}	Average light intensity
$i_{C,ALG}$	Fraction of carbon in microalgae
$I_{CO2,ALG}$	Inhibition constant of microalgae on dissolved carbon
$i_{H,ALG}$	Fraction of hydrogen in microalgae
$i_{N,ALG}$	Fraction of nitrogen in microalgae
I_o	Incident light intensity
$i_{O,ALG}$	Fraction of oxygen in microalgae
j	Number of processes

J	Unit matrix
k	Number of components (Chapter 5)
K_{a,NH_3}	Mass transfer coefficient for ammonia
K_{a,O_2}	Mass transfer coefficient for oxygen
K_{a,CO_2}	Mass transfer coefficient for dioxide carbon
$K_{C,ALG}$	Saturation constant of microalgae on dissolved carbon
$K_{C,AOB}/K_{C,NOB}$	Saturation constant of nitrifying bacteria for bicarbonate
$k_{death,ALG}$	Decay constant of microalgae
$k_{death,H}$	Decay constant of heterotrophic bacteria
$k_{death,AOB}/$ $k_{death,NOB}$	Decay constant of nitrifying bacteria
$k_{eq,c}$	Dissociation constant
$k_{eq,1}$	Dissociation constant of $CO_2 \leftrightarrow HCO_3^-$
$K_{eq,1}$	Chemical equilibrium of $CO_2 \leftrightarrow HCO_3^-$
$k_{eq,2}$	Dissociation constant of $HCO_3^- \leftrightarrow CO_3^{2-}$
$K_{eq,2}$	Chemical equilibrium of $HCO_3^- \leftrightarrow CO_3^{2-}$
$k_{eq,3}$	Dissociation constant of $NH_4^+ \leftrightarrow NH_3$
$K_{eq,3}$	Chemical equilibrium of $NH_4^+ \leftrightarrow NH_3$
$k_{eq,w}$	Dissociation constant of $H^+ \leftrightarrow OH^-$
$K_{eq,w}$	Chemical equilibrium of $H^+ \leftrightarrow OH^-$
K_{HYD}	Hydrolysis rate constant
K_{I,NH_4}	Ammonia inhibition constant of nitrite oxidizing bacteria
$K_{N,ALG}$	Saturation constant of microalgae on nitrogen species
K_N	Saturation constant of heterotrophic bacteria on nitrogen species
$K_{NH_4,AOB}$	Saturation constant of ammonium oxidizing bacteria on ammonium
$K_{NO_3,H,ANOX}$	Saturation constant of heterotrophic bacteria for nitrate
$K_{NO_2,H,ANOX}$	Saturation constant of heterotrophic bacteria for nitrite
$K_{NO_2,NOB}$	Saturation constant of nitrite oxidizing bacteria for nitrite
$K_{O_2,AOB}/K_{O_2,NOB}$	Saturation constant of nitrifying bacteria for dissolved oxygen
$K_{O_2,H}$	Saturation constant of heterotrophic bacteria for dissolved oxygen
K_{PR}	Inhibition constant of photorespiration

k_q	Minimum subsistence quota
$k_{\text{resp,ALG}}$	Endogenous respiration constant
$k_{\text{resp,AOB}}/k_{\text{resp,NOB}}$	Endogenous respiration rate of nitrifying bacteria
$k_{\text{resp,H}}$	Endogenous respiration rate of heterotrophic bacteria
$K_{S,H}$	Saturation constant of heterotrophic bacteria for readily biodegradable soluble organic matter
K_S	Half-saturation coefficient for substrates
m	Number of rows (Chapter 5)
m	Number of components (Chapter 6)
M1, M2, M3	Triplicate Middle ponds
N	Number of simulations (Chapter 5)
p	Number of levels (Chapter 5)
P^*	k -dimensional matrix
r	Repetitions of elementary effects
Re	Reynolds number
r_i	Reaction rate for each component
s	Normalized parameter (Chapter 4)
S	Limiting substrate concentration (Chapters 3, 4)
S_c	Concentration of species in equilibrium (Chapter 4)
S_{CO_2}	Carbon dioxide
S_{CO_3}	Carbonate
S_{cT}	Turbulent Schmidt number
$S_{\text{eq,c}}$	Concentration at equilibrium (Chapter 4)
S_g	Gas concentration in water (Chapter 4)
S_g^{WAT}	Gas saturation concentration in water (Chapter 4)
S_H	Hydrogen ions
S_{HCO_3}	Bicarbonate
S_{NH_3}	Ammonia nitrogen
S_{NH_4}	Ammonium nitrogen
S_{NO_2}	Nitrite nitrogen
S_{NO_3}	Nitrate nitrogen
S_{O_2}	Dissolved oxygen
$S_{\text{O}_2}^{\text{SAT}}$	Dissolved oxygen air saturation

S_{OH}	Hydroxide ions
S_{PO4}	Phosphate phosphorus
S_S	Readily biodegradable soluble organic matter
T_{OPT}	Optimum temperature
u	Culture velocity
v_{ij}	Stoichiometric coefficients
\mathbf{x}	Vector of components x_i
\mathbf{x}^*	Random vector
x_i	Parameters of sensitivity analysis
X	Design Matrix
X_{AOB}	Ammonium oxidizing bacteria
X_C	Sum of particulate components
X_H	Heterotrophic bacteria
X_I	Inert particulate organic matter
X_{NOB}	Nitrite oxidizing bacteria
X_S	Slowly biodegradable particulate organic matter
x_1	Open or resting state
x_2	Closed or activated state
x_3	Inhibited state
y	Model output
Y_{ALG}	Yield of microalgae
Y_{AOB}	Yield of ammonium oxidizing bacteria
Y_H	Yield of heterotrophic bacteria
Y_{NOB}	Yield of nitrite oxidizing bacteria
$Y_{H,NO3}$	Yield of heterotrophic bacteria on nitrate
$Y_{H,NO2}$	Yield of heterotrophic bacteria on nitrite
Y_{HYD}	Hydrolysis saturation constant

Greek symbol

α	Activation rate
β	Inhibition rate
γ	Production rate
δ	Recovery rate

δ	Sun declination (Chapter 4)
Δ	Magnitude of step length
η_H	Anoxic reduction factor for heterotrophic bacteria
θ	Temperature coefficient
μ	Dynamic viscosity
μ_{ALG}	Maximum specific growth rate of microalgae
μ_{AOB}	Maximum growth rate of ammonium oxidizing bacteria
μ_{NOB}	Maximum growth rate of nitrite oxidizing bacteria
μ_H	Maximum growth rate of heterotrophic bacteria
ν_T	Turbulent kinematic viscosity
κ	Index atmospheric clarity
ζ	Universal solar constant
ρ	Culture density
ρ_c	Chemical Reaction rate for each species (Chapter 4)
ρ_j	Reaction rate for each process j (Chapter 4)
σ_i	Standard deviations of the parameters x_i (Chapter 5)
σ_y	Standard deviations of model outputs y_j (Chapter 5)
τ	Excess of dissolved oxygen coefficient
φ	Latitude
ω	Hour angle
ω_s	Sunset hour angle
Ω	Domain, region of interest (Chapter 5)

List of contents

1	Introduction	21
1.2	Microalgae production systems	23
1.3	Application of microalgae cultures	26
1.4	Microalgae for wastewater treatment	28
2	Objectives and thesis outline	31
2.1	Objectives	32
2.2	Thesis outline	32
3	State of the art	35
3.1	Introduction	36
3.2	Activated sludge models (bacteria models)	39
3.3	Microalgae models	40
3.4	Microalgae-bacteria models	49
3.4.1	<i>River Water Quality Model No. 1</i>	52
3.4.2	<i>Sab et al. 2011</i> model	53
3.4.3	<i>Zambrano et al. 2016</i>	54
3.4.4	<i>ASM-A</i>	55
3.4.5	<i>BIO_ALGAE</i>	56
3.5	Discussion	57
3.5.1	Microalgae processes comparison	57
3.5.2	Bacteria processes comparison	62
3.5.3	Physical, chemical and additional processes	69
3.6	Conclusion	76
4	Microalgae model	77
4.1	Introduction	78
4.2	Model description	80
4.2.1	Conceptual model	80
4.2.2	Model components	81
4.2.3	Processes	82
4.2.4	Effects of temperature, irradiance and pH	90
4.2.5	Stoichiometry and parameter values	92

4.3	Experimental verification	92
4.4	Model implementation and calibration procedure	93
4.5	Results	95
4.6	Discussion	99
4.6.1	Innovative features of the model	99
4.6.2	Model limitations and future developments	102
4.7	Conclusions	103
4.8	Appendix	106
5	Sensitivity analysis	108
5.1	Introduction	109
5.2	Material and methods	111
5.2.1	Theoretical background	111
5.2.2	Trajectory construction	112
5.2.3	Morris's method indices	113
5.2.4	Parameter selection, additional parameterization, and sensitivity analysis: computational experiment	115
5.2.5	Implementation of the Morris's method	117
5.3	Results	120
5.4	Discussion	124
5.5	Conclusions	126
6	Application of the microalgae model to photobioreactors	127
6.1	Introduction	128
6.2	Methods	129
6.2.1	Pilot closed photobioreactors and experimental data	129
6.2.2	Conceptual model	133
6.2.3	Model domain	134
6.2.4	Hydrodynamics of the system, light attenuation and temperature	135
6.2.5	Calibration procedure	139
6.2.6	Study cases	140
6.3	Results	141
6.4	Discussion	146
6.4.1	New features of the model	146

6.4.2	Calibration of the model	146
6.4.3	Study case: microalgae production as a function of temperature and irradiance	151
6.4.4	Study case: oxygen concentration	150
6.5	Conclusion	152
6.6	Appendix	153
7	Integrated BIO_ALGAE model	164
7.1	Introduction	165
7.2	Model description	168
7.2.1	Conceptual model	168
7.2.2	Model components	169
7.2.3	Model processes	173
7.2.4	Stoichiometric and parameter values	175
7.3	Pilot plant and experimental verification	176
7.4	The BIO_ALGAE model	178
7.5	Results and discussion	182
7.5.1	Model calibration	182
7.5.2	Model validation	188
7.5.3	Model applications	193
7.6	Conclusion	197
7.7	Appendix	199
8	Long-term BIO_ALGAE validation	217
8.1	Introduction	218
8.2	Material and methods	220
8.2.1	Experimental data	220
8.2.2	Model implementation	222
8.2.3	Validation procedure	223
8.2.4	Case studies: relative proportion of microalgae and bacteria, and biomass production forecasting over a year cycle	226
8.3	Results and discussion	226
8.3.1	HRAP _{4d} validation (Period I)	228
8.3.2	HRAP _{8d} validation (Period II)	234

8.3.3 Study case: relative proportion of microalgae and bacteria, biomass production and ammonium removal efficiency of HRAP4d over a year cycle	239
8.3.4 Study case: relative proportion of microalgae and bacteria, biomass production and ammonium removal efficiency of HRAP8d over a year cycle	242
8.3.5 Study case: optimization of microalgae production and ammonium removal efficiency over a year cycle	245
8.4 Conclusion	246
8.5 Appendix	247
9 Conclusions	261
References	265
Curriculum vitae	288

1

Introduction

Social and productive activities require and use large amounts of water. Direct consequence of water use is the production of discharges which should necessarily be subjected to treatment in order to be returned and assimilated by the environment. Urban wastewater in the past contained almost exclusively biodegradable substances, but nowadays there is a growing presence of chemical compounds of synthetic origin with different levels of biodegradability. Seas, rivers and lakes cannot receive a quantity of pollutants exceeding its self-purification capacity without seeing compromised the quality of its water and the normal balance of ecosystems.

New technologies and strategies are being experimented with the objective of removing conventional contaminants as well as chemical compounds of synthetic origin. Also there is a growing trend to replace “conventional wastewater treatment plants” by “resource recovery plants” able to produce reusable water and by-products, as well as energy. In this context, wastewater treatment systems with microalgae represent an opportunity to help moving from pure sanitation systems towards a “productive industry”. In fact, microalgae systems like conventional waste stabilisation ponds are an ancient technology for wastewater treatment which was progressively abandoned in many advanced countries in the near past. However, the growing interest in resource recovery combined with their capacity for feedstock production has revived the interest in microalgae systems, although different from the old conventional waste stabilization ponds (Craggs et al., 2013, Park et al., 2011, Rawat et al., 2011).

Microalgae based technologies are complex systems that degrade organic pollutants through the activity of aerobic bacteria that use the oxygen released from microalgae photosynthetic activity. Carbon dioxide released by heterotrophic bacteria is in turn assimilated by microalgae to grow and produce new biomass. Thus, in these systems solar energy is converted into chemical energy and stored in microalgae cells through photosynthetic activity. This chemical energy can be converted into biofuel (methane) through anaerobic digestion, and also into bioproducts. Reactions and processes that occur in microalgae systems are difficult to understand because most of them take place simultaneously and they are strongly interdependent (García et al., 2006). Also these reactions and processes change with time depending on environmental variables such as solar

radiation, temperature, and flow and quality of the influent wastewater. It is very challenging to understand a microbiological system where completely metabolic processes such as photoautotrophy, lithotrophy and heterotrophy coexist in a synergistic form. In fact, a deep and realistic knowledge of the inner functioning of these systems is necessary to predict performance and optimize reactor design.

In the last decades mathematical models have proven to be useful tools for design, analysis, operation and control of wastewater treatment systems. Nowadays, models have become essential tools for testing operational scenarios in wastewater systems aiming to improve the removal efficiency at the lowest operational costs. Mathematical models for microalgae-based wastewater treatment systems are also increasing in popularity. However, models in these systems are still in the research stage and are not in common in practice because their complex bioprocesses and hydrodynamics.

1.2 Microalgae production systems

The culture and industrial production of microalgae (not specifically speaking of wastewater treatment) can be achieved with two main reactor typologies: open and closed reactors. Cultivation of microalgae in open reactors (also often named open ponds) has been extensively studied in the past (Boussiba et al., 1988; Hase et al., 2000; Tredici and Materassi, 1992). Open reactors usually consist in shallow raceway ponds with mechanical stirring of the mixed liquor (Fig. 1.1).

In raceway ponds microalgae, water and nutrients circulate around a track and microalgae are kept in suspension thanks to the mixing mechanism. They are shallow (0.3 to 0.5 m), so that the light can penetrate as much as possible in the water column. Raceway ponds for biomass production normally operate with continuously flows of nutrients and carbon dioxide.



Figure 1.1 Microalgae open reactors (raceway systems). An aerial view of a pilot plant (Seambiotic Ltd., Tel Aviv) growing *Nannochloropsis* (an algae are rich in oil) using flue gas CO₂ from a coal-fired Power Plant near Ashkelon, Israel. Small ponds used to inoculate the largest (Seibert, 2009).

The main advantage of raceway reactors in comparison to closed reactors is that they are easier to build and operate. The main disadvantages are lower cell exposure to light, evaporation losses, high mass transport of CO₂ to the atmosphere (losses) and the requirement of large land areas. Another important disadvantage is that the culture can be easily contaminated by other microorganisms (competitors or grazers), and are difficult to control. These inconveniences cause a lower microalgal biomass production of raceways reactors in comparison to closed reactors (Ugwu et al., 2008).

Closed reactors are usually named with the term “photobioreactors” (although open reactors are also photobioreactors). In this case microalgae grow in enclosed transparent vessels in the form of panels or tubes that can be oriented vertically or horizontally (Fig. 1.2). These systems can be quite sophisticated and even use additional artificial light to help boost production when biomass has a high value added. Photobioreactors allow a strict control of chemical, physical and biological parameters of the culture and allow attaining higher biomass production than raceway reactors (Wang et al., 2012).

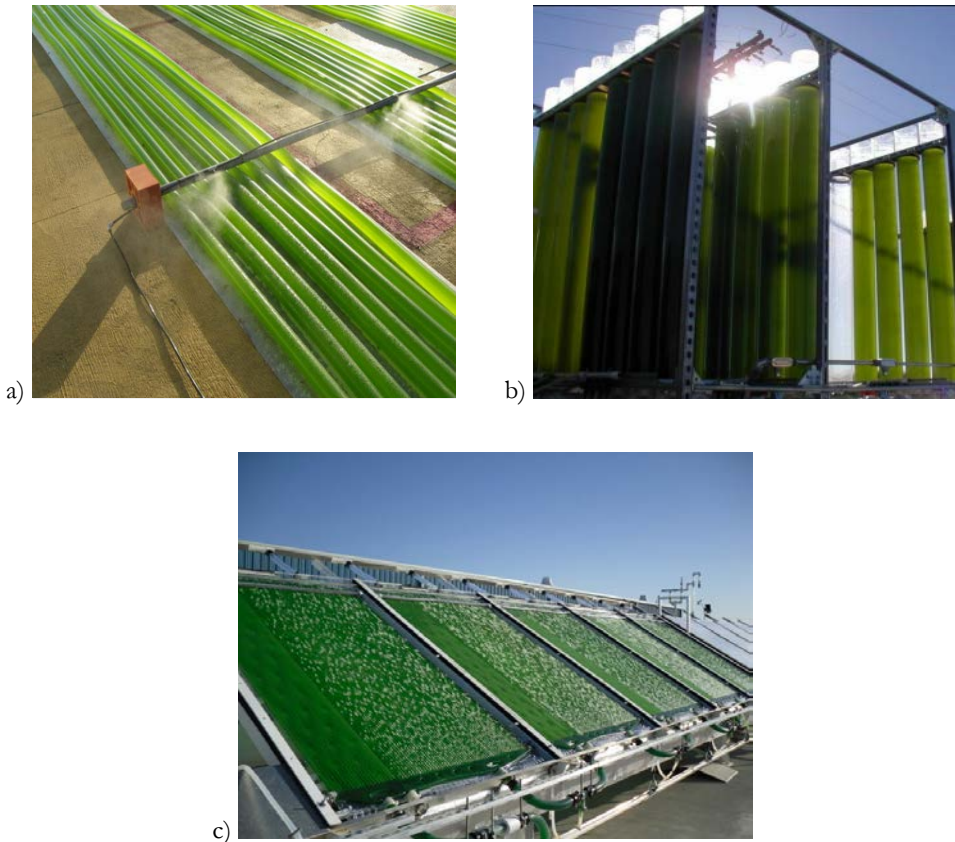


Figure 1.2 These images show: a) horizontal tubular photobioreactors made out of plastic tubing in Neste Oil's field trials in Andalusia (NesteOil, 2013); b) a column photobioreactor (NanoVoltaics, Inc. 2012) and c) scale-able rigid plastic photobioreactor (Joule Unlimited, 2013).

The great advantage of photobioreactors is that they can better match ideal conditions for growth of microalgae than raceway reactors optimizing light exposure due to turbulent conditions in the mixed liquor. Furthermore they reduce the possibility of contamination and allow to grow particular types of microalgae that are difficult to maintain in open raceway ponds. The two most critical issues of photobioreactors are their high sensitivity to temperature variations and the potential accumulation of high amounts of oxygen and subsequent inhibition. It should be noted that oxygen build-up becomes a problem when photobioreactors are scaled up (Molina Grima et al., 2001). Therefore photobioreactors often they require cooling and degasser systems (Weissman and Goebel, 1987).

1.3 Application of microalgae cultures

Nowadays several species of microalgae are already produced commercially in various countries and used for the production of food complements, nutraceuticals as well as pharmaceuticals, and biomass for aquaculture (Barbato and Simbolotti, 2009). In the field of environmental biotechnology, microalgae cultures are particularly suitable for wastewater treatment, biofuel production and sequestration of CO₂.

Biodiesel production from microalgal cultures aroused a great interest in the 2000 decade. However, this application is still under strong research and microalgae biodiesel prices are still not competitive with conventional fossil fuels. The cost of conventional diesel fuel in the last 16 years has ranged between \$1/gallon and \$4.70/gallon, with the current price just under \$3/gallon (EIA, 2017). While the price has been volatile in recent years, it is still much lower than biodiesel from microalgae. Since there are no large-scale production facilities of algal biodiesel, an accurate comparative cost per gallon is difficult to be attained. An analysis presented by Lundquist (2009) estimated the production cost to be around \$7.10/gallon of oil from a wastewater application. One of the bottlenecks of biodiesel from microalgae is biomass production, which depends on microalgae species, location for cultivation as well as cultivation techniques (Table 1.1). In fact one of the main challenges of microalgal biotechnology is prediction of biomass production.

According to Meisner (2007), by 2015 the products obtained from microalgae may have a potential world-wide market of 25-50 billion dollars per year, mainly due to the production of biodiesel (50%), the sequestration of CO₂ and the production of nutritional supplements.

Table 1.1 Algal production measured in experimental fresh water and wastewater treatment high rate algal ponds (Park et al., 2011).

HRAP	Location	Species	Areal production [g m ⁻² d ⁻¹]		Surface area [m ²]	Total volume [m ³]	References
			Total	Harvestable			
Commercial production	Hawaii	<i>Tetraselmis suecica</i>	40	-			Laws et al. (1988)
	Hawaii	<i>Cyclotella cryptica</i>	29.7	-			Laws et al. (1988)
	Hawaii	<i>Platymonas sp</i>	26	-	48	5.8	Sheehan et al. (1998)
	Hawaii	<i>Cyclotella cryptica</i>	30	-	9.2	1.1	Sheehan et al. (1998)
	Hawaii	<i>Tetraselmis suecica</i>	37.5	-	9.2	1.1	Sheehan et al. (1998)
	New Mexico	<i>Scenedesmus quadricauda</i>	14	-	100	22.5	Weissman and Goebel (1988)
	New Mexico	<i>Chlorella sp.</i>	21	-	100	22.5	Weissman and Goebel (1988)
	Israel	<i>Anabena siamensis</i>	12.9	-	2	0.3	Richmond et al. (1993)
Wastewater treatment	California	Mixed algal culture	18.4	14.8	1000	-	Benemann (1986)
	Israel		33	-	120	-	Shelef (1982)
	Israel		35	-	150	-	Shelef (1982)
	New Zealand		25	16.8	32	8	Park and Craggs (2010)
	Philippines		15.3	11.9	100	-	Oswald (1987)
	Scotland		18	-	13	-	Cromar et al. (1996)
	Spain		12.7 - 14.8	9.9 - 11.5	1.54	-	García et al. (2006)
	Kuwait		15	-	12	-	Banat et al. (1990)

In 2011, the total microalgae production has reached 9,000 tonnes dry weight (Acien et al., 2013). The value of the global marine biotechnology market in 2011, with microalgae as its main component, was estimated at €2.4 billion, with an expected yearly growth of 10 per cent (Gaudes et al., 2011). Note that this volume is still small compared to other food commodities. Global wheat production for instance is around 700 million tonnes annually, 70,000 times as much (Enzing et al., 2014).

1.4 Microalgae for wastewater treatment

Microalgae cultures can be used to treat wastewater. The most frequent type of microalgae wastewater reactor consist in shallow open raceway ponds (0.3 to 0.5 m deep), with devices such as paddlewheels to stir the mixed liquor. These types of systems have been referred to “high rate ponds”, “high rate oxidation ponds” or “high rate algal ponds”, being the latter the one used in the present document (acronym HRAP). Note that the old-type conventional waste stabilisation ponds as mentioned before are also microalgae based treatment systems, but because they are not designed for biomass production, they will not be covered in the present document. HRAPs constitute low energy wastewater treatment systems as well as energy generation systems through microalgae biomass that can be converted into biofuels.

HRAP technology was developed in California in the late 1950s with the main aim of improving the performance of conventional waste stabilisation ponds (García et al., 1998; Oswald 1988). In HRAPs low water depth and continuous stirring of the mixing liquor reduce the light limitation of algal growth that occurs in conventional waste stabilisation ponds, and gives place to a higher biomass production. However, algal production in these systems is usually limited by inorganic carbon and for this reason injection of carbon dioxide is seen as a promising strategy to increase production (Figure 1.3).

Within the context of a wastewater treatment plants, the main function of a HRAP unit is secondary treatment, which is to degrade and convert dissolved organic matter in microorganisms that can be subsequently separated. Moreover, another function can be microalgae biomass

production for biofuels providing economic and environmental benefits (Park et al., 2011).



Figure 1.3 Experimental high rate algal ponds on the roof of the GEMMA group building at UPC in Barcelona (Spain).

2

Objectives and thesis outline

2.1 Objectives

The overall objective of the present PhD thesis is to develop an integrated mathematical mechanistic model that includes physical, chemical and biokinetic processes for microalgae-based wastewater treatment systems simulation. The model is “integrated” because includes mixed populations of microalgae as well as bacteria. In this research we implement this mathematical model in a simulation platform for the prediction of different variables related to wastewater treatment and biomass production.

The specific objectives of this research are:

- To develop and calibrate a mechanistic microalgae model (without bacteria) and to evaluate the sensitivity of the microalgae model outputs in respect to a subset of key input parameters.
- To calibrate and apply the microalgae model to different tubular photobioreactors.
- To develop, calibrate and validate an integrated microalgae-bacteria mechanistic model and to evaluate the sensitivity of the integrated model outputs in respect to a subset of key input parameters.
- To validate the integrated model in a pilot HRAP over a year cycle.

2.2 Thesis outline

This PhD thesis is mostly based on six scientific articles (three of which have been already published). The reader should be aware that chapters are organized in chronological order of the works performed (except Chapter 3, which was written towards the end of thesis), therefore a few equations or parameters have been changed during the evolution of the model.

In Chapter 3, the state of the art of microalgae and bacteria models is presented. Moreover, the new mechanistic model BIO_ALGAE, which is

the final result of this thesis (the “integrated” model), is described in comparison with other mechanistic microalgae-bacteria models for wastewater treatment.

The following Chapters describe the development of the BIO_ALGAE model step-by-step: from a microalgae mechanistic model to the integrated microalgae-bacteria mechanistic model:

Chapter 4: *Microalgae model*

The mechanistic model to simulate microalgae growth is developed and described. The model is implemented in a software simulation platform, and calibrated using experimental data from a case study based on the cultivation of microalgae species in synthetic culture medium over 9 days of experimentation.

Chapter 5: *Sensitivity analysis*

The procedure and the sensitivity measurements of the Morris method of Elementary Effects (EEs) are described and applied for screening the most sensitive parameters on microalgae model outputs.

Chapter 6: *Application of the microalgae model to photobioreactors*

The model is calibrated for full-scale horizontal and vertical photobioreactors. The model is first calibrated using experimental data obtained from the vertical photobioreactor monitored for 24 hours. Afterwards, the model is calibrated with experimental data from the horizontal photobioreactor retrieved from three days batch experiment. By means of practical study cases microalgae production under different climatic conditions and oxygen accumulation throughout the photobioreactor are predicted.

Chapter 7: *Integrated BIO_ALGAE model*

The microalgae model is expanded with bacteria processes to create the integrated model, which is calibrated and validated in triplicate

pilot raceway ponds over a time period of 4 days. The relative effect of the factors that affect microalgae growth and the effect of different influent organic matter concentration on total biomass production are investigated by means numerical experiments. Moreover, the relative proportion of microalgae and bacteria is predicted.

Chapter 8: *Long-term BIO_ALGAE validation*

The BIO_ALGAE is validated with data from a pilot raceway pond over a year cycle. Microalgae and bacteria proportions, the effect of different HRT operating strategies and variations of environmental conditions were studied in order to optimize biomass production and ammonium removal efficiency.

Finally, in Chapter 9 the main conclusions of this work are presented.

3

State of the art

This chapter is based on the article:

- ❖ A. Solimeno, J. García. (in preparation). Microalgae-bacteria models evolution: from microalgae steady-state models to integrated microalgae-bacteria wastewater treatment models – a comparative review.

3.1 Introduction

Interactions between microalgae and bacteria have been incidentally used for wastewater treatment for long time ago in waste stabilization ponds (WSPs). This type of treatment was intensively implemented worldwide from the Second World War. As an example, in the EE.UU in 1990 there were more than 7,000 WSPs which represented more than 1/3 of the operating wastewater treatment plants (WPCF, 1990). Important role of microalgae (as well as bacteria) in pollutant removal processes occurring in WSPs was already put into evidence in early studies by Myers (1948). However, the interest in WSPs decreased from 1990, especially in developed countries due to various reasons, but in particular the high content of microalgae in their effluents which makes difficult to meet usual effluent standards for Total Suspended Solids (García et al., 2000a).

A variant of the conventional WSPs are the high rate algal ponds (HRAPs), which were developed in California in late 1950s (Oswald and Gotaas, 1957). HRAPs are shallow raceway ponds with mechanical stirring of the mixed liquor to increase microalgae biomass production and enhance pollutant's removal. In last years, the search for alternative fuels neutral with the climate change had revived with great enthusiasm the interest of microalgae and bacteria systems such as HRAPs (Chisti, 2007). Nevertheless, biofuel production from microalgae is currently price prohibitive, and the interest is at this very moment much more oriented to develop wastewater treatment systems with neutral energy footprint which at the same time can produce marketable products and effluent water than can be reused (Dalrymple et al., 2013, Craggs et al., 2011, Park et al., 2011). In comparison to conventional wastewater treatment systems, the potential of costs savings, including electrical power, are great enough to promote HRAPs independent of biofuels production (Suganya et al., 2016).

Currently, in comparison to conventional technologies, less is known about the internal functioning of microalgae wastewater treatment systems, and in particular the interactions between microalgae and bacteria. In these systems, microalgae can promote or inhibit bacteria growth and vice versa (Awuah,

2006; Marsollier et al., 2004; Ruíz-Marín et al., 2004). The physical, chemical and biological processes that take place in these systems (e.g. growth, decay, light attenuation, gas mass transfer to atmosphere) occur simultaneously and they are strongly interdependent (García et al., 2006). In addition, the rates of these processes depend on ever-changing environmental variables such as light intensity and temperature. Within this framework, is necessary to gain insight on this complexity which will help to create a body of knowledge on the interactions between microalgae and bacteria. A deep and realistic knowledge of the inner functioning of these systems is necessary to predict performance and optimize reactor design. Mathematical models represent a powerful tool to get insight into complex systems such as microalgae-bacteria treatments.

Mechanistic bacteria mathematical models for conventional wastewater treatment systems such as the activated sludge have been successfully developed and proved, and nowadays are widely accepted and used (Van Loosdrecht et al., 2015). On the contrary, mechanistic models that describe the inner complexity of microalgae-bacteria wastewater treatment systems are still at development and testing stage.

Of course there is large number of simple microalgae steady-state models, which are based on deterministic biological kinetics. Steady-state models describe microalgae growth keeping the values of factors constant over time. These models were initially developed observing the behaviour of microalgae respect to a single factor (e.g. nitrogen, carbon, phosphorus, light intensity) (Aslan and Kapdan, 2006; Eilers and Peeters, 1988; Martínez et al., 1997; Novak and Brune, 1985). More recently, researchers have developed more complicated dynamic models that take into account multiple substrate or physical factors limitations following a structure according to Droop's or Monod kinetics (Bernard, 2011; Brennan and Owende, 2010; Mata et al., 2011; Quinn et al., 2011). In opposition to steady-state models, in these dynamic models values of factors change with time.

A number of different types of mathematical models have been developed for understanding the interaction between microalgae and bacteria. Buhr and Miller (1983) produced the first simple dynamic mathematical model to describe the symbiotic growth of microalgae and bacteria in HRAPs. Since

Buhr and Miller (1983), other models with more complexity have appeared with a progressive increase of features and processes. The River Water Quality Model 1 (RWQM1) (Reichert et al., 2011), for instance, is a mechanistic model that includes the growth of microalgae and bacteria (i.e. heterotrophs as well as nitrifiers) on N (ammonium and nitrate) and P (orthophosphate), but does not include any reference on carbon limiting growth. In the mechanistic model by Sah et al. (2011) microalgae and bacteria processes are also influenced by physical processes (such as re-aeration) and environmental factors (i.e. solar radiation, temperature and wind). These mechanistic models are usually based on Monod kinetics and microalgae-bacteria interactions are commonly written in a matrix format with several of kinetics and stoichiometric coefficients.

Much of the integrated microalgae-bacteria models currently available do not combine the overall biochemical processes involved in these systems and the simultaneous effects of light intensity, temperature, pH, or the effect of high dissolved oxygen concentration on biomass growth. The new integral mechanistic model BIO_ALGAE (Chapter 7; Solimeno et al., 2017a) was developed with the aim to overcome these microalgae-bacteria bottlenecks of the previous microalgae-bacteria mechanistic models.

The principal objective of this article is therefore to compare different and complementary approaches for microalgae-bacteria models. First the article deals briefly with the most famous mechanistic mathematical model for activated sludge systems (a bacterial model). Afterwards the evolution of microalgae models from steady-state models to dynamic models is described. Also the most relevant integrated mechanistic models are revised, and finally a critical discussion of microalgae-bacteria interactions and physical-chemical processes implemented in these mechanistic models is made. The target is to give an overview of the key differences and limitations between these models.

3.2 Activated sludge models (bacteria models)

The mechanistic models of the Activated Sludge Model (ASM) series were promoted by the International Water Association (IWA, former International Association on Water Pollution Research and Control). The first one, the Activated Sludge Model No. 1 (ASM1) was presented in 1986 by a defined IWA task group and is considered as the base model for conventional biological wastewater treatment. The task group revised previous existing models in order to produce a widely accepted mathematical model to predict the performance systems and optimize design (Jeppsson, 1997). Carbon (organic matter) oxidation, nitrification and denitrification were included in the model; conversely biological phosphorus removal was not taken into account (Gernaey et al., 2004).

The ASM1 is composed of 8 processes and 13 state variables (or factors). The kinetics and stoichiometry used to describe the ASM1 processes are mainly based on Monod formulation. The general specific growth rate for Monod formulation is:

$$\mu = \mu_{\max} \frac{S}{K_S + S} \quad (3.1)$$

where μ [T^{-1}] is the specific growth rate, μ_{\max} [T^{-1}] is the maximum specific growth rate coefficient, S [$M L^{-3}$] is the concentration of the limiting nutrient and K_S [$M L^{-3}$] is the Monod coefficient, also known as half-saturation coefficient (the nutrient concentration at which μ is half of its maximum) (Hiatt and Leslie Grady, 2006).

Subsequently, ASM1 was the starting point to further extensions: Activated Sludge Model No. 2 (ASM2) and Activated Sludge Model No. 2d (ASM2d), which added more processes to include biological phosphorus removal, and Activated Sludge Model No. 3 (ASM3), which incorporated a more realistic description of decay processes and more detailed description of cell internal storage compounds (Henze et al., 2000).

The main limitation of ASM models is attributable to the fact that kinetic parameters were calibrated based on experience in a temperature range of 8-

23 °C and pH 6.5-7.5 (Henze et al., 2000). Outside of this range, models might not represent adequately the behaviour of the system. Improvements of ASMs models have been made implementing temperature effects with specific equations proposed in the literature (Beran and Kargi, 2005; Wolf et al., 2007; Xu et al., 2010). Another limitation is that the values of coefficients related to bacteria processes (e.g. growth, decay) were considered constant for a given wastewater (Henze et al., 2000).

Despite their inherent restrictions, ASM models are considered the most important mathematical models for wastewater treatment simulation and are nowadays used as base model from which extensions can be incorporated to describe other processes not included in the original versions (Van Loosdrecht et al., 2015).

3.3 Microalgae models

A number of steady-state models have been developed to describe microalgae photosynthesis and growth kinetics, which can be expressed either in terms of biomass growth or nutrients uptake, and the influence of several factors, such as light, pH, temperature and nutrients availability, on these processes.

Research on microalgae growth kinetics modeling started with the pioneering work by Droop (1983). The Droop model relates the process rates to the internal content of substrate in the microalgae cell (Richmond, 2004; Sommer, 1991). The Droop model is described by the following equation (Eq. 3.2):

$$\mu = \mu_m \left(1 - \frac{k_q}{Q}\right) \quad (3.2)$$

where μ [T^{-1}] is the specific growth rate, μ_m [T^{-1}] is the theoretical growth rate at infinite quota, k_q [-] is the minimum (subsistence) quota and Q [-] is the cell quota.

Since the publication of Droop model, several different steady-state mathematical models have been used to predict microalgae specific growth rate with one process which depends on one factor (i.e. substrate or light intensity). Moreover, most of these models describe microalgae processes using the Monod formulation instead the Droop model because in the practice is easier to measure an external substrate than internal cell quotas.

These models were in general developed from experiments which were conducted to relate microalgae growth in relation to substrate concentration in the culture medium. Table 3.1 shows several of the most cited steady-state models, based on either Droop or Monod formulations (Aslan and Kapdan, 2006; Eilers and Peeters, 1988; Martínez et al., 1997; Molina-Grima et al., 1994; Novak and Brune, 1985; Sommer, 2011;). Neither of all these models considers that microalgae processes are influenced by multiple factors (two or more). Dynamic models describe changes in microalgae growth as a result of changing factors and are a prerequisite to predict microalgae biomass together with optimizing operation conditions. With this aim, dynamic models including two or more factors were developed (Bernard, 2011; Bonachela et al., 2011; Costache et al., 2013; Packer et al., 2011).

In the next paragraphs some of the most cited microalgae steady-state and dynamic model considering more than one factor (nitrogen or carbon limitation simultaneously affected by temperature and/or light intensity) are described.

Table 3.1 Microalgae steady-state models based on one factor to predict microalgae growth (μ_{ALG}).

Description	Process	Nomenclature	Reference
Inorganic carbon model	$\mu_{ALG} = \mu_m \frac{S_C}{K_{S,C} + S_C}$	μ_m : Maximum specific growth rate [T^{-1}] S_C : Inorganic carbon concentration [$M L^{-3}$] $K_{S,C}$: Half-saturation constant for inorganic carbon [$M L^{-3}$]	Novak and Brune, 1985; Tang et al., 2011
Nitrogen model	$\mu_{ALG} = \mu_m \left(1 - \frac{q_{N,Xmin}}{q_{N,X}} \right)$ $\mu_{ALG} = \mu_m \frac{S_N}{K_{S,N} + S_N}$	μ_m : Maximum specific growth rate [T^{-1}] $q_{N,X}$: Internal nitrogen cell quota [-] $q_{N,Xmin}$: Minimum nitrogen cell quota [-] μ_m : Maximum specific growth rate [T^{-1}] S_N : Nitrogen concentration [$M L^{-3}$] $K_{S,N}$: Half-saturation constant for nitrogen [$M L^{-3}$]	Droop, 1983 Smith, 2002; Aslan and Kapdan, 2006
Phosphorous model	$\mu_{ALG} = \mu_m \frac{S_P}{K_{S,P} + S_P}$ $\mu_{ALG} = \mu_m \left(1 - \frac{q_{P,Xmin}}{q_{P,X}} \right)$	μ_m : Maximum specific growth rate [T^{-1}] S_P : Phosphorus concentration [$M L^{-3}$] $K_{S,P}$: Half-saturation constant for phosphorus [$M L^{-3}$] μ_m : Maximum specific growth rate [T^{-1}] $q_{P,X}$: Internal phosphorous cell quota [-] $q_{P,Xmin}$: Minimum phosphorus cell quota [-]	Aslan and Kapdan, 2006 Sommer, 2011
Light intensity model	$\mu_{ALG} = \mu_m \frac{I}{K_I + I + K_I I^2}$	μ_m : Maximum specific growth rate [T^{-1}] I : Light intensity [$M T^{-3}$] K_I : Half-saturation constant for light intensity [$M T^{-3}$]	Aiba, 1982

	$\mu_{\text{ALG}} = \frac{k\alpha\delta\gamma I}{\alpha\beta I^2 + (\alpha + \beta)\delta I + \gamma\delta} - \text{Me}$ $\mu_{\text{ALG}} = \mu_m \frac{I_{\text{av}}}{K_1 + I_{\text{av}}}$ $\mu_{\text{ALG}} = \mu_m \frac{(I_{\text{av}})^{\left(n_2 + \frac{n_3}{I_0}\right)}}{\left(I'_k + \left(\frac{I_0}{K_1}\right)^{n_1}\right)^{\left(n_2 + \frac{n_3}{I_0}\right)} + (I_{\text{av}})^{\left(n_2 + \frac{n_3}{I_0}\right)}}$ $\mu_{\text{ALG}} = \mu_m (1 - \exp^{-I/K_1})$	<p>I: Light intensity [M T⁻³] k: Yield of photosynthesis production [-] Me: Maintenance [T⁻¹] α,β: Rate constants [M⁻¹ T²] γ,δ: Rate constants [T⁻¹]</p> <p>μ_m: Maximum specific growth rate [T⁻¹] I_{av}: Average light intensity [M T⁻³] K₁: Half-saturation constant for light intensity [M T⁻³]</p> <p>μ_m: Maximum specific growth rate [T⁻¹] K₁: Photoinhibition constant [M T⁻³] n₁, n₂, n₃: Characteristic parameters [-] I_{av}: Average light intensity inside the culture [M T⁻³] I₀: Light intensity [M T⁻³] I'_k: Specific irradiance constant [M T⁻³]</p> <p>μ_m: Maximum specific growth rate [T⁻¹] I: Light intensity [M T⁻³] K₁: Half-saturation constant for light intensity [M T⁻³]</p>	<p>Eilers and Peeters, 1988; Wu and Merchuck, 2001</p> <p>Molina-Grima et al., 1994; Martínez et al., 1997; Bordel et al., 2009</p> <p>Molina-Grima et al., 1996; Ación et al., 1998</p> <p>Martínez et al., 1997</p>
--	---	---	---

Microalgae growth as a function of nitrogen and temperature

Sterner and Grover (1998) described microalgae growth with a steady-state Monod formulation considering two factors:

$$\rho_{\text{ALG}} = \mu_T \cdot T \cdot \frac{S_N}{K_N + S_N} \cdot X_{\text{ALG}} \quad (3.3)$$

where ρ_{ALG} [$\text{M L}^{-3} \text{T}^{-1}$] is microalgae growth rate, μ_T [T^{-1}] is the specific growth coefficient, T [$^{\circ}\text{C}$] is the temperature, K_N [M L^{-3}] is the nitrogen half saturation constant, S_N [M L^{-3}] is the nitrogen concentration and X_{ALG} [M L^{-3}] is the microalgae concentration. This model was calibrated with experimental data from different depths of the Eagle Mountain Lake (Tarrant County, Texas, US). The authors observed that temperature had a clear and consistent effect on nutrient-saturated growth rate, and thus temperature effects combined with Monod function for N-limiting provided a reasonably good description of the experimental data. Although the model was able to fit well the experimental data, the authors recommended caution for applying a single Monod-microalgae nutrient formulation for modelling microalgal growth in natural ecosystems. This is because in natural ecosystems growth depends on factors that change continuously, and a single Monod model will be likely improper to describe the dynamics of microalgae.

Microalgae limited simultaneously by nitrogen and light intensity

In the dynamic model by Bernard (2011) microalgae growth rate is limited simultaneously by nitrogen and light availability. Based on classic Droop formulation, Bernard (2011) developed a model in which microalgae growth is related to internal concentration of inorganic nitrogen (nitrate or ammonium) and light (Eq. 3.4-3.7). Considering the nitrogen internal cell quota, microalgae can continue growing for some time even if the nitrogen concentration in the culture medium is completely consumed (Bernard et al., 2016). The four differential equations are expressed as:

$$s(t) = DS_{in} - \bar{\rho} \frac{S}{K_S + S} \left(1 - \frac{q}{Q_1}\right) X - DS \quad (3.4)$$

$$q(t) = \bar{\rho} \frac{S}{K_S + S} \left(1 - \frac{q}{Q_1}\right) - \bar{\mu} (I_0, I^*, X, q)(q - Q_0) \quad (3.5)$$

$$X(t) = \bar{\mu} (I_0, I^*, X, q)(q - Q_0) X - DX - RX \quad (3.6)$$

$$I^* = \bar{\mu} (I_0, I^*, X, q) \left(1 - \frac{Q_0}{q}\right) (\bar{I} - I^*) \quad (3.7)$$

where $s(t)$ [$M L^{-3}$] is the culture dissolved inorganic nitrogen concentration (i.e. nitrate and/or ammonium), $q(t)$ [-] the internal nitrogen cell quota, $X(t)$ [$M L^{-3}$] is the microalgae concentration and $I^*(t)$ [$M T^{-3}$] is the light intensity. The dilution rate is expressed as D [T^{-1}], $\bar{\rho}$ is the maximum nitrogen uptake [-], S_{in} [$M L^{-3}$] is the influent nitrogen concentration, R [T^{-1}] is the respiration rate, \bar{I} [$M T^{-3}$] and I_0 [$M T^{-3}$] are the average light intensity and light intensity over culture surface, respectively. Q_0 [dimensionless] is the minimum nitrogen quota, Q_1 [-] is the maximum nitrogen quota and $\bar{\mu}$ [T^{-1}] is the average growth rate. Observing Eq. 3.4-3.5, the maximum nitrogen uptake ($\bar{\rho}$) is associated with a Monod formulation where K_S [$M L^{-3}$] is the nitrogen half saturation constant [$M L^{-3}$]. In this model microalgae growth is described by a single process which already includes the respiration rate.

Parameters related to microalgae-nitrogen growth rate were calibrated with experiments conducted with *Dunaliella salina* using various light intensities and different nitrogen concentrations in chemostat experiments (Pawlowski, 2004). Parameters related to photosynthesis (equations not shown) were calibrated with experimental data from Anning et al. (2000), which analyzed the photosynthetic response of the diatom *Skeletonema costatum* at low and high irradiance. The model was validated with experimental data from Mairet et al. (2010) with the microalgae *Isochrysis* aff. *galbana*. The model was able to accurately reproduce experimental data.

Few models have used the model of Bernard. Zhou et al. (2014) applied the model to investigate the optimal value of culture factors (i.e. dilution rate, light intensity and influent nitrogen concentration) to maximize microalgae production. Yuan et al. (2014) taking as a starting point Bernard's model, developed a model guideline for microalgae growth introducing different expressions and coefficients from other previous models (Geider et al., 1998; Packer et al., 2011; Quinn et al., 2011). Thus, the authors made up several sub-models such as the light distribution sub-model following Quinn et al. (2011), the respiration sub-model according to Mairet et al. (2010), or the nitrogen uptake sub-model from Geider et al. (1998). This was done to compare model outputs from the original Bernard's model with those of integrated Bernard's model with the sub-models.

Mairet et al. (2011) proposed a model from Bernard's work to predict biomass, carbohydrate and neutral lipid production in a photobioreactor under light and nitrogen limitations. It is well-known that microalgae with a high content of neutral lipids are an excellent source for biofuel production (Metting, 1996). This model takes into account the ability of microalgae to synthesize and to accumulate lipids during the photosynthesis in order to optimize their production (Chisti, 2007). The model is based on Droop's formulation and parameters values were selected from the validated model of Bernard (2011). Moreover, the model considers light limitation and photoacclimation:

$$p(s) = p \frac{S}{S+K_S} \quad (3.8)$$

$$\mu(q_n) = \bar{\mu} \left(1 - \frac{Q_0}{q_n}\right) \quad (3.9)$$

$$\bar{\mu}(I) = \tilde{\mu} \frac{I}{I + K_{SI} + \frac{I^2}{K_{II}}} \quad (3.10)$$

where $p(s)$ [T^{-1}] is the nitrogen absorption rate, $\mu(q_n)$ [T^{-1}] is the growth rate and $\bar{\mu}(I)$ [T^{-1}] is the maximum growth rate dependent from light intensity I

$[M T^{-3}]$, $K_{SI} [M T^{-3}]$ is the half saturation coefficient for light and $K_{II} [M T^{-3}]$ is the inhibition coefficient (Eilers and Peeters, 1993). $K_s [M L^{-3}]$ is the half saturation constant for substrate uptake and $Q_0 [-]$ the minimal cell quota. $\bar{\rho} [T^{-1}]$ and $\tilde{\mu} [T^{-1}]$ are the maximum inorganic nitrogen uptake rate and the hypothetical growth rate, respectively.

The proposed model was calibrated with experimental data of *Isochrysis* aff. *galbana* under day/night cycles. MATLAB[®] software was used to minimize the square error between experimental data and simulation results. The model was able to fit experimental data but according to the authors more experiments are needed to validate the model.

Microalgae growth as a function of carbon and light intensity

He et al. (2012) developed a dynamic model to describe growth in a photobioreactor fed with flue gas as a source of inorganic carbon. Also light intensity was included as a factor limiting growth, and the model was experimentally validated. A Monod formulation was used to relate the dependence of growth on carbon and light:

$$X_{ALG}(t) = \mu_M \cdot \frac{S_{CO2}}{K_{CO2} + S_{CO2} + \frac{S_{CO2}^2}{K_{I,CO2}}} \cdot \frac{I}{I + K} \cdot X_{ALG} \quad (3.11)$$

$$S_{CO2}(t) = K_{La} \cdot (P/H - S_{CO2}) \cdot Y_{SCO2/X} \cdot \frac{S_{CO2}}{K_{CO2} + S_{CO2} + \frac{S_{CO2}^2}{K_{I,CO2}}} \cdot \frac{I}{I + K} \cdot X_{ALG} \quad (3.12)$$

where $K_{CO2} [M L^{-3}]$ and $K [M T^{-3}]$ are the half saturation constants for CO_2 and light intensity, respectively, $K_{I,CO2} [M L^{-3}]$ is the inhibition constant for CO_2 ; $\mu_M [T^{-1}]$ is the maximum specific growth rate of microalgae, and $S_{CO2} [M L^{-3}]$ and $X_{ALG} [M L^{-3}]$ are the concentration of carbon dioxide and microalgae, respectively. $P [M L^{-1} T^{-2}]$ is the CO_2 partial pressure in the gas phase, $H [L^2 T^{-2}]$ is the CO_2 Henry's constant of, $K_{La} [T^{-1}]$ is the mass transfer rate, and $Y_{SCO2/X} [-]$ is the yield coefficient. Experimental tests on

three different microalgae species (i.e. *Chlorella* sp., *Synechocystis* sp. and *Tetraselmis suecica*) were made to investigate growth response at different flue gas pulse modes. The model allowed finding the optimal time-dependent CO₂ injections to maximize microalgae growth. The most interesting feature of this model is the inclusion of a CO₂ inhibition function for microalgae growth (Silva and Pirt, 1984).

Microalgae growth as a function of irradiance, temperature, pH, and dissolved oxygen

Costache et al. (2013) developed dynamic model considering several important environmental parameters (light intensity, temperature, pH, and dissolved oxygen) on microalgae growth. The model equations were built, in steady-state analysing experimental data related on the influence of the environmental parameters on the photosynthesis rate of *Scenedesmus almeriensis*. After that, the model was validated using daily experimental data from an outdoor culture of *Scenedesmus almeriensis* growing in open raceway reactor. Biomass concentration was calculated measuring the oxygen production rate (RO₂) [T⁻¹] under different conditions of light intensity (RO₂[I_{av}]) [T⁻¹], temperature (RO₂[T]) [T⁻¹], pH (RO₂[pH]) [T⁻¹] and dissolved oxygen (RO₂[DO₂]) [T⁻¹] (Eq. 13). A detailed description of the effect of each factors respect to photosynthesis production rate is reported in Costache et al. (2013):

$$RO_2 [I_{av}; T; pH; DO_2] = RO_2 [I_{av}] \cdot RO_2 [T] \cdot RO_2 [pH] \cdot RO_2 [DO_2] \quad (3.13)$$

Experiments allowed to find optimal values for each factor (Temperature = 35 °C, pH = 8, dissolved oxygen <20 g m⁻³). The most interesting feature of this model is the inclusion of pH and dissolved oxygen concentration relationship with the photosynthesis rate. According with experimental results, the photosynthesis rate is reduced more slowly at pH values lower than 7.0 than higher than 9.0. Regarding dissolved oxygen, the photosynthesis rate is maximal at concentrations equal to, or lower than saturation (9.0 g m⁻³), but at higher dissolved oxygen the photosynthesis rate reduced exponentially until it reaches zero at 32 g m⁻³ (350 % saturation).

3.4 Microalgae-bacteria models

Mathematical microalgae steady-state and dynamic models presented in the previous section in general use a relatively low number of factors to describe the inherent complexity of algal cultures, and in particular for bacteria-microalgae cultures growing in wastewaters. Microalgae-bacteria models require a higher degree of complexity due to the multiple factors involved in wastewater treatment as well as the numerous interactions between organisms.

The very first integrated model considering simultaneous growth of microalgae and bacteria in HRAPs was developed by Buhr and Miller (1983). In this dynamic model algal growth was limited by carbon dioxide, total inorganic nitrogen and light availability, whereas bacteria were limited by organic substrates, dissolved oxygen and inorganic nitrogen. Since Buhr and Miller (1983), a few dynamic models integrating microalgae and bacteria processes were developed with different purposes. Beran and Kargi (2005) developed a model for predicting the effluent quality of WSPs considering the following variables: bacteria and microalgae biomass, soluble chemical oxygen demand (COD), dissolved oxygen and nutrients (nitrogen and phosphorous) concentrations. Microalgae growth was modeled using Liebig's "Law of the Minimum" as function of nitrogen (ammonium and nitrate), phosphorous, light intensity, pH and temperature. The Law of the Minimum allows no more than one substrate to be limiting at the same time. Moreno-Grau et al. (1996) developed a model for describing the dynamics of microalgae and bacteria and zoo-plankton in WSPs. Microalgae growth was described with ammonia and phosphorous Monod functions, while light intensity and temperature were modeled following Steel function and Arrhenius equations, respectively.

In the last 2 decades, the prospective of treating wastewater and at the same time producing microalgae biomass that can be valorized in the form of bioproducts and/or biofuels has promoted the development of more complex microalgae-bacteria mechanistic models. These models lead the way

forward to understand interactions among microalgae and bacteria, and to control reactions in microalgae treatment systems. Table 3.2 shows a feature comparison of some of the main mechanistic mathematical models applied to simulate biokinetic processes of microalgae-bacteria systems. In the next section we describe these integral mechanistic mathematical models.

Table 3.2 Comparison of the general features of integrated mechanistic microalgae-bacteria models.

Model	Base mechanistic model	Simulation platform	Number of Components	Number of processes	Additional processes	Hydrodynamics	Most relevant Features
RWQM1 (Reichert et al. (2001))	Their own	Conceptual model	24 (9 particulate and 15 soluble)	26	Light limitation, temperature dependence, chemical equilibria	Not included	pH dynamics; Water quality mass balance equations in terms of BOD
Sah et al. (2011)	ASM2, CWM1, RWQM1	Delft3D	18 (9 particulate and 9 soluble)	19	Light limitation and attenuation, temperature dependence	Navier-Stokes equations	Anaerobic processes; CFD solution of a coarse 3D facultative pond model
Zambrano et al. (2016)	ASM1, Solimeno et al., (2015)	MATLAB/ Simulink	8 (2 particulate and 6 soluble)	6	Light limitation	Not included	
ASM-A Wagner et al. (2016)	ASM-2d and their own	Conceptual model	11 (5 particulate and 6 soluble)	6	Light limitation	Not included	
BIO_ALGAE Solimeno et al. (2017)	ASM3, RWQM1	COMSOL Multiphysics™	19 (6 particulate and 13 soluble)	25	Light limitation and attenuation, temperature dependence, photorespiration, chemical equilibrium	Navier-Stokes equations; transport of diluted species by convection and diffusion	Carbon limitation; Photorespiration; Transfer of gasses to atmosphere; Dynamic model of light intensity

Note: Activated Sludge Model No. 1 (ASM1), (Henze et al., 1987); Activated Sludge Model No. 2 (ASM-2), (Henze et al., 1995); Activated Sludge Model No. 2d (ASM-2d), (Henze et al., 1999); Activated Sludge Model No. 3 (ASM3), (Henze et al., 2000); Constructed Wetland Model No.1 (CWM1), (Langergraber et al., 2009); River Water Quality Model No. 1 (RWQM1), (Reichert et al., 2011), Biochemical Oxygen Demand (BOD).

3.4.1 River Water Quality Model No. 1

Similar to the models of the ASM series, the River Water Quality Model No1 (RWQM1) is mainly a conceptual model that was developed by a defined IWA task group created *ad-hoc* for this purpose (Dekissa et al., 2004; Reichert et al., 2001). Despite of the RWQM1 come up as indicative model for water quality management, especially in rivers, it was used as basic model for microalgae treatment systems due to the fact that considered microalgae as well as bacteria. Respect to other existing river models such as QUAL2E (Brown and Barnwell, 1987) and MIKE11 (DHI, 1992), the RWQM1 is based on mass balance of chemical elements expressed as Biochemical Oxygen Demand (BOD). Moreover, the model considers the sedimentation of organic matter and also includes chemical equilibrium of nitrogen, carbon and phosphorus species.

The model is based on the main elementary composition of organisms (C, H, N, O and P) and stoichiometry of biochemical conversion processes, instead of only COD like other river water quality models (QUAL2E, Brow and Barnwell, 1987). The model is written in ASM like format and includes all variables of ASM series models. It considers 26 processes and 24 components (9 particulate and 15 soluble). The particulate fraction is composed by: heterotrophic bacteria (X_H), two types of nitrifying bacteria (X_{N1} , X_{N2}), microalgae (X_{ALG}) and animal consumers (X_{CON}). Particulate fractions further contain organic particulate inert (X_I), phosphate adsorbed to particles (X_P), inorganic particulate material (X_{II}) and biodegradable particulate materials (X_S). The soluble fraction is composed by: organic dissolved inert (S_I), biodegradable dissolved organic substances (SS), nitrogen compounds (S_{NH3} , S_{NH4} , S_{NO2} , S_{NO3}), phosphates (S_{HPO4} , S_{H2PO4}), oxygen (S_{O2}) and finally the components involved in the bicarbonate equilibrium, i.e. carbon dioxide (S_{CO2}), bicarbonate (S_{HCO3}), carbonate (S_{CO3}), calcium (S_{Ca}) and hydroxyl ions (S_{OH}) and protons (S_H). Such as the ASM series, the kinetic expressions of RWQM1 are based on switching functions of nutrient availability, light, and temperature (Monod, Lambert and Beer's Law, and Arrhenius equations, respectively).

The RWQM1 coupled with computational simulation platforms such as WEST[®] simulator (Vanhooren et al., 2002), or AQUASIM (Reichert et al., 1998) was used for practical study cases (Benedetti et al., 2007; Dekissa et al., 2004; Shrestha et al., 2016; Thrin Anh et al., 2006). In these studies water quality issues and flow or dynamic problems due to extreme pollution events in the river were investigated.

3.4.2 Sah et al. 2011 model

The mechanistic model of Sah et al. (2011) was developed in Delft3D software to simulate wastewater treatment in facultative ponds (one of the pond typologies commonly used in WSPs). The model was constructed coupling the ASM2 model (Henze et al., 1995) for describing aerobic and anoxic bacteria processes, CWM1 (Constructed Wetland Model No.1; Langergraber et al., 2009) for anaerobic bacteria processes and RWQM1 (Reichert et al., 2001) for simulating microalgae growth. Moreover, the model describes the hydrodynamics of the system (i.e. hydraulic and transport equations) using a 3D domain, and physical and environmental factors such as re-aeration, solar radiation, temperature and wind effects.

This model uses the same notation and structure of the ASM series and considers 19 processes and 18 components (9 particulate and 9 soluble). Among particulate components there are 5 functional groups of bacteria, including heterotrophic, nitrifying, fermenting, sulphate reducing and sulphide oxidising bacteria (X_H , X_A , X_{FB} , X_{ASRB} and X_{AMB} , respectively), inert and particulate organic matter (X_I and X_S , respectively), microalgae (X_{ALG}) and *E. coli* ($X_{E.coli}$). Among the dissolved components there are: dissolved oxygen (S_O), ammonium, nitrite and nitrogen gas (S_{NH_4} , S_{NO_3} and S_{N_2} , respectively), soluble fermentable COD (S_F), sulphate sulphur (S_{SO_4}), methane (S_{CH_4}) and fermentation products as acetate (S_A) and soluble inert COD (S_I).

Processes rates are based on Monod type rate equations, while light attenuation and temperature are based on Lambert Beer's Law and

Arrhenius type equation, respectively. The hydraulic and water quality processes were simulated by Sah et al. (2011) using FLOW and WAQ modules presented in Delft3D software. For turbulence flow, Delft3D software solves the hydrodynamics of systems with Navier-Stokes equation for incompressible fluids under shallow water and Boussinesq assumptions using an inbuilt standard k- ϵ model (Delft3D manual, 2006).

The model was tested using as scenario a secondary facultative pond in León (Nicaragua), treating domestic wastewater with variable flow rate (Baldizon et al., 2002), but not calibrated and validated due to the lack of consistent data. Therefore, this model is considered to be at a conceptual stage since it still requires calibration and validation against experimental data.

3.4.3 Zambrano et al. 2016

Recently, Zambrano et al. (2016) have presented a simplified mechanistic model to describe the growth of microalgae and bacteria consortia in a photobioreactor. The model was developed in MATLAB[®]/Simulink[®] platform by the authors, and was inspired by the ASM1 for describing bacteria processes and by the new mechanistic model for microalgae growth presented by Solimeno et al. (2015) (this model is implemented in the integrated BIO_ALGAE model described afterwards). The model considers 6 processes and 6 components (2 particulate and 4 soluble). Particulate components are nitrifying bacteria (X_{BAC}) and microalgae (X_{ALG}), while soluble components are nitrogen fractions (S_{NH_4} , S_{NO_3}), oxygen (S_{O_2}) and carbon dioxide (S_{CO_2}).

The model was calibrated comparing ammonium, nitrate and oxygen data from batch experiments performed in two lab-scale photobioreactors fed with municipal wastewater over six days. The dominant species of microalgae populations was *Scenedesmus obliquus*. The most sensitive parameters of the model were identified via Monte Carlo simulations: maximum growth rate of microalgae (μ_{ALG}), maximum growth rate and yield of bacteria (μ_{BAC} , Y_{BAC}), and the microalgae half saturation constant for

inorganic carbon (K_{CO_2}). These parameters were calibrated and simulations matched well experimental results, except for dissolved oxygen outputs, which reached levels above the saturation value for oxygen in the water. Not considering any processes that describe the effect of excess of dissolved oxygen in the culture medium, microalgae concentration was over-estimated.

The model is in development phase; the idea of authors is to implement more processes such as light attenuation and pH dynamics.

3.4.4 ASM-A

The ASM-A model (Wágner et al., 2016) was developed as an extension to the ASM-2d (Henze et al., 1999) for describing microalgae growth in WSPs, HRAPs and closed photobioreactors fed with wastewater. The model was implemented in MATLAB[®] and uses the same format of ASM models. It considers 6 processes and 11 components (5 particulate and 6 soluble, all related to microalgae). Particulate components include: microalgae (X_{Alg}), organic inert (X_I) and biodegradable substance (X_S). Particulate fractions further contain the internal cell quota of nitrogen and phosphorous ($X_{Alg,N}$ and $X_{Alg,PP}$) in microalgae. Soluble fraction includes: ammonium and nitrate nitrogen (S_{NH_4} and S_{NO}), inorganic phosphorous (S_{PO_4}), inorganic carbon (S_{ALK}), dissolved oxygen (S_{O_2}) and acetate as organic carbon substrate (S_A). Microalgae nitrogen and phosphorus limitations are described according to Droop formulation, while the consumption of inorganic carbon is formulated using Monod kinetics. Light limitation was implemented by the Steele equation (Steele, 1962), considering a constant average light intensity (type I light model, Béchet et al., 2013).

The model was calibrated with experimental data from 24-L photobioreactor operated in sequenced mode under controlled temperature at 20 °C. *Chlorella sorokiniana* and *Scenedesmus* sp. were cultivated in a mixed culture using a MWC + Se synthetic medium (Guillard and Lorenzen, 1972). The model was able to predict accurately microalgae biomass, ammonium and

phosphorous uptake and storage minimizing the relative root mean square normalized error (RMSNE).

The ASM-A model only presents the biochemical processes related to microalgae. The aim of ASM-A is to present photoautotrophic and heterotrophic microalgae processes in the ASM framework in order to allow their integration in bacteria models (such as the ASM-2d).

3.4.5 BIO_ALGAE

The model BIO_ALGAE (Chapter 7; Solimeno et al., 2017a) was implemented in COMSOL Multiphysics™ platform and was mainly built by coupling the RWQM1 (Reichert et al., 2011) with the modify ASM3 (Iacopozzi et al., 2007). This model is applicable for WSP, HRAP_s and photobioreactors. The model uses the common nomenclature of the IWA models and considers 19 components (6 particulate and 13 dissolved) implicated as variables in 25 physical, chemical and biokinetic processes.

Particulate components include: heterotrophic bacteria (X_H), two types of nitrifying bacteria (X_{AOB} , X_{NOB}), microalgae (X_{ALG}), organic inert (X_I) and biodegradable materials (X_S). Dissolved components include: inert organic matter (S_I) and biodegradable organic matter (S_S), nitrogen fractions (S_{NH_3} , S_{NH_4} , S_{NO_2} , S_{NO_3}), phosphate (S_{PO_4}), oxygen (S_{O_2}) and inorganic carbon components (S_{CO_2} , S_{HCO_3} , S_{CO_3}), hydroxyl ions (S_{OH}) and hydrogen ions (S_H).

Such as in ASM series and RWMQ1, the kinetic expressions of BIO_ALGAE are based on Monod type functions for carbon, nitrogen and phosphorus limitation. Carbon limitation for microalgae and nitrifying bacteria was one of the main features included in the model. The model also includes temperature dependence for microalgae and bacteria using Arrhenius type equation, and for microalgae the dynamic model by Eilers and Peters for describing the effect of light intensity on photosynthesis (Eilers and Peters, 1988). Moreover, light attenuation, pH dynamics and the effect of excess of oxygen were included.

The model was calibrated and validated with experimental data from triplicate HRAPs located at the Delhi, California wastewater pond treatment plant over 4 days of experiments. From previous sensitivity analyses, the maximum growth rate of microalgae (μ_{ALG}), the maximum growth rate and the inactivation of heterotrophic bacteria (μ_H and $k_{death,H}$), and the mass transfer coefficients for oxygen, carbon dioxide and ammonia (K_{a,O_2} , K_{a,CO_2} and K_{a,NH_3}) were calibrated. Results of the calibration and validation indicated that the model was able to match accurately experimental data. The model was used to simulate microalgae and bacteria population dynamics.

Furthermore, BIO_ALGAE model demonstrated to be a useful tool to simulate biomass production, and in particular to infer the relative proportion of microalgae and bacteria.

3.5 Discussion

In this section, we provide a comparison on the different integrated models considered in Section 3.4 to approach microalgae and bacteria interactions and physical-chemical processes in microalgae-bacteria systems. We conduct a critical discussion on the key differences between the five selected mechanistic models.

3.5.1 Microalgae processes comparison

Table 3.3 shows the microalgae process rates of the five selected mechanistic models, as well as their parameter values. In this section growth and decay processes and parameters are discussed separately.

Growth and uptake processes

In general corrective factors that limit or inhibit the maximum microalgae growth rates are described by Monod functions. Only the ASM-A model uses the internal cell quota according to Droop formulation. The Droop

model accounts for the luxury uptake and storage of nutrients for later growth by means the intracellular concentration of the limiting nutrient ('cell quota', q) (Sommer, 1991). Therefore ASM-A can predict microalgae growth for some time after the drop of nutrient concentration. Luxury uptake and storage are processes need to be strictly taken into account in aquatic natural ecosystems, which usually have very low nutrient concentrations (Powell et al., 2009, Sommer, 1991). On the other hand, in wastewater systems which are intrinsically rich in nutrients, the use of external nutrient limiting concentrations are more easily measured and known, and guarantee enough modelling accuracy. This makes the Monod model to be preferred, in conjunction with the fact that simultaneous nutrient limitations can be easily implemented with the Monod model, while the extension of Droop's model from single to multiple nutrient limitations is not so straightforward (Cherif and Loreau, 2010). Surprisingly, the ASM-A model considers luxury uptake and storage for N and P, while not for C.

Microalgae growth is usually not limited by inorganic carbon in aquatic ecosystems (Anesio et al., 1999). However, in dense microalgae cultures like WSP, HRAP and photobioreactors, carbon limitation can occur (García et al., 2000b; Park and Craggs, 2010). In fact, in photobioreactors used for microalgae cultures, carbon is usually supplied in the form of CO_2 in order to increase microalgae production (Park and Craggs, 2010a; Sutherland et al., 2014). Inorganic biogenic carbon includes CO_2 and HCO_3^- , whereas CO_3^{2-} is not biogenic and therefore has not to be considered as substrate.

BIO_ALGAE and Zambrano et al. (2016) models consider inorganic carbon (both CO_2 and HCO_3^-) as a limiting substrate for microalgae growth, while the RWQM1, and Sah et al. (2001) model do not address carbon (Table 3). The ASM-A model includes inorganic carbon limitation using a Monod formulation for alkalinity (S_{ALK}). But expressing inorganic carbon by alkalinity, the model runs the risk to slightly overestimate microalgae growth since CO_3^{2-} is not directly biogenic. On the other hand, excessively high concentrations of carbon dioxide can also inhibit the growth of microalgae (Kurano and Myachi, 2005). In this sense, BIO_ALGAE is the only one that implements in the model the inhibitory effect of high concentrations of

carbon dioxide through the parameter $I_{\text{CO}_2, \text{ALG}}$ (Table 3.3). This is especially relevant in closed photobioreactors with CO_2 injection in which partial pressures above 0.6 atm can acidify the culture medium (Silva and Pirt, 1984).

A relevant difference between the ASM-A model and the rest of models is that the ASM-A considers microalgae heterotrophic growth. Therefore in ASM-A microalgae can grow with carbon dioxide as an inorganic carbon source using light as energy source (autotrophic growth), as well as with acetate as carbon and energy source in the dark (heterotrophic growth) (Moya et al., 1997). This capacity of growing on inorganic as well as organic C sources is named mixotrophy (Kang et al., 2004; Wang et al., 2004) and seems to be unlikely to occur or at least to be not very important in wastewater treatment systems, where conspicuous populations of heterotrophic bacteria would successfully outcompete microalgae for organic carbon. Several studies on microalgae cultures have demonstrated an increase in microalgae biomass production in mixotrophic conditions (Andrade et al., 2007; Park et al., 2012), but this has not been yet proved in wastewater treatment systems.

With regards nitrogen, microalgae can grow on both ammonium (and/or ammonia) and nitrate as nitrogen source. When ammonium (and/or ammonia) and nitrate are both present, ammonium is generally preferred (Mostert and Grobbelaar, 1987; Stewart, 1974; Syrett, 1981). Therefore, an inhibition term by ammonium is included in the growth process of microalgae with nitrate in all the models. The 5 revised models have the same criteria regarding nitrogen.

Phosphorus is another important macronutrient for microalgae metabolism necessary for nucleic acids (RNA and DNA), membrane phospholipids and ATP (Geider and La Roche, 2002). Moreover, phosphorus tends to be a limiting nutrient in natural aquatic ecosystems (Correll, 1999), while it is not in wastewater treatment systems, where is largely available (Larsdotter, 2006). Therefore phosphorus is not really needed to be considered in wastewater models; however, the models RWQM1, ASM-A and BIO_ALGAE include phosphorus limitations.

Table 3.3 Microalgae processes of integrated mechanistic microalgae-bacteria models.

Model	Process	Process rate [M L ⁻³ T ⁻¹]	Parameter values
RWQM1 (Reichert et al., 2001)	Growth of X _{ALG} on S _{NH4}	$k_{gro,ALG} \cdot f(T) \cdot f(L) \cdot \frac{S_{NH3} + S_{NH4} + S_{NO3}}{K_{N,ALG} + S_{NH3} + S_{NH4} + S_{NO3}} \cdot \frac{S_{NH3} + S_{NH4}}{K_{N,ALG} + S_{NH3} + S_{NH4}} \cdot \frac{S_{HPO4} + S_{H2PO4}}{K_{HPO4,ALG} + S_{HPO4} + S_{H2PO4}} \cdot X_{ALG}$	$k_{gro,ALG} = 2 \text{ d}^{-1}$ $k_{resp,ALG} = 0.1 \text{ d}^{-1}$ $k_{death,ALG} = 0.1 \text{ d}^{-1}$ $K_{N,ALG} = 0.1 \text{ gN m}^{-3}$ $K_{HPO4,ALG} = 0.02 \text{ gP m}^{-3}$ $K_{O2,ALG} = 0.2 \text{ gO}_2 \text{ m}^{-3}$
	Growth of X _{ALG} on S _{NO3}	$k_{gro,ALG} \cdot f(T) \cdot f(L) \cdot \frac{S_{NH3} + S_{NH4} + S_{NO3}}{K_{N,ALG} + S_{NH3} + S_{NH4} + S_{NO3}} \cdot \frac{K_{N,ALG}}{K_{N,ALG} + S_{NH3} + S_{NH4}} \cdot \frac{S_{HPO4} + S_{H2PO4}}{K_{HPO4,ALG} + S_{HPO4} + S_{H2PO4}} \cdot X_{ALG}$	
	Endogenous respiration of X _{ALG}	$k_{resp,ALG} \cdot f(T) \cdot \frac{S_{O2}}{K_{O2,ALG} + S_{O2}} \cdot X_{ALG}$	
	Death of X _{ALG}	$k_{death,ALG} \cdot f(T) \cdot f(L) \cdot X_{ALG}$	
Sah et al., 2011	Growth of X _{ALG} on S _{NH4}	$\mu_{ALG} \cdot f(T) \cdot f(L) \cdot \frac{S_{NH}}{K_{NH,ALG} + S_{NH}} \cdot X_{ALG}$	$\mu_{ALG} = 2 \text{ d}^{-1}$ $b_{ALG} = 0.1 \text{ d}^{-1}$ $K_{NH,ALG} = 0.01 \text{ gN m}^{-3}$ $K_{NO,ALG} = 0.01 \text{ gN m}^{-3}$
	Growth of X _{ALG} on S _{NO3}	$\mu_{ALG} \cdot f(T) \cdot f(L) \cdot \frac{S_{NO}}{K_{NO,ALG} + S_{NO}} \cdot \frac{K_{NH,ALG}}{K_{NH,ALG} + S_{NH}} \cdot X_{ALG}$	
	Decay of X _{ALG}	$b_{ALG} \cdot f(T) \cdot X_{ALG}$	
Zambrano et al., 2016	Growth of X _{ALG} on S _{NH4}	$\mu_{ALG} \cdot f(L) \cdot \frac{S_{CO2}}{K_{CO2} + S_{CO2}} \cdot \frac{S_{NH4}}{K_{N,ALG} + S_{NH4}} \cdot X_{ALG}$	$\mu_{ALG} = 1.6 \text{ d}^{-1}$ $b_{ALG} = 0.1 \text{ d}^{-1}$ $K_{N,ALG} = 0.1 \text{ gN m}^{-3}$ $K_{CO2} = 4.32 \cdot 10^{-3} \text{ gC m}^{-3}$
	Growth of X _{ALG} on S _{NO3}	$\mu_{ALG} \cdot f(L) \cdot \frac{S_{CO2}}{K_{CO2} + S_{CO2}} \cdot \frac{S_{NO3}}{K_{N,ALG} + S_{NO3}} \cdot \frac{K_{N,ALG}}{K_{N,ALG} + S_{NH4}} \cdot X_{ALG}$	

	Decay of X_{ALG}	$b_{ALG} \cdot X_{ALG}$	
ASM-A (Wagner et al., 2016)	Uptake and storage of S_{NH4}	$k_{NH4,ALG} \cdot \frac{S_{NH4}}{K_{NH4,ALG} + S_{NH4}} \cdot \frac{X_{ALG,Nmax} \cdot X_{ALG} - X_{ALG,N}}{X_{ALG,Nmax} \cdot X_{ALG}} \cdot X_{ALG}$	$\mu_{A,max} = 3.6 \text{ d}^{-1}$ $\mu_{H,max} = 4.5 \text{ d}^{-1}$ $b_{ALG} = 0.21 \text{ d}^{-1}$ $K_{NH4,ALG} = 7.87 \text{ gN m}^{-3}$ $K_{NO,ALG} = 12.61 \text{ gN m}^{-3}$ $K_{PO4,ALG} = 4.49 \text{ gP m}^{-3}$ $K_{ALK} = 3 \text{ gC m}^{-3}$ $K_A = 7.1 \text{ gCOD m}^{-3}$ $K_{O2} = 0.2 \text{ gO}_2 \text{ m}^{-3}$
	Uptake and storage of S_{NO3}	$k_{NO,ALG} \cdot \frac{S_{NO}}{K_{NO,ALG} + S_{NO}} \cdot \frac{K_{NH4,ALG}}{K_{NH4,ALG} + S_{NH4}} \cdot \frac{X_{ALG,Nmax} \cdot X_{ALG} - X_{ALG,N}}{X_{ALG,Nmax} \cdot X_{ALG}} \cdot X_{ALG}$	
	Uptake and storage of S_{PO4}	$k_{PO4,ALG} \cdot \frac{S_{PO4}}{K_{PO4,ALG} + S_{PO4}} \cdot \frac{X_{ALG,Nmax} \cdot X_{ALG} - X_{ALG,N}}{X_{ALG,Nmax} \cdot X_{ALG}} \cdot X_{ALG}$	
	Autotrophic growth	$\mu_{A,max} \cdot \left(1 - \frac{X_{ALG,Nmin} \cdot X_{ALG}}{X_{ALG,N}}\right) \cdot \left(1 - \frac{X_{ALG,PPmin} \cdot X_{ALG}}{X_{ALG,PP}}\right) \cdot \frac{S_{ALK}}{K_{ALK} + S_{ALK}} \cdot f(L) \cdot X_{ALG}$	
	Heterotrophic growth	$\mu_{H,max} \cdot \left(1 - \frac{X_{ALG,Nmin} \cdot X_{ALG}}{X_{ALG,N}}\right) \cdot \left(1 - \frac{X_{ALG,PPmin} \cdot X_{ALG}}{X_{ALG,PP}}\right) \cdot \frac{S_A}{K_A + S_A} \cdot \frac{S_{O2}}{K_{O2} + S_{O2}} \cdot f(L) \cdot X_{ALG}$	
	Decay of X_{ALG}	$b_{ALG} \cdot X_{ALG}$	
BIO_ALGAE (Chapter 7; Solimeno et al., 2017a)	Growth of X_{ALG} on S_{NH4}	$\mu_{ALG} \cdot f_{T,FS}(T) \cdot \eta_{PS}(I, S_{O2}) \cdot \frac{S_{CO2} + S_{HCO3}}{K_{C,ALG} + S_{CO2} + S_{HCO3} + \frac{S_{CO2}^2}{I_{CO2,ALG}}} \cdot \frac{S_{NH3} + S_{NH4}}{K_{N,ALG} + S_{NH3} + S_{NH4}} \cdot \frac{S_{PO4}}{K_{P,ALG} + S_{PO4}} \cdot X_{ALG}$	$\mu_{ALG} = 1.5 \text{ d}^{-1}$ $k_{resp,ALG} = 0.1 \text{ d}^{-1}$ $k_{death,ALG} = 0.1 \text{ d}^{-1}$ $K_{N,ALG} = 0.1 \text{ gN m}^{-3}$ $K_{C,ALG} = 0.004 \text{ gC m}^{-3}$ $I_{CO2,ALG} = 120 \text{ gC m}^{-3}$ $K_{O2,ALG} = 0.2 \text{ gO}_2 \text{ m}^{-3}$ $K_{P,ALG} = 0.02 \text{ gP m}^{-3}$
	Growth of X_{ALG} on S_{NO3}	$\mu_{ALG} \cdot f_{T,FS}(T) \cdot \eta_{PS}(I, S_{O2}) \cdot \frac{S_{CO2} + S_{HCO3}}{K_{C,ALG} + S_{CO2} + S_{HCO3} + \frac{S_{CO2}^2}{I_{CO2,ALG}}} \cdot \frac{S_{NO3}}{K_{N,ALG} + S_{NO3}} \cdot \frac{K_{N,ALG}}{K_{N,ALG} + S_{NH3} + S_{NH4}} \cdot \frac{S_{PO4}}{K_{P,ALG} + S_{PO4}} \cdot X_{ALG}$	
	Endogenous respiration of X_{ALG}	$k_{resp,ALG} \cdot f_{T,FS}(T) \cdot \frac{S_{O2}}{K_{O2,ALG} + S_{O2}} \cdot X_{ALG}$	
	Decay of X_{ALG}	$k_{death,ALG} \cdot f_{T,FS}(T) \cdot X_{ALG}$	

Decay processes

The models of Sah et al. (2011), ASM-A and Zambrano et al. (2016) describe with a global decay rate the biomass endogenous respiration and the death. On the contrary, RWQM1 and BIO_ALGAE distinguish endogenous respiration and decay as two different processes. In the models endogenous respiration produces CO_2 and transforms alive biomass into inert organic matter (X_I), while decay of microalgae transforms alive biomass into dead slowly biodegradable (X_S) and inert (X_I) organic matter (Van Loosdrecht and Henze, 1999). Slowly biodegradable particulate organic matter (X_S) originating from decay process is assumed to be 80% of the total loss microalgae biomass. These processes are actually in revision because it is not clear that endogenous respiration produces inert organic matter (X_I) when decay is considered as an another process.

Parameter values

The saturation constants of X_{ALG} for nutrients (i.e. carbon, nitrogen and phosphorous) and the decay constant present in BIO_ALGAE, Sah et al. (2011) and Zambrano et al. (2016) were obtained from the well accepted RWQM1. Uncertainty analysis conducted for each model confirmed that the maximum growth rate of microalgae is the parameter that had a greater influence on the simulation response. Therefore, it was calibrated in each case, giving values ($\mu_{\text{ALG}} = 1.5 \text{ d}^{-1}$ for BIO_ALGAE, $\mu_{\text{ALG}} = 2 \text{ d}^{-1}$ for Sah et al. (2011), $\mu_{\text{ALG}} = 1.6 \text{ d}^{-1}$ for Zambrano et al. (2016) and $k_{\text{gro_ALG}} = 2 \text{ d}^{-1}$ for RWQM1) that fit well within literature ranges [0.4-2 d^{-1}] (Reichert et al., 2001).

ASM-A model presents a notable difference in parameters values (Table 3.3). Maximum microalgae growth rate and the saturation constant of nutrients are quite high respect to the other models maybe due to microalgae are able to growth under both heterotrophic and photoautotrophic conditions, as well bacteria interactions were neglected during the calibration of the model.

3.5.2 Bacteria processes comparison

Table 3.4 shows the bacteria process rates of the five selected mechanistic models, as well as their parameter values. In this section growth and decay/respiration processes and parameters related to bacteria are discussed separately.

Growth and uptake processes

In all mechanistic models considered the main source of inspiration for bacteria processes description was the ASM series. In the model by Zambrano et al. (2016) a notable simplification of bacteria processes was implemented in comparison to the other models. Only the growth of nitrifying bacteria was considered, and therefore this model can be only applied to low strength wastewater (e.g. secondary effluent), where the growth of heterotrophic bacteria could be neglected.

ASM-A model is an extension of the ASM-2d and includes several interactions between microalgae and bacteria such as oxygen and dissolved carbon exchange or the competition for organic carbon between heterotrophic bacteria and microalgae under heterotrophic growth. Although the model does not include microalgae and bacteria processes with the same matrix format, interactions were taken into account indirectly during the formulation of microalgae processes.

The model of Sah et al. (2011) is the most complex and includes processes related to aerobic autotrophic and heterotrophic bacteria, and anaerobic fermenting, acetotrophic sulphate reducing and acetotrophic methanogenic bacteria. Aerobic heterotrophic bacteria can also growth in anoxic conditions and are limited by ammonium (S_{NH}), soluble fermentable COD (S_F), and fermentation products as acetate (S_A). Autotrophic bacteria are limited only by nitrogen and oxygen. The most noticeable feature of the model is the inclusion of anaerobic processes, which is fact are very necessary to describe reactions occurring at the bottom of facultative ponds.

The description of bacteria processes is also quite complete in both RWQM1 and BIO_ALGAE. Using Monod kinetics, bacteria processes were modelled in the same way as microalgae processes. A certain number of simplifications were made in order to make easier the control of biochemical processes. Anaerobic biological processes, such as fermentation and sulfate reduction, which can sometimes be important in wastewater treatment (e.g. as mentioned before in facultative ponds), were also omitted because the relatively oxidized nature of microalgae-bacteria processes occurring in HRAPs and photobioreactors. Moreover, likewise the model of Sah et al. (2011) and Zambrano et al. (2016), these models do not consider processes related to the storage of readily

biodegradable soluble organic matter (S_s) which are included in some of the ASM models.

Respect to RWQM1, BIO_ALGAE does not consider the limitation of phosphorous species on the growth of heterotrophic and autotrophic bacteria, since phosphorous is usually highly available in wastewaters (Larsdotter, 2006). On the other hand, BIO_ALGAE includes carbon limitation on the growth of autotrophic bacteria, which is a key factor for competition between microalgae and nitrifying bacteria.

Decay and respiration processes

Different approaches to implement the loss of bacteria biomass were considered in each model depending on which ASM series were base to. The model of Sah et al. (2011) is based on ASM1 decay approach, including in the same global process endogenous respiration as well as decay. Decay is assumed to be identical all bacteria groups and transforms alive biomass into dead slowly biodegradable (X_s) and inert (X_i) organic matter. Conversely, in the RWQM1, which is based on ASM3, the loss of bacteria biomass is implemented by the endogenous respiration producing inert organic matter (X_i); the formation of slowly biodegradable (X_s) organic matter was neglected. Surprisingly, in the RWQM1 microalgae have endogenous respiration and decay separately, while bacteria have a global process for the two.

The BIO_ALGAE includes both decay and respiration of heterotrophic and autotrophic bacteria, but in separate processes. These processes are formulated in the same way as the aerobic endogenous respiration and decay of microalgae to maintain congruence between the processes of the model.

Zambrano et al. (2016) not consider the slowly biodegradable (X_s) and inert (X_i) organic matter components. The product of nitrifiers decay is only the release of the ammonium fraction contained in bacteria biomass, which can be used again as substrate for both microalgae and bacteria growth.

Table 3.4 Bacteria processes of integrated mechanistic microalgae-bacteria models.

Model	Process	Process rate [M L ⁻³ T ⁻¹]	Parameter values
RWQM1 (Reichert et al., 2001)	Aerobic growth of X _H on S _{NH4}	$k_{gro,H,aer} \cdot f(T) \cdot \frac{S_S}{K_{S,H} + S_S} \cdot \frac{S_{O_2}}{K_{O_2,H} + S_{O_2}} \cdot \frac{S_{NH_4} + S_{NH_3}}{K_{N,H} + S_{NH_4} + S_{NH_3}} \cdot \frac{S_{HPO_4} + S_{H_2PO_4}}{K_{HPO_4,H} + S_{HPO_4} + S_{H_2PO_4}} \cdot X_H$	$k_{gro,H,aer} = 2.0 \text{ d}^{-1}$ $k_{resp,H} = 0.2 \text{ d}^{-1}$ $k_{resp,H,anox} = 0.1 \text{ d}^{-1}$ $k_{gro,H,anox} = 1.6 \text{ d}^{-1}$ $k_{gro,N_1} = 0.8 \text{ d}^{-1}$ $k_{gro,N_2} = 1.1 \text{ d}^{-1}$ $K_{S,H} = 2.0 \text{ gCOD m}^{-3}$ $K_{N,H} = 0.2 \text{ gN m}^{-3}$ $K_{O_2,H} = 0.2 \text{ gO}_2 \text{ m}^{-3}$ $K_{HPO_4,H} = 0.02 \text{ gP m}^{-3}$ $K_{NO_3,H} = 0.5 \text{ gN m}^{-3}$ $K_{NO_2,H} = 0.2 \text{ gN m}^{-3}$ $K_{O_2,N_1} = 0.2 \text{ gO}_2 \text{ m}^{-3}$ $K_{O_2,N_2} = 0.2 \text{ gO}_2 \text{ m}^{-3}$ $K_{NH_4,N_1} = 0.5 \text{ gO}_2 \text{ m}^{-3}$ $K_{HPO_4,N_1} = 0.5 \text{ gO}_2 \text{ m}^{-3}$
	Aerobic growth of X _H on S _{NO3}	$k_{gro,H,aer} \cdot f(T) \cdot \frac{S_S}{K_{S,H} + S_S} \cdot \frac{S_{O_2}}{K_{O_2,H} + S_{O_2}} \cdot \frac{K_{N,H,aer}}{K_{N,H} + S_{NH_4} + S_{NH_3}} \cdot \frac{S_{NO_3}}{K_{N,H} + S_{NO_3}} \cdot \frac{S_{HPO_4} + S_{H_2PO_4}}{K_{HPO_4,H} + S_{HPO_4} + S_{H_2PO_4}} \cdot X_H$	
	Aerobic respiration of X _H	$k_{resp,H,aer} \cdot f(T) \cdot \frac{S_{O_2}}{K_{O_2,H} + S_{O_2}} \cdot X_H$	
	Anoxic growth of X _H on S _{NO2}	$k_{gro,H,anox} \cdot f(T) \cdot \frac{S_S}{K_{S,H} + S_S} \cdot \frac{K_{O_2,H}}{K_{O_2,H} + S_{O_2}} \cdot \frac{S_{NO_2}}{K_{NO_2,H} + S_{NO_2}} \cdot \frac{S_{HPO_4} + S_{H_2PO_4}}{K_{HPO_4,H} + S_{HPO_4} + S_{H_2PO_4}} \cdot X_H$	
	Anoxic growth of X _H on S _{NO3}	$k_{gro,H,anox} \cdot f(T) \cdot \frac{S_S}{K_{S,H} + S_S} \cdot \frac{K_{O_2}}{K_{O_2,H} + S_{O_2}} \cdot \frac{S_{NO_3}}{K_{NO_3,H} + S_{NO_3}} \cdot \frac{S_{HPO_4} + S_{H_2PO_4}}{K_{HPO_4,H} + S_{HPO_4} + S_{H_2PO_4}} \cdot X_H$	
	Anoxic respiration of X _H	$k_{resp,H,anox} \cdot f(T) \cdot \frac{S_{O_2}}{K_{O_2,H} + S_{O_2}} \cdot \frac{S_{NO_3}}{K_{NO_3,H} + S_{NO_3}} \cdot X_H$	
	Growth of X _{N1}	$k_{gro,N_1} \cdot f(T) \cdot \frac{S_{O_2}}{K_{O_2,N_1} + S_{O_2}} \cdot \frac{S_{NH_4} + S_{NH_3}}{K_{NH_4,N_1} + S_{NH_4} + S_{NH_3}} \cdot \frac{S_{HPO_4} + S_{H_2PO_4}}{K_{HPO_4,N_1} + S_{HPO_4} + S_{H_2PO_4}} \cdot X_{N_1}$	
	Growth of X _{N2}	$k_{gro,N_2} \cdot f(T) \cdot \frac{S_{O_2}}{K_{O_2,N_2} + S_{O_2}} \cdot \frac{S_{NO_2}}{K_{NO_2,N_2} + S_{NO_2}} \cdot \frac{S_{HPO_4} + S_{H_2PO_4}}{K_{HPO_4,N_1} + S_{HPO_4} + S_{H_2PO_4}} \cdot X_{N_2}$	
	Aerobic respiration of X _{N1}	$k_{gro,N_1} \cdot f(T) \cdot \frac{S_{O_2}}{K_{O_2,N_1} + S_{O_2}} \cdot X_{N_1}$	

	Aerobic respiration of X_{N2}	$k_{gro,N2} \cdot f(T) \cdot \frac{S_{O2}}{K_{O2,N2} + S_{O2}} \cdot X_{N2}$	
Sah et al., 2011	Aerobic growth of X_H on S_A	$\mu_H \cdot f(T) \cdot \frac{S_A}{K_{SAH} + S_A} \cdot \frac{S_A}{S_F + S_A} \cdot \frac{S_O}{K_{OH} + S_O} \cdot \frac{S_{NH}}{K_{NHH} + S_{NH}} \cdot X_H$	$\mu_H = 6 \text{ d}^{-1}$ $\mu_{FB} = 6 \text{ d}^{-1}$
	Aerobic growth of X_H on S_F	$\mu_H \cdot f(T) \cdot \frac{S_F}{K_{SFH} + S_F} \cdot \frac{S_F}{S_F + S_A} \cdot \frac{S_O}{K_{OH} + S_O} \cdot \frac{S_{NH}}{K_{NHH} + S_{NH}} \cdot X_H$	$\mu_{ASRB} = 0.18 \text{ d}^{-1}$ $\mu_{AMB} = 0.085 \text{ d}^{-1}$ $b_H = 0.4 \text{ d}^{-1}$
	Anoxic growth of X_H on S_A	$\mu_H \cdot \eta_H \cdot f(T) \cdot \frac{S_A}{K_{SAH} + S_A} \cdot \frac{S_A}{S_F + S_A} \cdot \frac{S_O}{K_{OH} + S_O} \cdot \frac{S_{NH}}{K_{NHH} + S_{NH}} \cdot \frac{S_{NO}}{K_{NOH} + S_{NO}} \cdot X_H$	$b_A = 0.015 \text{ d}^{-1}$ $b_{FB} = 0.02 \text{ d}^{-1}$
	Anoxic growth of X_H on S_F	$\mu_H \cdot \eta_H \cdot f(T) \cdot \frac{S_F}{K_{SFH} + S_A} \cdot \frac{S_A}{S_F + S_A} \cdot \frac{S_O}{K_{OH} + S_O} \cdot \frac{S_{NH}}{K_{NHH} + S_{NH}} \cdot \frac{S_{NO}}{K_{NOH} + S_{NO}} \cdot X_H$	$b_{ASRB} = 0.012 \text{ d}^{-1}$ $b_{AMB} = 0.008 \text{ d}^{-1}$ $\eta_H = 0.8$
	Growth of X_A	$\mu_A \cdot f(T) \cdot \frac{S_O}{K_{OA} + S_O} \cdot \frac{S_{NH}}{K_{NHA} + S_{NH}} \cdot X_A$	$K_{SAH} = 4 \text{ gCOD m}^{-3}$ $K_{OH} = 0.2 \text{ gO}_2 \text{ m}^{-3}$ $K_{SFH} = 3 \text{ gCOD m}^{-3}$ $K_{NOH} = 0.5 \text{ gN m}^{-3}$
	Growth of X_{FB}	$\mu_{FB} \cdot f(T) \cdot \frac{S_F}{K_{SFB} + S_F} \cdot \frac{K_{OFB}}{K_{OFB} + S_O} \cdot \frac{K_{NOFB}}{K_{NOFB} + S_{NO}} \cdot \frac{S_{NH}}{K_{NHFB} + S_{NH}} \cdot X_{FB}$	$K_{NHH} = 0.05 \text{ gN m}^{-3}$ $K_{OA} = 0.5 \text{ gO}_2 \text{ m}^{-3}$
	Growth of X_{AMB}	$\mu_{ASRB} \cdot f(T) \cdot \frac{S_A}{K_{SASRB} + S_F} \cdot \frac{S_{SO4}}{K_{SOASRB} + S_{SO4}} \cdot \frac{K_{OASRB}}{K_{OASRB} + S_O} \cdot \frac{K_{NOASRB}}{K_{NOASRB} + S_{NO}} \cdot \frac{S_{NH}}{K_{NHASRB} + S_{NH}} \cdot X_{ASRB}$	$K_{NHA} = 0.2 \text{ gN m}^{-3}$ $K_{SFB} = 28 \text{ gCOD m}^{-3}$ $K_{OFB} = 0.2 \text{ gO}_2 \text{ m}^{-3}$ $K_{NOFB} = 0.5 \text{ gN m}^{-3}$
	Growth of X_{ASRB}	$\mu_{AMB} \cdot f(T) \cdot \frac{S_A}{K_{SAMB} + S_F} \cdot \frac{K_{OAMB}}{K_{OAMB} + S_O} \cdot \frac{K_{NOAMB}}{K_{NOAMB} + S_{NO}} \cdot \frac{S_{NH}}{K_{NHAMB} + S_{NH}} \cdot X_{AMB}$	$K_{NHFB} = 0.01 \text{ gN m}^{-3}$ $K_{SASRB} = 24 \text{ gCOD m}^{-3}$ $K_{OASRB} = 3E-4 \text{ gO}_2 \text{ m}^{-3}$ $K_{SOASRB} = 19 \text{ gS m}^{-3}$
	Decay of X_H	$b_H \cdot f(T) \cdot X_H$	$K_{NOASRB} = 5E-4 \text{ gN m}^{-3}$ $K_{NHASRB} = 0.01 \text{ gN m}^{-3}$ $K_{OAMB} = 2E-4 \text{ gO}_2 \text{ m}^{-3}$
	Decay of X_A	$b_A \cdot f(T) \cdot X_A$	$K_{NOAMB} = 5E-4 \text{ gN m}^{-3}$ $K_{SAMB} = 56 \text{ gCOD m}^{-3}$
	Decay of X_{FB}	$b_{FB} \cdot f(T) \cdot X_{FB}$	$K_{NHAMB} = 0.01 \text{ gN m}^{-3}$
	Decay of X_{AMB}	$b_{AMB} \cdot f(T) \cdot X_{AMB}$	

	Decay of X_{ASRB}	$b_{ASRB} \cdot f(T) \cdot X_{ASRB}$	
Zambrano et al., 2016	Bacteria growth	$\mu_{BAC} \cdot \frac{S_{NH4}}{K_{N,BAC} + S_{NH4}} \cdot \frac{S_{O2}}{K_{O2} + S_{O2}} \cdot X_{BAC}$	$\mu_{BAC} = 0.5 \text{ d}^{-1}$ $b_{BAC} = 0.05 \text{ d}^{-1}$ $K_{N,BAC} = 1 \text{ gN m}^{-3}$ $K_{O2} = 0.4 \text{ gO}_2 \text{ m}^{-3}$
	Bacteria decay	$b_{BAC} \cdot X_{BAC}$	
ASM-A (Wagner et al., 2016)	*		
BIO_ALGAE (Chapter 7; Solimeno et al., 2017a)	Aerobic growth of X_H on S_{NH4}	$\mu_H \cdot f_{T,MB}(T) \cdot \frac{S_S}{K_{S,H} + S_S} \cdot \frac{S_{O2}}{K_{O2,H} + S_{O2}} \cdot \frac{S_{NH4} + S_{NH3}}{K_{N,H} + S_{NH4} + S_{NH3}} \cdot X_H$	$\mu_H = 1.5 \text{ d}^{-1}$ $\mu_{AOB} = 0.63 \text{ d}^{-1}$ $\mu_{NOB} = 1.1 \text{ d}^{-1}$ $\eta_H = 0.6$ $k_{resp,H} = 0.2 \text{ d}^{-1}$ $k_{resp,AOB} = 0.5 \text{ d}^{-1}$ $k_{resp,NOB} = 0.5 \text{ d}^{-1}$ $k_{death,H} = 0.3 \text{ d}^{-1}$ $k_{death,AOB} = 0.2 \text{ d}^{-1}$ $k_{death,NOB} = 0.2 \text{ d}^{-1}$ $K_{S,H} = 20 \text{ gCOD m}^{-3}$ $K_{N,H} = 0.2 \text{ gN m}^{-3}$ $K_{NO2,H,anox} = 0.2 \text{ gN m}^{-3}$ $K_{NO2,NOB} = 0.5 \text{ gN m}^{-3}$ $K_{NO3,H,anox} = 0.5 \text{ gN m}^{-3}$ $K_{NH4,AOB} = 0.5 \text{ gN m}^{-3}$ $K_{I,NH4} = 5 \text{ gN m}^{-3}$ $K_{O2,H} = 0.2 \text{ gO}_2 \text{ m}^{-3}$ $K_{O2,AOB} = 0.5 \text{ gO}_2 \text{ m}^{-3}$ $K_{O2,NOB} = 0.5 \text{ gO}_2 \text{ m}^{-3}$
	Aerobic growth of X_H on S_{NO3}	$\mu_H \cdot f_{T,MB}(T) \cdot \frac{S_S}{K_{S,H} + S_S} \cdot \frac{S_{O2}}{K_{O2,H} + S_{O2}} \cdot \frac{S_{NO3}}{K_{N,H} + S_{NO3}} \cdot X_H$	
	Anoxic growth of X_H on S_{NO2}	$\mu_H \cdot \eta_H \cdot f_{T,MB}(T) \cdot \frac{S_S}{K_{S,H} + S_S} \cdot \frac{K_{O2,H}}{K_{O2,H} + S_{O2}} \cdot \frac{S_{NO2}}{K_{NO2,H,anox} + S_{NO2}} \cdot X_H$	
	Anoxic growth of X_H on S_{NO3}	$\mu_H \cdot \eta_H \cdot f_{T,MB}(T) \cdot \frac{S_S}{K_{S,H} + S_S} \cdot \frac{K_{O2,H}}{K_{O2,H} + S_{O2}} \cdot \frac{S_{NO3}}{K_{NO3,H,anox} + S_{NO3}} \cdot X_H$	
	Aerobic respiration of X_H	$k_{resp,H} \cdot f_{T,MB}(T) \cdot \frac{S_{O2}}{K_{O2,H} + S_{O2}} \cdot X_H$	
	Anoxic respiration of X_H	$k_{resp,H} \cdot \eta_H \cdot f_{T,MB}(T) \cdot \frac{K_{O2,H}}{K_{O2,H} + S_{O2}} \cdot \frac{S_{NO3} + S_{NO2}}{K_{NO3,H,anox} + S_{NO2} + S_{NO3}} \cdot X_H$	
	Decay of X_H	$k_{death,H} \cdot f_{T,MB}(T) \cdot X_H$	

Growth of X_{AOB}	$\mu_{AOB} \cdot f_{T,MB}(T) \cdot \frac{S_{O_2}}{K_{O_2,AOB} + S_{O_2}} \cdot \frac{S_{NH_3} + S_{NH_4}}{K_{NH_4,AOB} + S_{NH_4} + S_{NH_3}} \cdot \frac{S_{CO_2} + S_{HCO_3}}{K_{C,AOB} + S_{CO_2} + S_{HCO_3}} \cdot X_{AOB}$	$K_{C,AOB} = 0.5 \text{ gC m}^{-3}$ $K_{C,NOB} = 0.5 \text{ gC m}^{-3}$
Growth of X_{NOB}	$\mu_{NOB} \cdot f_{T,MB}(T) \cdot \frac{S_{O_2}}{K_{O_2,NOB} + S_{O_2}} \cdot \frac{K_{I,NH_4}}{K_{I,NH_4} + S_{NH_4} + S_{NH_3}} \cdot \frac{S_{NO_2}}{K_{NO_2,NOB} + S_{NO_2}} \cdot \frac{S_{CO_2} + S_{HCO_3}}{K_{C,NOB} + S_{CO_2} + S_{HCO_3}} \cdot X_{NOB}$	
Respiration of X_{AOB}	$k_{resp,AOB} \cdot f_{T,MB}(T) \cdot \frac{S_{O_2}}{K_{O_2,AOB} + S_{O_2}} \cdot X_{AOB}$	
Respiration of X_{NOB}	$k_{resp,NOB} \cdot f_{T,MB}(T) \cdot \frac{S_{O_2}}{K_{O_2,NOB} + S_{O_2}} \cdot X_{NOB}$	
Decay of X_{AOB}	$k_{death,AOB} \cdot f_{T,MB}(T) \cdot X_{AOB}$	
Decay of X_{NOB}	$k_{death,NOB} \cdot f_{T,MB}(T) \cdot X_{NOB}$	

* Bacteria processes are directly ASM-2d.

Parameter values

Most of the parameters were obtained from the well validated ASM series (Table 3.4). Likewise for microalgae parameters, the maximum growth rate of heterotrophic bacteria resulted the most sensitive parameter in all the models. The RWQM1 and BIO_ALGAE had a very similar value of maximum growth rate of heterotrophic bacteria ($k_{gro,H, aer} = 2.0 \text{ d}^{-1}$ and $\mu_H = 1.5 \text{ d}^{-1}$, respectively), while in the model of Sah et al. (2011) is comparatively very high ($\mu_H = 6 \text{ d}^{-1}$). It is important to remark that parameters presented in the Sah et al. (2011) were not calibrated with experimental data.

The value of maximum growth rate of nitrifying bacteria is significantly low in comparison to maximum growth rate of aerobic heterotrophic bacteria in all models. These values are in agreement with previous simulation studies (e.g. Krasnits et al., 2009; Samsó and García, 2013), which have demonstrated that the amount of nitrifying's bacteria is very low in comparison to other bacteria groups.

3.5.3 Physical, chemical and additional processes

Microalgae-bacteria systems are considerably affected by ever-changing environmental factors: temperature and light. pH and dissolved oxygen are factors greatly influenced by fluctuations in environmental factors. Altogether these factors have a strong influence on growth, endogenous respiration and decay, and greatly influence metabolism sometimes causing severe inhibitory effects (Gordillo et al., 1998). Table 3.5 shows physical, chemical and additional processes of the five selected mechanistic models, as well as their parameter values. In this section temperature, light intensity, pH and other additional factors are discussed.

Temperature

Temperature has remarkable effects on all biological systems, and microalgae and bacteria grow under different range of temperatures (from

15 to 25 °C for many microalgae species, and from 15 to 40 °C for bacteria) (Bitog et al., 2011; Henze et al., 2011; Larsdotter, 2006). Below or above optimal temperatures, the growth rate drastically decreases. Note that BIO_ALGAE model describes the microalgae temperature dependency with a normal distribution. The thermic photosynthetic factor ($f_{T_{FS}}(T)$) is highest at the optimal temperature ($T_{opt} = 25$ °C) and declines as temperature deviates from the optimum towards either higher or lower limits. Bacteria temperature dependency is described by means Arrhenius equation, like the ASM series. In the models by Zambrano et al. (2016) and ASM-A temperature influence is not considered, while in the RWQM1 and Sah et al. (2011) both microalgae and bacteria temperature dependency are described by Arrhenius equation.

Light intensity and light attenuation

Incident light intensity and light attenuation in the culture affect light availability and therefore photosynthesis rates. The amount of light available for microalgae photosynthesis is a function of sun position, amount photosynthetically active radiation (PAR = 400-700 nm), concentration of particulate matter in the culture and the light path length (Molina-Grima et al., 1994). Also an excess of light can lead to oxidative damage to chlorophyll and other key photosynthetic pigments, and therefore can inhibit photosynthesis.

Sah et al. (2011) and BIO_ALGAE are the only two models that implement the attenuation of the light intensity. It is described using Lambert-Beer's Law and is attenuated by the presence of particulate components inside the reactors, and also by the depth of system. The resulting light availability as well the efficiency of microalgae to absorption photons is described with different formulations.

Table 3.5 Physical, chemical and additional processes of integrated mechanistic microalgae-bacteria models.

Model	Process	Process rate [M L ⁻³ T ⁻¹]	Parameter values
RWQM1 (Reichert et al., 2001)	Temperature	$f(T) = e^{\beta(T-20)}$	$k_{\text{hyd}} = 3 \text{ d}^{-1}$ $k_{\text{eq},1} = 100000 \text{ d}^{-1}$ $k_{\text{eq},2} = 10000 \text{ d}^{-1}$ $k_{\text{eq},3} = 10000 \text{ d}^{-1}$ $k_{\text{eq},P} = 10000 \text{ d}^{-1}$ $k_{\text{eq},w} = 10000 \text{ d}^{-1}$ $k_{\text{eq},s0} = 2 \text{ d}^{-1}$ $\beta = 0.046 - 0.08 \text{ }^{\circ}\text{C}^{-1}$ $K_I = 500 \text{ W m}^{-1}$ $k_{\text{ads}} = 2 \text{ d}^{-1}$ $k_{\text{des}} = 7 \text{ d}^{-1}$
	Light intensity	$f(L) = \frac{1}{K_I} \cdot \exp\left(1 - \frac{1}{K_I}\right)$	
	Hydrolysis	$k_{\text{hyd}} \cdot f(T) \cdot X_s$	
	Eq. $\text{CO}_2 \leftrightarrow \text{HCO}_3^-$	$k_{\text{eq},1} \cdot (S_{\text{CO}_2} - S_{\text{H}}S_{\text{HCO}_3}/K_{\text{eq},1}^*)$	
	Eq. $\text{HCO}_3^- \leftrightarrow \text{CO}_3^{2-}$	$k_{\text{eq},2} \cdot (S_{\text{HCO}_3} - S_{\text{H}}S_{\text{CO}_3}/K_{\text{eq},2}^*)$	
	Eq. $\text{NH}_4^+ \leftrightarrow \text{NH}_3$	$k_{\text{eq},3} \cdot (S_{\text{NH}_4} - S_{\text{H}}S_{\text{NH}_3}/K_{\text{eq},3}^*)$	
	Eq. $\text{H}_2\text{PO}_4^- \leftrightarrow \text{PO}_4^{2-}$	$k_{\text{eq},P} \cdot (S_{\text{H}_2\text{PO}_4} - S_{\text{H}}S_{\text{HPO}_4}/K_{\text{eq},P}^*)$	
	Eq. $\text{H}^+ \leftrightarrow \text{OH}^-$	$k_{\text{eq},w} \cdot (1 - S_{\text{H}}S_{\text{OH}}/K_{\text{eq},w}^*)$	
	Eq. $\text{Ca}^{2+} \leftrightarrow \text{CO}_3^{2-}$	$k_{\text{eq},s0} \cdot (1 - S_{\text{Ca}}S_{\text{CO}_3}/K_{\text{eq},s0}^*)$	
	Adsorption of phosphate	$k_{\text{ads}} \cdot S_{\text{HPO}_4}$	
	Desorption of phosphate	$k_{\text{des}} \cdot X_P$	

Sah et al., 2011	Temperature	$f(T) = \theta^{(T-20)}$	$b_{E.coli} = 0.25 \text{ d}^{-1}$ $K_S = 0.01 \text{ gN m}^{-3}$ $K_I = 198 \text{ } \mu\text{E m}^{-2} \text{ s}^{-1}$ $k = 13 \text{ m}^{-1}$ $K = 0.09 \text{ m d}^{-1}$ $\theta = 1.07$ $k_h = 3 \text{ d}^{-1}$ $\eta_H = 3 \text{ d}^{-1}$ $K_X = 0.1 \text{ gCOD}_{SF} / \text{gCOD}_{BM}$
	Light attenuation	$I_Z = I_0 e^{(-kz)}$	
	Light intensity	$f(L) = \frac{I_Z}{K_I + I_Z}$	
	Hydrolysis	$k_h \cdot \frac{X_S / (X_H + X_{FB})}{K_X + X_S / (X_H + X_{FB})} \cdot (X_H + \eta_H \cdot X_{FB})$	
	Reaeration	$\frac{K(C_S - C)}{d}$	
	Decay of E.coli	$b_{E.coli} \cdot f(T) \cdot X_{E.coli}$	
Zambrano et al., 2016	Oxygen transfer	$k_L a_{O_2} \cdot (S_{O_2}^{SAT} - S_{O_2})$	$k_L a_{O_2} = 4 \text{ d}^{-1}$ $S_{O_2}^{SAT} = 8.58 \text{ gO}_2 \text{ m}^{-3}$ $K_I = 0.1 \text{ } \mu\text{E m}^{-2} \text{ s}^{-1}$
	Light intensity	$f(L) = \frac{I}{K_I + I}$	
ASM-A (Wagner et al., 2016)	Light intensity	$f(L) = \frac{I_{av}}{I_s} \cdot \exp\left(1 - \frac{I_{av}}{I_s}\right)$	$I_s = 758 \text{ } \mu\text{E m}^{-2} \text{ s}^{-1}$
	Microalgae Temperature	$f_{T,FS}(T) = e^{-\frac{(T-T_{opt})}{s}}$	$\alpha = 0.001935 \text{ (} \mu\text{E m}^{-2} \text{)}^{-1}$ $\beta = 5.7E-7 \text{ (} \mu\text{E m}^{-2} \text{)}^{-1}$ $\delta = 0.0004769 \text{ s}^{-1}$ $\gamma = 0.1460 \text{ s}^{-1}$ $K_I = 0.07 \text{ m}^2 \text{ g}^{-1}$ $s = 30$ $\theta = 1.07$
	Bacteria Temperature	$f_{T,MB}(T) = \theta^{(T-T_{opt})}$	
	Photosynthetic factor	$\eta_{PS}(I, S_{O_2}) = f(L) \cdot f_{PR}(S_{O_2})$ $f(L) = \frac{\alpha \delta I_{av}}{\alpha \beta I_{av}^2 + (\alpha + \beta) \delta I_{av} + \gamma \delta}$	

BIO_ALGAE (Chapter 7; Solimeno et al., 2017a)		$f_{PR}(S_{O_2}) = \begin{cases} 1 - \tanh\left(\frac{K_{PR} \cdot \frac{S_{O_2}}{\tau \cdot S_{O_2}^{SAT}}}{1 - \frac{S_{O_2}}{\tau \cdot S_{O_2}^{SAT}}}\right), & S_{O_2} \leq \tau \cdot S_{O_2}^{SAT} \\ 0, & S_{O_2} > \tau \cdot S_{O_2}^{SAT} \end{cases}$	$K_{PR} = 0.03 \text{ gO}_2 \text{ m}^{-3}$ $S_{O_2}^{SAT} = 9.07 \text{ gO}_2 \text{ m}^{-3}$ $\tau = 3.5$
	Light attenuation	$I_{av} = \frac{I_0 \cdot (1 - \exp(-K_I \cdot X_C \cdot d))}{K_I \cdot X_C \cdot d}$	$k_{HYD} = 3 \text{ d}^{-1}$ $Y_{HYD} = 1 \text{ gCOD gCOD}^{-1}$
	Hydrolysis	$k_{HYD} \cdot \frac{X_S/X_H}{Y_{HYD} + (X_S/X_H)} \cdot X_H$	$k_{eq,1} = 100000 \text{ d}^{-1}$ $k_{eq,2} = 10000 \text{ d}^{-1}$ $k_{eq,N} = 10000 \text{ d}^{-1}$
	Eq. $\text{CO}_2 \leftrightarrow \text{HCO}_3^-$	$k_{eq,1} \cdot (S_{CO_2} - S_H S_{HCO_3} / K_{eq,1}^*)$	$k_{eq,w} = 10000 \text{ d}^{-1}$ $k_{a,O_2} = 0.16 \text{ h}^{-1}$
	Eq. $\text{HCO}_3^- \leftrightarrow \text{CO}_3^{2-}$	$k_{eq,2} \cdot (S_{HCO_3} - S_H S_{CO_3} / K_{eq,2}^*)$	$k_{a,CO_2} = 0.14 \text{ h}^{-1}$ $k_{a,NH_3} = 0.14 \text{ h}^{-1}$
	Eq. $\text{NH}_4^+ \leftrightarrow \text{NH}_3$	$k_{eq,3} \cdot (S_{NH_4} - S_H S_{NH_3} / K_{eq,3}^*)$	
	Eq. $\text{H}^+ \leftrightarrow \text{OH}^-$	$k_{eq,w} \cdot (1 - S_H S_{OH} / K_{eq,w}^*)$	
	Oxygen transfer	$k_{a,O_2} \cdot (S_{O_2}^{WAT} - S_{O_2})$	
	Carbon dioxide transfer	$k_{a,CO_2} \cdot (S_{CO_2}^{WAT} - S_{CO_2})$	
	Ammonia transfer	$k_{a,NH_3} \cdot (-S_{NH_3})$	

* $K_{eq,1} = 10^{17.843 - \frac{3404.71}{273.15+T} - 0.032786(273.15+T)}$; $K_{eq,2} = 10^{9.494 - \frac{2902.39}{273.15+T} - 0.02379(273.15+T)}$; $K_{eq,3} = 10^{2.891 - \frac{2727}{(273.15+T)}}$; $K_{eq,w} = 10^{-\frac{4470.99}{273.15+T} + 12.0875 - 0.01706(273.15+T)}$;

$K_{eq,s0} = 10^{19.87 - \frac{3059}{273.15+T} - 0.04035(273.15+T)}$; $K_{eq,P} = 10^{-3.46 - \frac{219.4}{(273.15+T)}}$ [-]

In BIO_ALGAE model the effects of light availability are included in the photosynthetic factor (η_{ps}) and are described by the ‘photosynthetic factories’ model (PSF) as proposed by Eilers and Peters (1988). At low light intensity, photosynthesis is limited by the rate of capture of photons by microalgae, while at high light intensity microalgae become ‘light saturated’ because photosynthesis cannot process more photons. If irradiance increases above saturation limit, photosynthesis is therefore inhibited.

Sah et al. (2011) as well Zambrano et al. (2016), describes the effect of light on growth by a Monod formulation, while in the ASM-A model microalgae were limited by a constant average light intensity (type I light model, Béchet et al., 2013). These models neglect any effect due light inhibition. The RWQM1 takes into account light limitation and photoinhibition by the Steele relationship (Wu et al., 2013).

pH

In microalgae-bacteria systems pH greatly changes following daily and seasonal rhythms. These fluctuations are mostly due to photosynthetic activity, which impacts bicarbonate buffer system producing pH changes (Solimeno et al., 2015; Sutherland et al., 2014). Usually the main concern is the high pH values attained during the central hours of the day, because can negatively affect microalgae and bacteria growth (Avoz and Goldman, 1982; Borowitzka and Moheimani 2013; García et al., 2000b). Values up to 10 or even more can be reached depending on the alkalinity of water (García et al., 2006). The pH dynamics is included in the RWQM1 and also in BIO_ALGAE. In turn carbon, nitrogen and phosphorus species are in chemical equilibrium which is affected by pH. Phosphorous equilibrium is neglected in BIO_ALGAE, because the model considers only phosphate as phosphorus species.

Nevertheless, all the models don’t include any limitation factor to microalgae and bacteria growth at high or low pH. Elevated pH (>8.3) can inhibit aerobic bacteria and shift the equilibrium of carbon species towards to carbonate concentrations, inhibiting microalgae growth (Avoz and Goldman, 1982). However, the influence of pH on photosynthesis rate and bacteria growth can be easily implemented in the models following, as example, the Arrhenius equation proposed in the model of Costache et al. (2013) for microalgae growth.

Additional processes

In comparison to the other models, BIO_ALGAE considers the excess of dissolved oxygen in the mixed liquor or the culture. Concentrations of dissolved oxygen in the culture above 250% air saturation can dangerously inhibit microalgae activity. This is known to be especially critical in closed photobioreactors, where the oxygen exchange with the atmosphere is very limited (Costache et al., 2013; Weissmand and Gobel, 1987). But also could be important in full-scale HRAPs in locations far away from the mixing paddle-wheel device. The effect of dissolved oxygen concentrations are taken into account by the photorespiration factor ($f_{PR}(S_{O_2})$) (Solimeno et al., 2015). This factor describes that for a dissolved oxygen concentration of approximately $250\%S_{O_2}^{SAT}$ ($22.67 \text{ gO}_2 \text{ m}^{-3}$ at 20°C) the photosynthesis rate is reduced by 10%. Above this value, the photosynthesis rate decreases more quickly with a vertical asymptote, and is equal at zero when dissolved oxygen reaches the 350% saturation limit ($32 \text{ gO}_2 \text{ m}^{-3}$ at 20°C).

According to model results provided by Solimeno et al. (2015, 2017b), in microalgae-bacteria systems is imperative to implement the transfer of gases to the atmosphere. Oxygen, carbon dioxide and ammonia nitrogen are involved in the majority of biological processes, and can either promote or inhibit microalgae and bacteria growth depending on their concentrations. In BIO_ALGAE the transfer rates of oxygen, carbon dioxide and ammonia depend on the different concentrations of the gases between culture medium and atmosphere, temperature, and extension of the surface interface. Without transfer rates is almost impossible to attain good nitrogen predictions because with high pH most of the ammonium is converted to ammonia which can be volatilized (García et al., 2000b).

The model by Zambrano et al. (2016) includes the transfer of oxygen to the atmosphere. Carbon dioxide and ammonia transfer were neglected. In Sah et al. (2011) the equation of re-aeration depends on the difference between dissolved oxygen concentration in the culture medium and saturation concentrations, depth and interfacial transfer coefficient (Moreno-Grau et al., 1996). On the other side RWQM1 and ASM-A not consider this process.

Additional processes such as absorption and desorption of phosphate on particular matter were included only in the RWQM1. Regarding hydrolysis

process, that describes how fast slowly biodegradable substrate is turned into readily biodegradable substrate, the RWQM1 presents a simply equation respect more complicated process implemented by Sah et al. (2011) and BIO_ALGAE.

3.6 Conclusion

In this paper a literature review of microalgae and bacteria models was made to better understand how integrated microalgae-bacteria mechanistic models were built. In comparison with widely accepted bacteria models (ASMs), less is known about microalgae models, thus exhaustive review of models evolution from steady-state to dynamic models has been presented. Moreover, an in depth comparative review of five integrates mechanistic models for microalgae-bacteria systems has been conducted.

4

Microalgae model

This chapter is based on the article:

- ❖ A. Solimeno, R. Samsó, E. Uggetti, B. Sialve, J.P. Steyer, A. Gabarró, J. García. 2015. New mechanistic model to simulate microalgae growth. *Algal Research*, 12:350-358.

4.1 Introduction

Microalgae are nowadays used to produce a variety of compounds of interest for different industrial sectors such as aquaculture and animal feed, human nutrition, cosmetics and nutraceuticals as well as pharmaceuticals (Acién et al., 2013; Spolaore et al., 2006). In addition, these microorganisms have a great potential for CO₂ capture and biofuels production such as biodiesel (Craggs et al., 2011). In fact, in recent years a tremendous effort has been made in numerous research centres to obtain biodiesel from microalgae; however the industrial production of biodiesel is still far from becoming a consolidated technology (Brennan and Owende, 2010; Chisti, 2007).

Another biotechnological application of microalgae is their use for wastewater treatment. Since the late 1950s, the growth of mixed consortia of microalgae and bacteria has been promoted in high rate algal ponds (HRAP) with that aim. In these treatment systems microalgae provide the required oxygen for the degradation of certain wastewater constituents by aerobic bacteria. Though the interest in this technology decreased over the years, in the current context of energy crisis it is skyrocketing again due to its dual benefit: treating wastewater and producing algal biomass that can be valorised in the form of biofuels or bioproducts (Park et al., 2011).

All these microalgal biotechnology applications require tools that allow us to forecast biomass production in order to ensure feasibility for valorisation of microalgae as products or biofuels (Béchet et al., 2013). At the same time production forecasting is challenging because microalgae growth depends on many parameters such as solar radiation, nutrients availability (e.g. carbon and nitrogen) as well as on certain inhibitory conditions (e.g. excess of oxygen in the algal culture).

Mathematical models offer a great opportunity to study the simultaneous effect of different factors affecting algal growth and allow forecasting algal production. Research on microalgae growth kinetics modeling started with the pioneering work by Droop (1968, 1974). Since then a number of researchers have developed models based on single factors such as light

intensity (Huisman, 1999), temperature (Franz et al., 2012), nitrogen (Bernard et al., 2009) and photosynthesis and photoinhibition effects (Wu and Merchuk, 2001). In fact, there is a vast array of models that predict biomass production as a function of light intensity (Yuan et al., 2014). This results from the fact that light cannot be easily controlled at full-scale microalgae cultures, in contrast to other factors which are maintained at optimal conditions to avoid limiting or inhibitory effects (e.g. pH, nutrients and mixing conditions). Recently, models of increasing complexity with two or more factors have been developed (Bonachela et al., 2011; Packer et al., 2011). As an example, in the model by Bernard (2011) light intensity and nitrogen are the limiting factors for microalgae growth. Most of these previous models use few parameters to describe the inherent complexity of algal cultures, especially so in the particular case of microalgae grown in wastewaters, where carbon and nitrogen limitations can be significant. Therefore the main objective of this paper is to present a new mechanistic model that includes crucial physical and biokinetic processes for the description of microalgae growth in different types of cultures, and most particularly in wastewater.

The main source of inspiration for building the presented model was the River Water Quality Model 1 (RWQM1) of the International Water Association (Reichert et al., 2011). RWQM1 was selected because it belongs to a family of widely accepted models (e.g. the Activated Sludge Models (ASM)) which share the same presentation, notation and structure for compounds, processes, and kinetic constants (Henze et al., 2000; Sah et al., 2011). Moreover, RWQM1 is the unique in the IWA family models because it considers microalgae activity.

The model was implemented in the COMSOL MultiphysicsTM software, which solves differential equations using the finite elements method (FEM). For calibration we used experimental data obtained from a culture medium simulating treated urban wastewater (i.e. secondary effluent). This model will provide new insight into the functioning of microalgae cultures, and will help to explore the simultaneous effects of factors affecting microalgae growth. It is also a part of a more ambitious project through which we intend to develop a complete model to simulate mixed cultures of

microalgae and bacteria treating wastewater (like HRAP or photobioreactors).

4.2 Model description

4.2.1 Conceptual model

The conceptual understanding that we have of the modelled system is shown in Figure 4.1. This figure shows that microalgae grow with light, consume substrates (i.e. carbon and nitrogen) and release oxygen. Note that other nutrients (e.g. phosphorus) and micronutrients are not considered to be limiting factors because are usually highly available in wastewater (which is the type of culture that mainly addresses the present model) (Larsdotter, 2006) As a result of microalgal activity, hydroxide ions concentration and pH increase. Increasing pHs displace the equilibrium of the carbon species towards the formation of carbonates.

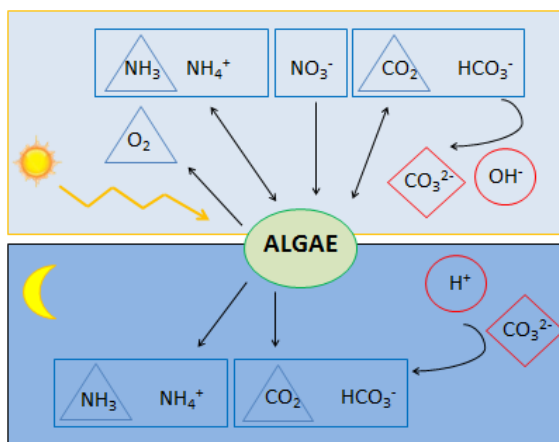


Figure 4.1 General schematic representation of the conceptual model. Microalgae (green ellipse), substrates (rectangles), gaseous species (triangles) and species depending on algal activity which are neither substrates nor gases (diamonds and circles). Other nutrients (e.g. phosphorus) and micronutrients are not limiting factors.

In darkness, endogenous respiration and decay of microalgae release carbon dioxide, the concentration of hydrogen ions increase and pH decreases. By

decreasing pH the carbon equilibrium shifts and carbonate turns into bicarbonate, which can be used as substrate again in the presence of light.

4.2.2 Model components

The model follows the most commonly used nomenclature in the IWA models and considers 10 components. From these components, there are 9 dissolved components and one particulate component corresponding to microalgae biomass (X_{ALG}).

Dissolved components

S_{NH_4} [gNH₄⁺-N m⁻³]: *Ammonium nitrogen*. Nitrogen present in the water as ammonium. It is produced through the processes of endogenous respiration and through inactivation of microalgae. It is consumed through the growth of microalgae.

S_{NH_3} [gNH₃-N m⁻³]: *Ammonia nitrogen*. Nitrogen in the form of ammonia. It is in chemical equilibrium with ammonium (S_{NH_4}). Its concentration decreases by volatilization to the atmosphere.

S_{NO_3} [gNO₃⁻-N m⁻³]: *Nitrate nitrogen*. Nitrogen available as nitrate. It is consumed by microalgae (X_{ALG}).

S_{O_2} [gO₂ m⁻³]: *Dissolved oxygen*. Concentration of dissolved oxygen in the water. It is produced by the growth of microalgae due to photosynthesis and consumed during the processes of endogenous respiration and inactivation of microalgae. It can also be transferred to the atmosphere.

S_{CO_2} [gCO₂-C m⁻³]: *Carbon dioxide*. Carbon as carbon dioxide. It is consumed by microalgae and is produced through the processes of endogenous respiration and inactivation. Moreover, it is in chemical equilibrium with bicarbonate (S_{HCO_3}) and carbonate (S_{CO_3}), and like dissolved oxygen (S_{O_2}), it can be transferred to the atmosphere.

S_{HCO_3} [$\text{gHCO}_3^- \cdot \text{C m}^{-3}$]: *Bicarbonate*. Carbon as bicarbonate. It is in chemical equilibrium with carbon dioxide (S_{CO_2}) and carbonate (S_{CO_3}). It is consumed by microalgae.

S_{CO_3} [$\text{gCO}_3^{2-} \cdot \text{C m}^{-3}$]: *Carbonate*. Carbon in the form of dissolved carbonate. It is in chemical equilibrium with bicarbonate (S_{HCO_3}) and carbon dioxide (S_{CO_2}). Carbonate is not used by microalgae as carbon source.

S_{H} [gH m^{-3}]: *Hydrogen ions*. Concentration of hydrogen ions in the water. They are involved in carbon and ammonium equilibrium systems. The concentration of hydrogen ions decreases with the growth of microalgae and increases with endogenous respiration and inactivation.

S_{OH} [$\text{gOH}^- \cdot \text{H m}^{-3}$]: *Hydroxide ions*. Concentration of hydroxide ions in the water. They are in equilibrium with hydrogen ions.

Particulate components

X_{ALG} [gCOD m^{-3}]: *Microalgae biomass*. Concentration of microalgae. It increases with growth processes and decreases by endogenous respiration and inactivation.

Note that in the model it is expressed in gCOD (chemical oxygen demand) m^{-3} as it is common practice to express organic matter concentrations in all IWA models. Microalgae biomass is transformed from COD to TSS (total suspended solids) assuming a ratio $\text{COD}/\text{TSS} = 0.80$ (Sperling, 2007; Khorsandi et al., 2014) in order to compare experimental and simulation results.

4.2.3 Processes

Table 4.1 shows a list of the processes included in the model and the equations describing their rates. Table 4.2 shows the matrix of stoichiometric parameters.

Algal processes

- **Growth of microalgae** (processes 1a and 1b in Table 4.1). The increase of microalgae biomass per unit of time (growth rate) is expressed as the product of their maximum specific growth rate (μ_{ALG}) [T^{-1}] by their concentration at that point in time (X_{ALG}) and by corrective factors (in the form of Monod functions) that limit or inhibit their growth.

Microalgae grow with both carbon dioxide (S_{CO_2}) and bicarbonate (S_{HCO_3}). Note that in the matrix of stoichiometric parameters (Table 4.2) only the reaction rate of carbon dioxide is affected by microalgae growth because the concentration of bicarbonate is already in chemical equilibrium with it. Carbon dioxide (S_{CO_2}) inhibits microalgae growth at very high concentrations based on the results of Silva and Pirt (1984). More precisely, it has been observed that in closed photobioreactors CO_2 behaves as an inhibitor at partial pressures above 0.6 atm, which is equivalent to a dissolved CO_2 concentration of $440 \text{ gCO}_2 \text{ m}^{-3}$ at $37 \text{ }^\circ\text{C}$ (Silva and Pirt, 1984). Inhibition caused by CO_2 is due to the compound itself as well as its effect on acidity, which in the current status of the model cannot be distinguished.

Microalgae grow with ammonia and ammonium ($S_{\text{NH}_4} - S_{\text{NH}_3}$) or with nitrate (S_{NO_3}) as nitrogen source. When ammonium (or ammonia, note that they are in chemical equilibrium) and nitrate are both present, ammonium is generally preferred (Monstert and Grobbelar, 1987; Stewart, 1974; Syrett, 1981). To represent this phenomenon, the highlighted term that describes the inhibiting effect of ammonia and ammonium on growth of microalgae once nitrate has been introduced in Eq. (4.1) (process 1b in Table 4.1).

$$\rho_{1b} = \mu_{\text{ALG}} \cdot f_{\text{T,FS}}(T) \cdot \eta_{\text{PS}}(I, S_{\text{O}_2}) \cdot \frac{S_{\text{CO}_2} + S_{\text{HCO}_3}}{K_{\text{C,ALG}} + S_{\text{CO}_2} + S_{\text{HCO}_3} + \frac{S_{\text{CO}_2}^2}{I_{\text{CO}_2,\text{ALG}}}} \cdot \frac{S_{\text{NO}_3}}{K_{\text{N,ALG}} + S_{\text{NO}_3}} \cdot \frac{K_{\text{N,ALG}}}{K_{\text{N,ALG}} + S_{\text{NH}_3} + S_{\text{NH}_4}} \cdot X_{\text{ALG}} \quad (4.1)$$

Here again note that microalgae growth only affects the reaction rate of ammonia because it is in equilibrium with ammonium (Table 4.2).

Table 4.1 Mathematical description of the processes of the model (processes rates).

Processes	Process rate [M L ⁻³ T ⁻¹]
1a. Growth of X _{ALG} on S _{NH4}	$\rho_{1a} = \mu_{ALG} \cdot f_{T,FS}(T) \cdot \eta_{PS}(I, S_{O_2}) \cdot \frac{S_{CO_2} + S_{HCO_3}}{K_{C,ALG} + S_{CO_2} + S_{HCO_3} + \frac{S_{CO_2}^2}{I_{CO_2,ALG}}} \cdot \frac{S_{NH_3} + S_{NH_4}}{K_{N,ALG} + S_{NH_3} + S_{NH_4}} \cdot X_{ALG}$
1b. Growth of X _{ALG} on S _{NO3}	$\rho_{1b} = \mu_{ALG} \cdot f_{T,FS}(T) \cdot \eta_{PS}(I, S_{O_2}) \cdot \frac{S_{CO_2} + S_{HCO_3}}{K_{C,ALG} + S_{CO_2} + S_{HCO_3} + \frac{S_{CO_2}^2}{I_{CO_2,ALG}}} \cdot \frac{S_{NO_3}}{K_{N,ALG} + S_{NO_3}} \cdot \frac{K_{N,ALG}}{K_{N,ALG} + S_{NH_3} + S_{NH_4}} \cdot X_{ALG}$
2. Endogenous respiration of X _{ALG}	$\rho_2 = k_{resp,ALG} \cdot f_{T,FS}(T) \cdot \frac{S_{O_2}}{K_{O_2,ALG} + S_{O_2}} \cdot X_{ALG}$
3. Decay of X _{ALG}	$\rho_3 = k_{death,ALG} \cdot f_{T,FS}(T) \cdot X_{ALG}$
4. Chemical equilibrium CO ₂ ↔ HCO ₃ ⁻	$\rho_4 = k_{eq,1} \cdot (S_{CO_2} - \frac{S_H S_{HCO_3}}{K_{eq,1}})$
5. Chemical equilibrium HCO ₃ ⁻ ↔ CO ₃ ²⁻	$\rho_5 = k_{eq,2} \cdot (S_{HCO_3} - \frac{S_H S_{CO_3}}{K_{eq,2}})$
6. Chemical equilibrium NH ₄ ⁺ ↔ NH ₃	$\rho_6 = k_{eq,3} \cdot (S_{NH_4} - \frac{S_H S_{NH_3}}{K_{eq,3}})$
7. Chemical equilibrium H ⁺ ↔ OH ⁻	$\rho_7 = k_{eq,w} \cdot (1 - \frac{S_H S_{OH}}{K_{eq,w}})$
8. Transfer of S _{O2} to the atmosphere	$\rho_{O_2} = K_{a,O_2} \cdot (S_{O_2}^{WAT} - S_{O_2})$
9. Transfer of S _{CO2} to the atmosphere	$\rho_{CO_2} = K_{a,CO_2} \cdot (S_{CO_2}^{WAT} - S_{CO_2})$
10. Transfer of S _{NH3} to the atmosphere	$\rho_{NH_3} = K_{a,NH_3} \cdot (-S_{NH_3})$

Table 4.2 Matrix of stoichiometric parameters that relates processes and components through stoichiometric coefficients in Appendix A4.1.

State variables $\rightarrow i$		S_{NH4}	S_{NH3}	S_{NO3}	S_{O2}	S_{CO2}	S_{HCO3}	S_{CO3}	S_H	S_{OH}	X_{ALG}
Processes $\downarrow j$											
1a. Growth of X_{ALG} on S_{NH4}	ρ_{1a}	$v_{1,1a}$			$v_{4,1a}$	$v_{5,1a}$			$v_{8,1a}$		$v_{10,1a}$
1b. Growth of X_{ALG} on S_{NO3}	ρ_{1b}			$v_{3,1b}$	$v_{4,1b}$	$v_{5,1b}$			$v_{8,1b}$		$v_{10,1b}$
2. Endogenous respiration of X_{ALG}	ρ_2	$v_{1,2}$			$v_{4,2}$	$v_{5,2}$			$v_{8,2}$		$v_{10,2}$
3. Decay of X_{ALG}	ρ_3	$v_{1,3}$			$v_{4,3}$	$v_{5,3}$			$v_{8,3}$		$v_{10,3}$
4. Chemical equilibrium $CO_2 \leftrightarrow HCO_3^-$	ρ_4					$v_{5,4}$	$v_{6,4}$		$v_{8,4}$		
5. Chemical equilibrium $HCO_3^- \leftrightarrow CO_3^{2-}$	ρ_5						$v_{6,5}$	$v_{7,5}$	$v_{8,5}$		
6. Chemical equilibrium $NH_4^+ \leftrightarrow NH_3$	ρ_6	$v_{1,6}$	$v_{2,6}$						$v_{8,6}$		
7. Chemical equilibrium $H^+ \leftrightarrow OH^-$	ρ_7								$v_{8,7}$	$v_{9,7}$	
8. Transfer of S_{O2} to the atmosphere	ρ_{O2}				$v_{4,O2}$						
9. Transfer of S_{CO2} to the atmosphere	ρ_{CO2}					$v_{5,CO2}$					
10. Transfer of S_{NH3} to the atmosphere	ρ_{NH3}		$v_{2,NH3}$								

The photosynthetic factor (η_{PS}) [-] takes into account the effects of light intensity (I) [$M T^{-3}$] and excess of oxygen (S_{O_2}) [$M L^{-3}$] on photosynthesis and therefore on microalgae growth. The following relationship was introduced:

$$\eta_{PS}(I, S_{O_2}) = f_L(I) \cdot f_{PR}(S_{O_2}) \quad (4.2)$$

where, f_L [-] is the light factor and f_{PR} [-] the photorespiration factor.

The effects of light intensity on photosynthesis are described by the ‘photosynthetic factories’ model (PSF) as proposed by Eilers and Peeters (1988): at low light irradiance, the rate of photosynthesis is proportional to light intensity because photosynthesis is limited by the rate of capture of photons. When irradiance increases to a certain point, microalgae become ‘light saturated’ because photosynthesis cannot process more photons. If irradiance increases beyond an inhibitory threshold, the rate of photosynthesis starts to decrease (Béchet et al., 2013; Camacho-Rubio et al., 2003; Crill, 1977).

In the PSF model it is assumed that microalgae are present in three different states: resting or ‘open’ (x_1), activated or ‘closed’ (x_2), and inhibited (x_3) (Figure 4.2).

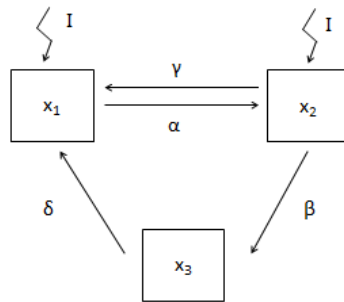


Figure 4.2 Three different states and relationships of the photosynthetic factories model (PSF): open (x_1), closed (x_2) and inhibited (x_3) (Adapted from Eilers and Peeters (1998)).

Initially microalgae are in open state x_1 , ready to capture a photon. When the photon is captured and biochemical reactions start, microalgae turn to activated state x_2 . This reaction depends on the rate of activation α [$M^{-1}T^{-1}$]. In activated state microalgae can go back to open state x_1 in dark conditions, or can capture another photon and pass to inhibited state x_3 . These two reactions depend on a rate constant of production γ [T^{-1}] and on a rate constant of inhibition β [$M^{-1}T^{-1}$]. Microalgae in the inhibited state turn back to the open state with a rate of recovery δ [T^{-1}].

Considering the principle of mass conservation, the three states can be described by the following system of differential equations (Equation 4.3-4.6):

$$\frac{dx_1}{dt} = -\alpha \cdot I \cdot x_1 + \gamma \cdot x_2 + \delta \cdot x_3 \quad (4.3)$$

$$\frac{dx_2}{dt} = \alpha \cdot I \cdot x_1 - \gamma \cdot x_2 - \beta \cdot I \cdot x_2 \quad (4.4)$$

$$\frac{dx_3}{dt} = \beta \cdot I \cdot x_2 - \delta \cdot x_3 \quad (4.5)$$

$$x_1 + x_2 + x_3 = 1 \quad (4.6)$$

When irradiance is not constant, but is a nonlinear function of time ($I(t)$), this system of differential equations does not have an analytical solution. However, under outdoor conditions, variations of I [$M T^{-3}$] during the daily solar cycle are very slow with respect to the dynamics of photosynthesis (Camacho-Rubio et al., 2002; Eilers and Peeters, 1988). In these conditions x_1 and x_2 are close to equilibrium within less than a second. Therefore it can be assumed that equilibrium is reached instantly, making the left hand side of differential terms equal to zero.

Under this assumption, the solution to this system of differential equations is:

$$x_1 = \frac{\gamma\delta + \beta I\delta}{\alpha\beta I^2 + (\alpha + \beta)\delta I + \gamma\delta} \quad (4.7)$$

$$x_2 = \frac{\alpha\delta I}{\alpha\beta I^2 + (\alpha + \beta)\delta I + \gamma\delta} \quad (4.8)$$

$$x_3 = \frac{\alpha\beta I^2}{\alpha\beta I^2 + (\alpha + \beta)\delta I + \gamma\delta} \quad (4.9)$$

The state in which microalgae can grow is x_2 , and therefore in our model the photosynthetic factor is:

$$f_L(I) = x_2 \quad (4.10)$$

As shown before (Eq. 4.2), in microalgae cultures photosynthesis not only depends on the solar irradiance, but is also a function of oxygen concentration (for high concentrations). Especially in closed photobioreactors where there is little (if any) oxygen exchange with the atmosphere, the accumulation of this component may inhibit photosynthesis (Molina-Grima et al., 2001). According to Chisti (2007), to prevent such inhibitory effects the dissolved oxygen concentration should never exceed about 400% of air saturation value. The photorespiration factor is introduced in this work to represent this phenomenon in mathematical terms:

$$f_{PR}(S_{O_2}) = \begin{cases} 1 - \tanh\left(\frac{K_{PR} \cdot \frac{S_{O_2}}{\tau \cdot S_{O_2}^{SAT}}}{1 - \frac{S_{O_2}}{\tau \cdot S_{O_2}^{SAT}}}\right), & S_{O_2} \leq \tau \cdot S_{O_2}^{SAT} \\ 0, & S_{O_2} > \tau \cdot S_{O_2}^{SAT} \end{cases} \quad (4.11)$$

where $S_{O_2}^{SAT}$ [M L⁻³] is the saturation concentration of oxygen in the air. The photorespiration inhibition constant (K_{PR}) [M L⁻³] and the coefficient of

excess dissolved oxygen (τ) are parameters that have to be calibrated during the application of the model.

The effect of photorespiration does not affect microalgal production if the concentration of oxygen in water is clearly lower than τ times the saturation concentration, as is the case of open photobioreactors (Chisti, 2007). However, when the concentration of oxygen tends towards saturation ($\tau S_{O_2}^{SAT}$) [M L⁻³] the photorespiration factor decreases, hindering microalgae growth.

The thermic photosynthetic factor ($f_{T,FS}$) [-] takes into account the effects of temperature on microalgae growth and also on endogenous respiration and inactivation processes (1a, 1b, 2 and 3 in Table 4.1, respectively). Water temperature varies on both diurnal and seasonal scales, affecting both microalgal photosynthesis and respiration rates. The optimal temperature for algal growth ranges between 15°C and 25°C, depending on the species (Bitog et al., 2011; Larsdotter, 2006). The thermic photosynthetic factor is represented in the model following the work of Dauta et al. (1990):

$$f_{T,FS}(T) = e^{-\left(\frac{T-T_{OPT}}{s}\right)} \quad (4.12)$$

where T_{OPT} was assumed equal to 25 °C (Dauta et al., 1990) and s [-] is a parameter value for empirical fitting.

- **Endogenous respiration** (process 2 in Table 4.1). The rate of this process is expressed as the product between the maximum rate of endogenous respiration ($k_{resp,alg}$) [T⁻¹], the concentration of microalgae, the thermic photosynthetic factor (the same as used for the growth of microalgae) and Monod function relates limiting oxygen concentration to a microalgae growth rate.

- **Decay of microalgae** (process 3 in Table 4.1). The rate of this process is expressed as the product of the maximum rate of inactivation ($k_{death,alg}$) [T⁻¹] by the concentration of microalgae and by thermic photosynthetic factor (the same as for growth) (Reichert et al., 2001).

Chemical equilibrium reactions

Chemical equilibria affect carbon, nitrogen and the balance of hydrogen and hydroxide ions (processes 4, 5, 6 and 7 in Table 4.1). The rates of these chemical reactions (ρ_c) [$M L^{-3}T^{-1}$] are obtained with the following general equation (Batstone et al., 2002):

$$\rho_c = K_{eq,c} (S_c - S_{eq,c}) \quad (4.13)$$

Where $c=1\dots n$ and n is the number of chemical species in equilibrium, $k_{eq,c}$ [T^{-1}] is the dissociation constant of the c^{th} component, S_c [$M L^{-3}$] is the concentration of the c^{th} component and $S_{eq,c}$ [$M L^{-3}$] is the concentration at equilibrium.

Transfer of gases to the atmosphere

Transfer rates of oxygen, carbon dioxide and ammonia between water and the atmosphere (processes 8, 9 and 10 in Table 4.1) are given by the general equation (Batstone et al., 2002):

$$\rho_g = K_{a,g} (S_g^{WAT} - S_g) \quad (4.14)$$

where $g=1\dots m$ and m is the number of transfer rates, S_g^{WAT} [$M L^{-3}$] is the saturation concentration of g^{th} gas in the water, S_g [$M L^{-3}$] is the gas concentration in the water and $K_{a,g}$ is the overall mass transfer coefficient of g^{th} gas [T^{-1}]. K_a depends on the temperature, the nature of the gas and the liquid and the extension of the surface interface.

4.2.4 Effects of temperature, irradiance and pH

Temperature, irradiance and pH also affect the rates the processes described previously.

Irradiance ($I(\lambda)$) [$M T^{-3}$]: Wavelength-specific *irradiance or light intensity*. It is also known in literature as a photon flux density (PFD).

In the present model irradiance was expressed as photosynthetically active radiation (PAR), which includes wavelengths between 400 and 700 nm (Zonneveld, 1998):

$$PAR = \int_{400 \text{ nm}}^{700 \text{ nm}} I(\lambda) d\lambda \quad (4.15)$$

If measured PAR values are not available, estimated values at any Earth geographical location can be calculated from coordinates with the equations presented in Table 4.3 (Al-Rawahi et al., 2011).

Table 4.3 Mathematical equations for estimating irradiance at any point on Earth. Parameters and factors are described in Appendix A4.1.

Description	Mathematical Equation	Units
Total incident irradiance	$I_0 = \frac{\pi H E_f}{24} \{ [0.409 + 0.5016 \cdot \sin(\omega_s - 60)] + [0.6609 - 0.4767 \cdot (\omega_s - 60)] \cos \omega \} \cdot \left(\frac{\cos \omega \cdot \cos \omega_s}{\sin \omega_s - \omega_s \cdot \cos \omega_s} \right) \cdot 0.2174$	$\mu E m^{-2} s^{-1}$
Daily radiation	$H = \kappa H_0$	$J m^{-2} d^{-1}$
Total daily extraterrestrial radiation	$H_0 = \left(\frac{24\zeta}{\pi} \right) \left(1 + 0.003 \cdot \cos \left(\frac{360 N}{365} \right) \right) \left(\cos \phi \cdot \cos \delta \cdot \sin \omega_s + \frac{2\pi \omega_s}{360} \cdot \sin \phi \cdot \sin \delta \right)$	$J m^{-2} d^{-1}$

Water temperature (T [°C]): *Water temperature*. Microalgae processes are influenced by temperature described by thermic photosynthetic factor Eq. (4.12).

pH [-]. pH of the aqueous medium is obtained from hydrogen ions concentration (S_H). pH value displaces the equilibrium of the carbon and nitrogen species.

4.2.5 Stoichiometry and parameter values

The stoichiometric matrix is presented in Table 4.2 and is based on the structure of IWA models (Petersen matrix). Values of biokinetic, physical and chemical parameters are shown in Appendix A4.1-A4.2. Mathematical expressions of the stoichiometric coefficients of each process are shown in Appendix A4.3.

Using Tables 4.1 and 4.2, the reaction rate for each component of the model r_i is obtained with:

$$r_i = \sum_j v_{j,i} * \rho_j \quad (4.15)$$

where i is the number of components and j is the number of processes; ρ_j is the reaction rate for each process j and $v_{j,i}$ is the stoichiometric coefficient. The expressions of stoichiometric coefficients related to microalgae processes are based on the fractions of carbon ($i_{C,ALG}$), hydrogen ($i_{H,ALG}$), oxygen ($i_{O,ALG}$) and nitrogen ($i_{N,ALG}$) (Appendix, Table A4.4).

4.3 Experimental verification

Experiments were carried out in a batch mesocosm microalgae culture located outdoors at the facilities of the Laboratory of Environmental Biotechnology (LBE, INRA) in Narbonne, South of France (43°11'N, 3°00'E, 13 m A.M.S.L.). The mesocosm consisted of a cylindrical PVC container with a surface area of 1.30 m² and a depth of 0.55 m (nominal volume 0.5 m³). A drainage pump ensured continuous stirring of culture medium.

Experiments started on January 23rd 2012. The mesocosm (without replicates) was manually filled with 450 L of medium. 50 L of inoculum with the microalgae *Scenedemus* sp were added. The medium was prepared as to simulate the mineral composition of a wastewater. A commercial mineral fertilizer (Antys8, Frayssinet, France) (80 mg/L TN, 50 g/L P₂O₅) was diluted into tap water (0.16/1000), and 0.03g/L of NH₄Cl were added to

increase nitrogen concentration. The experiments lasted 9 days, and no new fresh medium was added during the entire experimental period.

Photosynthetically active radiation (PAR) was measured with a probe (Sky Instruments PAR Quantum Sensor) located on the surface of mesocosms; data were recorded every five minutes. Water temperature and pH were measured with pH and temperature probes (InPro 426i, Mettler Toledo, CH) every morning. During the 9 days water temperature varied between 9 and 18.7 °C (January and February are the coldest months in the region) and the light intensity (PAR) ranged from 3.25 and 655 $\mu\text{E m}^{-2}\text{s}^{-1}$.

Samples of the microalgae culture were taken after 2, 4, 8 and 9 days, and analyzed for total suspended solids (TSS) as indicator of algal biomass and ammonium (NH_4^+ -N) according to conventional procedures indicated in the Standard Methods (APHA-AWWA-WPCF, 2001).

4.4 Model implementation and calibration procedure

The model described in section 2 was implemented in COMSOL MultiphysicsTM v4.3b software. A 0D domain was used to represent the experimental reactor (mesocosms), which can be considered in perfect mixing, and therefore transport of aqueous phase species (i.e. dissolved and particulate) can be ignored.

The model was calibrated using available data for the 9 days of experimentation. Manual trial and error adjustment of parameters was used to match measured data as much as possible using graphical representations.

The concentrations of components in the mesocosms measured at the beginning of the experiment are shown in Table 4.3.

Table 4.3 Initial concentrations of the components in the mesocosms.

Component	Concentration	Units
Dissolved Components		
S_{NH4}	8.1	$gN-NH_4 m^{-3}$
S_{NH3}	0.685	$gN-NH_3 m^{-3}$
S_{NO3}	11.37	$gN-NO_3 m^{-3}$
S_{CO2}	0.8	$gC-CO_2 m^{-3}$
S_{HCO3}	100	$gC-HCO_3 m^{-3}$
S_{CO3}	1.17	$gC-CO_3 m^{-3}$
S_{O2}	8.0	$gO_2 m^{-3}$
S_H	3.16E-6	$gH m^{-3}$
S_{OH}	2.83E-3	$gH-OH m^{-3}$
Particulate Component		
X_{ALG}	80	$gCOD m^{-3}$

From the 31 parameters implemented in the model, 16 parameters were obtained from the existing River Water Quality Model (Reichert et al., 2001). Those parameters related to transfer of gases to the atmosphere, temperature, photorespiration and carbon limitation on microalgae growth are not included into the RWQM1 and they were obtained from other literature cited in Tables. Morris's uncertainty method (Morris, 1991) was applied to screening which parameters had a greater influence on the simulation response. Based on a previous uncertainty analysis, the model was calibrated by adjusting the values of the maximum growth rate of microalgae (μ_{ALG}), the transfer of gases to the atmosphere and the photorespiration inhibition constant (K_{PR}). Calibration was conducted by comparing simulated and experimental data curves.

4.5 Results

Biomass concentration in the mesocosm increased from 100 gTSS m^{-3} at the beginning of the experiment to around 210 gTSS m^{-3} after 9 days. Figure 4.3 shows that the model was able to reproduce such growth pattern with an acceptable accuracy. Interestingly, the simulated curve has a wavelike trend which indicates that the model is able to reproduce microalgae growth (crests) and inactivation (trough) cycles occurring during daytime and at night, respectively.

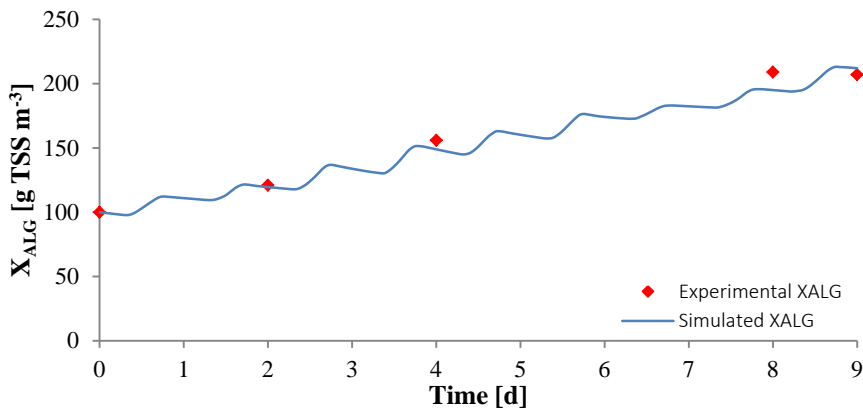


Figure 4.3 Experimental (red diamonds) and simulated (blue line) microalgae biomass growth over the 9 days. The crests and troughs of the simulated curve correspond to microalgae growth and inactivation periods during daytime and at night, respectively.

On the other hand, Figure 4.4 shows that pH increased with the growth of microalgae. Despite the fitting between experimental data and simulation results are not as good as in Figure 4.3, the model still predicts the general trend shown by the experimentally measured pH values. Again, daily pH variations related to the activity of microalgae can be clearly observed. In darkness, the pH decreases as a consequence of endogenous respiration and inactivation of microalgae which release both carbon dioxide and hydrogen ions, while during the day the pH increases due to photosynthesis.

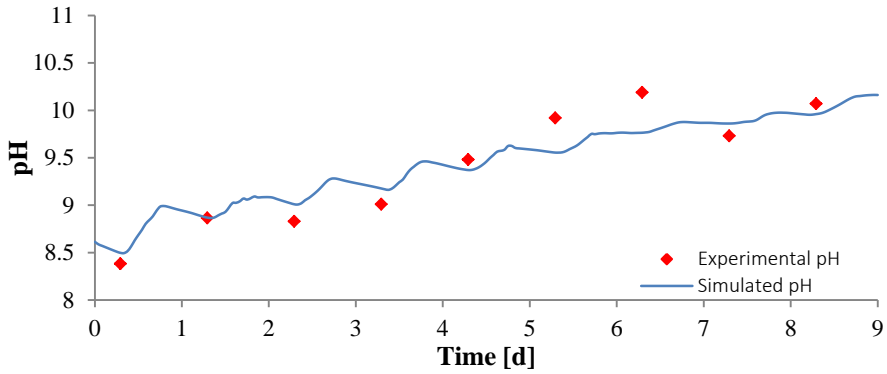


Figure 4.4 Experimental (red diamonds) and simulated (blue line) pH values over the 9 days period.

Figure 4.5 shows the experimental and simulated ammonium nitrogen concentrations within the mesocosm as well as the simulated nitrate concentration (note that nitrate concentrations were not measured in the experimental study). Once more, the simulated ammonium concentrations match the trend of the experimental measurements with a satisfactory degree of accuracy. Although this phenomenon cannot be demonstrated with the available experimental data, Figure 4.5 also shows to what extent microalgae growth used ammonium preferably to nitrate as nitrogen source. After 6 days, the concentrations of S_{NH_4} and S_{NH_3} were very low but microalgae continued growing, most likely by consuming S_{NO_3} . Once again, the daily $S_{\text{NH}_4} + S_{\text{NH}_3}$ variations related to the activity of microalgae can be clearly observed.

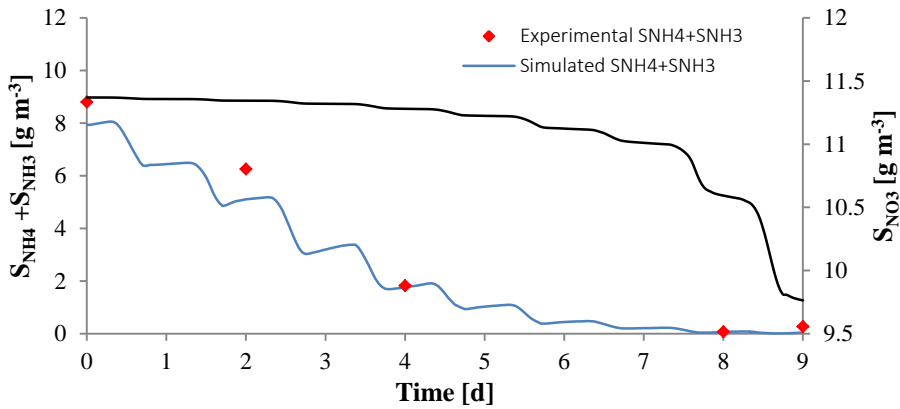


Figure 4.5 Comparison between experimental (red diamonds) and simulated (blue line) concentrations of ammonium and ammonia and simulated concentrations of nitrate (black line).

Figure 4.6 shows simulation results for $S_{CO_2} + S_{HCO_3}$ and S_{CO_3} concentrations. $S_{CO_2} + S_{HCO_3}$ decreased with the growth of microalgae while the concentration of S_{CO_3} followed the opposite trend. For increasing values of pH, the equilibrium of the carbon species is displaced towards the formation of carbonates CO_3^{2-} . Daily variations of these carbon species are again related to growth and endogenous respiration and inactivation cycles during daytime and at night, respectively.

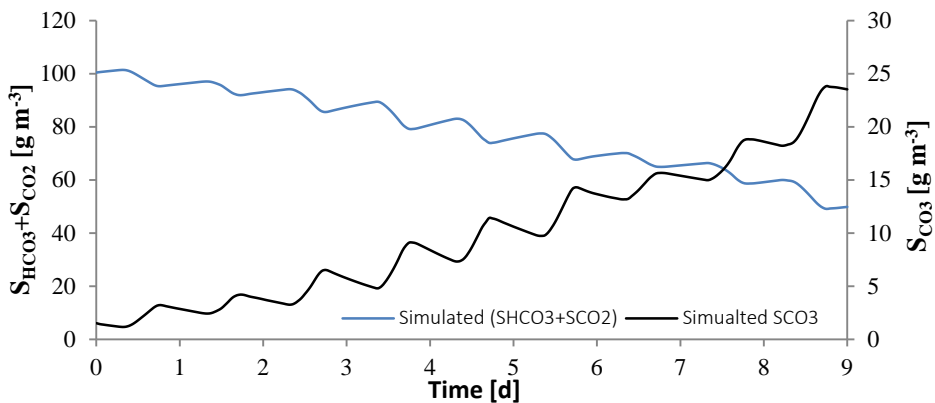


Figure 4.6 Microalgae uptake of carbon ($S_{HCO_3} + S_{CO_2}$) (blue line) and S_{CO_3} (black line) simulated curves.

The thermic photosynthetic factor ($f_{T,FS}(T)$) which depends exclusively on temperature can range between 0 and 1, where higher values are favourable for algae growth. According to Figure 4.7 at the beginning of the experimental study (first 5 days) the conditions were more favourable for microalgae growth, and slightly worsened after that (Figure 4.7). Temperature values (shown in Figure 4.8, from 9 °C up to 18 °C), give values of the photosynthetic thermal factor oscillating between 0.38 and 0.8. Meanwhile low temperature from day 6 to 9 (from 9 °C up to 12 °C) decreased microalgae activity. This phenomenon can be observed by looking at the biomass growth rate (slope of the curve of Figure 4.3), which decreases slightly after day 5.

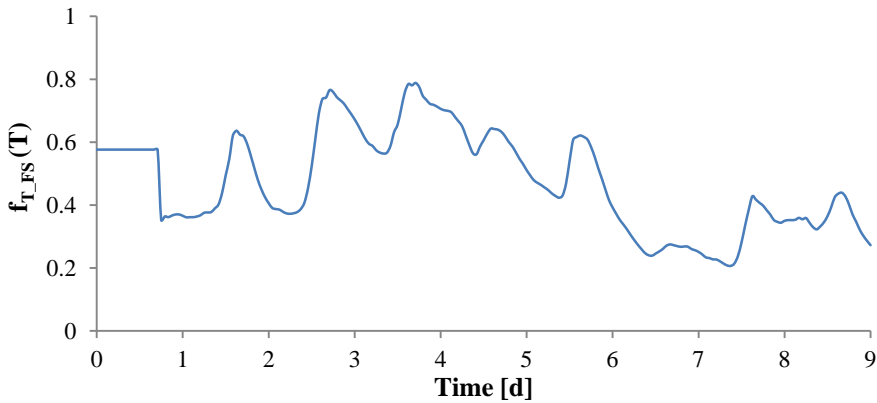


Figure 4.7 Evolution of the thermic photosynthetic factor ($f_{T,FS}$) over the 9 days of the experiment.

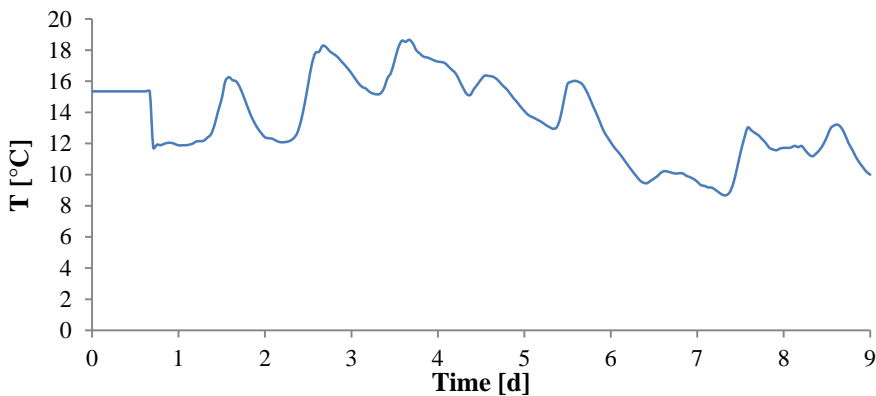


Figure 4.8 Temperature measurements (T) over the 9 days of the experiment.

Table 4.4 presents the values of the parameters that were calibrated to obtain the results of Figures 4.3 to 4.7.

Table 4.4 Values of calibrated parameters.

Parameter	Description	Value
μ_{ALG}	Maximum specific growth rate of microalgae	1.5 d^{-1}
K_{a,O_2}	Mass transfer coefficient for oxygen	4 d^{-1}
K_{a,CO_2}	Mass transfer coefficient for carbon dioxide	0.6 d^{-1}
K_{a,NH_3}	Mass transfer coefficient for ammonia	0.6 d^{-1}

4.6 Discussion

4.6.1 Innovative features of the model

The main innovation of the current model comes from considering inorganic carbon as a limiting substrate for the growth of microalgae. Previous research on microalgae growth modeling focused on properly describing the dependence of microalgae growth on light, while carbon limitation was not addressed (Franz et al., 2012; Wu and Merchuk, 2001). This approach was justified by the fact the growth of microalgae was studied in photobioreactors in which carbon dioxide was supplied through injection and thus carbon availability was always ensured (Bitog et al., 2011). However, microalgae grown in wastewater systems such as HRAP, in which no external carbon dioxide is supplied, are usually carbon limited (Buhr and Miller, 1983). Hence, in this case, it is essential to consider carbon limitation for a correct estimation of biomass production. In the scenario simulated in this work it was shown how the model was able to simulate the dynamics of the carbon species and in this case it was observed that they did not hinder algae growth. Carbon limitation was implemented in the model by introducing the correction factor $K_{C,ALG}$ in the equation describing the growth rate of microalgae (processes 1a and 1b in Table 4.1).

On the other hand, excessively high concentrations of carbon dioxide can also be counter-productive and inhibit the growth of microalgae (Kurano and Miyachi, 2005). Although in our experimental setup the excess of carbon dioxide is released to the atmosphere and does not inhibit algae growth, this effect has to be taken into account in closed reactors. To this end, the presented model also implements the inhibitory effect of high concentration of carbon dioxide through the parameter $I_{\text{CO}_2, \text{ALG}}$ (Silva and Pirt, 1984) (processes 1a and 1b in Table 4.1) .

Temperature has also an effect on the chemical equilibrium of species, pH and gas solubility (Bouterfas et al., 2002). In the current scenario, when temperatures decreased, photosynthetic activity also decreased. It is translated into lower pH oscillations (± 0.2) during the day/night cycle (Figure 4.4).

Photosynthetic processes (e.g. photoinhibition and photolimitation) and photorespiration phenomena were lumped together into a single parameter called photosynthetic factor $\eta_{\text{PS}}(I, S_{\text{O}_2})$. Among others, the photosynthetic factor includes the influence of irradiance on microalgal growth. In fact, this parameter is considered the main limiting factor in microalgae systems (Larsdotter, 2006; Park and Craggs, 2011).

The dynamic model of photosynthesis and photoinhibition presented by Eilers and Peeters (1992) solves the system of differential equations 3 to 6 considering constant light intensity (I). In the current work this approach was also adopted. To reproduce the daily variation of light intensity we assume that photosynthetic processes are fast compared to the rate of change of irradiance; hence, the activated photosynthetic factor (x_2) quickly reaches equilibrium with instantaneous irradiance (Camacho-Rubio et al., 2002). This simplification was required to obtain the analytical solution of the system of differential equations (4.3-4.6).

The second term of the Equation (4.2) $f_{\text{PR}}(S_{\text{O}_2})$ considers the effects of photorespiration on microalgae growth, a phenomenon so far never modelled in large-scale algal cultures. Chisti (2007) imposed a maximum concentration of oxygen dissolved in water equal to four times the value of air saturation. This concentration can be considered equal to $7.1904 \text{ gO}_2 \text{ m}^{-3}$

at 20 °C (Camacho-Rubio and Fernández, 1999). To this restriction must be added the fact that photorespiration phenomenon starts suddenly at high concentration of dissolved oxygen, without significant impact to low concentrations.

Despite the scarce information available on modelling photorespiration, a photorespiration factor $f_{PR}(S_{O_2})$ has been proposed in the current work (Equation 4.11), representing the effects of high oxygen concentration in the culture medium. To obtain this expression, the limiting function of the Monod equation was reversed (Figure 4.9a). Figure 4.9b describes a function that equals zero for negligible dissolved oxygen concentration and increases suddenly with a vertical asymptote when dissolved oxygen concentration reaches the limit saturation ($\tau S_{O_2}^{SAT}$). The parameter K_{PR} , based on the affinity constant of Monod switching functions, is responsible for the velocity at which the value of the function increases for increasing dissolved oxygen concentrations. The expression that describes the behaviour of photorespiration was obtained by subtracting a unit from the resulting function (Figure 4.9c).

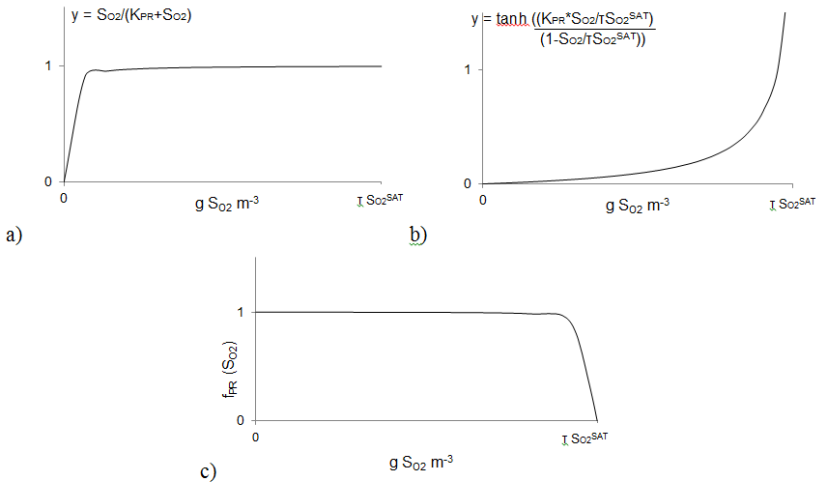


Figure 4.9 a) Monod-function for limiting substrate, b) hyperbolic tangent function, c) photorespiration factor.

In an open reactor oxygen is gradually transferred from the culture medium to the atmosphere, so the effect of photorespiration is negligible (as in our experiment). Photorespiration should be considered in closed photobioreactors.

The calibrated value of the maximum specific growth rate of microalgae ($\mu_{\text{ALG}} = 1.5 \text{ [d}^{-1}\text{]}$) fits well within literature ranges $[0.4\text{-}2 \text{ d}^{-1}]$ (Reichert et al., 2001). Model results proved to be very sensitive to mass transfer coefficients to the atmosphere (Table 4.4), perhaps because all of these gases participate in a number of processes that either promote or inhibit microalgae growth depending on their concentrations. Indeed, intense photosynthesis can increase daytime dissolved oxygen levels in pond water up to more than 200% of the saturation concentration (García et al., 2000b, Molina-Grima et al., 2001). The exchange of dissolved oxygen between water and the atmosphere occurs rapidly. Thus, to prevent high levels of dissolved oxygen in water, the coefficient of volatilization of oxygen (K_{a,O_2}) was set so that the oxygen concentration in the culture medium would remain between 9 and 20 $\text{gO}_2 \text{ m}^{-3}$. Carbon dioxide and nitrogen mass transfer were also calibrated. Although the values of these parameters can be found in the literature as a function of surface interface, in this work we had to calibrate them due to the 0D domain used.

In accordance with daily variation of light intensity, simulated curves show a wavelike trend which indicates that model is able to reproduce the effects related to microalgae processes occurring during daytime and at night.

4.6.2 Model limitations and future developments

In the current work a 0D domain was used to represent the microalgae culture in the mesocosm. This approach was adequate for the specific characteristics of our experimental system, since we assumed complete mixing conditions. However, HRAP and photobioreactors are characterized by more complex geometries and hydrodynamic regimes. In those cases both flow and transport equations will have to be coupled to the current model to obtain realistic results.

Light attenuation caused by pigments absorption and by the scattering and the shading effect of the microalgae cells themselves (Sutherland et al., 2014) was not included in the current version of the model. However, numerous models (Quinn et al., 2011, Yuan et al. 2014) have been developed to estimate the gradient of light taking into account the aspects listed above.

Phosphorous species and their effects on biological processes were not included in this model since this component is usually highly available in wastewaters and hence it does not cause any growth-limiting effects on microalgae (Larsdotter, 2006). However, predictions on the rate of removal of phosphorous species will require their inclusion in the model, which in fact can be easily done following the approach of the RWQM1. Once all the above mentioned ameliorations are included in the model, it will be capable to predict biomass production in HRAP and photobioreactors. A following step to fulfil our final objective will be to complete the model with the addition of bacterial processes and to validate the model with other experimental data.

4.7 Conclusions

In this paper a complex biokinetic model to simulate the dynamics of microalgae growth is presented. The biokinetic model is based on RWQM1 formulation and was implemented in COMSOL Multiphysics™ together with several other processes affecting microalgal biomass production in the widest possible range of microalgal cultures.

The most relevant features of the model is the inclusion an allowance for carbon limitation on the growth of microalgae, as well as the dynamic model of photosynthesis and photolimitation and the description of the effect of photorespiration.

The model was calibrated by comparing simulated results to experimental data on microalgae growth in a mesocosm fed with synthetic culture medium (simulating a secondary effluent) for a period of 9 days. Although the results of the calibration indicate that the model was able to accurately reproduce microalgae growth, changes in nutrient concentrations and pH,

the model will require a subsequent verification with other real dataset. The results of this paper have to be considered as a conceptual exercise that could be manually adjusted to fit one single experiment. The value of the exercise is in fact in the development of the equations set and showing that a model based on the set can be run and calibrated to fit a real dataset. Furthermore, the growth of microalgae under natural light/dark cycles and a dynamic model of photosynthesis (PSF) were implemented. The model was able to represent the complex system of photosynthetic growth with simultaneous photoinhibition and photorespiration.

4.8 Appendix

A4.1 Values of biokinetic and physic parameters.

Parameters	Description	Value	Unit	Source
Microalgae processes				
μ_{ALG}	Maximum growth rate of X_{ALG}	1.6	d^{-1}	Calibrated
$k_{\text{resp,ALG}}$	Endogenous respiration constant	0.1	d^{-1}	Reichert et al., 2001
$k_{\text{death,ALG}}$	Decay constant	0.1	d^{-1}	Reichert et al., 2001
$K_{\text{C,ALG}}$	Saturation constant of X_{ALG} on S_{CO_2}	4E-3	gC m^{-3}	Novak and Brune, 1985
$I_{\text{CO}_2,\text{ALG}}$	Inhibition constant of X_{ALG} on S_{CO_2}	120	gC m^{-3}	Silva and Pirt, 1984
$K_{\text{N,ALG}}$	Saturation constant of X_{ALG} on nitrogen sp	0.1	gN m^{-3}	Reichert et al., 2001
$K_{\text{O}_2,\text{ALG}}$	Saturation constant of X_{ALG} on S_{O_2}	0.2	$\text{gO}_2 \text{m}^{-3}$	Reichert et al., 2001
Photorespiration factor				
K_{PR}	Inhibition constant of photorespiration	0.01	–	Assumption
τ	Excess of S_{O_2} coefficient	4	–	Camacho-Rubio et al., 1999
$C_{\text{O}_2}^{\text{SAT}}$	S_{O_2} air saturation	7.19	$\text{gO}_2 \text{m}^{-3}$	Camacho-Rubio et al., 1999
Photosynthetic thermal factor				
T_{OPT}	Optimum temperature for X_{ALG} growth	25	$^{\circ}\text{C}$	Dauta et al., 1990
s	Normalized parameter	13	–	Dauta et al., 1990
Light factor				
α	Activation rate	1.9E-3	$(\mu\text{E m}^{-2})^{-1}$	Wu and Merchuk, 2001
β	Inhibition rate	5.7E-7	$(\mu\text{E m}^{-2})^{-1}$	Wu and Merchuk, 2001
γ	Production rate	0.14	s^{-1}	Wu and Merchuk, 2001
δ	Recovery rate	4.7E-4	s^{-1}	Wu and Merchuk, 2001
Irradiance solar incident				
E_f	Photosynthetic efficiency of solar radiation	1.74	$\mu\text{E J}^{-1}$	Al-Rawahi et al., 2011
κ	Index atmospheric clarity	0.74	–	Al-Rawahi et al., 2011
ζ	Universal solar constant	1353	W m^{-2}	Al-Rawahi et al., 2011
ω	Hour angle	Calculated	$^{\circ}$	Molina-Grima et al., 2001
ω_s	Sunset hour angle	Calculated	$^{\circ}$	Molina-Grima et al., 2001
φ	Latitude	Observed	$^{\circ}$	-
δ	Sun declination	Calculated	$^{\circ}$	Molina-Grima et al., 2001
Transfer of gases to the atmosphere				
$K_{\text{a,O}_2}$	Mass transfer coefficient for S_{O_2}	4	d^{-1}	Calibrated
$K_{\text{a,CO}_2}$	Mass transfer coefficient for S_{CO_2}	0.7	d^{-1}	Calibrated
$K_{\text{a,NH}_3}$	Mass transfer coefficient for S_{NH_3}	0.7	d^{-1}	Calibrated

A4.2 Values of chemical parameters.

Parameters		Equations		
Chemical equilibrium $\text{CO}_2 \leftrightarrow \text{HCO}_3^-$.		$K_{\text{eq},1} = 10^{17.843 - \frac{3404.71}{273.15+T} - 0.032786(273.15+T)}$		
Chemical equilibrium $\text{HCO}_3^- \leftrightarrow \text{CO}_3^{2-}$		$K_{\text{eq},2} = 10^{9.494 - \frac{2902.39}{273.15+T} - 0.02379(273.15+T)}$		
Chemical equilibrium $\text{NH}_4^+ \leftrightarrow \text{NH}_3$		$K_{\text{eq},3} = 10^{2.891 - \frac{2727}{(273.15+T)}}$		
Chemical equilibrium $\text{H}^+ \leftrightarrow \text{OH}^-$		$K_{\text{eq},w} = 10^{-\frac{4470.99}{273.15+T} + 12.0875 - 0.01706(273.15+T)}$		
Kinetics parameters				
$k_{\text{eq},1}$	Dissociation constant of $\text{CO}_2 \leftrightarrow \text{HCO}_3^-$.	10000	d^{-1}	Reichert et al., 2001
$k_{\text{eq},2}$	Dissociation constant of $\text{HCO}_3^- \leftrightarrow \text{CO}_3^{2-}$	1000	d^{-1}	Reichert et al., 2001
$k_{\text{eq},3}$	Dissociation constant of $\text{NH}_4^+ \leftrightarrow \text{NH}_3$	1000	d^{-1}	Reichert et al., 2001
$k_{\text{eq},w}$	Dissociation constant of $\text{H}^+ \leftrightarrow \text{OH}^-$	1000	$\text{g m}^{-1}\text{d}^{-1}$	Reichert et al., 2001

A4.3 Mathematical expressions of the stoichiometric coefficients of each process.

Stoichiometric coefficient	Unit
Growth of X_{ALG} on S_{NH_4}	
$v_{1,1a} = -i_{\text{N,ALG}}$	gN gCOD^{-1}
$v_{4,1a} = 8i_{\text{C,ALG}}/3 + 8i_{\text{H,ALG}} - i_{\text{O,ALG}} - 12i_{\text{N,ALG}}/7$	$\text{gO}_2 \text{gCOD}^{-1}$
$v_{5,1a} = -i_{\text{C,ALG}}$	gC gCOD^{-1}
$v_{8,1a} = i_{\text{N,ALG}}/14$	gH gCOD^{-1}
$v_{10,1a} = 1$	gCOD gCOD^{-1}
Growth of X_{ALG} on S_{NO_3}	
$v_{3,1b} = -i_{\text{N,ALG}}$	gN gCOD^{-1}
$v_{4,1b} = 8i_{\text{C,ALG}}/3 + 8i_{\text{H,ALG}} - i_{\text{O,ALG}} - 20i_{\text{N,ALG}}/7$	$\text{gO}_2 \text{gCOD}^{-1}$
$v_{5,1b} = -i_{\text{C,ALG}}$	gC gCOD^{-1}
$v_{8,1b} = -i_{\text{N,ALG}}/14$	gH gCOD^{-1}
$v_{10,1b} = 1$	gCOD gCOD^{-1}
Endogenous respiration of X_{ALG}	
$v_{1,2} = i_{\text{N,ALG}}$	gN gCOD^{-1}
$v_{4,2} = (i_{\text{O,ALG}}) - 8(i_{\text{H,ALG}}) - 8/3(i_{\text{C,ALG}}) + 12/7(i_{\text{N,ALG}})$	$\text{gO}_2 \text{gCOD}^{-1}$
$v_{5,2} = i_{\text{C,ALG}}$	gC gCOD^{-1}
$v_{8,2} = -1/14(i_{\text{N,ALG}})$	gH gCOD^{-1}
$v_{10,2} = -1$	gCOD gCOD^{-1}
Decay of X_{ALG}	

$v_{1,3} = i_{N,ALG}$	gN gCOD ⁻¹
$v_{4,3} = (i_{O,ALG}) - 8(i_{H,ALG}) - 8/3(i_{C,ALG}) + 12/7(i_{N,ALG})$	gO ₂ gCOD ⁻¹
$v_{5,3} = i_{C,ALG}$	gC gCOD ⁻¹
$v_{8,3} = -1/14(i_{N,ALG})$	gH gCOD ⁻¹
$v_{10,3} = -1$	gCOD gCOD ⁻¹
Chemical equilibria CO₂ ↔ HCO₃⁻	
$v_{5,4} = -1$	gC gC ⁻¹
$v_{6,4} = 1$	gC gC ⁻¹
$v_{8,4} = 1/12$	gH gC ⁻¹
Chemical equilibria HCO₃⁻ ↔ CO₃²⁻	
$v_{6,5} = -1$	gC gC ⁻¹
$v_{7,5} = 1$	gC gC ⁻¹
$v_{8,5} = 1/12$	gH gC ⁻¹
Chemical equilibria NH₄⁺ ↔ NH₃	
$v_{1,6} = -1$	gN gN ⁻¹
$v_{2,6} = 1$	gN gN ⁻¹
$v_{8,6} = 1/14$	gH gN ⁻¹
Chemical equilibria H⁺ ↔ OH⁻	
$v_{8,7} = 1$	gH gH ⁻¹
$v_{9,7} = 1$	gH gH ⁻¹
Oxygen transfer to the atmosphere	
$v_{4,O_2} = 1$	—
Carbon dioxide transfer to the atmosphere	
$v_{5,CO_2} = 1$	—
Ammonia transfer to the atmosphere	
$v_{2,NH_3} = 1$	—

A4.4 Values of fraction of carbon, hydrogen, oxygen and nitrogen in microalgae biomass.

Parameter	Description	Value	Unit	Source
Fractions of microalgal biomass				
$i_{C,ALG}$	Fraction of carbon in microalgae	0.387	gC gCOD ⁻¹	Reichert et al., 2001
$i_{H,ALG}$	Fraction of hydrogen in microalgae	0.075	gH gCOD ⁻¹	Reichert et al., 2001
$i_{O,ALG}$	Fraction of oxygen in microalgae	0.538	gO ₂ gCOD ⁻¹	Reichert et al., 2001
$i_{N,ALG}$	Fraction of nitrogen in microalgae	0.065	gN gCOD ⁻¹	Reichert et al., 2001

5

Sensitivity analysis

This chapter is based on the article:

- ❖ A. Solimeno, R. Samsó, J. García. 2015. Parameter sensitivity analysis of a mathematical model to simulate microalgae growth. *Algal Research*, 15:217–223.

5.1 Introduction

Full-scale microalgae cultures are used to produce a variety of compounds for different economic sectors such as: aquaculture and animal feed; human nutrition; cosmetics and nutraceuticals; and pharmaceuticals (Ación et al., 2013; Spolaore et al., 2016). Moreover, mixed cultures of microalgae and bacteria are being used for wastewater treatment in ways that may convert “conventional wastewater treatment plants” into “resource recovery plants”, able to produce purified water and by-products such as biodiesel (Brennan and Owende, 2010; Chisti, 2007).

A thorough understanding of the internal functioning of microalgae-based technologies is essential to predict performance and update design guidelines. The physical, chemical, and biological processes that occur in microalgae cultures systems are difficult to study because most of them take place simultaneously and are strongly interdependent. In addition, the rates of many of these processes depend on environmental variables such as light intensity and temperature. In the case of wastewater treatments with mixed cultures, it is very challenging to understand a microbiological system where metabolic processes such as photoautotrophy and heterotrophy coexist.

The increasing number of applications of microalgae-based technologies has encouraged the development of new mathematical models to study the main processes, factors and variables that influence microalgae growth in different types of cultures, including wastewaters. In the last decade, an array of mathematical models that predict microalgae biomass production has been developed (Bernard et al., 2009; Packer et al., 2011). One general limitation of these models is the use of very few parameters to describe the inherent complexity of algal cultures, especially in the particular case of microalgae grown in wastewaters, where carbon and/or nitrogen limitation can be significant.

Recently, a complex mechanistic model to simulate microalgae growth in various cultures was developed (Chapter 4; Solimeno et al., 2015). This model is a part of a more ambitious project through which we intend to

develop a complete model to simulate mixed cultures of microalgae and bacteria treating wastewater (e.g. high rate algal ponds). Therefore, in this first version of the model, only microalgal processes were included, while bacterial processes were not taken into account.

River Water Quality Model 1 (RWQM1) of the International Water Association (Reichert et al., 2011) was used as a reference for the new model. Carbon-limited microalgae growth, transfer of gases to the atmosphere and photorespiration, photosynthesis kinetics and photoinhibition were not included in RWQM1, but were considered as candidate parameters for new model. Furthermore, we felt that growth of microalgae would be dependent on light intensity, temperature, and availability of nitrogen and carbon species.

The model was calibrated using experimental data from a case study based on the cultivation of different microalgae species in a culture medium simulating treated urban wastewater (secondary effluent).

Sensitivity analysis is an important step during model development, promotes better understanding of the complex interactions of engineered systems (Sin and Gernaey, 2009), and can be an important tool for building a mechanistic model for microalgae growth. With this in mind, the aim of the present study was to identify the parameters that have the greatest impact on a new model for microbial culture. Sensitivity analysis of whole set of model parameters (31) is quite an unattainable objective unless high-end computational facilities are available. For this reason, a subset of the most influential parameters on output model was analysed. These subset parameters were selected because they turned out the parameters that most influenced the results obtained with the model and are therefore likely to be changed during calibration.

The Morris method of Elementary Effects (EEs) (Morris, 1991) was selected over other commonly used global sensitivity analysis methods (Saltelli et al., 2000) based on previous work by Ruano et al. 2011 for screening the most influential parameters in wastewater treatment plant models. The Morris method corresponds to a typically randomized One-At-a-Time (OAT) approach. OAT designs are an efficient technique in which the factors are

varied individually by the same relative amount around the nominal point (Summer et al., 2012). The basic idea is to reproduce individually randomized experiments that evaluate the elementary effects along trajectories obtained by changing one parameter at a time.

The work described here was necessary to complete the model previously described in Chapter 4. Little information was available for several additional parameters related to microbial growth that were thought to be necessary for development of this model.

After model calibration was optimized, the sensitivity analysis described here promoted interpretation of model outputs, and refined our understanding of which parameters were required. As a result, the model provided new insight into the functioning of microalgae cultures, and promoted investigation of the many factors that may influence microalgae growth.

5.2 Material and methods

5.2.1 Theoretical background

The Elementary Effects method represents an effective screening strategy to identify the most important factors in highly parametrized models (Campolongo et al., 2011), and is summarized here.

Here is presented a summary of the method following the explanation by Campolongo et al. 1999.

Suppose a general model, the model output $y = y(\mathbf{x})$ is a scalar function of k -dimensional factors (parameters and input values) constituting a general vector \mathbf{x} that identify an exact point in the experimental domain Ω of k -dimensional factor, which corresponds to an exact value of y . The vector $\mathbf{x} = \{x_1, x_2, \dots, x_k\}$ has k components, x_i , each of which can be take p level in the set $\{0, 1/(p-1), 2/(p-1), 3/(p-1), \dots, (p-2)/(p-1), 1\}$. This assume that range of any k -dimensional factors has been scaled to the set levels $\{0, 1/(p-1), 2/(p-1), \dots, 1\}$. The region of experimentation Ω is thus a k -dimensional p -level grid.

Morris defines the elementary effect of the i^{th} input parameter at given value of $\mathbf{x} \in \Omega$ (Morris, 1991):

$$EE_i(\mathbf{x}) = [y(x_1, x_2, \dots, x_{i-1}, x_{i+\Delta}, x_{i+1}, \dots, x_k) - y(\mathbf{x})]/\Delta \quad (5.1)$$

where Δ is the magnitude of step length that can be assumed value in the set $\{1/(p-1), \dots, 1-1/(p-1)\}$ so that $\mathbf{x}+\Delta$ is still in Ω .

5.2.2 Trajectory construction

The basic principle of Morris's method (Morris, 1991) was applied to build r random orientation in the region of experimentation, Ω , constituted by p levels. The magnitude of the experiment step, Δ , is a multiple of $1/(p-1)$. It will be convenient to restrict attention to the case in which p is even and $\Delta = p/[2(p-1)]$ for more economical design construction (Alam et al., 2004).

A base value, \mathbf{x}^* , is randomly chosen from the vector \mathbf{x} values ranging from 0 to $1-\Delta$, so that increasing by Δ one of the k components, the vector $\mathbf{x}^{(1)}$ that it still in Ω .

After calculating the elementary effect of the i^{th} component of $\mathbf{x}^{(1)}$ following the Eq. 5.1, $k+1$ new sampling points are selected such that two consecutive points differ in just one component and the elementary effect for each factor are calculated.

The vector so created $\mathbf{x}^{(1)}, \mathbf{x}^{(2)}, \dots, \mathbf{x}^{(k+1)}$ define a trajectory in the parameter space, and an orientation matrix B^* .

The final trajectory matrix, B^* , as given in the following equation is:

$$B^* = (J_{m,1} \mathbf{x}^* + \Delta B')P^* \quad (5.2a)$$

$$B^* = (J_{m,1} \mathbf{x}^* + (\Delta/2)[(2B - J_{m,k})D^* + J_{m,k}])P^* \quad (5.2b)$$

where

- J is $(m \cdot 1)$ unit matrix;

- D^* is a k -dimensional diagonal matrix which the diagonal elements may be take a value of +1 of -1 with the same probability (King and Perrera, 2013).

- P^* is a k -dimensional matrix where each column and row contains only single element equal to 1 and the rest 0's. The random location of the 1's changes the order that the variables are perturbed, and increases the number of trajectories (King and Perrera, 2013).

To determine the random directions of the trajectory the matrix B' was created:

$$B' = \frac{1}{2} [(2B - J_{m,k}) D^* + J_{m,k}] \quad (5.3)$$

where:

- J is $(m \cdot k)$ unit matrix with $m=k+1$;

- B is a random $(m \cdot k)$ lower left triangle unit matrix with two rows that differ in only one element;

The design matrix X is constructed by changing the base value \mathbf{x}^* , or the random selected matrices B, D^* and P^* r times. The total number of simulations (N) needed in the Morris's method is $N = r(k + 1)$.

5.2.3 Morris's method indices

To obtain a non-dimensional measure in this study, the scaled elementary effects $SEE_{i,j}$ proposed by Sin et al. 2009 were applied. The unscaled elementary effect $EE_{i,j}$ given by Eq. (5.1) yields an incorrect classification of parameters for the model, especially when model outputs differ by an order of magnitude (Sin et al., 2009; Smith, 2014). This condition justifies the use of the scaled elementary effects:

$$SEE_{i,j}(\mathbf{x}): [y_j(x_1, x_2, \dots, x_{i-1}, x_{i+\Delta}, x_{i+1}, \dots, x_k) - y_j(\mathbf{x})] / \Delta \cdot \sigma_i / \sigma_y \quad (5.4)$$

where σ_i and σ_y are the standard deviations of the parameters x_i and model outputs y_j . The finite distribution of the $SEE_{i,j}$ due to the i^{th} input variable on j^{th} model output is denoted as $F_{i,j}$.

The method proposed by Morris provides a global sensitivity measure (mean and standard deviation) of the finite distribution of $p^{k-1} [p - \Delta(p-1)]$ elementary effects associated with each input (Alam et al., 2004). Each $F_{i,j}$ contains r independent scaled elementary effects built by sampling \mathbf{x} from Ω . The mean μ Eq. (5.5) and standard deviation σ Eq. (5.6) of the distribution $F_{i,j}$ provide an approximate global sensitivity measure. Mean and standard deviation carried out information about the impact of the i^{th} input factor on the output j^{th} and the dependence of its sensitivity on the values of other parameters (King and Perrera, 2013).

A high mean, μ , indicates a parameter with an important overall effect on the output. A high standard deviation, σ , indicates a parameter with a non-linear effect on the output, or one which interacts with other parameters (Campolongo and Braddock, 1999). Campolongo et al. 2007, modified the calculation of μ , denoted μ^* Eq. (5.7), when the distribution $F_{i,j}$ is non-monotonic.

$$\mu_i = \frac{\sum_{n=1}^r SEE_n}{r} \quad (5.5)$$

$$\sigma_i = \sqrt{\frac{1}{r} \sum_{n=1}^r (SEE_n - \mu_i)^2} \quad (5.6)$$

$$\mu_i^* = \frac{\sum_{n=1}^r |SEE_n|}{r} \quad (5.7)$$

Based on the values of μ_i^* and σ_i the Morris method identifies factors having: negligible effects, linear and additive effects, or nonlinear or

interactions effects (Santiago et al., 2012). Fig. 5.1 illustrates this interpretation of the values μ_i^* and σ_i .

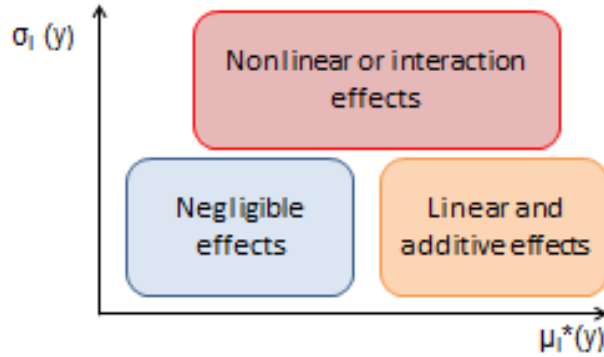


Figure 5.1 Schematic representation of theoretical disposition of means μ_i^* and standard deviations σ_i of the effects distribution (Adapted from Santiago et al. 2012).

To identify the most influential parameters, these sensitivity measures were interpreted using the graphical approach proposed by Morris, 1991. In this approach, the value of $\mu_{i,j}$ and $\sigma_{i,j}$ obtained for all the $F_{i,j}$ distributions are displayed together with two lines corresponding to $\mu_{i,j} = \pm 2SEM_{i,j}$, where $SEM_{i,j}$ represents the standard error of the mean that can be estimated as $SEM_{i,j} = \sigma_{i,j}/\sqrt{r}$. Parameters that lie inside the “wedge” created by the two lines are deemed as non-influential or negligible. Parameters that lie outside the wedge have significant effect on the output (Morris, 1991; Sin et al., 2009).

5.2.4 Parameter selection, additional parameterization, and sensitivity analysis: computational experiment

Parameter selection

The mechanistic model developed by the authors includes a total of 31 parameters (Solimeno et al., 2015). The values of 16 parameters were taken from RWQM1 (Reichert et al., 2001). Because RWQM1 does not include the parameters related to transfer of gases to the atmosphere, temperature, photorespiration, or carbon limitation on microalgae growth; values of these

parameters were obtained from other literature (Dauta et al., 1990; Novak and Brune, 1985; Silva and Pirt, 1984).

The subset parameters evaluated were: the maximum specific rate of microalgae growth (μ_{ALG}) and those related to the transfer of gases to the atmosphere (oxygen: K_{a,O_2} , carbon dioxide: K_{a,CO_2} and ammonia: K_{a,NH_3}). The effects of these parameters were investigated respect to the model outputs (Table 5.1). Note that these four parameters were selected because a global sensitivity analysis of whole set of model parameters (31) is quite an unattainable objective unless high-end computational facilities are available. These four demonstrated to be the parameters that most influenced the results obtained with the model and are therefore likely to be changed during calibration (Solimeno et al., 2015). The global sensitivity analysis was carried out using the same initial conditions, parameters value and geometry (Solimeno et al. 2015).

Table 5.1 List of model outputs.

Model outputs	Description
X_{ALG}	Concentration of microalgae biomass. It increases with growth processes and decreases by endogenous respiration and inactivation.
$S_{NH_3} + S_{NH_4}$	Concentration of nitrogen present in the water as ammonium and ammonia. Nitrogen as ammonium (S_{NH_4}) is produced through the processes of endogenous respiration and through inactivation of microalgae. It is consumed through the growth of microalgae. Nitrogen in form of ammonia (S_{NH_3}) is in chemical equilibrium with ammonium (S_{NH_4}). Its concentration decreases by volatilization to the atmosphere.
S_{NO_3}	Nitrogen available as nitrate. It is consumed by microalgae (X_{ALG}).
$S_{HCO_3} + S_{CO_2}$	Concentration of carbon as carbon dioxide and bicarbonate. Carbon as carbon dioxide (S_{CO_2}) is consumed by microalgae and is produced through the processes of endogenous respiration and inactivation. Carbon as bicarbonate (S_{HCO_3}) is in chemical equilibrium with carbon dioxide (S_{CO_2}) and carbonate (S_{CO_3}).
S_{CO_3}	Carbon in the form of dissolved carbonate. It is in chemical equilibrium with bicarbonate (S_{HCO_3}) and carbon dioxide (S_{CO_2}). Carbonate is not used by microalgae as carbon source.

5.2.5 Implementation of the Morris's method

The software used for the sensitivity analysis was COMSOL Multiphysics™ v4.3b. As noted above, the total number of simulations (N) needed in the Morris's method is $N = r(k + 1)$, and previous studies have demonstrated that using $p = 4$ levels and $r = 10$ produces satisfactory results (Campolongo et al., 1999). Therefore, we used $k = 4$ uncertain parameters for the screening, and $r = 10$ repetitions of elementary effects to obtain a good balance between computational cost and results robustness. Thus, fifty-five simulations were required. Processing time was determined to be 16 seconds per simulation (PC computer, 3.4 GHz Intel Core i7_3770 processor).

The elementary effects were calculated using Eq. 5.4, which provides random observations of the distribution function F_{ij} .

The parameters of the experiment were set to $p = 4$, $\Delta = p/[2(p-1)] = 2/3$ and $r = 10$. Four different levels ($p = 4$) for each factor were considered. So, the p values in the set $\{0, 1/(p-1), 2/(p-1), \dots, 1\}$ would be equivalent to $\{0, 1/3, 2/3, 1\}$ in our experiment.

Following Morris's method, 10 orientation matrices were generated, and the respective elementary effects for 4 different factors per orientation matrix were estimated from the model output.

The first base values $\mathbf{x}^* = \{0, 1/3, 0, 1/3\}$ were randomly selected from the possible combinations of $\mathbf{x} = \{0, 1/3, 2/3, 1\}$ ranging from 1 to $1 - \Delta$. After that the matrices presented in Eq. 5.2 and 5.3 were defined:

$$\mathbf{B}_{(5,4)} = \begin{pmatrix} 0 & 0 & 0 & 0 \\ 1 & 0 & 0 & 0 \\ 1 & 1 & 0 & 0 \\ 1 & 1 & 1 & 0 \\ 1 & 1 & 1 & 1 \end{pmatrix} \quad (5.8)$$

$$\mathbf{J}_{(5,4)} = \begin{pmatrix} 1 & 1 & 1 & 1 \\ 1 & 1 & 1 & 1 \\ 1 & 1 & 1 & 1 \\ 1 & 1 & 1 & 1 \\ 1 & 1 & 1 & 1 \end{pmatrix} \quad (5.9)$$

$$D^*_{(4,4)} = \begin{pmatrix} 1 & 0 & 0 & 0 \\ 0 & -1 & 0 & 0 \\ 0 & 0 & 1 & 0 \\ 0 & 0 & 0 & -1 \end{pmatrix} \quad (5.10)$$

$$P^*_{(4,4)} = \begin{pmatrix} 1 & 0 & 0 & 0 \\ 0 & 0 & 1 & 0 \\ 0 & 1 & 0 & 0 \\ 0 & 0 & 0 & 1 \end{pmatrix} \quad (5.11)$$

The modified sampling matrix B' is shown in below.

$$B'_{(5,4)} = \begin{pmatrix} 0 & 1 & 0 & 1 \\ 1 & 1 & 0 & 1 \\ 1 & 0 & 0 & 1 \\ 1 & 0 & 1 & 1 \\ 1 & 0 & 1 & 0 \end{pmatrix} \quad (5.12)$$

B' is then multiplied by $\Delta = 2/3$ defined earlier, to create the following matrix:

$$\Delta B'_{(5,4)} = \begin{pmatrix} 0 & 2/3 & 0 & 2/3 \\ 2/3 & 2/3 & 0 & 2/3 \\ 2/3 & 0 & 0 & 2/3 \\ 2/3 & 0 & 2/3 & 2/3 \\ 2/3 & 0 & 2/3 & 0 \end{pmatrix} \quad (5.13)$$

Matrices D^* and P^* define the orientation of trajectory (for $k = 4$, there are 2^4 different possibilities for D^* each one with probability $1/16$ and $4! = 24$ possibilities for P^* each one with probability $1/24$). Then B^* becomes:

$$J_{(4,1)}(\mathbf{x}^* + \Delta B')^* P^* = \left\{ \begin{pmatrix} 1/3 & 0 & 1/3 & 0 \\ 1/3 & 0 & 1/3 & 0 \\ 1/3 & 0 & 1/3 & 0 \\ 1/3 & 0 & 1/3 & 0 \\ 1/3 & 0 & 1/3 & 0 \end{pmatrix} + \begin{pmatrix} 0 & 2/3 & 0 & 2/3 \\ 2/3 & 2/3 & 0 & 2/3 \\ 2/3 & 0 & 0 & 2/3 \\ 2/3 & 0 & 2/3 & 2/3 \\ 2/3 & 0 & 2/3 & 0 \end{pmatrix} \right\} \cdot \begin{pmatrix} 1 & 0 & 0 & 0 \\ 0 & 0 & 1 & 0 \\ 0 & 1 & 0 & 0 \\ 0 & 0 & 0 & 1 \end{pmatrix}$$

$$= \begin{pmatrix} 1/3 & 2/3 & 1/3 & 2/3 \\ 1 & 2/3 & 1/3 & 2/3 \\ 1 & 0 & 1/3 & 2/3 \\ 1 & 0 & 1 & 2/3 \\ 1 & 0 & 1 & 0 \end{pmatrix} \cdot \begin{pmatrix} 1 & 0 & 0 & 0 \\ 0 & 0 & 1 & 0 \\ 0 & 1 & 0 & 0 \\ 0 & 0 & 0 & 1 \end{pmatrix} \quad (5.14)$$

Finally, matrix B^* becomes

$$B^* = \begin{pmatrix} 1/3 & 1/3 & 2/3 & 2/3 \\ 1 & 1/3 & 2/3 & 2/3 \\ 1 & 1/3 & 0 & 2/3 \\ 1 & 1 & 0 & 2/3 \\ 1 & 1 & 0 & 0 \end{pmatrix} \quad (5.15)$$

Each row of B^* design the factorization of k parameters. Applying Eq. (5.4), an elementary effect will be estimated for each input factor. In order to get an estimation of the distribution of elementary effects for each input factor, the process was repeated $r = 10$ times. As a result, the design matrix for the entire experiment becomes:

$$X = \begin{pmatrix} B_1^* \\ B_2^* \\ \dots \\ B_{10}^* \end{pmatrix} \quad (5.16)$$

In supplementary material readers can find an Excel file which contains a simplified numerical example of trajectory construction of Morris method. In this example only 2 trajectories out of the 10 selected in this paper are described to make it easier.

5.3 Results

The Morris's method results were evaluated by comparing the means and standard deviations of the distribution function $F_{i,j}$ for each input. Table 5.2 shows the resulting sensitivity measures ($\mu_{i,j}$, $\mu_{i,j}^*$ and $\sigma_{i,j}$) of input parameters (μ_{alg} , K_{a,O_2} , K_{a,CO_2} , K_{a,NH_3}) for each output variable analysed at $r = 10$.

Means and standard deviations of the 4 input parameters were plotted in Fig. 5.2 for the 6 output variables considered (X_{ALG} , pH, $(S_{NH_3}-S_{NH_4})$, S_{NO_3} , $(S_{HCO_3^-}-S_{CO_2})$, S_{CO_3}).

In addition there are two lines corresponding to $\mu_{i,j} = \pm 2SEM_{i,j}$ to facilitate the interpretation of the results. Parameters that lie inside the wedge obtained by the two lines are deemed as non-influential or negligible. Otherwise, if the parameters lie outside the wedge, it indicates to have significant effect on the output (Morris, 1991; Sin et al., 2009).

Furthermore, Fig. 5.3 includes the mean effect measures $\mu_{i,j}^*$ and the standard deviations $\sigma_{i,j}$ of the distribution of input parameters on model outputs, and illustrates the linearity and interaction effects of the parameters.

Table 5.2 Sensitivity measures of input parameter at $r = 10$ for each output variables.

X_{alg}				pH				$S_{NH3}+S_{NH4}$			
Parameters	μ	σ	μ^*	Parameters	μ	σ	μ^*	Parameters	μ	σ	μ^*
μ_{alg}	0.876	0.128	0.876	μ_{alg}	0.981	0.121	0.981	μ_{alg}	0.141	1.185	1.039
$K_{a,O2}$	0.073	0.116	0.079	$K_{a,O2}$	0.037	0.153	0.040	$K_{a,O2}$	-0.392	1.006	0.920
$K_{a,CO2}$	-0.040	0.093	0.068	$K_{a,CO2}$	-0.075	0.071	0.075	$K_{a,CO2}$	-0.592	1.218	1.142
$K_{a,NH3}$	0.034	0.254	0.152	$K_{a,NH3}$	0.011	0.080	0.050	$K_{a,NH3}$	0.029	1.694	1.700
S_{NO3}				$S_{HCO3}+S_{CO2}$				S_{CO3}			
Parameters	μ	σ	μ^*	Parameters	μ	σ	μ^*	Parameters	μ	σ	μ^*
μ_{alg}	-0.827	0.064	0.827	μ_{alg}	-1.548	2.790	1.548	μ_{alg}	-0.223	1.454	1.446
$K_{a,O2}$	-0.069	0.022	0.075	$K_{a,O2}$	-0.002	0.002	0.002	$K_{a,O2}$	-0.414	0.610	0.487
$K_{a,CO2}$	0.050	0.082	0.065	$K_{a,CO2}$	-0.098	0.322	0.116	$K_{a,CO2}$	1.049	0.757	1.049
$K_{a,NH3}$	-0.078	0.227	0.179	$K_{a,NH3}$	-0.001	0.003	0.004	$K_{a,NH3}$	0.309	1.254	1.124

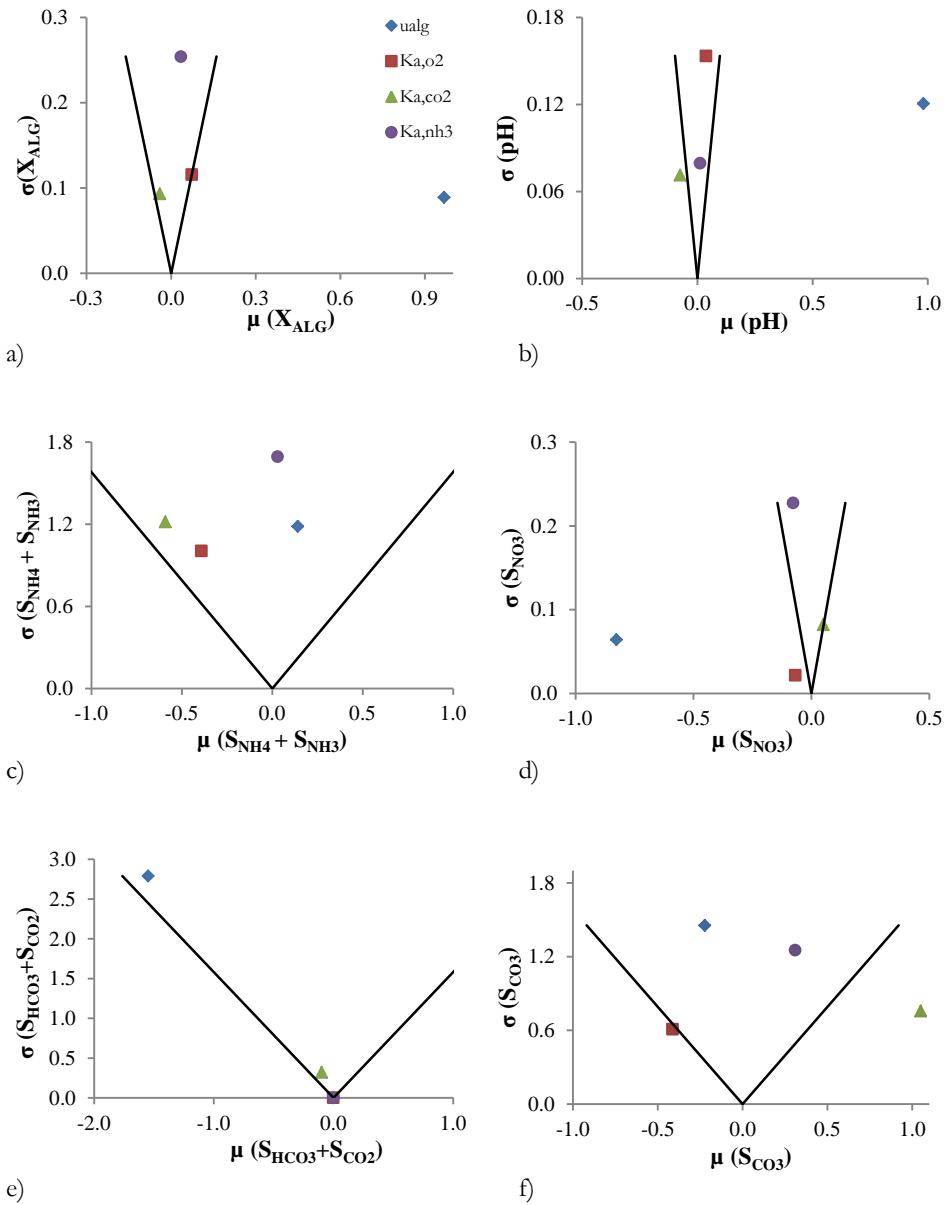


Figure 5.2 Sensitivity measures of the distribution of elementary effects of the inputs on the model outputs a) X_{ALG} , b) pH , c) $S_{NH3}+S_{NH4}$, d) S_{NO3} , e) $S_{HCO3}+S_{CO2}$, f) S_{CO3} . Lines correspond to $\mu_i = \pm 2SEM_i$. Figure legends for graphics shown in the upper right graph.

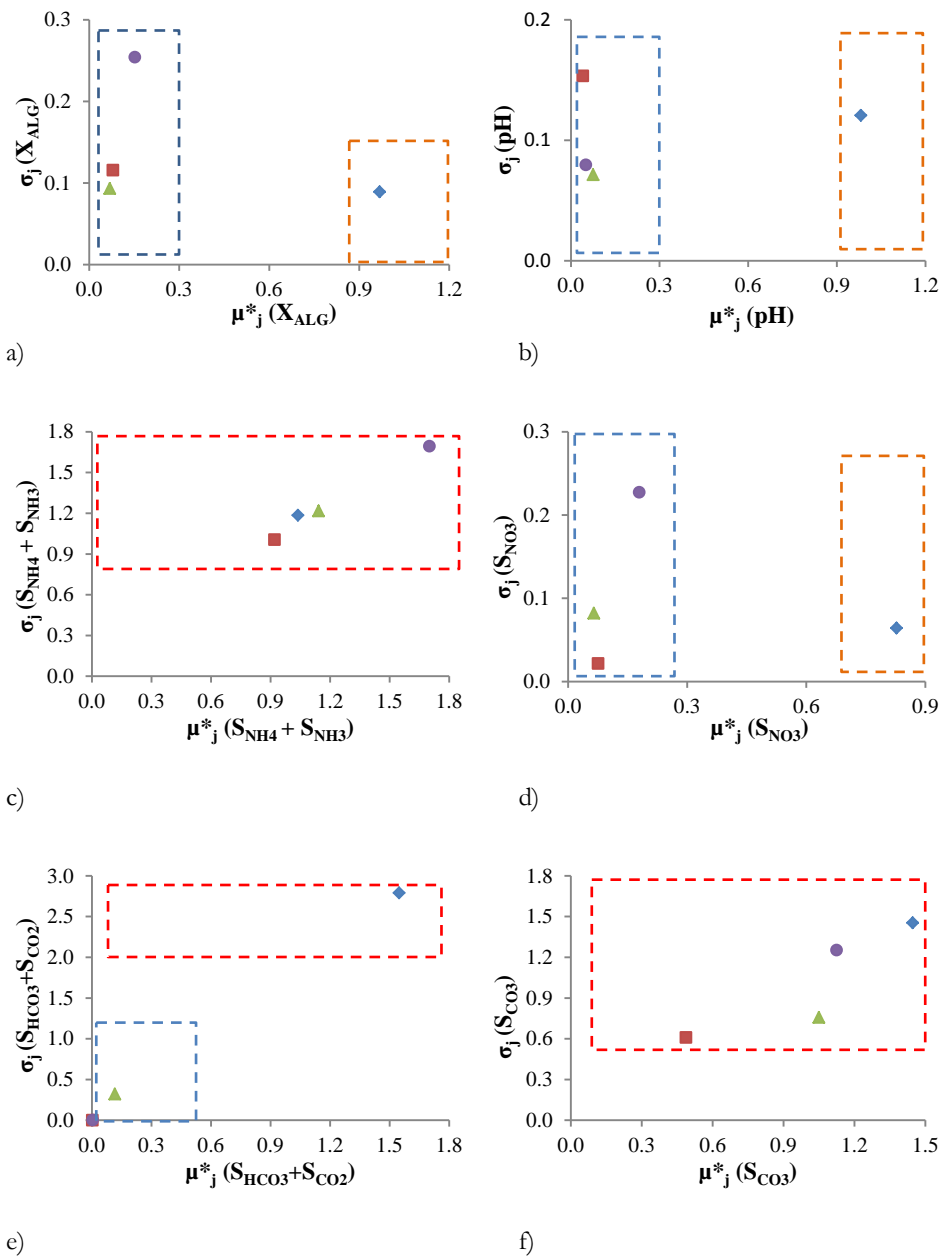


Figure 5.3 Sensitivity measures $\mu_{i,j}^*$ versus $\sigma_{i,j}$ for the model outputs a) X_{ALG} , b) pH, c) $S_{NH3}+S_{NH4}$, d) S_{NO3} , e) $S_{HCO3}+S_{CO2}$, f) S_{CO3} . Dotted lines represent the theoretical distribution of effects: negligible effects (blue dotted line), non-linear effects (red dotted line) and linear effect (orange dotted line).

5.4 Discussion

Despite the mechanistic model includes more than 31 parameters, only the sensitivity related to the maximum specific growth rate of microalgae (μ_{ALG}) and the parameters of gas transfer to the atmosphere (K_{a,O_2} , K_{a,CO_2} and K_{a,NH_3}) were analysed the ranges of those obtained from literature were totally unknown unlike the parameters obtained from RWQM1. Moreover, RWQM1's parameters have already been subjected to sensitivity analyses (Reichert and Vanrolleghem, 2001).

From the graphical Morris approach (Fig. 5.2) it was clear that the maximum specific growth rate of microalgae (μ_{ALG}) had the greatest influence on microalgae biomass output (X_{ALG}) (Fig. 5.2a).

This parameter was distributed outside of the “wedge” formed by $\mu_{i,j} = \pm 2 SEM_{i,j}$, indicating that model output was very sensitive to this parameter. Altering this parameter by $\pm 60\%$ caused a change in microalgae concentration of $\pm 32\%$. Nitrate and pH were also very sensitive to microalgae growth rate.

The model was not very sensitive to the transference of gases to the atmosphere. The majority of these parameters (K_{a,O_2} , K_{a,CO_2} and K_{a,NH_3}) were distributed inside the wedge formed by $\mu_{i,j} = \pm 2 SEM_{i,j}$, indicating that their effects on model output were negligible (Fig. 5.2b-e). Only the transfer of carbon dioxide (K_{a,CO_2}) had a clear effect on carbonate in the model output (Fig. 5.2f).

To evaluate with more details the effects of these parameters on model outputs, the values of the sensitivity measures $\mu_{i,j}^*$ and $\sigma_{i,j}$ were reported in Fig. 5.3. Maximum specific growth rate of microalgae (μ_{ALG}) was the most sensitive input parameter exhibiting a linear relationship with microalgae (X_{ALG}), pH and nitrate (S_{NO_3}), indicated by high $\mu_{i,j}^*$ and low $\sigma_{i,j}$ (Fig. 5.3a-d). Otherwise, μ_{ALG} exhibited non-linear effects with nitrogen as ammonium and ammonia, and with (dissolved) carbon species (Fig. 5.3c-f).

It is important to note that these simulation outputs were sensitive to pH, which in turn was influenced by K_{a,NH_3} and K_{a,CO_2} . Thus the transfer of

ammonia (K_{a,NH_3}) and carbon dioxide (K_{a,CO_2}) presented a non-linear or interaction effect on nitrogen ($S_{NH_3}+S_{NH_4}$) uptake and carbonate concentrations.

The effect of growth rate on pH and nitrate in the model was mediated through microalgae biomass (X_{ALG}): growth of microalgae consumes substrates (nitrogen and inorganic carbon) and releases hydroxide ions that increase pH. Similarly, the concentration of nitrate depended exclusively on microalgae uptake, in contrast with ammonia which was also affected by transfer to the atmosphere.

Although parameters related to dissolved carbon were also influenced by values of other parameters (i.e., K_{a,O_2} , K_{a,CO_2} and K_{a,NH_3}) through interactions effects, the effects of the transfer of gases to the atmosphere (K_{a,O_2} , K_{a,CO_2} and K_{a,NH_3}) directly on model outputs were typically negligible. The exceptions to this included transfer of ammonia (K_{a,NH_3}) and carbon dioxide (K_{a,CO_2}) with respect to carbonate and ammonium and ammonia concentrations, respectively; these were characterized by high mean and standard deviations outputs.

The value ($\mu_{ALG} = 1.5 [d^{-1}]$) used during the calibration of the model was in agreement within literature ranges $[0.4-2 d^{-1}]$ (Reichert et al., 2001). Despite model results obtained during the calibration, the results from sensitivity analysis have shown that the model was not sensitive to the parameters related to the transfer of gases to the atmosphere (K_{a,O_2} , K_{a,CO_2} and K_{a,NH_3}). The range of these parameters for 0D geometry is not known. Because transfer of gases to atmosphere depends on the dimensions of the air-water interface, we initially applied a range of $144-408 d^{-1}$ for 2D geometry (Powell et al., 2009).

In this case, model outputs were very sensitive to parameters related to transfer of these gases to the atmosphere. Subsequently, we determined an optimal range $[0.7-4 d^{-1}]$ for 0D geometry during model calibration. However, as a result of the present study, we found that the parameters related to the transfer of gases to the atmosphere may vary +/- 60% of the optimal range with negligible effect on model outputs.

5.5 Conclusions

A sensitivity analysis of the maximum specific rate of microalgae growth (μ_{ALG}) and the parameters related to the transfer of gases to the atmosphere (K_{a,O_2} , K_{a,CO_2} , K_{a,NH_3}) was conducted on a mechanistic model developed to simulate microalgae growth in wastewater. The Morris method was used to identify the sensitivity of model outputs to 4 parameters calibrated during model building.

The results of the sensitivity analysis indicated that model outputs were especially sensitive to the maximum specific growth rate of microalgae (μ_{ALG}), while the parameters related to transfer of ammonia (K_{a,NH_3}) and carbon (K_{a,CO_2}) to the atmosphere had a non-linear effect on the nitrogen uptake and carbonate concentrations. Thus, maximum specific growth rate of microalgae (μ_{ALG}) must be calibrated with great accuracy. The results of this paper have to be considered as a conceptual exercise that has to be verified experimentally.

6

Application of the microalgae model to photobioreactors

This chapter is based on the article:

- ❖ A. Solimeno, F. Gabriel Acién, J. García. 2017. Mechanistic model for design, analysis, operation and control of microalgae cultures: calibration and application to tubular photobioreactors. *Algal research* 21, 236-246.

6.1 Introduction

Industrial production of microalgae can be accomplished in open or closed photobioreactors. Open systems are shallow channels in the shape of race tracks (raceway reactors) and have been extensively studied in the past (Camacho-Rubio et al., 1999; Fernández et al., 2014). Though open photobioreactors represent an efficient economic solution in front of closed photobioreactors, they can be easily contaminated by microorganisms and difficult to control. These disadvantages make closed photobioreactors more suitable when high-value products are the target of the culture. Closed systems strictly control chemical, physical and biological factors and can improve conditions for microalgae growth by optimizing light absorption due to turbulent conditions in the culture (Camacho-Rubio et al., 1999; Chisti, 2007; Craggs et al., 2011, Ugwu et al., 2008; Wang et al., 2012).

Closed photobioreactors (as well as open raceways) are sensitive to carbon limitations and pH variations that could limit photosynthesis and therefore biomass production (Fernández et al., 2012). Carbon and pH limitations can be corrected by supplying carbon dioxide (CO₂) in order to maintain high photosynthesis rates and pH control. However the two most critical issues of closed photobioreactors are the risk of overheating and their potential for oxygen accumulation and subsequent growth inhibition (Molina-Grima et al., 2001). To prevent overheating, closed photobioreactors often require cooling as well as degasser systems (Weissmand and Goebel, 1987). Concentrations of dissolved oxygen (DO) in the culture above 250% air saturation can dangerously inhibit microalgae activity (Costache et al., 2013).

Over the last few decades, mathematical models have proven to be useful tools for the design, analysis, operation and control in multiple engineering problems (Bitog et al., 2011). Nowadays, models have become essential tools for understanding complex processes, such as those occurring in photobioreactors. In the case of microalgae cultures, models are less developed than those seen in other fields. When models contain too few parameters, they risk the capability of not capturing the complexity of microalgae cultures in long-term scenarios, and therefore can be unreliable. Having this in mind, in Chapter 4 was developed a complete mechanistic

mathematical model that includes crucial physical and biokinetic processes that describe microalgae growth in different types of cultures, particularly in wastewater (where growth is controlled by carbon and nitrogen limitations). This model was calibrated with data from a complete stirred culture fed with simulated treated wastewater using a 0D domain (Chapter 4; Solimeno et al., 2015). A global sensitivity analysis was carried out using the same set of data (Chapter 5; Solimeno et al., 2016). In the present paper we intend to go beyond our previous work, calibrating the model with data from two different pilot scale tubular closed photobioreactors fed with different types of medium culture. In this present case, a 2D domain, which represents the hydrodynamics of the system (i.e., transport of diluted species and mass transfer phenomena), is coupled with the previous mechanistic model (Chapter 5; Solimeno et al., 2016). The resulting model has been implemented into the COMSOL Multiphysics™ software, which solves equations using the finite elements method (FEM).

The aim of the present study is to calibrate the new and more complex mechanistic model described in Chapter 4 using experimental data from two different tubular photobioreactors. The potential of the model is demonstrated by means of practical study cases in which we simulate oxygen concentrations (the most critical growth inhibition factor of closed photobioreactors) and predict microalgae production as a function of temperature and light intensity. Simulations show the potential of photobioreactor configurations to optimize microalgae production. The overall objective of this model is to become a reference to simulate physical, chemical and biokinetic microalgae processes in different types of photobioreactors fed with different types of medium cultures.

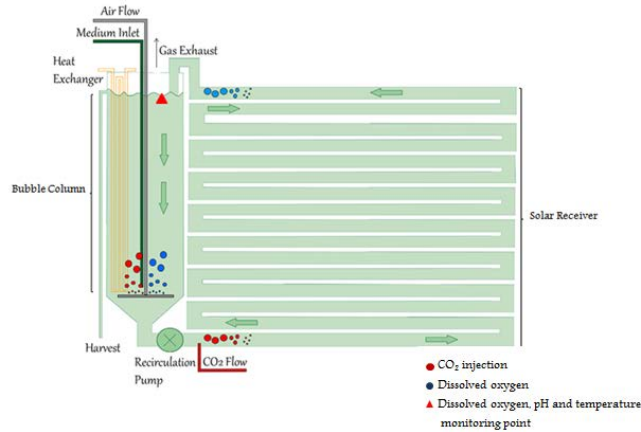
6.2 Methods

6.2.1 Pilot closed photobioreactors and experimental data

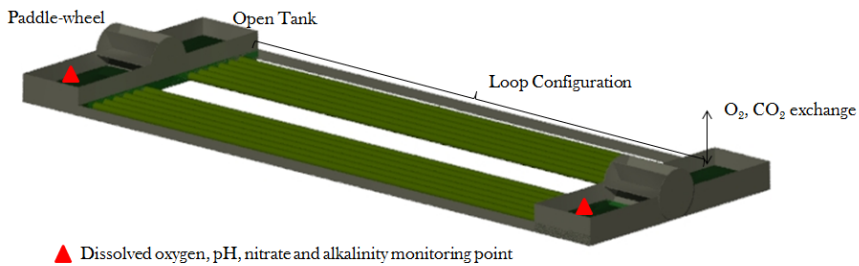
Both photobioreactors were located in Spain, one in “Estación Experimental Las Palmerillas”, property of Fundación CAJAMAR in Almeria, and the other in “Agropolis”, property of Universitat Politècnica de

Catalunya-BarcelonaTech in Barcelona (Fig. 6.1). The vertical tubular photobioreactor (PBR) in Almeria includes a loop solar receiver made of transparent plastic tubes of 0.09 m diameter with a total horizontal length of 400 m, and a 0.4 m diameter bubble column with 3.5 m of height, and has a total working volume of 3,000 L. The PBR unit is used to produce the microalgae *Scenedesmus almeriensis*, which is characterized by a high growth rate and tolerance temperatures up to 45 °C and pH values up to 10 (Acien et al., 2013; Sanchez et al, 2008). The PBR works by creating continuous flow of culture between loop and bubble column by means of a centrifuge pump located at the bottom of the column. The pump provides a constant flow velocity of 0.8 m s⁻¹ inside the loop. The pH of the culture is controlled by injection of pure CO₂ at 5 L min⁻¹. In the bubble column, excess DO is removed by a constant airflow rate of 140 L min⁻¹. The culture temperature is maintained by passing cooling water at 1,500 L h⁻¹ through an internal heat exchanger located inside the bubble column. When fresh culture medium is poured into the system, the culture is harvested through an overflow located on top of the column. Temperature, pH and DO are measured at several locations along the tube using Crison probes (Crison Instruments, Spain) connected to a control-transmitter unit MM44 (Crison Instrument, Spain). Liquid and gas flow rates are measured using digital flowmeters (PF2W540 and PF2A510, from SMC, Japan). All of these monitoring systems are in turn connected to a control computer through a data acquisition device NI Compact FieldPoint (National Instruments, USA) (Fernández et al., 2013). Data for the present study were obtained at the end of a two month experiment in which the photobioreactor was operated in continuous mode, medium flow rate of 1,020 L d⁻¹, and under controlled pH (7.8) and temperature (lower than 35 °C). As a result, the amount of microalgae biomass was kept fairly constant. Culture medium used was Mann&Myers, prepared using agricultural fertilizers. Collected data were retrieved in batch mode by switching off the feeding for 24 hours (at the end of the two months). Dissolved oxygen and pH data were recorded every 30 minutes, while temperature and irradiance were measured every hour. The horizontal tubular photobioreactor in Barcelona is composed of two open-air tanks made of polypropylene and is 1.8 x 1 x 0.4 m (L x W x H) in size. These tanks include paddlewheels that provide enough head pressure to move the culture through 12 (6 per each flow direction) transparent 0.125 m diameter

polyethylene tubes (each 50 m length). Culture flows from one tank to the other at a constant velocity of 0.125 m s^{-1} .



a)



b)

Figure 6.1 a) Tubular vertical photobioreactor located in Almeria (Spain) with details of the solar receiver (a continuous tubular loop) and a mixing unit (a bubble column). The culture is continuously recirculating from one to the other part using airlift and mechanical pumps (Fernández et al., 20129; b) Tubular horizontal photobioreactor located in Barcelona (Spain) with details of the two open-air tanks and the loop configurations (6 tubes per each flow direction). Mechanical paddlewheels promote the recirculation of the culture through the system.

Tanks also allow release of exceeding oxygen accumulated along tubes. The PBR has an effective volume of 8.5 m^3 . Note that in this PBR there is no

CO₂ injection or pH control. Data used for the present work were retrieved from a three days batch experiment and measured in each tank. For this experiment the PBR was filled with 8 m³ of agricultural runoff from a nearby agriculture canal which were inoculated with 0.5 m³ of inoculum with microalgae from a previous experiment (Table 6.1). The PBR contained different microalgae species belonging to the genus *Pediastrum* sp., *Chlorella* sp. and *Scenedesmus* sp.

Table 6.1 Agricultural runoff characteristics during batch experiment in the tubular horizontal photobioreactor located in Barcelona (Spain).

Parameter	Agricultural runoff
pH	8.4
Dissolved oxygen (g m ⁻³)	6.6
NO ₃ ⁻ -N (g m ⁻³)	0.6
Alkalinity (g CaCO ₃ m ⁻³)	42

The horizontal PBR has dissolved oxygen and pH online sensors in each tank that record data every hour, and temperature and irradiance online sensors that record data every two to three hours. Gathered data are stored using a Programmable Logic Controller (PLC) that is connected to a computer with supervisory control and a data management system (Green web manager 2.0). During the three days of experiments, offline samples were taken every two-three hours and analyzed in the laboratory for nitrates and alkalinity. Analysis of nitrate ion chromatography was accomplished using a Thermo Finnigan chromatograph with a metallic detector TCD (thermal conductivity detector). Alkalinity was analysed using conventional titrimetric procedures indicated in Standard Methods (APHA, 2001). Note that bicarbonate was calculated using alkalinity measurements, pH, and equilibrium constants of carbon species (Eq. 6.1).

$$\text{Alkalinity} = 50 \cdot \left[\frac{S_{\text{HCO}_3}}{12} + 2 * \frac{S_{\text{CO}_3}}{12} + S_{\text{OH}} - S_{\text{H}} \right] \quad (6.1)$$

6.2.2 Conceptual model

The new mechanistic model presented in Chapter 4 considers crucial physical, chemical and biokinetic processes for the description of microalgae growth in different types of cultures, particularly in wastewaters. The main relevant feature of the model, respect to any previous model for microalgae production (Bernard et al., 2009; Bonachela et al., 2011; Packer et al., 2011), consists in the inclusion of a carbon limitation on the growth of microalgae, as well as a dynamic model for photosynthesis, photolimitation, light attenuation, and photorespiration. In the model, microalgae grow with light, consume nutrients (i.e., carbon and nitrogen), and release oxygen (Fig. 6.2).

Note that other nutrients (e.g., phosphorus) and micronutrients are not considered to be limiting factors because are usually highly available in wastewaters (which is the type of culture mainly addresses by the model) (Larsdotter, 2006). Dependency of microalgae growth on phosphorus could easily be implemented in the model by creating a limiting Monod function, similar how the other nutrients (i.e., carbon and nitrogen) were represented.

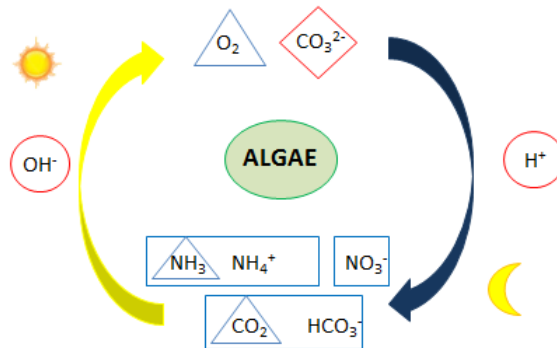


Figure 6.2 General schematic representation of the conceptual model by Solimeno et al. (2015). Microalgae (green ellipse), substrates (rectangles), gaseous species (triangles) and species depending on algal activity which are neither substrates nor gases (diamonds and circles). Other nutrients (e.g. phosphorus) and micronutrients are not limiting factors.

In the model, as a result of microalgal activity in the presence of light, hydroxide ions concentration and pH increase. Increases in pH displace the equilibrium of the carbon species towards the formation of carbonates (which are not bioavailable for growth). Note that this model assumes that carbon dioxide as well as bicarbonate are bioavailable for growth. In darkness, endogenous respiration of microalgae release carbon dioxide, the concentration of hydrogen ions increase and the pH decreases. With decreasing pH, the carbon equilibrium shifts and carbonate turns into bicarbonate, which can be used as substrate again in the presence of light (Ugwu et al., 2008). A detailed description of the model, including components, and processes can be found in Solimeno et al. (2015). A list of the processes included in the model, the equations describing their rates and the matrix of stoichiometric parameters are shown in Appendix A6.1-A6.2).

6.2.3 Model domain

The photobioreactor's configuration was assumed to have a 2D geometry. The domain was divided into two sub-domains (D1 and D2) corresponding to the loop configuration and the bubble column for the vertical system in Almeria, and to the open-air tanks and the tubes for the horizontal system in Barcelona (Fig. 6.3). In the case of the vertical system, D1 was 400 m long in the longitudinal direction and 0.09 m in diameter, while in the horizontal system it was 50 m long and 0.125 m in diameter. D2 domains were designed allocating the volume of the bubble column (vertical system) and open-air tank (horizontal system) along a surface interface area where gases were transferred to the atmosphere, fixing the corresponding D1 diameter. Thus, the bubble column is 5.1 m long and 0.09 m deep, while the tank is 5.76 m long and 0.125 m deep. These simplifications allow to simulate of hydrodynamics within the system. Note that in the present model it was necessary to divide the domain into two sub-domains due to the different domain conditions. Transfer of gases to the atmosphere took place exclusively in the bubble column and open-air tanks. A periodic condition was applied at boundaries 1 and 2 to reproduce the continuous culture flow from domain 2 to 1 (degasser to loop and tank to tube).

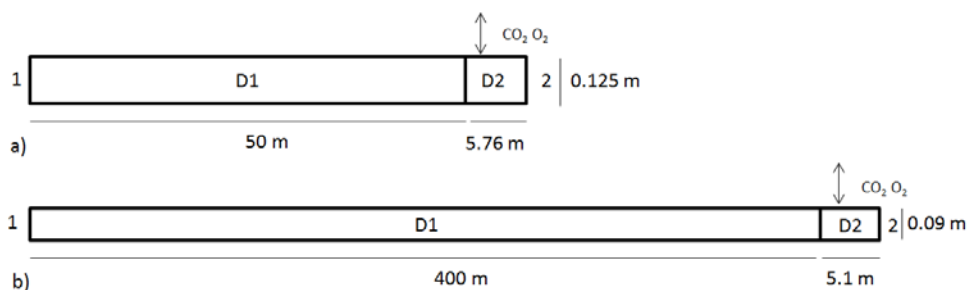


Figure 6.3 Schematic representation of the model domain, a) simplification of the horizontal photobioreactor located in Barcelona (Spain), b) simplification of the vertical photobioreactor in Almeria (Spain). D1 represents the loop configuration of both PBRs and D2 is the the total volume of open-air tank (a) and bubble column (b) respectively for horizontal and vertical photobioreactor. A periodic condition was applied at boundaries 1 and 2 to reproduce the continuous culture flow.

6.2.4 Hydrodynamics of the system, light attenuation and temperature

In Chapter 4, the calibration of the model was conducted in a complete mixed reactor represented by a 0D domain in order to simplify hydrodynamic's complexity. In the present work, as a result of the motion of the culture through the tubes and bubble column or open-air tank, a 2D domain was needed, which include hydraulic and transport equations. On the other hand, in the previous work (Chapter 4; Solimeno et al., 2015), it was assumed that microalgae cells captured photons at all depths (light attenuation was neglected due to 0D domain). The present work incorporates light attenuation due to the presence of microalgae.

In the model microalgae processes are influenced by temperature (Solimeno et al., 2015). It is known that the growth rate of microalgae is highly dependent on temperature; it increases when optimum temperature is reached and drastically decreases when optimum temperature is exceeded (Dauta et al., 1990). In the present study, microalgae production was

simulated in a study case at different temperatures, showing the dependence of microalgae growth on temperature.

Hydrodynamics of system was modelled through the COMSOL Multiphysics™ software, previously used for the calibration of the microalgae model in a completely stirred experiment, which solves differential equations using the finite elements method (FEM).

Hydraulic Considerations

In the PBR used in this work the culture is set in motion by an external pump (vertical system) or by paddlewheels (horizontal system), and enters the model domain with a certain velocity. To predict the flow regime without starting a simulation, the Reynolds number was firstly calculated. The Reynolds number quantifies the ratio of inertia to viscous forces, characterizing the flow regime (Eq. 6.2):

$$\text{Re} = \frac{\rho * u * d}{\mu} \quad (6.2)$$

where ρ is the culture density (assumed to have the same density as water, 1000 kg m^{-3}), u is the culture velocity (m s^{-1}), d is the tube diameter (0.09 m and 0.125 m for vertical and horizontal systems, respectively), and μ is the dynamic viscosity of the culture (assumed to be the same as water $0.003 \text{ kg m}^{-1}\text{s}^{-1}$). The Reynolds number was calculated to be approximately 27,000 for the vertical system and 5,000 for the horizontal. Note that in tubes with a flow with a Reynolds number above 4,000 is already considered turbulent (Stokes, 1851), and in these conditions transversal variations of culture properties (temperature, dissolved oxygen, biomass concentration, etc.) may be neglected and Navier-Stokes equations can be solved directly. With such high Reynolds number's temperature does not significantly influence the motion because viscous forces (μ) are very small when compared to inertial forces (v).

For turbulent flow, COMSOL Multiphysics™ solves the Navier-Stokes as well as continuity equations. Turbulent effects are modelled using “Turbulent Mixing” interfaces for “Transport of Diluted Species” physics.

In “Turbulent Mixing” models the additional mixing caused by turbulence is estimated by adding turbulent diffusivity to the molecular diffusivity considering:

$$D_T = \frac{\nu_T}{S_{cT}} \quad (6.3)$$

where D_T is the turbulent diffusion, ν_T is the turbulent kinematic viscosity at 20 °C ($1.004E-06 \text{ m}^2 \text{ s}^{-1}$) and S_{cT} is the turbulent Schmidt number (0.7).

Transport of dissolved and particulate components

Transport of diluted and particulate components with a concentration S_i [M L^{-3}] by convection and diffusion is given by:

$$\frac{\delta S_i}{\delta t} + (-D_T \cdot S_i) + u \cdot c_i = r_i \quad (6.4)$$

$$r_i = \sum_j v_{ij} \cdot \rho_j \quad (6.5)$$

where $i = 1, 2 \dots m$ are the different components considered (Table 6.2), and j is the number of processes shown in Appendix A6.1; u [L T^{-1}] is the vector of velocity, r_i [$\text{M L}^{-3} \text{T}^{-1}$] is the reaction rate, ρ_j [$\text{M L}^{-3} \text{T}^{-1}$] is the process rate corresponding to the biokinetic and chemical j processes described in Chapter 4 and v_{ij} is the stoichiometric coefficient. Mathematical expressions of the stoichiometric coefficient and values of biokinetic, physical and chemical parameters are shown in Appendix A6.3-A6.6.

Table 6.2 Dissolved and particulate components considered in the model.

Component	Description	Units
Dissolved Components		
S _{NH4}	Ammonium nitrogen	gN-NH ₄ m ⁻³
S _{NH3}	Ammonia nitrogen	gN-NH ₃ m ⁻³
S _{NO3}	Nitrate nitrogen	gN-NO ₃ m ⁻³
S _{CO2}	Carbon dioxide	gC-CO ₂ m ⁻³
S _{HCO3}	Bicarbonate	gC-HCO ₃ m ⁻³
S _{CO3}	Carbonate	gC-CO ₃ m ⁻³
S _{O2}	Dissolved oxygen	gO ₂ m ⁻³
S _H	Hydrogen ions	gH m ⁻³
S _{OH}	Hydroxide ions	gH-OH m ⁻³
Particulate Component		
X _{ALG}	Microalgae biomass	gTSS m ⁻³

Light attenuation

In the present study light intensity decay was described using Lambert-Beer's Law, which dictates that intensity decreases exponentially as it penetrates into a perfectly homogeneous section of culture with a short penetration pathway (Sanchez et al., 2008), as it is the case of both PBR. In this case light is attenuated by the presence of microalgae inside the reactors. The average light intensity (I_{av} , [MT⁻³]) at any point within the culture is therefore calculated as (Hase et al., 2000):

$$I_{av} = I_o \cdot \frac{1 - e^{(-K_I \cdot X_{ALG} \cdot d)}}{K_I \cdot X_{ALG} \cdot d} \quad (6.6)$$

where I_o [MT⁻³] is the incident light intensity, K_I is the extinction coefficient for microalgae biomass [0.1 M⁻¹L²] (Camacho-Rubio et al., 2003), X_{ALG} is the concentration of microalgae and d [L] is the diameter of tube.

Temperature

In our model, the influence of temperature on microalgae activity was implemented by the thermic photosynthetic factor ($f_{T,FS}$), which takes into account the effects of temperature on microalgae growth, endogenous respiration and inactivation processes (1a, 1b, 2 and 3 in Appendix A6.1, respectively). Water temperature varies both on hourly and daily scales, affecting microalgal photosynthesis and respiration rates. The thermic photosynthetic factor is represented in the model following the work of Dauta et al. (1990):

$$f_{T,FS}(T) = e^{-\left(\frac{T-T_{OPT}}{s}\right)^2} \quad (6.7)$$

where T_{OPT} (optimum temperature) was assumed to be 25 °C (Dauta et al., 1990) and s equal to 13 (Dauta et al., 1990) (it is a parameter value for empirical fitting).

6.2.5 Calibration procedure

Model output results are highly sensitive to the maximum specific growth rate of microalgae (μ_{ALG}), mass transfer coefficient for oxygen (K_{a,O_2}), and carbon dioxide (K_{a,CO_2}). The mass transfer coefficients depend on the extension of the surface interface and photobioreactor design (Solimeno et al., 2015). Therefore, these parameters were calibrated in the two different tubular photobioreactors. The model was first calibrated using experimental data obtained from the vertical photobioreactor located in Almeria (Spain). Dissolved oxygen, pH, temperature and irradiance were monitored for 24 hours on February 28th, 2012. Afterwards, the model was calibrated with experimental data from the horizontal photobioreactor located in Barcelona (Spain). Data used for this calibration were retrieved from three days batch experiment from April 16th, 2012 to April 19th, 2012. Available data used for the calibration procedure are shown in Appendix A6.7-A6.8. The initial concentrations of components in the vertical and horizontal photobioreactors at the beginning of the experiments are shown in Table

6.3. In the horizontal PBR the concentrations of S_{NH_4} and S_{NH_3} were lower than the analytical method's detection limit and therefore considered to be zero for this model. Note the difference in initial concentrations of microalgae (X_{ALG}) between the two PBRs due to their different operating conditions.

Table 6.3 Initial concentrations of the components in the vertical photobioreactor of Almeria (Spain) and horizontal photobioreactor of Barcelona (Spain).

Components	Concentrations		Units
	Vertical PBR	Horizontal PBR	
X_{ALG}	619	200	$gCOD\ m^{-3}$
S_{NH_4}	14	-	$gN-NH_4\ m^{-3}$
S_{NH_3}	0.684	-	$gN-NH_3\ m^{-3}$
S_{NO_3}	4.2	0.6	$gN-NO_3\ m^{-3}$
S_{CO_2}	1.59	0.068	$gC-CO_2\ m^{-3}$
S_{HCO_3}	100	7.59	$gC-HCO_3\ m^{-3}$
S_{CO_3}	0.62	0.085	$gC-CO_3\ m^{-3}$
S_{O_2}	7.2	6.64	$gO_2\ m^{-3}$
S_H	6.31E-6	3.55E-6	$gH\ m^{-3}$
S_{OH}	1.58E-3	2.82E-3	$gH-OH\ m^{-3}$

6.2.6 Study cases

Practical study cases have been done to evaluate the influence of both temperature and irradiance on microalgae production, and the effect of oxygen concentration in the loop. The vertical photobioreactor of Almeria (Spain) was selected as reference for these studies.

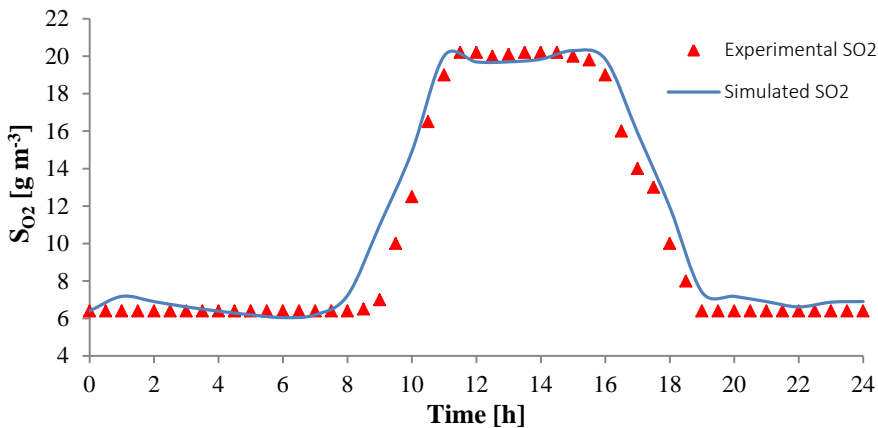
Starting from the initial concentrations used for calibration of the model in the vertical photobioreactor, average daily microalgae production was simulated using daily temperature and irradiance variations from 17th day of each month of year. Two scenarios were evaluated. In the first set of simulations the vertical photobioreactor was under controlled temperature by passing cooling water at $1500\ L\ h^{-1}$ through an internal heat exchanger located in the bubble column of the photobioreactor. In a second set of simulations, temperature was obtained from meteorological annals of

Almeria (Spain). These two scenarios were compared and an estimation of the total annual production using monthly irradiance variations was calculated. Irradiance, expressed as photosynthetically active radiation (PAR), was estimated for Almeria (Spain) from the mathematical equations presented in Appendix A6.9 (Al-Rawahi et al., 2011).

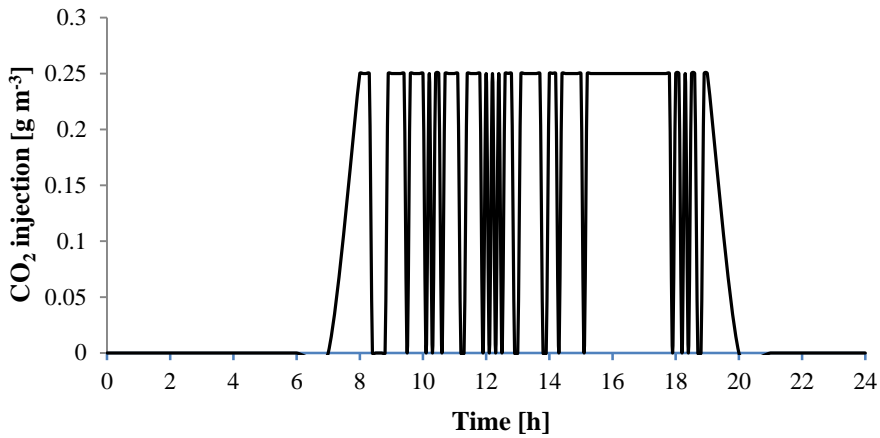
Moreover, oxygen concentration throughout the 400 m of vertical photobioreactor was evaluated while maintaining the reactor under controlled temperature, Dissolved oxygen profile in the loop configuration was simulated at noon in the months of July and January, when the highest and lowest temperature, respectively, were recorded.

6.3 Results

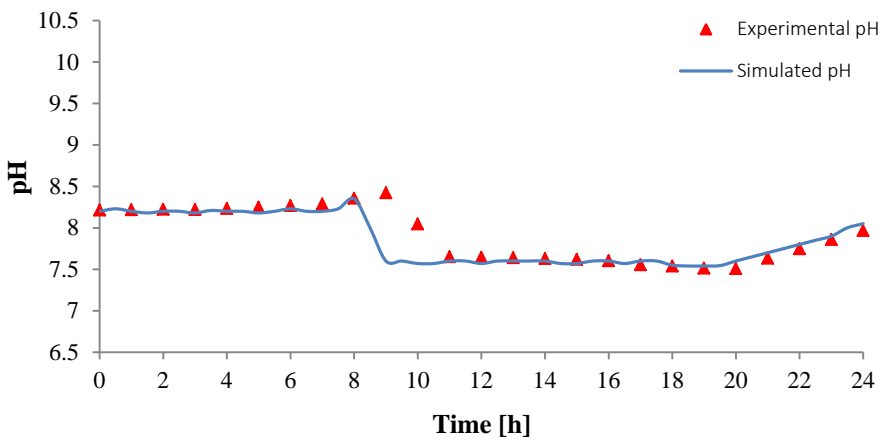
In this work simulations for two different photobioreactors were studied. First we present the results of the model calibration for the vertical photobioreactor. Fig. 6.4 shows that the model was able to accurately match DO and pH trends over the course of one day inside the system, with decreasing pH due to CO₂ injection (which displaces the equilibrium of carbon species).



a)



b)



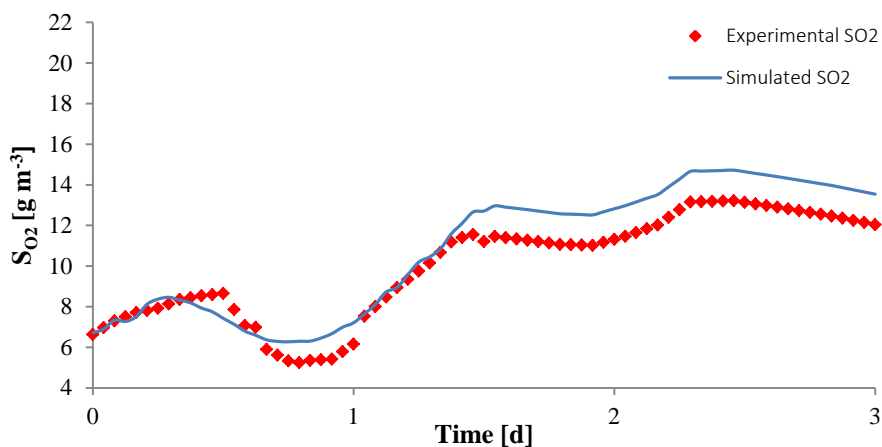
c)

Figure 6.4 Experimental (red triangles) and simulated (blue line) (a) dissolved oxygen (DO) and (c) pH values as a function of CO₂ injection (b) over the 24 hours in the vertical photobioreactor in Almeria (Spain).

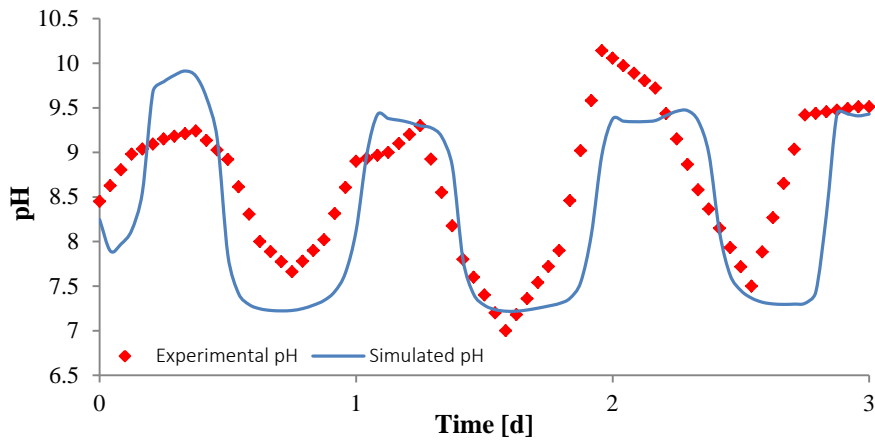
Fig. 6.5 shows the results of the calibration in the horizontal photobioreactor. Experimental and simulated dissolved oxygen and pH values inside the open-air tanks of the horizontal photobioreactor are presented. As can be seen, the wavelike trend of pH varied due to microalgae activity, which is quite well simulated by the model. Moreover, Fig. 6.6 shows the experimental and simulated nitrate (S_{NO_3}) and bicarbonate (S_{HCO_3}) concentrations in the horizontal system. The model was able to

reproduce quite well the trend of experimental data. In absence of ammonia species, only nitrates are used as nitrogen substrates for microalgae growth. The low concentration of nitrate in the culture medium limited the activity of microalgae. As can be seen, microalgae consumed nitrate concentrations quickly in the first hours of experiment (Fig. 6.6). Likewise, Fig. 6.6 shows that bicarbonate concentrations decreased faster in the first hours due to intense microalgae activity. After 22 hours, in absence of nitrate, daily variations of bicarbonate are related to changes in equilibrium species of carbon.

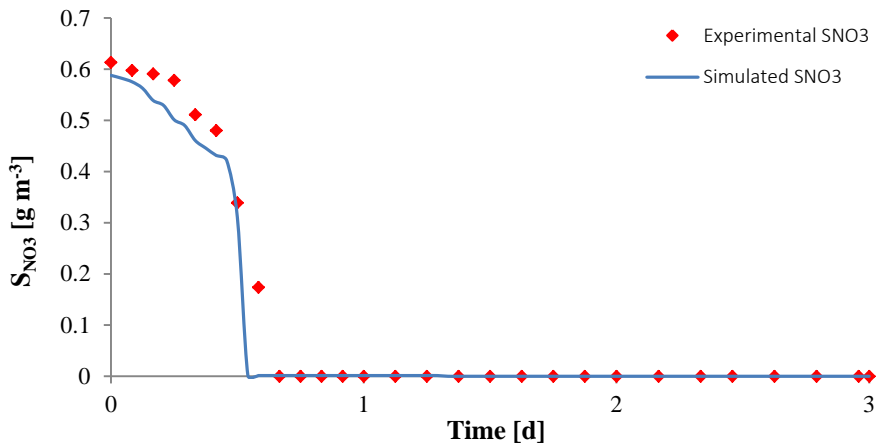
Note that, in general, simulations of the vertical PBR were more accurate than those of the horizontal due to in the horizontal system there was some growth of other microorganisms different from microalgae (e.g., bacteria and protozoa). This was to be expected as the culture water was from an irrigation channel. The activity of these microorganisms affected simulated factors though it is not known to what extent, because unfortunately we do not have values for these organisms.



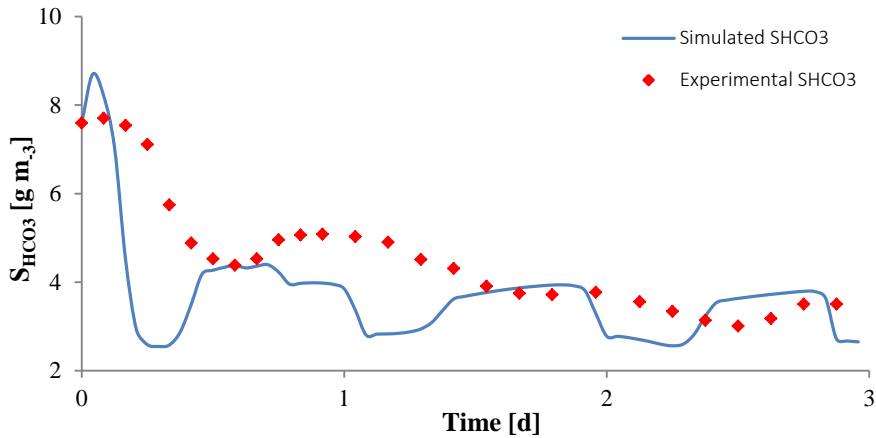
a)



b) **Figure 6.5** Experimental (red diamonds) and simulated (blue line) (a) dissolved oxygen (DO) and (b) pH values over the three days in the horizontal photobioreactor in Barcelona (Spain).



a)



b)
Figure 6.6 Experimental (red diamonds) and simulated (blue line) (a) nitrate and (b) bicarbonate concentrations over the three days in the horizontal photobioreactor in Barcelona (Spain).

Table 6.4 presents the values of the parameters that were calibrated in each photobioreactor. Note that maximum specific growth rate (μ_{ALG}) and the transfer of gases to the atmosphere (K_{a,O_2} and K_{a,CO_2}) were also calibrated in our previous works (Solimeno et al., 2015, 2016). In this previous work the model output results are very sensitive to these parameters (Solimeno et al., 2015, 2016), and therefore should be calibrated with great accuracy. Furthermore, gas transfer parameters depend on the extension of the surface interface. Due to different PBRs design, modifications of these parameters were considered worthwhile.

Table 6.4. Values of calibrated parameters in the vertical and horizontal photobioreactors.

Parameter	Description	Value	
		Vertical PBR	Horizontal PBR
μ_{ALG}	Maximum specific growth rate of microalgae	1.7 d^{-1}	1.7 d^{-1}
K_{a,O_2}	Mass transfer coefficient for oxygen	$2.9E-03 \text{ s}^{-1}$	$9.2E-03 \text{ s}^{-1}$
K_{a,CO_2}	Mass transfer coefficient for carbon dioxide	$2.8E-03 \text{ s}^{-1}$	$9.0E-03 \text{ s}^{-1}$

6.4 Discussion

6.4.1 New features of the model

In comparison to our previous work (Chapter 4; Solimeno et al., 2015), where a 0D domain was applied, here 2D domain was used to represent the two tubular photobioreactors. The domain was divided in two sub-domains (D1 and D2), where different conditions from the tubes (D1) to the open body (D2) of the photobioreactors were applied. According to the function of bubble column in the vertical system and the open-air tank in the horizontal system, the transfer of gases to the atmosphere was only applied to the D2 domain that corresponds to the total volume of these specific parts.

A periodic condition was applied at boundaries 1 and 2 to reproduce the recirculation of flow from the loop configuration to the bubble column in the vertical system, and from the tubes to the open-tank in the horizontal system. Simulation results demonstrated that these simplifications were adequate to describe the specific parts of different tubular photobioreactors. Moreover, fluid flow and transport equations were added in the current model to obtain a realistic representation of the hydrodynamics in the photobioreactors.

In addition to the previous mechanistic model presented in Chapter 4 (Solimeno et al., 2015) light attenuation through the medium was implemented. Light intensity decays exponentially due to microalgae biomass accumulation inside the reactors. Assuming a perfect mixing of medium, due to turbulent flow regime, an irradiance average I_{av} was used to represent any point within the reactor.

6.4.2 Calibration of the model

Results of the sensitivity analysis, reported in Chapter 5 (Solimeno et al., 2016), had indicated that the maximum specific growth rate of microalgae (μ_{ALG}) and the mass transfer coefficient for oxygen (K_{a,O_2}) and carbon

dioxide (K_{a,CO_2}) were the parameters with the greatest impact on simulation outputs. Therefore, calibration of these parameters must occur in each particular case.

The calibrated maximum specific growth rate of microalgae ($\mu_{ALG} = 1.7 [d^{-1}]$) in the vertical photobioreactor fits well within literature range [0.4-2.0 d^{-1}]. Also, the mass transfer coefficient in the bubble column for oxygen which was $K_{a,O_2} = 2.9E-03 s^{-1}$ fits into the range values for vertical photobioreactors [1.2E-03 to 7.7E-03 s^{-1}] (Hulatt and Thomas, 2011). The mass transfer coefficient for carbon dioxide ($K_{a,CO_2} = 2.8E-03 s^{-1}$) was consistent with range values [1.1E-03 to 7.0E-03 s^{-1}] for bubble column systems (Hulatt and Thomas, 2011). These same parameters were calibrated with experimental data over three days from the horizontal photobioreactor located in Barcelona (Spain). Likewise as in the previous calibration, the values generated for the maximum growth rate of microalgae ($\mu_{ALG} = 1.7 [d^{-1}]$), the mass transfer of oxygen ($K_{a,O_2} = 9.2E-03 [s^{-1}]$) and carbon dioxide ($K_{a,CO_2} = 9.0E-03 [s^{-1}]$) were all in agreement with literature ranges for tubular photobioreactors (Camacho-Rubio et al., 1999).

Mass transfer coefficients depend on, temperature, mixing and most importantly, the extension of the surface interface. Thus, variable values of mass transfer coefficients from vertical and horizontal photobioreactors are due to different design and scale-up of bubble column and open-tanks, respectively.

Also the culture medium influences the mass transfer coefficients and the maximum growth rate of microalgae. In this work the horizontal photobioreactor was filled with agricultural runoff which could contain few concentrations of bacteria and other microorganisms. The activity of these microorganisms could influence dissolved oxygen and carbon dioxide concentrations in the medium culture, and therefore could slightly affect the values of the calibrated parameters. However, single microscopic observations during the experiment indicated that their concentration was irrelevant in comparison to microalgae (as usual in this type of PBR), and thus their influence is considered very low or almost negligible. Calibrating the model in two different photobioreactors (e.g., horizontal and vertical)

with different types of media has proved the robustness and resilience of the mathematical model to operate under variables conditions.

6.4.3 Study case: microalgae production as a function of temperature and irradiance

Irradiance and temperature play an important role in microalgae production. These physical factors influence biokinetic and chemical processes related to microalgae growth. Irradiance is strictly correlated to photosynthesis rate. At high level of irradiance, microalgae become 'light saturated' because photosynthesis cannot process more photons. As result, the rate of photosynthesis progressively starts to stabilize (Camacho-Rubio et al., 1999; Craggs et al., 2011)). Temperature influences the equilibrium of chemical species (carbon and nitrogen), uptake of nutrients, transfer of gases to the atmosphere, and especially the microalgae growth rates. The optimal temperature for microalgae growth ranges between 15°C and 25°C, depending on the species (Bitog et al., 2011; Larsdotter, 2006). Temperature above or below this range negatively affects biomass yield.

Thanks to the model, previously calibrated with daily experimental data, has been possible to make predictions of microalgae production over long-term with different environmental factors, such as temperature and irradiance. Simulations of the average daily microalgae production at a monthly scale in the vertical photobioreactor are presented in Fig 6.7. As can be observed simulations indicate that production is generally higher under daily temperature variations due to a more favourable temperature range (Appendix A6.10).

Table 6.5 presents the annual microalgae production comparing the two scenarios studied: under controlled temperature and with daily temperature variations. Although the growth of microalgae decreases with high temperature and irradiance during the months of June, July and August (when the highest temperatures of the year occur), total annual production of microalgae exposed to daily temperature variations is higher than the reactor under controlled temperature. To optimize production, it might be

considered to only use cooling water during the hottest months (June, July and August). Moreover, simulations results show that during the summer the production is also inhibited due to high dissolved oxygen concentrations throughout loop configuration up to 250% of air saturation (see next section).

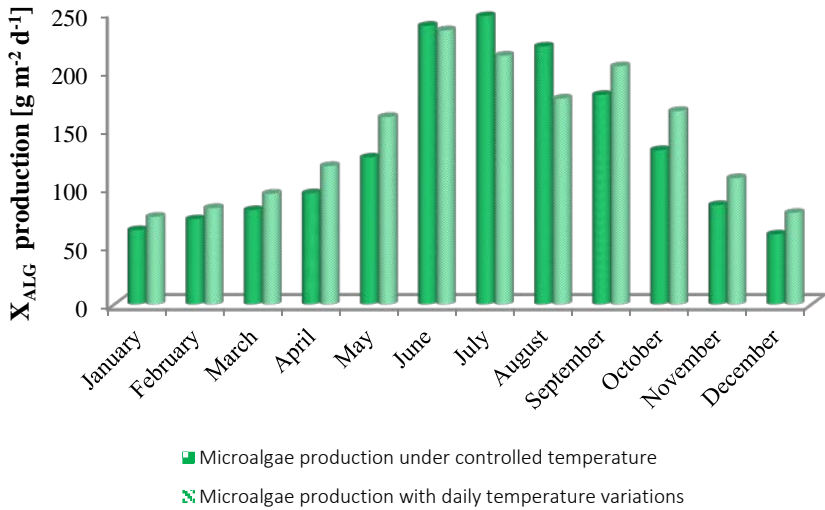


Figure 6.7 Average daily microalgae production for each month of the year under controlled temperature and with daily temperature variations.

Table 6.5 Comparing total annual production under controlled temperature and daily temperature variations versus optimizing system using cooling water during summer.

Total annual production	Value
Optimizing system	1796.86 gTSS m ⁻³
Daily temperature variations	1714.53 gTSS m ⁻³
Under controlled temperature	1604.48 gTSS m ⁻³

6.4.4 Study case: oxygen concentration

Fig. 6.8 shows the simulations of the dissolved oxygen profile throughout the 400 m length of the vertical photobioreactor at noon (when the highest temperature occurs) in the months of January and July. These two months were selected as they represent the minimum and maximum microalgae activity in a monthly basis time scale. As can be seen, the lower light intensity and temperature in January gives as a result lower dissolved oxygen concentrations in contrast to July. Also it can be observed in both months how dissolved oxygen concentration increases throughout the loop and decreases in the bubble column. In July, transfer of excess of dissolved oxygen to the atmosphere throughout the airlift permits to re-establish, at the beginning of loop configuration, the oxygen level under the maximum concentration of oxygen dissolved in water ($32 \text{ gO}_2 \text{ m}^{-3}$ at $20 \text{ }^\circ\text{C}$) equal 350% of saturation ($9.07 \text{ gO}_2 \text{ m}^{-3}$ at $20 \text{ }^\circ\text{C}$) (Acién et al., 2013; Camacho-Rubio et al., 1999). This property of the photobioreactor design is especially important in warm months (such as July), when a high photosynthetic activity could cause inhibition due to oxygen accumulation.

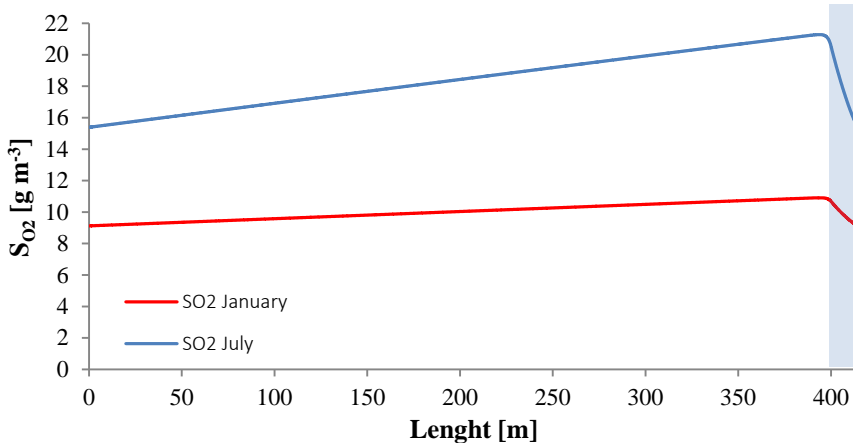


Figure 6.8 Simulations of dissolved oxygen concentration profile throughout the vertical photobioreactor in Almeria (Spain) in the months of January and July. Bubble column position is represented by blue region.

The model presented in this work allows to simulate and study microalgae growth inhibition due to high dissolved oxygen concentrations thanks to the inclusion of a photorespiration factor $f_{PR}(S_{O_2})$ (Solimeno et al., 2015). The function ($f_{PR}(S_{O_2})$) in Fig. 6.9 describes that for dissolved oxygen concentrations lower than the $250\%S_{O_2}^{SAT}$ ($22.67 \text{ gO}_2 \text{ m}^{-3}$ at $20 \text{ }^\circ\text{C}$) the photosynthesis rate is reduced by 10%. Above this value, the photosynthesis rate decreases more quickly with a vertical asymptote and is equal at zero when dissolved oxygen reaches the 350% saturation limit ($\tau S_{O_2}^{SAT} = 32 \text{ gO}_2 \text{ m}^{-3}$ at $20 \text{ }^\circ\text{C}$).

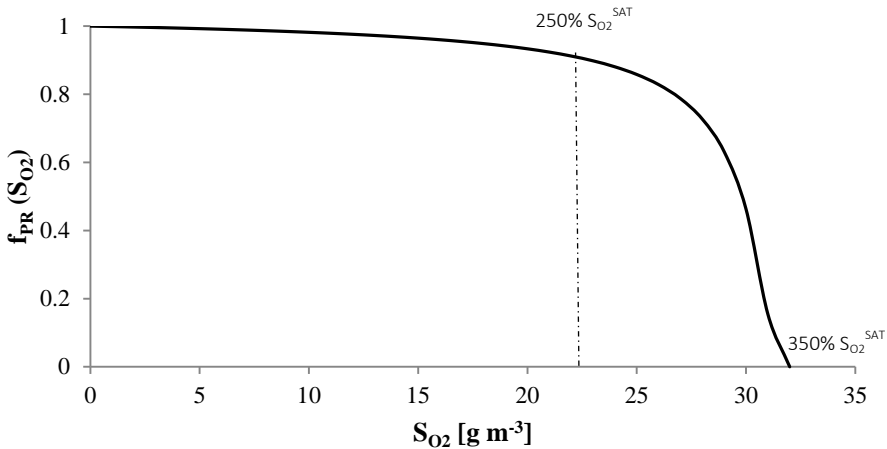


Figure 6.9 Profile of photorespiration factor function for value of dissolved oxygen concentrations below the saturation limit ($\tau S_{O_2}^{SAT}$).

In process design, the current model can be used to find the maximum photobioreactor length to avoid oxygen inhibition. For example, for the month of July, simulations were conducted using half the previous bubble column volume (from 0.44 m^3 to 0.22 m^3) in the vertical photobioreactors loops (400 m and 250 m). As seen in Fig. 6.10, reducing the volume of the bubble column and keeping the original loop configuration length (400 m), the simulation results show that the DO exceeds the saturation limit 1 inhibiting microalgae growth. The volume of bubble column is not enough to transfer the excess of dissolved oxygen to the atmosphere. On the contrary, simulations indicate that a 250 m length, photobioreactor greatly reduces the oxygen accumulation.

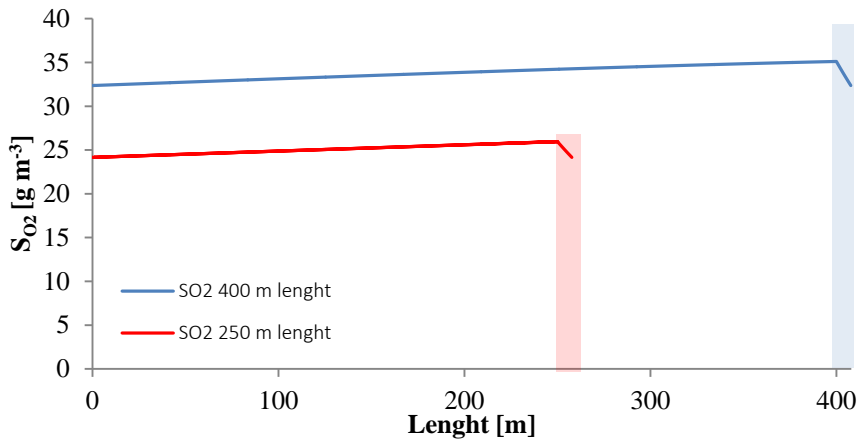


Figure 6.10 Simulations of dissolved oxygen concentration profile throughout 400 m and 250 m length of the vertical photobioreactor in Almeria (Spain) in the months of July. Bubble column position is represented by blue and red rectangle, for 400 m and 250 m length of vertical photobioreactor, respectively.

6.5 Conclusion

In this paper a new mechanistic model to simulate microalgae growth was calibrated in two different tubular photobioreactors. Fluid flow, transport equations and light attenuation were included in the model described in our previous work and implemented in COMSOL MultiphysicsTM software. Uncertainty parameters from previous sensitivity analysis were calibrated in each photobioreactor. The results of calibration indicate that the mass transfer of gases and the maximum specific growth rate of microalgae fit well within literature ranges. Moreover, the developed model demonstrates potential prediction of oxygen accumulation throughout the loop configuration and daily microalgae production as a function of temperature and irradiance. The model proves to be an efficient tool for photobioreactor design and production optimization.

6.6 Appendix

Table A6.1 Mathematical description of the processes of the model (processes rates).

Processes	Process rate [M L ⁻³ T ⁻¹]
1a. Growth of X _{ALG} on S _{NH4}	$\rho_{1a} = \mu_{ALG} \cdot f_{T,FS}(T) \cdot \eta_{PS}(I, S_{O_2}) \cdot \frac{S_{CO_2} + S_{HCO_3}}{K_{C,ALG} + S_{CO_2} + S_{HCO_3} + \frac{S_{CO_2}^2}{I_{CO_2,ALG}}} \cdot \frac{S_{NH_3} + S_{NH_4}}{K_{N,ALG} + S_{NH_3} + S_{NH_4}} \cdot X_{ALG}$
1b. Growth of X _{ALG} on S _{NO3}	$\rho_{1b} = \mu_{ALG} \cdot f_{T,FS}(T) \cdot \eta_{PS}(I, S_{O_2}) \cdot \frac{S_{CO_2} + S_{HCO_3}}{K_{C,ALG} + S_{CO_2} + S_{HCO_3} + \frac{S_{CO_2}^2}{I_{CO_2,ALG}}} \cdot \frac{S_{NO_3}}{K_{N,ALG} + S_{NO_3}} \cdot \frac{K_{N,ALG}}{K_{N,ALG} + S_{NH_3} + S_{NH_4}} \cdot X_{ALG}$
2. Endogenous respiration of X _{ALG}	$\rho_2 = k_{resp,ALG} \cdot f_{T,FS}(T) \cdot \frac{S_{O_2}}{K_{O_2,ALG} + S_{O_2}} \cdot X_{ALG}$
3. Decay of X _{ALG}	$\rho_3 = k_{death,ALG} \cdot f_{T,FS}(T) \cdot X_{ALG}$
4. Chemical equilibrium CO ₂ ↔ HCO ₃ ⁻	$\rho_4 = k_{eq,1} \cdot \left(S_{CO_2} - \frac{S_H S_{HCO_3}}{K_{eq,1}} \right)$
5. Chemical equilibrium HCO ₃ ⁻ ↔ CO ₃ ²⁻	$\rho_5 = k_{eq,2} \cdot \left(S_{HCO_3} - \frac{S_H S_{CO_3}}{K_{eq,2}} \right)$
6. Chemical equilibrium NH ₄ ⁺ ↔ NH ₃	$\rho_6 = k_{eq,3} \cdot \left(S_{NH_4} - \frac{S_H S_{NH_3}}{K_{eq,3}} \right)$
7. Chemical equilibrium H ⁺ ↔ OH ⁻	$\rho_7 = k_{eq,w} \cdot \left(1 - \frac{S_H S_{OH}}{K_{eq,w}} \right)$
8. Transfer of S _{O2} to the atmosphere	$\rho_{O_2} = K_{a,O_2} \cdot (S_{O_2}^{WAT} - S_{O_2})$
9. Transfer of S _{CO2} to the atmosphere	$\rho_{CO_2} = K_{a,CO_2} \cdot (S_{CO_2}^{WAT} - S_{CO_2})$
10. Transfer of S _{NH3} to the atmosphere	$\rho_{NH_3} = K_{a,NH_3} \cdot (-S_{NH_3})$

Table A6.2 Matrix of stoichiometric parameters that relate processes and components through stoichiometric coefficients in Appendix A6.3.

State variables $\rightarrow i$		S_{NH4}	S_{NH3}	S_{NO3}	S_{O2}	S_{CO2}	S_{HCO3}	S_{CO3}	S_H	S_{OH}	X_{ALG}
Processes $\downarrow j$											
1a. Growth of X_{ALG} on S_{NH4}	ρ_{1a}	$v_{1,1a}$			$v_{4,1a}$	$v_{5,1a}$			$v_{8,1a}$		$v_{10,1a}$
1b. Growth of X_{ALG} on S_{NO3}	ρ_{1b}			$v_{3,1b}$	$v_{4,1b}$	$v_{5,1b}$			$v_{8,1b}$		$v_{10,1b}$
2. Endogenous respiration of X_{ALG}	ρ_2	$v_{1,2}$			$v_{4,2}$	$v_{5,2}$			$v_{8,2}$		$v_{10,2}$
3. Decay of X_{ALG}	ρ_3	$v_{1,3}$			$v_{4,3}$	$v_{5,3}$			$v_{8,3}$		$v_{10,3}$
4. Chemical equilibrium $CO_2 \leftrightarrow HCO_3^-$	ρ_4					$v_{5,4}$	$v_{6,4}$		$v_{8,4}$		
5. Chemical equilibrium $HCO_3^- \leftrightarrow CO_3^{2-}$	ρ_5						$v_{6,5}$	$v_{7,5}$	$v_{8,5}$		
6. Chemical equilibrium $NH_4^+ \leftrightarrow NH_3$	ρ_6	$v_{1,6}$	$v_{2,6}$						$v_{8,6}$		
7. Chemical equilibrium $H^+ \leftrightarrow OH^-$	ρ_7								$v_{8,7}$	$v_{9,7}$	
8. Transfer of S_{O2} to the atmosphere	ρ_{O2}				$v_{4,O2}$						
9. Transfer of S_{CO2} to the atmosphere	ρ_{CO2}					$v_{5,CO2}$					
10. Transfer of S_{NH3} to the atmosphere	ρ_{NH3}		$v_{2,NH3}$								

A6.3 Values of biokinetic and physic parameters.

Parameters	Description	Value	Unit	Source
Microalgae processes				
μ_{ALG}	Maximum growth rate of X_{ALG}	1.7	d^{-1}	Calibrated
$k_{\text{resp,ALG}}$	Endogenous respiration constant	0.1	d^{-1}	Reichert et al., 2001
$k_{\text{death,ALG}}$	Decay constant	0.1	d^{-1}	Reichert et al., 2001
$K_{\text{C,ALG}}$	Affinity constant of X_{ALG} on S_{CO_2}	4E-3	gC m^{-3}	Novak and Brune, 1985
$I_{\text{CO}_2,\text{ALG}}$	Inhibition constant of X_{ALG} on S_{CO_2}	120	gC m^{-3}	Silva and Pirt, 1984
$K_{\text{N,ALG}}$	Affinity constant of X_{ALG} on nitrogen sp.	0.1	gN m^{-3}	Reichert et al., 2001
$K_{\text{O}_2,\text{ALG}}$	Affinity constant of X_{ALG} on S_{O_2}	0.2	$\text{gO}_2 \text{m}^{-3}$	Reichert et al., 2001
Photorespiration factor				
K_{PR}	Inhibition constant of photorespiration	0.03	–	Assumption
τ	Excess of S_{O_2} coefficient	3.5	–	Fernández et al., 2014
$S_{\text{O}_2}^{\text{SAT}}$	S_{O_2} air saturation	9.07	$\text{gO}_2 \text{m}^{-3}$	Fernández et al., 2014
Photosynthetic thermal factor				
T_{OPT}	Optimum temperature for X_{ALG} growth	25	$^{\circ}\text{C}$	Dauta et al., 1990
s	Normalized parameter	13	–	Dauta et al., 1990
Light factor				
α	Parameter activation	1.9E-3	$(\mu\text{Em}^{-2})^{-1}$	Wu and Merchuk, 2001
β	Parameter inhibition	5.7E-7	$(\mu\text{Em}^{-2})^{-1}$	Wu and Merchuk, 2001
γ	Parameter production	0.14	s^{-1}	Wu and Merchuk, 2001
δ	Parameter recovery	4.7E-4	s^{-1}	Wu and Merchuk, 2001
Irradiance solar incident				
E_f	Photosynthetic efficiency of solar radiation	1.74	$\mu\text{E J}^{-1}$	Al-Rawahi et al., 2011
κ	Index atmospheric clarity	0.74	–	Al-Rawahi et al., 2011
ζ	Universal solar constant	1353	W m^{-2}	Al-Rawahi et al., 2011
ω	Hour angle	Calculated	$^{\circ}$	Molina-Grima et al., 2001
ω_s	Sunset hour angle	Calculated	$^{\circ}$	Molina-Grima et al., 2001
φ	Latitude	Observed	$^{\circ}$	-
δ	Sun declination	Calculated	$^{\circ}$	Molina-Grima et al., 2001

A6.4 Values of chemical parameters.

Parameters		Equations		
Chemical equilibrium $\text{CO}_2 \leftrightarrow \text{HCO}_3^-$.		$K_{\text{eq},1} = 10^{17.843 - \frac{3404.71}{273.15+T} - 0.032786(273.15+T)}$		
Chemical equilibrium $\text{HCO}_3^- \leftrightarrow \text{CO}_3^{2-}$		$K_{\text{eq},2} = 10^{9.494 - \frac{2902.39}{273.15+T} - 0.02379(273.15+T)}$		
Chemical equilibrium $\text{NH}_4^+ \leftrightarrow \text{NH}_3$		$K_{\text{eq},3} = 10^{2.891 - \frac{2727}{(273.15+T)}}$		
Chemical equilibrium $\text{H}^+ \leftrightarrow \text{OH}^-$		$K_{\text{eq},w} = 10^{-\frac{4470.99}{273.15+T} + 12.0875 - 0.01706(273.15+T)}$		
Kinetics parameters				
$k_{\text{eq},1}$	Dissociation constant of $\text{CO}_2 \leftrightarrow \text{HCO}_3^-$.	10000	d^{-1}	Reichert et al., 2001
$k_{\text{eq},2}$	Dissociation constant of $\text{HCO}_3^- \leftrightarrow \text{CO}_3^{2-}$	1000	d^{-1}	Reichert et al., 2001
$k_{\text{eq},3}$	Dissociation constant of $\text{NH}_4^+ \leftrightarrow \text{NH}_3$	1000	d^{-1}	Reichert et al., 2001
$k_{\text{eq},w}$	Dissociation constant of $\text{H}^+ \leftrightarrow \text{OH}^-$	1000	$\text{g m}^{-1} \text{d}^{-1}$	Reichert et al., 2001

A6.5 Mathematical expressions of the stoichiometric coefficients of each process.

Stoichiometric coefficient	Unit
Microalgae growth on ammonia	
$v_{1,1a} = -i_{\text{N,ALG}}$	gN gCOD^{-1}
$v_{4,1a} = 8i_{\text{C,ALG}}/3 + 8i_{\text{H,ALG}} - i_{\text{O,ALG}} - 12i_{\text{N,ALG}}/7$	$\text{gO}_2 \text{ gCOD}^{-1}$
$v_{5,1a} = -i_{\text{C,ALG}}$	gC gCOD^{-1}
$v_{8,1a} = i_{\text{N,ALG}}/14$	gH gCOD^{-1}
$v_{10,1a} = 1$	gCOD gCOD^{-1}
Microalgae growth on nitrate	
$v_{3,1b} = -i_{\text{N,ALG}}$	gN gCOD^{-1}
$v_{4,1b} = 8i_{\text{C,ALG}}/3 + 8i_{\text{H,ALG}} - i_{\text{O,ALG}} - 20i_{\text{N,ALG}}/7$	$\text{gO}_2 \text{ gCOD}^{-1}$
$v_{5,1b} = -i_{\text{C,ALG}}$	gC gCOD^{-1}
$v_{8,1b} = -i_{\text{N,ALG}}/14$	gH gCOD^{-1}
$v_{10,1b} = 1$	gCOD gCOD^{-1}
Microalgae endogenous respiration	
$v_{1,2} = i_{\text{N,ALG}}$	gN gCOD^{-1}
$v_{4,2} = (i_{\text{O,ALG}}) - 8(i_{\text{H,ALG}}) - 8/3(i_{\text{C,ALG}}) + 12/7(i_{\text{N,ALG}})$	$\text{gO}_2 \text{ gCOD}^{-1}$
$v_{5,2} = i_{\text{C,ALG}}$	gC gCOD^{-1}
$v_{8,2} = -1/14(i_{\text{N,ALG}})$	gH gCOD^{-1}
$v_{10,2} = -1$	gCOD gCOD^{-1}
Microalgae inactivation	
$v_{1,3} = i_{\text{N,ALG}}$	gN gCOD^{-1}

$v_{4,3} = (i_{O,ALG}) - 8(i_{H,ALG}) - 8/3(i_{C,ALG}) + 12/7(i_{N,ALG})$	$gO_2 \text{ gCOD}^{-1}$
$v_{5,3} = i_{C,ALG}$	$gC \text{ gCOD}^{-1}$
$v_{8,3} = -1/14(i_{N,ALG})$	$gH \text{ gCOD}^{-1}$
$v_{10,3} = -1$	$gCOD \text{ gCOD}^{-1}$
Chemical equilibria $CO_2 \leftrightarrow HCO_3^-$	
$v_{5,4} = -1$	$gC \text{ gC}^{-1}$
$v_{6,4} = 1$	$gC \text{ gC}^{-1}$
$v_{8,4} = 1/12$	$gH \text{ gC}^{-1}$
Chemical equilibria $HCO_3^- \leftrightarrow CO_3^{2-}$	
$v_{6,5} = -1$	$gC \text{ gC}^{-1}$
$v_{7,5} = 1$	$gC \text{ gC}^{-1}$
$v_{8,5} = 1/12$	$gH \text{ gC}^{-1}$
Chemical equilibria $NH_4^+ \leftrightarrow NH_3$	
$v_{1,6} = -1$	$gN \text{ gN}^{-1}$
$v_{2,6} = 1$	$gN \text{ gN}^{-1}$
$v_{8,6} = 1/14$	$gH \text{ gN}^{-1}$
Chemical equilibria $H^+ \leftrightarrow OH^-$	
$v_{8,7} = 1$	$gH \text{ gH}^{-1}$
$v_{9,7} = 1$	$gH \text{ gH}^{-1}$
Oxygen transfer to the atmosphere	
$v_{4,O_2} = 1$	—
Carbon dioxide transfer to the atmosphere	
$v_{5,CO_2} = 1$	—
Ammonia transfer to the atmosphere	
$v_{2,NH_3} = 1$	—

A6.6 Values of fraction of carbon, hydrogen, oxygen and nitrogen in microalgae biomass.

Parameter	Description	Value	Unit	Source
Fractions of microalgal biomass				
$i_{C,ALG}$	Fraction of carbon in microalgae	0.387	$gC \text{ gCOD}^{-1}$	Reichert et al., 2001
$i_{H,ALG}$	Fraction of hydrogen in microalgae	0.075	$gH \text{ gCOD}^{-1}$	Reichert et al., 2001
$i_{O,ALG}$	Fraction of oxygen in microalgae	0.538	$gO_2 \text{ gCOD}^{-1}$	Reichert et al., 2001
$i_{N,ALG}$	Fraction of nitrogen in microalgae	0.065	$gN \text{ gCOD}^{-1}$	Reichert et al., 2001

Table A6.7 Experimental data obtained from vertical photobioreactor in Almeria (Spain).

Date	Temperature [°C]	Irradiance [$\mu\text{mol m}^{-2} \text{s}^{-1}$]	S_{O_2} [$\text{gO}_2 \text{ m}^{-3}$]	pH
28/2/12 0:00	13.5	0	6.4	8.2
28/2/12 0:30			6.4	8.23
28/2/12 1:00	13.5	0	6.4	8.2
28/2/12 1:30			6.4	8.18
28/2/12 2:00	13.5	0	6.4	8.2
28/2/12 2:30			6.4	8.2
28/2/12 3:00	13.5	0	6.4	8.18
28/2/12 3:30			6.4	8.21
28/2/12 4:00	13.5	0	6.4	8.2
28/2/12 4:30			6.4	8.2
28/2/12 5:00	13.5	0	6.4	8.18
28/2/12 5:30			6.4	8.2
28/2/12 6:00	13.5	0	6.4	8.23
28/2/12 6:30			6.4	8.2
28/2/12 7:00	13.5	0	6.4	8.2
28/2/12 7:30			6.4	8.23
28/2/12 8:00	13.5	250	6.72	8.35
28/2/12 8:30			7.36	8
28/2/12 9:00	13.5	350	9.6	7.6
28/2/12 9:30			12.16	7.6
28/2/12 10:00	13.5	500	14.4	7.57
28/2/12 10:30			16.64	7.57
28/2/12 11:00	13.5	800	19.2	7.6
28/2/12 11:30			20.16	7.6
28/2/12 12:00	13.5	1100	20.16	7.57
28/2/12 12:30			19.68	7.6
28/2/12 13:00	13.5	1300	19.84	7.6
28/2/12 13:30			20.16	7.6
28/2/12 14:00	13.5	1100	20.16	7.6
28/2/12 14:30			20	7.57
28/2/12 15:00	13.5	800	19.68	7.57
28/2/12 15:30			19.52	7.6
28/2/12 16:00	13.5	500	18.24	7.6
28/2/12 16:30			16	7.57
28/2/12 17:00	13.5	350	14.4	7.6
28/2/12 17:30			12.8	7.6
28/2/12 18:00	13.5	250	10.56	7.55
28/2/12 18:30			8	7.54
28/2/12 19:00	13.5	0	6.4	7.54
28/2/12 19:30			6.4	7.54
28/2/12 20:00	13.5	0	6.4	7.6

28/2/12 20:30			6.4	7.65
28/2/12 21:00	13.5	0	6.4	7.7
28/2/12 21:30			6.4	7.75
28/2/12 22:00	13.5	0	6.4	7.8
28/2/12 22:30			6.4	7.85
28/2/12 23:00	13.5	0	6.4	7.9
28/2/12 23:30			6.4	8
29/2/12 0:00	13.5	0	6.4	8.05

Table A6.8 Experimental data obtained from horizontal photobioreactor in Barcelona (Spain).

Date	Temperature [°C]	Irradiance [$\mu\text{mol m}^{-2} \text{s}^{-1}$]	pH	S _{O2} [$\text{gO}_2 \text{m}^{-3}$]	S _{NO3} [gN m^{-3}]	S _{HCO3} [gC m^{-3}]
16/4/12 11:00	17.4	154.99	8.45	6.64	0.613	7.59
16/4/12 12:00			8.63	6.97		
16/4/12 13:00	22.8	185.31	8.80	7.30	0.598	7.70
16/4/12 14:00			8.98	7.51		
16/4/12 15:00	24.6	163.57	9.04	7.71	0.591	7.54
16/4/12 16:00			9.09	7.82		
16/4/12 17:00	24.2	126.35	9.15	7.92	0.578	7.11
16/4/12 18:00			9.18	8.14		
16/4/12 19:00	21.8	3.37	9.21	8.36	0.511	5.74
16/4/12 20:00			9.24	8.45		
16/4/12 21:00	16.8	0.00	9.13	8.54	0.480	4.88
16/4/12 22:00			9.03	8.60		
16/4/12 23:00	15.5	0.00	8.92	8.66	0.339	4.52
17/4/12 0:00			8.61	7.87		
17/4/12 1:00	12.5	0.00	8.31	7.07	0.174	4.38
17/4/12 2:00			8.00	6.99		
17/4/12 3:00	11.2	0.00	7.89	5.90	0.000	4.52
17/4/12 4:00			7.77	5.62		
17/4/12 5:00	9.4	0.00	7.66	5.34	0.000	4.95
17/4/12 6:00			7.78	5.25		
17/4/12 7:00	8.5	3.37	7.90	5.36	0.000	5.06
17/4/12 8:00			8.02	5.39		
17/4/12 9:00	9.8	16.85	8.31	5.42	0.000	5.08
17/4/12 10:00			8.61	5.79		

17/4/12 11:00	19.6	143.20	8.90	6.16	0.000	5.01
17/4/12 12:00			8.93	7.53		
17/4/12 13:00			8.97	8.00		
17/4/12 14:00	27	185.31	9.00	8.48	0.000	5.06
17/4/12 15:00			9.10	8.95		
17/4/12 16:00			9.20	9.35		
17/4/12 17:00	29.6	122.98	9.30	9.75	0.000	4.58
17/4/12 18:00			8.93	10.15		
17/4/12 19:00			8.55	10.67		
17/4/12 20:00	20.8	6.74	8.18	11.19	0.000	4.38
17/4/12 21:00			7.80	11.41		
17/4/12 22:00			7.60	11.56		
17/4/12 23:00	15.8	0.00	7.40	11.21	0.000	4.04
18/4/12 0:00			7.20	11.46		
18/4/12 1:00			7.00	11.40		
18/4/12 2:00	14.1	0.00	7.18	11.34	0.000	3.76
18/4/12 3:00			7.36	11.28		
18/4/12 4:00			7.54	11.21		
18/4/12 5:00	13.4	0.00	7.72	11.14	0.000	3.73
18/4/12 6:00			7.90	11.07		
18/4/12 7:00			8.46	11.06		
18/4/12 8:00	12.7	8.42	9.02	11.04	0.000	3.74
18/4/12 9:00			9.58	11.02		
18/4/12 10:00			10.14	11.17		
18/4/12 11:00	14.1	38.75	10.06	11.32	0.000	3.72
18/4/12 12:00			9.97	11.47		
18/4/12 13:00			9.89	11.66		
18/4/12 14:00			9.80	11.84		
18/4/12 15:00	19.9	92.66	9.72	12.02	0.000	3.50
18/4/12 16:00			9.44	12.40		
18/4/12 17:00			9.15	12.78		
18/4/12 18:00			8.87	13.16		
18/4/12 19:00	22.8	55.59	8.58	13.18	0.000	3.18
18/4/12 20:00			8.36	13.19		
18/4/12 21:00			8.15	13.21		
18/4/12 22:00	15.8	0.00	7.93	13.22	0.000	3.05
18/4/12 23:00			7.72	13.14		

19/4/12 0:00			7.50	13.06		
19/4/12 1:00			7.88	12.98		
19/4/12 2:00	14.3	0.00	8.27	12.90	0.000	3.18
19/4/12 3:00			8.65	12.82		
19/4/12 4:00			9.04	12.73		
19/4/12 5:00			9.42	12.64		
19/4/12 6:00	12.5	3.37	9.44	12.56	0.000	3.50
19/4/12 7:00			9.46	12.47		
19/4/12 8:00			9.47	12.36		
19/4/12 9:00			9.49	12.26		
19/4/12 10:00	19	47.17	9.51	12.15	0.000	3.50

Table A6.9 Mathematical equations for estimating irradiance at any point on Earth. Parameters and factors are described in Appendix A6.3.

Description	Mathematical Equation	Units
Total incident irradiance	$I_0 = \frac{\pi H E_f}{24} \{ [0.409 + 0.5016 \cdot \sin(\omega_s - 60)] + [0.6609 - 0.4767 \cdot (\omega_s - 60)] \cos \omega \}$ $\cdot \left(\frac{\cos \omega \cdot \cos \omega_s}{\sin \omega_s - \omega_s \cdot \cos \omega_s} \right) \cdot 0.2174$	$\mu\text{E m}^{-2}\text{s}^{-1}$
Daily radiation	$H = \kappa H_0$	$\text{J m}^{-2}\text{d}^{-1}$
Total daily extraterrestrial radiation	$H_0 = \left(\frac{24\zeta}{\pi} \right) \left(1 + 0.003 \cdot \cos \left(\frac{360 N}{365} \right) \right) \left(\cos \phi \cdot \cos \delta \cdot \sin \omega_s + \frac{2\pi \omega_s}{360} \cdot \sin \phi \cdot \sin \delta \right)$	$\text{J m}^{-2}\text{d}^{-1}$

Table A6.10 Comparison of temperature range used during the simulations with daily temperature variations and under controlled temperature.

Months	Daily temperature variations [°C]		Controlled temperature [°C]
	Min	Max	Constant value
January	8	17	12.5
February	9	18	13.5
March	10	20	15.5
April	12	21	17.5
May	14	24	20.5
June	18	28	23
July	21	31	24
August	22	31	24.5
September	20	29	21

7

Integrated BIO_ALGAE model

This chapter is based on the article:

- ❖ A. Solimeno, L. Parker, T. Lundquist, J. García. (submitted). Integral microalgae-bacteria model (BIO_ALGAE): application to wastewater high rate algal ponds.

7.1 Introduction

In the past decade, an increasing amount of research has been conducted on microalgae-bacterial systems for wastewater treatment. These efforts were initially stimulated by the interest in producing biofuel from microalgae (Park and Craggs, 2011a; Milano et al., 2016), but, compared to conventional wastewater treatment technologies, the potential total cost savings, including in electrical power, are great enough to pursue this topic independently of biofuels production (Suganya et al., 2016).

The system is based on the interactions of microalgae and bacteria in wastewater exposed to light. Algae photosynthesize and produce the oxygen used by bacteria, reducing or eliminating the need for mechanical aeration (Tricolici et al., 2014, Sayeda et al., 2016). Assimilation of nutrients (i.e. nitrogen and phosphorus) by algae is a further form of treatment (Liang et al., 2013), and pathogen inactivation also occurs in these algal-bacterial systems (Abdel et al., 2012).

Algal-bacterial wastewater treatment was originally carried-out in unmixed ponds – shallow oxidation ponds and deeper facultative ponds (Oswald and Gotaas, 1957), with mixed raceway ponds (specifically named high rate algal ponds) being introduced at full scale for increased cultivation control and algal productivity (Oswald et al., 1957). Using the produced algae biomass for biofuel feedstock was suggested shortly thereafter Oswald and Golueke (1960). Various other reactor designs have been proposed such as transparent vessels (e.g. tubular photobioreactors) and attached growth systems (e.g., algal turf scrubbers, Christenson and Sims, 2012). However, these other types of reactors are not a full scale reality, and belong to a more experimental domain in the field of wastewater treatment. These more complex and costly designs in comparison to mixed raceway ponds will be less competitive with conventional electromechanical treatment technologies.

In comparison with conventional treatment technologies, less is known about the physical, chemical and biochemical reactions and processes that occur in microalgae-bacteria wastewater treatment systems. Most of these

reactions and processes take place simultaneously and they are strongly interdependent (García et al., 2006). Also, they are dependent on ever-changing outdoor environmental conditions such as light intensity, temperature, and the flow and quality of the influent wastewater. In order to predict performance and optimize reactor design, it is necessary to have a deep pond wastewater treatment system ecological understanding.

Mathematical models offer an opportunity to study microalgae-bacteria interactions, can provide useful tools for design, and can control real-world parameters, which can all lead to increase bioreactor efficiency (Bitog et al., 2011). While much research has been conducted on microalgae models over the years (e.g. Dropp, 1968; Bernard et al., 2009), only recently has research intensively began on the integration of microalgal growth on biological wastewater treatment (microalgae-bacteria models). The very first modeling in this area was pioneered by Buhr and Miller (1983), and it focused on the simultaneous growth of algae and bacteria in high-rate algae ponds (HRAPs). HRAPs, which are shallow, low-energy, and paddle-wheel mixed treatment ponds, are typical in advanced pond wastewater treatment systems. Since Buhr and Miller (1983), other more sophisticated models have been developed mostly based on parameters and processes similar to those defined by the River Water Quality Model 1 (RWQM1) of the International Water Association (Reichert et al., 2011). However, while RWQM1 includes expressions for growth of microalgae on N (ammonium and nitrate) and P (orthophosphate), it does not include expressions for essential C limitations (carbon dioxide and bicarbonate) which can occur in algae growing in wastewater systems (Gehring et al., 2010). In the model by Sah et al. (2011) algal growth was described as a function of either ammonium or nitrate, with preference for ammonium. Halfhide et al. (2015) developed a simplified algae-bacteria model to simulate ammonia removal from wastewater, assuming the irradiance as limiting factor for algae growth. Likewise, Steen et al. (2015) proposed a simplified version of the Activated Sludge Model no. 3 (ASM3) based on the biomass growth of ammonia oxidizing bacteria, nitrite oxidizing bacteria, and microalgae.

Most of these previous models use a relatively low number of parameters to describe the inherent complexity of algae cultures and/or focus on single processes within the system, neither of which considers that microalgae-

bacterial technologies are systemic processes that involve multiple components (e.g. carbon, nitrogen, and dissolved oxygen (DO)). Other more complex models (such as the RWQM1 or the one by Sah et al. (2011)) do not include carbon limitation on the growth of microalgae and autotrophic bacteria, and lack the possible effect of high dissolved oxygen concentration in mixed liquor on microalgae activity.

In this paper we complete the microalgae model previously developed by the authors (Chapter 4 and 6; Solimeno et al., 2015, 2017b), including crucial physical, chemical and biokinetic processes of microalgae as well as bacteria in wastewater treatment systems. The model, which is called BIO_ALGAE was mainly built by coupling the model of the authors (Solimeno et al., 2015) with the modify ASM3 (Iacopozzi et al., 2007). These models were used as base model to represent the microalgae and bacteria activity, respectively. The new most relevant feature of the model is the inclusion of carbon limitation on the growth of microalgae and the growth of autotrophic bacteria. Also, other relevant features are photolimitation, light attenuation, photorespiration, temperature dependency and the implementation of hydrodynamics in the system.

Altogether the main purpose of this study was to develop, calibrate and validate the integral microalgae and bacteria model with high quality experimental data from triplicate raceway ponds located at the Delhi, California wastewater pond treatment plant. The implementation of BIO_ALGAE in the COMSOL MultiphysicsTM software allowed to simulate the dynamics of different components in the ponds and the relative proportion of microalgae and bacteria. Also the model was used for to applications: 1) to analyze the relative effect of the factors that affect microalgae growth, and 2) a study case on the effect of influent concentration of organic matter on the relative proportions of microalgae and bacteria. Our idea is to create a basis for a highly accepted platform that will be extensively used for different research purposes. Also, in the future, we believe that this model could help the industry to design and operate efficient microalgae-bacteria systems.

7.2 Model description

7.2.1 Conceptual model

In order to facilitate the comprehension of the model, Fig. 7.1 shows a general simplified schematic representation of the conceptual model describing the complexity of microalgal-bacterial interactions.

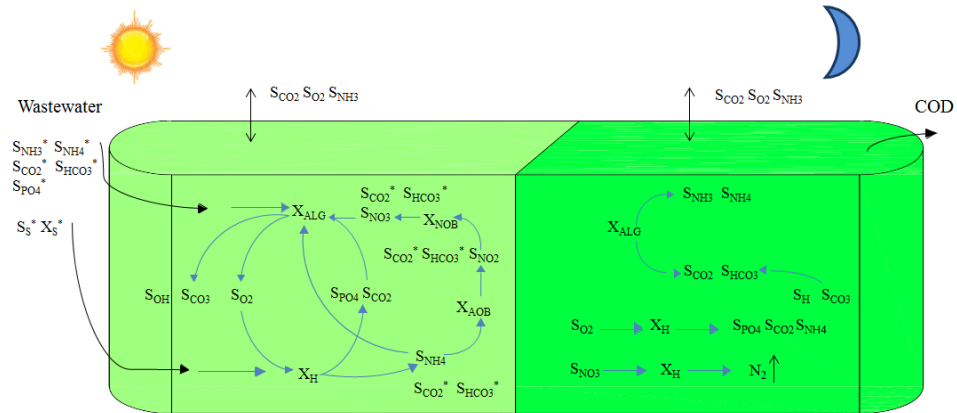


Figure 7.1 General simplified schematic representation of the conceptual integrated model showing the main algal-bacterial interactions in a high rate algal pond, during day (left) and night (right). Components which enter the ponds with the influent are marked with * and processes are indicated by arrows. Particulate and dissolved components and processes are described in Section 7.2.2.

Photosynthetic processes are activated with light. While microalgae (X_{ALG}) grow, they fix inorganic carbon (S_{CO2} and S_{HCO3}), consume substrates (S_{NH4} , S_{NO3} and S_{PO4}) present in wastewater and supply oxygen (S_{O2}) required by heterotrophic bacteria (X_H) to oxidize organic matter. During bacterial organic matter oxidation, CO_2 is produced and it is available for photosynthesis and nitrification. Nitrification is a two-step process: first ammonium oxidizing bacteria (X_{AOB}) convert ammonia and ammonium to nitrite (S_{NO2}) and second nitrite oxidizing bacteria (X_{NOB}) convert nitrite to nitrate (S_{NO3}) (Diehl et al., 2007).

As result of microalgal activity, hydroxide ion concentrations (S_{OH}) and pH increase. With increasing pH, bicarbonate-carbonate equilibrium is displaced, pushing carbon species towards the formation of carbonate

(S_{CO_3}), lead ammonia volatilization, and phosphorus precipitation (Nurdogan and Oswald, 1995; Serodes et al., 1991).

In darkness, both heterotrophic bacteria (X_{H}) and microalgae (X_{ALG}) have a net CO_2 release through oxidation of organic matter and endogenous respiration, respectively. With this release, concentrations of hydrogen ions increase and pH decreases, and the bicarbonate-carbonate equilibrium shifts and the carbonate turn into bicarbonate (S_{HCO_3}). This bicarbonate can be used as a substrate again in the presence of light. Microalgae respiration and bacterial growth reduce the oxygen level within the water. When oxygen levels are low, nitrate can become the primary source of oxygen, and denitrification occurs. This process is performed under anoxic conditions by denitrifying bacteria that reduce nitrate (S_{NO_3}) into nitrogen gas. In fact, denitrifying bacteria are considered to be the same heterotrophic bacteria (X_{H}) that under oxygen depletion circumstances can facultative use S_{NO_3} instead of S_{O_2} .

Microalgae and bacteria processes are influenced by temperature, which also affects chemical equilibria, pH and gas solubility (Bouterfas et al., 2002). Furthermore, in HRAPs the excess of DO and CO_2 is gradually transferred from the culture medium to the atmosphere.

7.2.2 Model components

The model uses the common nomenclature of the IWA models and considers 19 components – 6 particulate and 13 dissolved – implicated as variables in the physical, chemical and biokinetic processes. In the following two sections components are described, as well as their main role in processes and their interactions with other components.

Particulate components

X_{ALG} [g COD m^{-3}]: *Microalgae biomass*. It increases with growth processes pertinent to microalgae and decreases by endogenous respiration and inactivation of microalgae. Not present in influent wastewater.

X_H [g COD m⁻³]: *Heterotrophic bacteria*. These organisms use organic matter as a source of carbon and energy. They grow in aerobic as well as anoxic heterotrophic conditions and decrease by endogenous respiration and decay. These bacteria are responsible for hydrolysis processes and they are also present in the wastewater influent.

X_{AOB} [g COD m⁻³]: *Ammonium oxidizing bacteria*. Bacteria responsible for the first step of nitrification, the conversion of ammonium to nitrite. These microorganisms are produced by aerobic growth and decrease by endogenous respiration and decay. They are assumed to be present in the wastewater influent.

X_{NOB} [g COD m⁻³]: *Nitrite oxidizing bacteria*. Bacteria responsible for the second step of nitrification, the conversion of nitrite to nitrate. These microorganisms are produced by aerobic growth and decrease by endogenous respiration and decay. They are assumed to be present in the wastewater influent.

X_S [g COD m⁻³]: *Slowly biodegradable particulate organic matter*. Fraction of the particulate organic matter COD which can be hydrolyzed and converted into readily biodegradable organic matter COD (S_S) and inert organic matter (S_I). A large fraction of X_S is assumed to originate from decay of microorganisms and it is also present in the wastewater influent.

X_I [g COD m⁻³]: *Inert particulate organic matter*. It is the remainder after particulate organic matter hydrolysis and it increases by decay of microorganisms. It is also present in the wastewater influent.

Note that particulate components are expressed in g COD m⁻³, as it is common practice to express organic matter concentrations in all IWA models. In the present work microalgae and bacteria biomass is transformed from COD to TSS (total suspended solids) assuming a ratio COD/TSS= 0.80 (Sperling, 2007; Khorsandi et al., 2014) in order to compare experimental and simulation results.

Dissolved components

S_{NH_4} [g $\text{NH}_4^+\text{-N m}^{-3}$]: *Ammonium nitrogen*. Ammonium enters the ponds with the influent and is produced through endogenous respiration of all types of microorganisms in the model and decay of microorganisms. It is consumed through the growth of microalgae, heterotrophic bacteria (X_{H}) and during the first step of nitrification by ammonium oxidizing bacteria (X_{AOB}).

S_{NH_3} [g $\text{NH}_3\text{-N m}^{-3}$]: *Ammonia nitrogen*. It is in acid-base equilibrium with ammonium (S_{NH_4}), and comes into play in the model only as a gaseous compound. Its volatilization rate is modeled as a function of pH, temperature, and mixing intensity.

S_{NO_3} [g $\text{NO}_3^-\text{-N m}^{-3}$]: *Nitrate nitrogen*. Nitrate can enter the pond with the influent, although usually in negligible concentration. It is produced during nitrification by nitrite oxidizing bacteria (X_{NOB}). Nitrate can be assimilated by microalgae (X_{ALG}) and heterotrophic bacteria (X_{H}), and can also be used (consumed) as electron acceptor by heterotrophic bacteria, which are assumed to be facultative.

S_{NO_2} [g $\text{NO}_2\text{-N m}^{-3}$]: *Nitrite nitrogen*. Nitrite can enter the pond with the influent, although usually in negligible concentration. It is generated as an intermediate step the nitrification process. It is consumed by nitrite oxidizing bacteria (X_{NOB}) and heterotrophic bacteria (X_{H}) during denitrification.

S_{PO_4} [g $\text{PO}_4^-\text{-P m}^{-3}$]: *Phosphate phosphorus*. It enters with influent wastewater and is released from oxidation of organic matter. It is assimilated during the growth of microalgae, heterotrophic bacteria (X_{H}) and autotrophic bacteria (X_{AOB} , X_{NOB}). It is generated during respiration and decay of all microorganisms.

S_{O_2} [g $\text{O}_2 \text{ m}^{-3}$]: *Dissolved oxygen*. It is produced during photosynthetic growth of microalgae and it can be transferred to/from the atmosphere. It is consumed during aerobic respiration and decay of all types of microorganisms.

S_{CO_2} [g $\text{CO}_2\text{-C m}^{-3}$]: *Dissolved carbon dioxide*. It is in chemical equilibrium with bicarbonate (S_{HCO_3}) and carbonate (S_{CO_3}). It is generated during respiration

and decay, and can be transferred to/from the atmosphere. It is consumed by both microalgae (X_{ALG}) and autotrophic bacteria (X_{AOB} and X_{NOB}), and is produced during the growth of heterotrophic bacteria, and respiration and decay of all types of microorganisms.

S_{HCO_3} [g HCO_3^- -C m^{-3}]: *Bicarbonate*. It is in chemical equilibrium with carbon dioxide (S_{CO_2}) and carbonate (S_{CO_3}). It is consumed by microalgae.

S_{CO_3} [g CO_3^{2-} -C m^{-3}]: *Carbonate*. It is in chemical equilibrium with bicarbonate (S_{HCO_3}) and carbon dioxide (S_{CO_2}). Carbonate cannot be directly used by microalgae and autotrophic bacteria.

S_{H} [g H^+ m^{-3}]: *Hydrogen ions*. They are involved in acid-base equilibria including the carbonate, ammonium, and phosphate systems. Hydrogen ions are produced by ammonium oxidizing bacteria (X_{AOB}) and heterotrophic bacteria (X_{H}). They decrease during the growth of microalgae and nitrifying bacteria (X_{NOB}), and during endogenous respiration and decay of all microorganisms.

S_{OH} [g OH^- -H m^{-3}]: *Hydroxide ions*. They are in equilibrium with hydrogen ions.

S_{s} [g COD m^{-3}]: *Readily biodegradable soluble organic matter*. Fraction of the soluble organic matter directly available for biodegradation by heterotrophic bacteria (X_{H}). It is contained in the influent wastewater and is produced during the hydrolysis of biodegradable particulate organic matter (X_{s}).

S_{I} [g COD m^{-3}]: *Inert soluble organic matter*. Fraction of the soluble organic matter that is not readily available for biodegradation by heterotrophic bacteria (X_{H}). It is in the influent wastewater and is produced during the hydrolysis of biodegradable particulate organic matter (X_{s}).

7.2.3 Model processes

In this section, bacterial processes involved in wastewater treatment are presented. A description of the microalgae processes, chemical equilibrium reactions, and transfer of gases to the atmosphere was reported previously in Chapter 4 (Solimeno et al., 2015).

Using Monod kinetics, bacterial processes were modelled in the same way as microalgae processes. The main inspiration for building the bacteria processes was the River Water Quality Model 1 (RWQM1) and Activated Sludge Model 3 (ASM3) (Reichert et al., 2001, Iacopozzi et al., 2007). A certain number of simplifications were made in order to make easier the control of biochemical processes. This means that in comparison to ASM3, the model does not consider processes related to the storage of readily biodegradable soluble organic matter (S_S). Anaerobic biological processes, such as fermentation and sulfate reduction, which can sometimes be important in wastewater treatment, were also omitted because the relatively oxidized nature of microalgal-bacterial processes. Moreover, absorption and desorption of phosphate on particular matter were neglected.

Table A7.1 in the Appendix shows a list of the processes included in the complete model (bacteria and microalgae) and the equations describing their rates. Table A7.2 in Appendix shows the matrix of stoichiometric parameters. A complete list of parameters and stoichiometric coefficients used in the model is located in Appendix, Tables A7.3-A7.5.

- **Aerobic and anoxic growth of heterotrophic bacteria (X_H)** (Processes 4a, 4b, 5 and 6 in Table A7.1). Growth of heterotrophic bacteria was modeled with Monod kinetics. Anoxic and aerobic heterotrophic processes use the same parameter and coefficient values. Anoxic processes include an additional reduction factor (η_H), similar to the ASM3 model (Gujer et al., 1999).

In aerobic conditions, heterotrophic bacteria assimilate the readily biodegradable substrate (S_S) (coming with the influent or produced during the hydrolysis of biodegradable particulate organic matter (X_S)), and growth consuming both ammonium and ammonia (S_{NH_4} , S_{NH_3}) and nitrate (S_{NO_3}) as

nitrogen source. Note that in the matrix of stoichiometric parameters (Table A7.2) only the ammonium reaction rate is affected by bacterial growth because the concentration of ammonia is already in chemical equilibrium with it.

At dissolved oxygen concentrations less than 0.5 g m^{-3} heterotrophic bacteria use nitrate (S_{NO_3}) as electron acceptor and convert it in nitrogen gas (N_2) (denitrification) (Korner and Zumft, 1986). The denitrification is implemented in the model as separating processes with S_{NO_3} and S_{NO_2} as substrates for heterotrophic bacteria (processes 5 and 6 in Table A7.1), (Iacopozzi et al., 2007). In HRAP this process can occur at night, when photosynthesis is not happening (García et al., 2000b).

The temperature dependence of bacterial processes is modeled with an Arrhenius type thermal factor ($f_{\text{T,MB}}$)[-] (Sah et al., 2011; Langergraber et al., 2009; Reichert et al., 2001). This factor increases exponentially with temperature (T , given in $^{\circ}\text{C}$) (Reichert et al., 2001):

$$f_{\text{T,MB}}(T) = \theta^{T-T_{\text{OPT}}} \quad (7.1)$$

where T_{OPT} was assumed equal to $20 \text{ }^{\circ}\text{C}$, and θ is the temperature coefficient, which was assumed equal for both heterotrophic and autotrophic bacteria.

- **Aerobic and anoxic endogenous respiration of heterotrophic bacteria (X_{H})** (Processes 7 and 8 in Table A7.1). These processes are modeled as the product between the maximum rate of endogenous respiration ($k_{\text{resp,H}}$), the concentration of heterotrophic bacteria, the thermal factor (the same as used for growth), and the Monod function as it relates limiting oxygen and nitrogen concentrations respectively for aerobic and anoxic conditions. Endogenous respiration produces CO_2 and transforms alive biomass into inert organic matter (X_{I}).

- **Decay of heterotrophic bacteria (X_{H})** (Process 9 in Table A7.1). Decay of bacteria transforms alive biomass into dead slowly biodegradable (X_{S}) and inert (X_{I}) organic matter (Van Loosdrecht and Henze, 1999). This process is

expressed as the product of the maximum rate of decay ($k_{\text{decay,H}}$) by the concentration of bacteria and the thermal factor. The process is assumed to continue with the same rate under aerobic and anoxic conditions (Henze et al., 1987).

- **Growth of autotrophic bacteria (X_{AOB} and X_{NOB})** (Processes 10 and 11 in Table A7.1). These bacteria are responsible for the biological conversion of ammonium to nitrate nitrogen (nitrification) using molecular oxygen as electron acceptor. Nitrification is implemented in a two-step process (Iacopozzi et al., 2007).

- **Endogenous respiration of autotrophic bacteria (X_{AOB} and X_{NOB})** (Processes 12 and 13 in Table A7.1). This process is modeled in the same way as the aerobic endogenous respiration of heterotrophic bacteria.

- **Decay of autotrophic bacteria (X_{AOB} and X_{NOB})** (Process 14 in Table A7.1). This process is modeled in the same way as the decay of heterotrophic bacteria using different decay rates, $k_{\text{decay,AOB}}$ and $k_{\text{decay,NOB}}$, respectively for X_{AOB} and X_{NOB} .

- **Hydrolysis** (Process 15 in Table A7.1). Hydrolysis is the process of transformation of slowly biodegradable particulate organic matter (X_s) into readily biodegradable soluble organic matter (S_s) catalyzed by heterotrophic bacteria.

7.2.4 Stoichiometric and parameter values

The complete stoichiometric matrix is presented in Table A7.2 in the Appendix and is based on the structure of IWA models (Petersen matrix). Values of physical, chemical and biokinetic parameters are shown in Table A7.3. Mathematical expressions of the stoichiometric coefficients for each process are shown in Table A7.4. Using Tables (A7.1-A7.2), the reaction rate for each component of the model (r_i) is obtained using:

$$r_i = \sum_j v_{j,i} \cdot \rho_j$$

(7.2)

where i is the number of the component and j is the number of the processes; q_j is the reaction rate for each process j and v_{ij} is the stoichiometric coefficient.

The expressions of stoichiometric coefficients related to microalgae and bacteria processes are based on the fractions of carbon hydrogen, oxygen, nitrogen and phosphorus (Table A7.5).

7.3 Pilot plant and experimental verification

High quality experimental data for model calibration and validation were collected from three sets of triplicate HRAPs (3.5 m² and 0.3 m deep), named South, Middle, and North, which were fed municipal wastewaters (Fig. 7.2). These small pilot raceways were located at a full-scale facultative pond-HRAP facility treating an average of 2,300 m³d⁻¹ of wastewater from the inland community of Delhi, California (Fig. 7.3). Data for this work were obtained during experiments conducted to optimize wastewater treatment in conjunction with algae biomass production, harvesting, and conversion to liquid biofuel.



Figure 7.2 Real view of triplicate South, Middle and North high rate algal ponds of Delhi facilities.

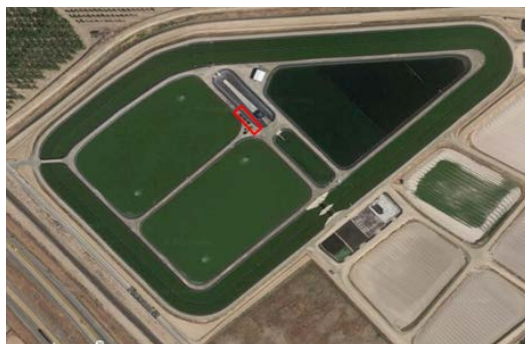


Figure 7.3 Area view of full-scale facultative pond-high rate algal pond in Delhi (California). The red box indicates the area where are located the triplicate high rate algal ponds.

Experimental data from the Middle pilot ponds were used. These ponds had 4.2-days hydraulic retention time (HRT), were fed with facultative pond effluent and were mechanically aerated at night from 6:00 pm to 6:00 am. Mechanical aeration was applied in order to maintain enough dissolved oxygen (DO) in the ponds at night, when oxygen was not produced by photosynthesis in order to ensure nitrification activity. The ponds received regular influent pulses (approximately 26.5 L/pulse) during the hours of 7:00 am to 4:00 pm. Each pond had a rotating paddle wheel with a rotation speed of approximately 10 rpm. In order to monitor the hourly DO, pH, and temperature ($^{\circ}\text{C}$), probes were installed per each pond set. The probes recorded measurements using Neptune System's Apex Fusion software program.

Samples from influent and pond effluents were taken at 9:00 am ± 2 hours for four to six consecutive days in June and July of 2016. Within 48 hours of sampling, assays were conducted to determine the concentration of ammonia (gN m^{-3}), nitrite (gN m^{-3}), nitrate (gN m^{-3}), total nitrogen (g N m^{-3}), alkalinity ($\text{gCaCO}_3 \text{ m}^{-3}$) and total suspended solids (gTSS m^{-3}). COD ($\text{g O}_2 \text{ m}^{-3}$) influent was analyzed only from the first sample of each experiment. These concentrations, as well as the hourly data from the Neptune software probes, were the main data for the model. Additionally, microscopic algal analyses were conducted on one of the four to six consecutive days for each experiment to identify the biological make-up within the ecosystem of each pond. Genera of microalgae common to the pilot ponds included *Chlorella*,

Closterium, Chlorococcum, Oscillatoria, Spirogyra, Synedra, Ulothrix, Westella, Coelastrum, Micratinium, Cyclotella, Nitzschia, Pediastrum, Scenedesmus, and Stigeoclonium.

Samples were analyzed according to Standard Methods (APHA, 1995). Modifications were made to the methods for nitrate and total nitrogen according to Hach Company Methods 10206 and 10071 (Hach, 1992), respectively. Nitrite, nitrate, and total nitrogen analysis were conducted using a Hach DR 3800 spectrophotometer (Hach, Loveland, Colorado) instrument. Ammonia analysis was conducted using a Timberline Model TL-2800 Ammonia/Nitrate Analyzer (Timberline Instruments, Boulder, Colorado) instrument.

7.4 The BIO_ALGAE model

The model was implemented in COMSOL Multiphysics™ v5.1 software. The pilot raceways were represented in a 1D domain 3.5 m long and a periodic condition was applied at boundaries to reproduce the hydrodynamics of the pilots. Hydraulic and transport equations of aqueous phase species (i.e. dissolved and particulate) were added to represent the motion of the culture through the pond. Injection of oxygen at night from 6:00 pm to 6:00 am was implemented in the model to reproduce the mechanical aeration of the HRAPs.

On the other hand, assuming that each point of a section receives the same quantity of photons due to perfectly homogeneous of the pond, it was possible to calculate the light attenuation through an average light intensity representing any point of the culture medium. In this way though the pond depth was not incorporated into the domain design (1D), the exponential decrease of light intensity as it penetrates into the pond has been considered.

Average light intensity (I_{av} [$\mu\text{mol m}^{-2}\text{s}^{-1}$]) was described using Lambert-Beer's Law and is attenuated by the presence of particulate components ($X_C = X_{ALG} + X_H + X_I + X_S + X_{AOB} + X_{NOB}$ [gTSS m^{-3}]) and the depth (d [m]) of the pilot raceways (Eq. 3).

$$I_{av} = \frac{I_o \cdot (1 - e^{(-K_I \cdot X_C \cdot d)})}{K_I \cdot X_C \cdot d} \quad (7.3)$$

where, I_o [$\mu\text{mol m}^{-2}\text{s}^{-1}$] is the incident light intensity and K_I is the extinction coefficient for particulate biomass [$0.07 \text{ m}^2 \text{ g}^{-1}$] (Molina-Grima et al., 1994).

A detailed description of hydrodynamic, transport of species, light intensity and the equations used in the model are reported in Chapter 6.

The model was calibrated using data collected during June 27th, 2016 to June 30th, 2016, from the first two Middle ponds (M1 and M2) in the triplicate set. Data from the third pond (M3) was not used due to lack of DO data.

Influent pond concentrations were used to run simulations. Average influent concentrations are shown in Table 7.1. Fractions of influent COD were estimated using values recommended by Henze et al. (2000). Accordingly, the proportion of each fraction was defined as: 22% S_S , 50% X_S , 10% S_I , 8% X_I , and 10% X_H . The initial concentrations of components in the Middle ponds M1 and M2 at the beginning of the experiments, temperature and irradiance are shown in Table 7.2. Initial conditions from M1 pond were considered to run simulations. The concentration of each particulate component in the pilot raceway at the beginning of the experiment was not known. Therefore, initial ratio of X_{ALG} , X_S , X_I , X_H , X_{AOB} and X_{NOB} concentrations were quantified from initial TSS value (from M1 pond) based on previous simulation tests in order to match the initial pattern trend of pH, dissolved oxygen, and nutrients (i.e. nitrogen and carbon) data.

In this model 46 additional parameters were added to the 31 originally-implemented microalgae parameters (Solimeno et al., 2015), for a total of 87 parameters. Most of these parameters were obtained from the existing RWQM1 (Reichert et al., 2001), ASM1, and ASM3 (Gujer et al., 1999, Henze et al., 2000, Iacopozzi et al., 2007). Parameters related to temperature, photorespiration, carbon limitation and light attenuation were obtained from other literature cited in Appendix (Table A7.3).

Table 7.1 Influent average (standard deviation) high-rate algal pond characteristics used for calibration and validation. $n = 4$. Note that all pilot ponds had the same influent.

Parameter	Influent wastewater
COD (g COD m ⁻³)	185.6 (35)
S _s (g CODm ⁻³)	27.8 (7.7)
X _s (g COD m ⁻³)	93 (17.5)
X _I (g COD m ⁻³)	15 (2.8)
X _H (g COD m ⁻³)	18.5 (3.5)
pH	7.8 (0.1)
NH ₄ ⁺ -N (g m ⁻³)	30.9 (1.5)
NO ₂ -N (g m ⁻³)	0.16 (0.2)
NO ₃ ⁻ -N (g m ⁻³)	0.4 (0.7)
Alkalinity (g CaCO ₃ m ⁻³)	288 (8.2)

Note: S_s, X_s, X_I and X_H concentrations were estimated from COD concentration using values recommended by Henze et al. (2000).

Morris uncertainty method was applied to screening which parameters had the greater influence on the simulation response (Morris, 1991). The detailed implementation of Morris's uncertainty method is described Chapter 5 (Solimeno et al., 2016). Here, based on previously uncertainty analysis, the model was calibrated by adjusting the values of maximum growth rate of microalgae (μ_{ALG}), the maximum growth rate and the decay of heterotrophic bacteria (μ_H and $k_{death,H}$) and the parameters related to the transfer of gases to the atmosphere (K_{a,O_2} , K_{a,CO_2} and K_{a,NH_3}). Calibration was performed comparing real data with simulation curves. Manual trial of parameters was used to match measured data as much as possible using graphical representations. Moreover, characteristic parameters (μ_{ALG} , μ_H , $k_{death,H}$, K_{a,O_2} , K_{a,CO_2} and K_{a,NH_3}), values were adjusted in order to minimize the root mean square error (RMSE) between experimental data and simulated curves. After calibration the model was validated using data collected from July 17th to July 20th, 2016 from the two Middle ponds M1 and M2.

Table 7.2 a) Initial concentrations of the components in Middle ponds (M1 and M2) used for simulations: calibration (June 27th, 2016) and validation (July 17th, 2016). b) Maximum and minimum water temperature and irradiance.

a)

Components	Concentrations				Units
	June 27 th , 2016		July 17 th , 2016		
	M1	M2	M1	M2	
TSS	163	160	174	172	g COD m ⁻³
X _S	4	5	4	4	g COD m ⁻³
X _{ALG}	97	96	108	118	g COD m ⁻³
X _H	50	49	50	40	g COD m ⁻³
X _I	13	11	13	12	g COD m ⁻³
X _{AOB}	0.1	0.15	0.1	0.1	g COD m ⁻³
X _{NOB}	0.05	0.07	0.05	0.05	g COD m ⁻³
S _S	6	6	5	5	g COD m ⁻³
S _{NH4}	1.50	1.70	2.44	2.45	g N-NH ₄ m ⁻³
S _{NH3}	0.15	0.15	0.11	0.11	g N-NH ₃ m ⁻³
S _{NO3}	38.0	37.8	33.2	33.8	g N-NO ₃ m ⁻³
S _{NO2}	0.82	0.96	0.63	0.57	g N-NO ₂ m ⁻³
S _{HCO3}	19.99	20.79	22.40	22.23	g C-CO ₂ m ⁻³
S _{CO2}	0.4	0.5	1.6	1.6	g C-HCO ₃ m ⁻³
S _{CO3}	0.05	0.05	0.08	0.08	g C-CO ₃ m ⁻³
S _{O2}	11	10	12.19	13.44	g O ₂ m ⁻³
S _H	2.00E-8	2.51E-8	1.17E-7	1.29E-7	g H m ⁻³
S _{OH}	5.00E-7	3.98E-7	4.51E-8	7.76E-8	g H-OH m ⁻³

Note: X_{ALG}, X_S, X_H, X_I, X_{AOB} and X_{NOB} concentrations were estimated from TSS concentration.

b)

	Water temperature [°C]		Irradiance [μmol m ⁻² s ⁻¹]	
	Min	Max	Min	Max
Calibration, June 27 th , 2016	17.4	30.2	0	930
Validation, July 17 th , 2016	16	28	0	901

Phosphorus was not considered in the simulations presented here since usually does not cause any growth limiting effect in high rate algal ponds treating wastewaters (Shilton, 2005, García et al., 2002).

Practical study cases were conducted to evaluate the relative effect of nutrients availability (i.e. nitrogen and carbon), temperature and light attenuation on microalgae growth. Moreover, total biomass production and the relative proportion of microalgae and bacteria as a function of different influent concentrations of organic matter were also investigated. In this case, keeping the same nutrient concentrations of the influent wastewater in the pond used for the calibration of the model and the same concentration of components (particulate and dissolved) at beginning of the experiment, three scenarios were evaluated reducing COD influent of 50% and 70%.

7.5 Results and discussion

7.5.1 Model calibration

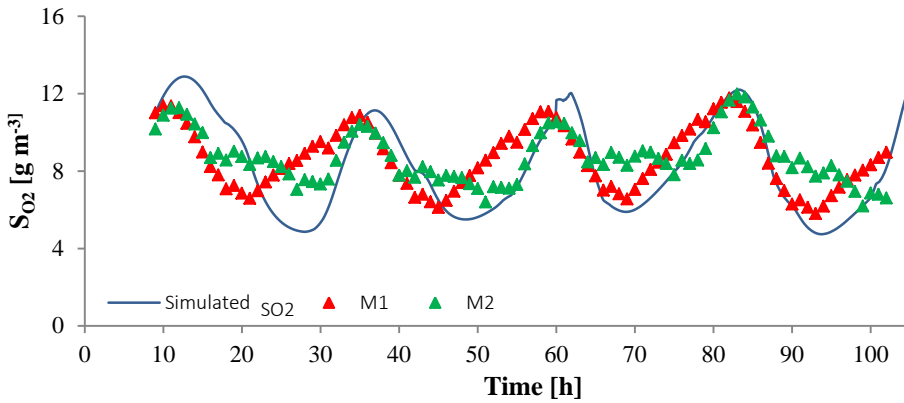
The model was calibrated using duplicate experimental data of pH, DO, TSS, alkalinity, and nitrogen species concentrations from Delhi, California's pilot raceway ponds. From the 93 parameters included in the BIO_ALGAE model (Appendix, A7.3), a global sensitivity analysis of the maximum growth rate of microalgae (μ_{ALG}), the maximum growth rate and the inactivation of heterotrophic bacteria (μ_H and $k_{death,H}$) was performed to evaluate the impact of these parameters on simulation response. In this work, the sensitivity analysis of mass transfer coefficients for oxygen, carbon dioxide and ammonia (K_{a,O_2} , K_{a,CO_2} and K_{a,NH_3}) was not conducted because the results from our previous works already proven that they were very sensitive and likely to be calibrated in each application of the model (Solimeno et al., 2017b, 2015). Note that the μ_{ALG} , μ_H and $k_{death,H}$ were selected because a global sensitivity analysis of whole set of model parameters (93) is quite unattainable objective unless high-end computational facilities are available. Moreover, these three parameters have demonstrated to influence mostly the model response during the calibration. Results of the sensitivity analysis are shown in Appendix and confirmed that

the three selected parameters (μ_{ALG} , μ_{H} and $k_{\text{death,H}}$) have a great impact on simulation outputs, and therefore need to be calibrated. Once the sensitive parameters of the model were identified (6 in total, μ_{ALG} , μ_{H} , $k_{\text{death,H}}$, $K_{\text{a,O}_2}$, $K_{\text{a,CO}_2}$ and $K_{\text{a,NH}_3}$) the calibration was performed in order to fit the model with the experimental data. Table 7.3 presents the values of the six calibrated parameters which were used to obtain the results shown in Figures 7.4 to 7.6.

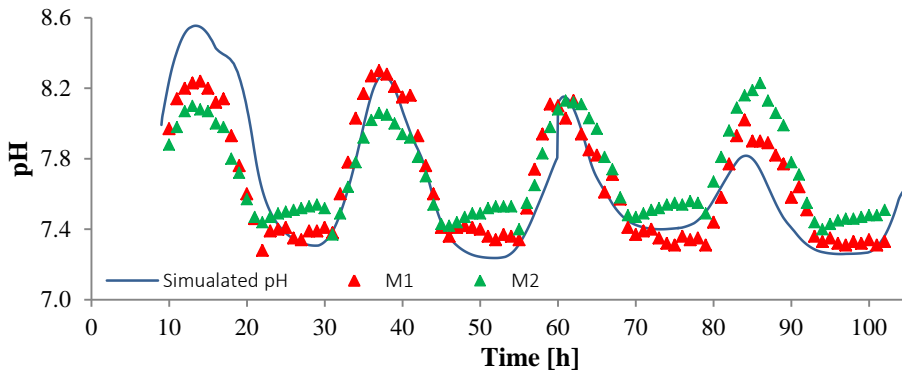
Table 7.3 Values of calibrated parameters.

Parameter	Description	Value
μ_{ALG}	Maximum specific growth rate of microalgae	1.5 d ⁻¹
μ_{H}	Maximum specific growth rate of heterotrophic bacteria	1.3 d ⁻¹
$k_{\text{death,H}}$	Inactivation constant of heterotrophic bacteria	0.3 d ⁻¹
$K_{\text{a,O}_2}$	Mass transfer coefficient for oxygen	0.16 h ⁻¹
$K_{\text{a,CO}_2}$	Mass transfer coefficient for dioxide carbon	0.14 h ⁻¹
$K_{\text{a,NH}_3}$	Mass transfer coefficient for ammonia	0.14 h ⁻¹

Fig. 7.4 shows the wave-like pattern of pH and S_{O_2} concentrations in both the simulated and experimental data, which is consistent with known pond microalgae and bacteria activity. During night S_{O_2} was not near 0 due to mechanical aeration. The model was able to match pretty well pH and S_{O_2} values, in fact the root mean square error of the simulation was low in relation to measured values ($\text{RMSE}_{\text{pH}} = 0.11$ and $\text{RMSE}_{S_{\text{O}_2}} = 0.62 \text{ gO}_2 \text{ m}^{-3}$). This meant a good agreement between experimental data and simulations (Willmott et al., 1985; Bennet et al., 2013).



a)

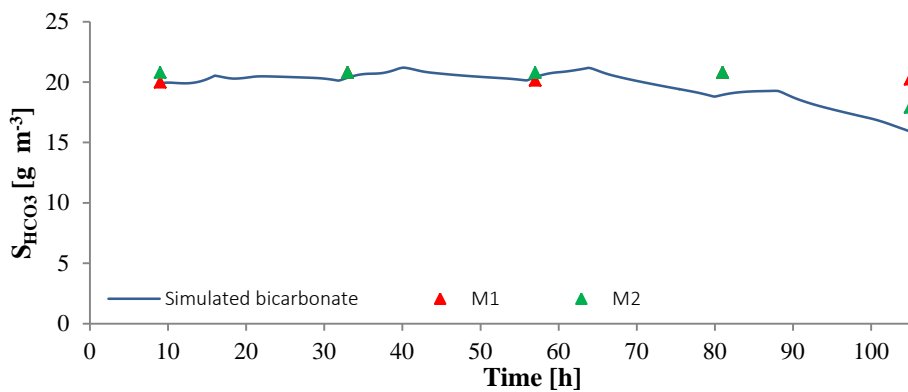


b)

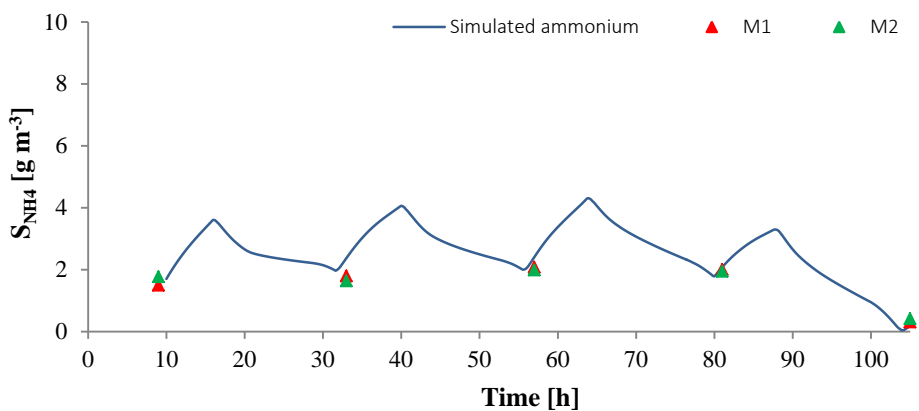
Figure 7.4 Experimental (red and green triangles) and simulated (blue line) a) dissolved oxygen (S_{O_2}) and b) pH values over June 27th-30th 2016 in both high-rate algal ponds. Data used for calibration.

Fig. 7.5 shows the changes in both experimental and simulated bicarbonate (S_{HCO_3}), ammonium nitrogen (S_{NH_4}), nitrate (S_{NO_3}) and nitrite (S_{NO_2}) concentrations in the HRAPs. Bicarbonate and nitrate had relatively constant values in the different days, and the model was able to reproduce quite well the pattern of these experimental data. Ammonium and nitrite had clearly lower concentration than nitrate and much more relative variation. The RMSE values were $1.26 \text{ gC}_{HCO_3} \text{ m}^{-3}$, $0.73 \text{ gN}_{NH_4} \text{ m}^{-3}$, $1.72 \text{ gN}_{NO_3} \text{ m}^{-3}$, $0.16 \text{ gN}_{NO_2} \text{ m}^{-3}$. Altogether these results are indicative of a great nitrification activity, and it is very interesting to see how the model is very sensitive and can show slight diurnal variations which are not detected with the experimental samples. For example, it can be seen that higher

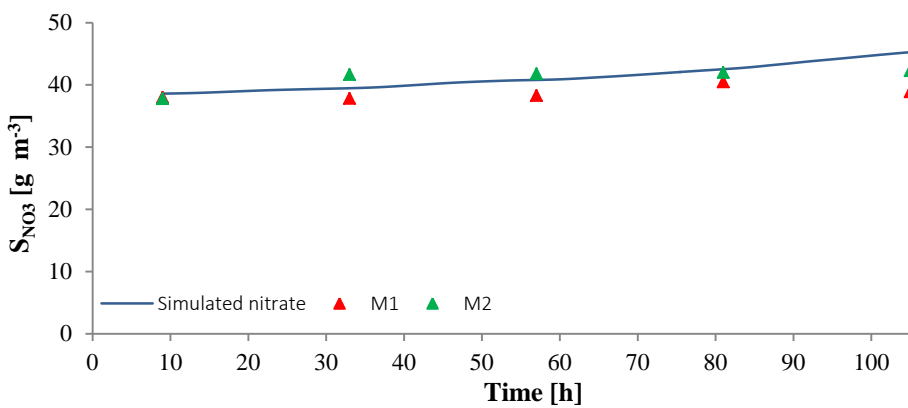
simulated ammonia concentrations are observed at night when microalgae do not grow and S_{O_2} concentrations are the lowest.



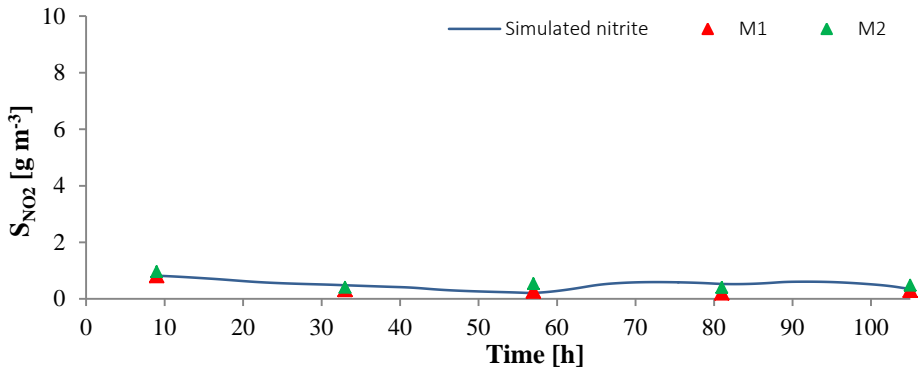
a)



b)



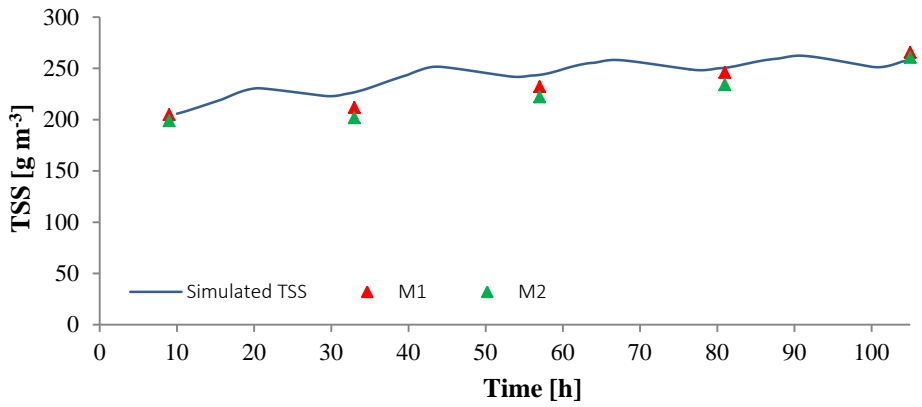
c)



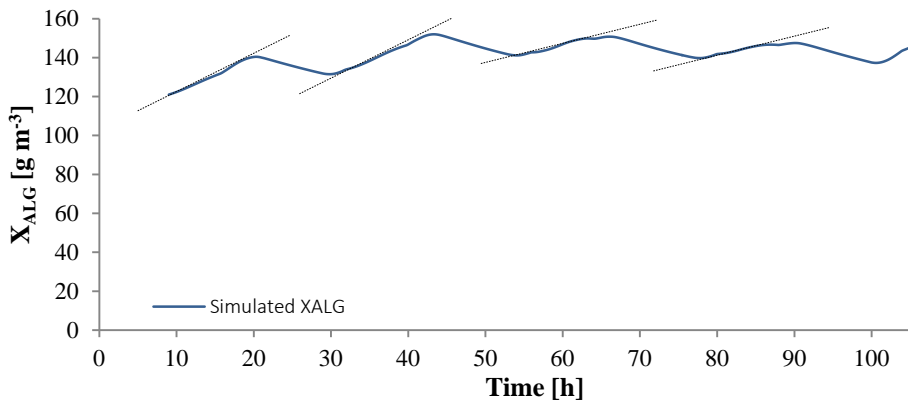
d)

Figure 7.5 Experimental (red and green triangles) and simulated (blue line) a) bicarbonate, b) ammonium nitrogen, c) nitrate and d) nitrite concentrations over June 27th-30th 2016 in both high-rate algal ponds. Data used for calibration.

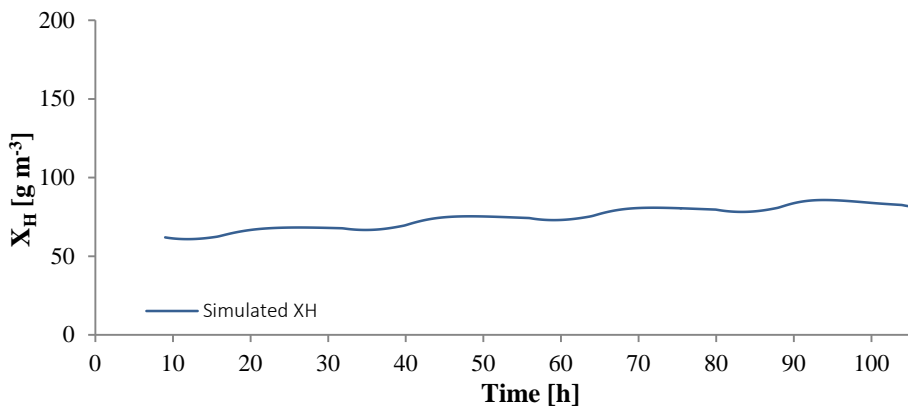
Average total biomass concentration in M1 and M2 changed from approximately 204 gTSS m^{-3} at the beginning of the experiment to 258 gTSS m^{-3} within four days. Simulated TSS concentrations (Fig. 7.6) match such growth patterns with a good accuracy ($\text{RMSE}_{\text{TSS}} = 8.11 \text{ gTSS m}^{-3}$). Moreover, Fig. 6 shows the simulated curve of microalgal (X_{ALG}) and bacterial biomass (X_{H} , X_{AOB} and X_{NOB}). As can be seen much of the biomass corresponds to microalgae (58% in average of TSS) and heterotrophic bacteria (30%). Nitrifiers biomass is comparatively very low (0.15%), however their activity is very important. The remaining solids are attributable to X_{s} (3%) and X_{I} (8.2%). This low amount of nitrifiers in comparison to other bacteria groups has been also obtained in previous simulation studies (Samsó and García, 2013; Krasnits et al., 2009; Silyn-Roberts and Lewis, 2001).



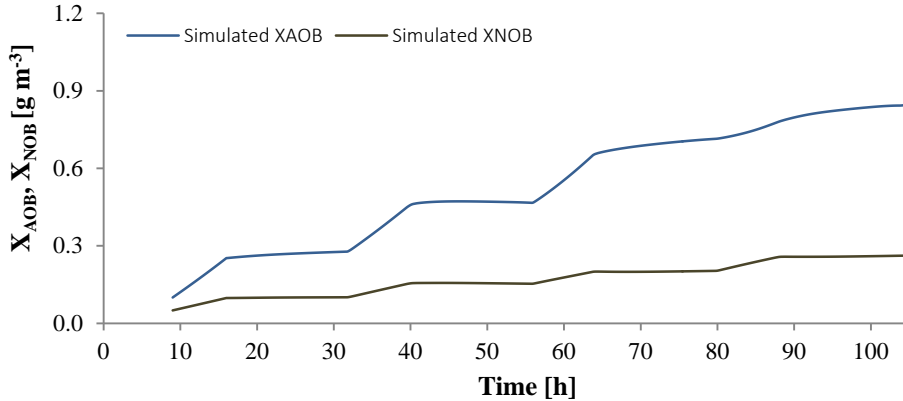
a)



b)



c)



d)

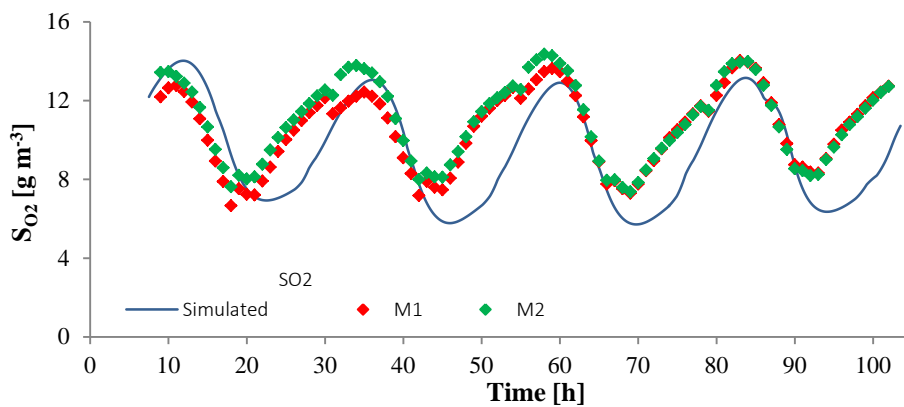
Figure 7.6 Experimental (red and green triangles) and simulated (blue line) a) TSS, b) microalgae, c) heterotrophic and d), autotrophy bacteria biomass over June 27th-30th 2016 in both high-rate algal ponds. Dotted lines indicate the different slope of microalgae growth rate from days 1-2 to 3-4 (see text). Data used for calibration.

7.5.2 Model validation

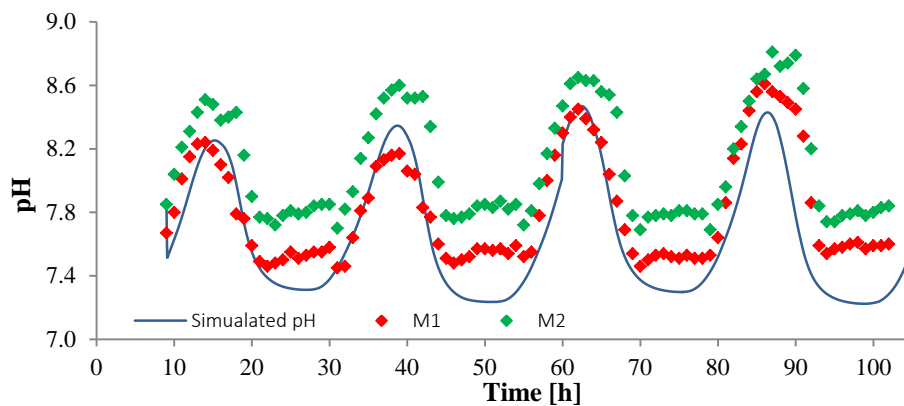
The model was validated with experimental data obtained over four days. Solar radiation, temperature, and initial conditions of culture medium were slightly different in the calibration and validation data sets (Table 7.2). Validation was conducted using the previous calibrated parameter values (Table 7.3).

Experimental results of the validation were similar to those of the calibration, and simulations matched pretty well the data. Fig. 7.7 shows the pH and S_{O2} fluctuations. The global error of the simulations was slightly higher than in the calibration (RMSE_{pH} = 0.38 and RMSE_{S_{O2}} = 1.88 gO₂ m⁻³), but also the range of variation of the two parameters was much higher. Nitrates were again the N species with the higher concentration (Fig. 7.8). The RMSE values of each component were: RMSE_{HCO₃} = 2.25 gC_HCO₃ m⁻³, RMSE_{NH₄} = 0.85 gN_NH₄ m⁻³, RMSE_{NO₃} = 4.80 gN_NO₃ m⁻³, RMSE_{NO₂} = 0.18 gN_NO₂ m⁻³. Simulated ammonium curve shows that the model was able to reproduce a wavelike trend of ammonium observed during the calibration, although with less accuracy (RMSE_{NH₄} values of

validation was $0.85 \text{ gN_NH}_4 \text{ m}^{-3}$ against $0.73 \text{ gN_NH}_4 \text{ m}^{-3}$ calculated from calibration result).

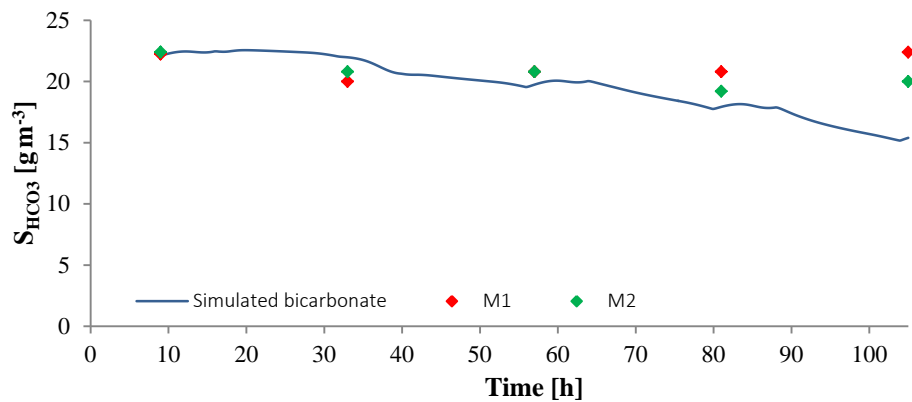


a)

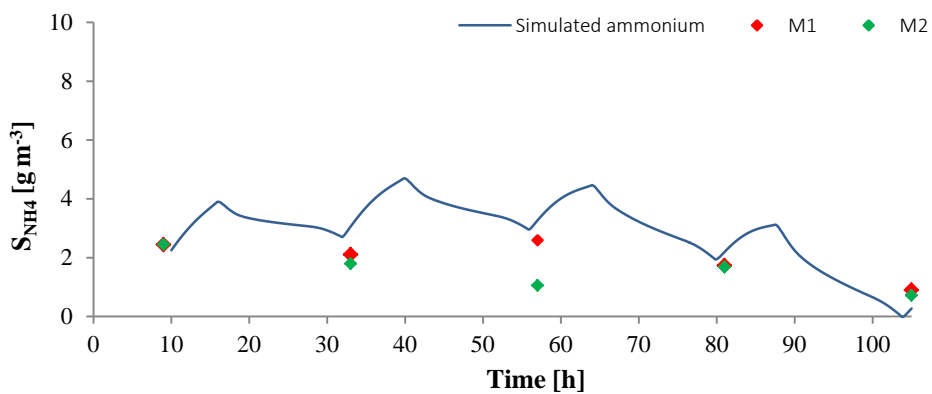


b)

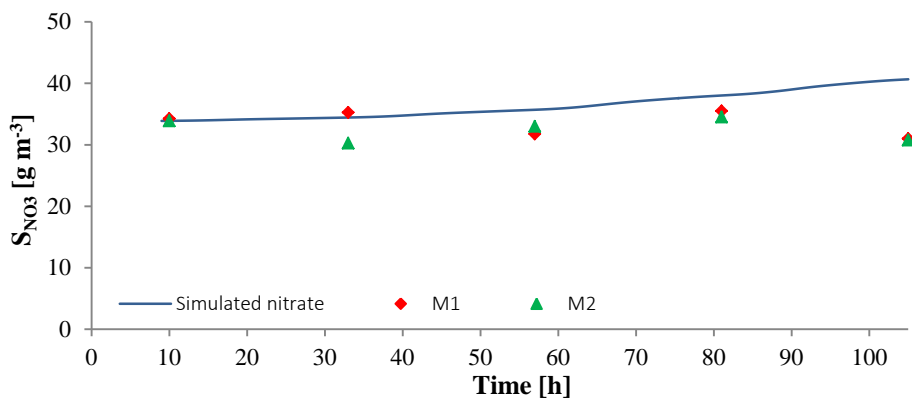
Figure 7.7 Experimental (red and green diamonds) and simulated (blue line) a) dissolved oxygen and b) pH values over July 17th-22th 2016 in both high-rate algal ponds. Data used for validation.



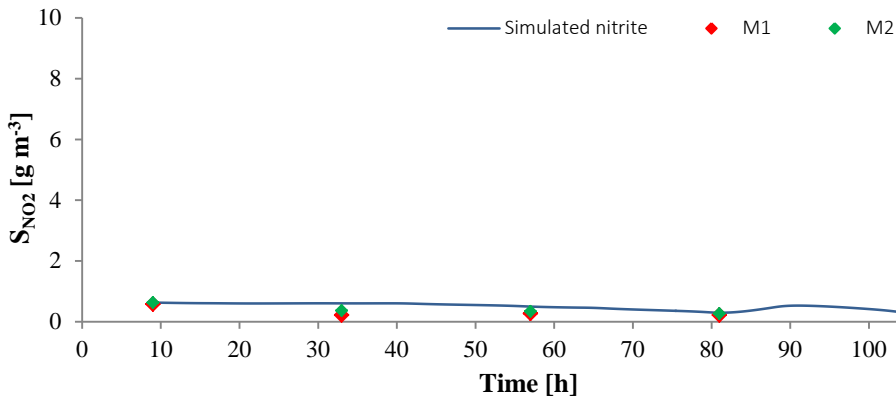
a)



b)



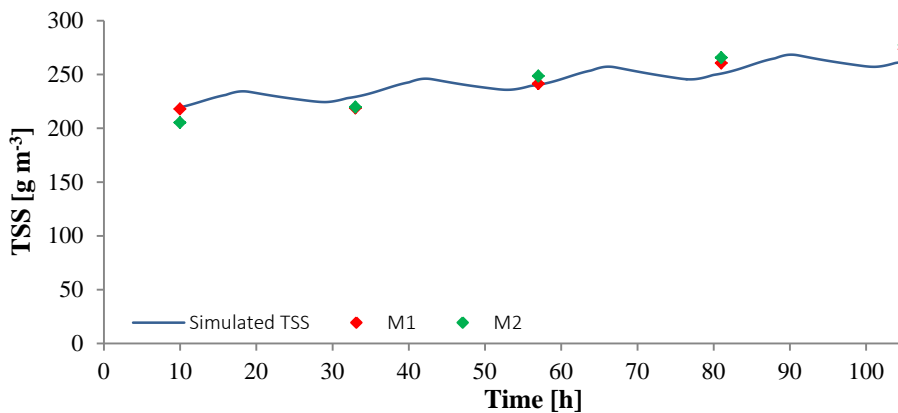
c)



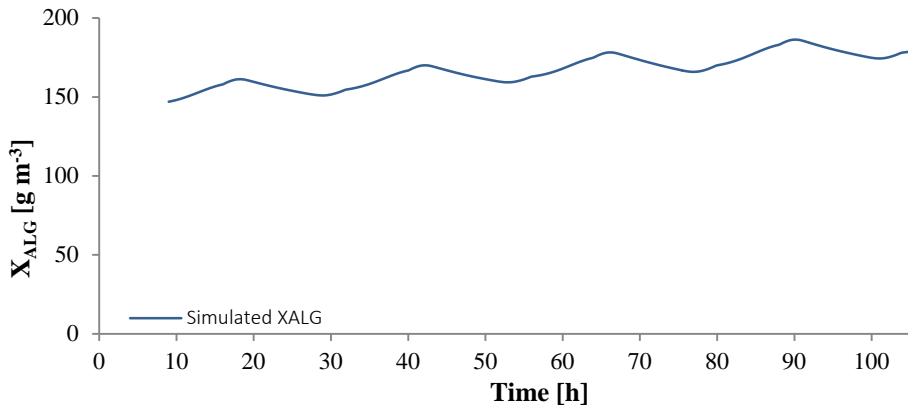
d)

Figure 7.8 Experimental (red and green diamonds) and simulated (blue line) a) bicarbonate, b) ammonium nitrogen, c) nitrate and d) nitrite concentrations over July 17th-22th 2016 in both high-rate algal ponds. Data used for validation.

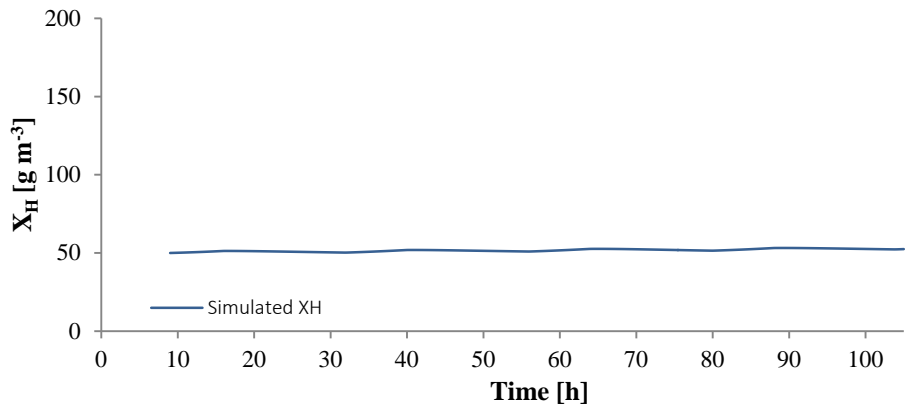
Simulated TSS concentrations fitted well the experimental data and the RMSE had a similar value to those obtained before during the calibration ($RMSE_{TSS} = 7.93 \text{ gTSS m}^{-3}$). Likewise of calibration, the model allowed to estimate microalgal (X_{ALG}) and bacterial biomass (X_H , X_{AOB} and X_{NOB}) over the four days of simulation (Fig. 7.9). Again much of the average biomass corresponds to microalgae (68.4% in average of TSS) and heterotrophic bacteria (21% in average), while nitrifiers (0.18%) had a low concentration. The remaining solids were X_S (2%) and X_I (8.2%). The relative proportion of particulate components respect to TSS obtained from model validation matches pretty well to those provided from the calibration.



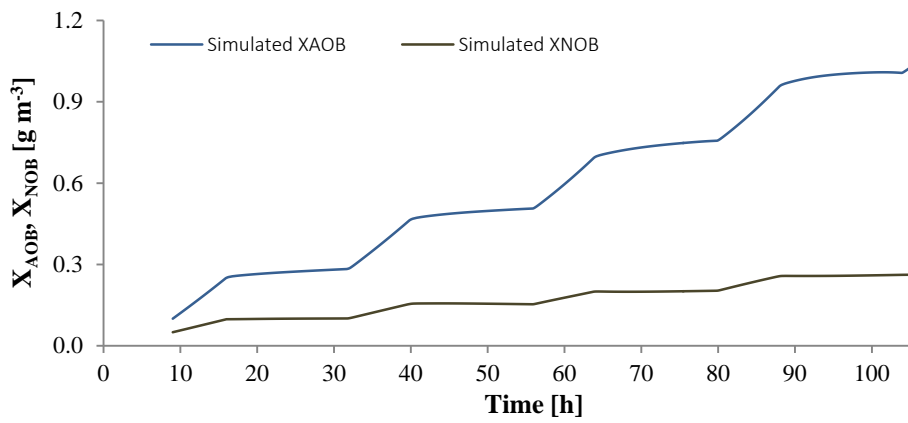
a)



b)



c)



d)

Figure 7.9 Experimental (red and green diamonds) and simulated (blue line) a) VSS, b) microalgae, c) heterotrophic and d) autotrophy bacteria biomass over July 17th-22th 2016 in both high-rate algal ponds. Data used for validation.

7.5.3 Model applications

Analysis of factors affecting microalgae growth

These results of high nitrate concentration (in average $41.2 \text{ gN_NO}_3 \text{ m}^{-3}$ from calibration results) in conjunction with the relatively low microalgae biomass (in average 128 gTSS m^{-3} from calibration results) suggest C limitation for the growth of microalgae (note that nitrifiers and microalgae compete for inorganic carbon). In fact the C:N average ratio in the mixed liquor of the HRAPs was 1:2. In general it is considered that microalgae growing in wastewater systems such as HRAP, in which no external carbon dioxide is supplied, are usually carbon limited (Park and Craggs, 2011a; García et al., 2006; Oswald, 1988; Buhr and Miller, 1983).

With a deep analysis of model outputs this hypothesis could be tested and it could be investigated which factor is more affecting microalgae concentration. Fig. 7.10 shows the changes of Monod-limited functions values for inorganic carbon, nitrate and ammonium, as well as the light factor $f_L(I)$ (Processes 1a, 1b, in Table A7.1). As can be seen, Monod functions had values near 1 and therefore microalgae were not limited by carbon or nitrogen, rejecting the hypothesis of carbon limitation. In fact, microalgae were strongly influenced by the light factor $f_L(I)$, that had values clearly lower than 1 and reduced growth from 40 to 60 %. This factor takes into account the effects of light intensity (e.g. photoinhibition, photolimitation and light attenuation) and is considered to be the main limiting factor in pure microalgae systems (Larsdotter, 2006).

Fig. 7.11 shows the changes in incident light intensity (I_o) and subsequent changes in pond average light intensity (I_{av}) (Eq. 7.3), which had a direct effect on the values of the light factor. The effect of the light factor $f_L(I)$ on microalgae growth can be detected in Fig. 6b (comparing with Fig. 7.11), where the slope of the main pattern of the curve slightly changes from days 1-2 to 3-4.

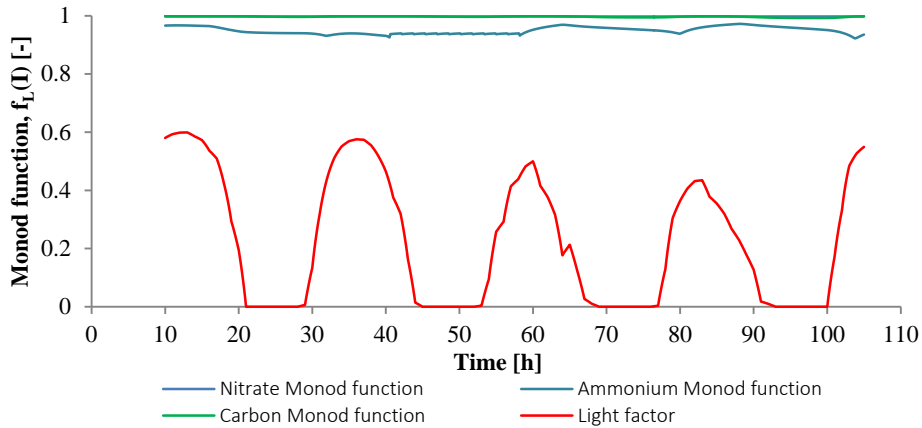


Figure 7.10 Changes in the values of microalgae Monod-limited functions for inorganic carbon, nitrate and ammonium, and in the light factor (f_L) over the 4 days of the experiment. Results obtained from calibration.

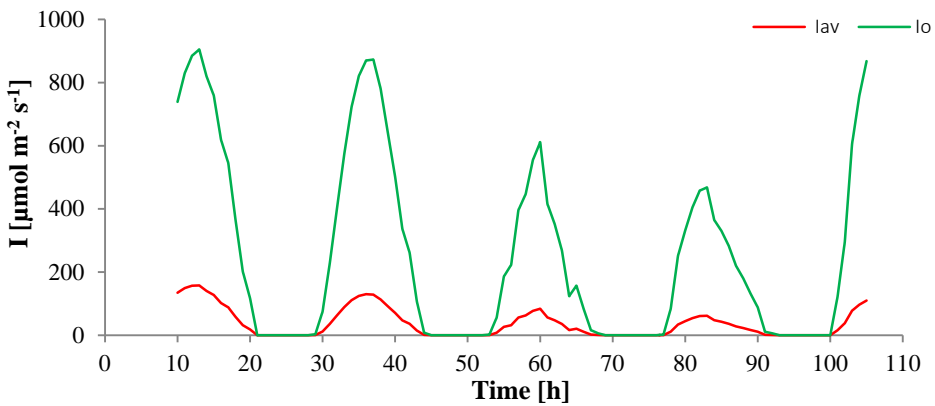


Figure 7.11 Changes in incident light intensity (I_o) (green line) and average light intensity in the pond (I_{av}) (red line) evolution over the 4 days of the experiment. Data used and obtained in the calibration.

In addition, it is known that the growth of microalgae is also highly dependent on temperature. Microalgae growth increases when optimum temperature is reached and decreases when is exceeded (Solimeno et al., 2017; Dauta et al., 1990). The effect of the photosynthetic thermal factor on microalgae growth is shown in Fig. 7.12 (Processes 1a, 1b, in Table A7.1). As can be seen this factor lowered growth at night and midday (when water

temperature was greater than 25 °C). However the global effect of the thermal factor was not as important as the light factor (having values ranging from 0.90 to 0.95 during the day).

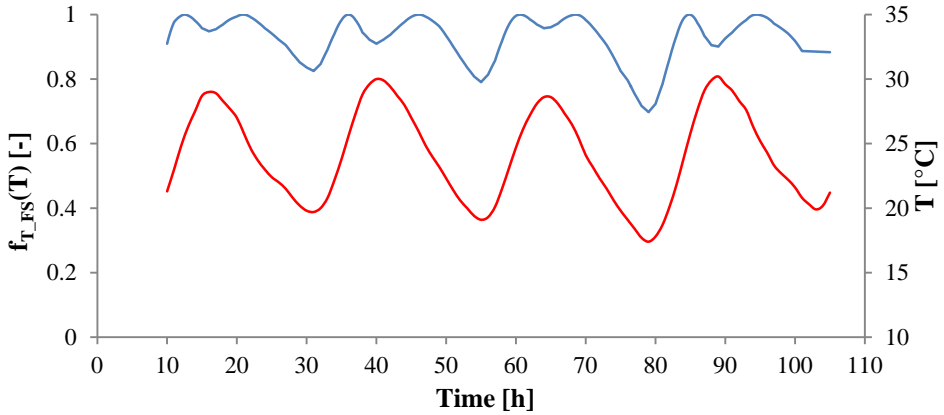


Figure 7.12 Changes of the values of the thermic photosynthetic factor ($f_{T-PS}(T)$) (blue line) and the water temperature (T) (orange line) over the 4 days of the experiment. Results used and obtained in the calibration.

Study case: effect of organic matter influent concentration on the relative proportion of microalgae and bacteria

According to the results presented in the previous section, attenuation of light within the pond was the main limiting factor on microalgae growth. Light attenuation depends strongly on particulate components concentration; therefore it could be expected that with lower organic matter influent concentrations the relative proportion of microalgae could increase, due to a lower growth of heterotrophic bacteria. To test this hypothesis, results from calibration were compared with two scenarios where total COD influent and initial concentration used for the calibration of particulate organic matter (except microalgae concentration) were reduced by 50% and 70%, respectively. As can be observed in Fig. 7.13, simulations indicated that the total biomass production (in average of TSS) increased from 15 gTSS m⁻²d⁻¹ to 16.2 gTSS m⁻²d⁻¹ with the lower organic matter. Also the

proportion of particulate components changed. Microalgae production is increased from 8.7 gTSS m⁻²d⁻¹ to 13.5 gTSS m⁻²d⁻¹, while heterotrophic bacteria and inert particulate organic matter are decreased.

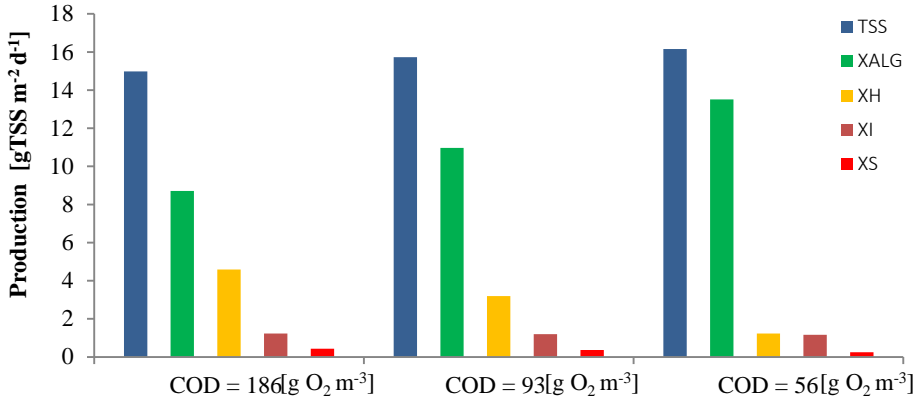


Figure 7.13 Comparison of average biomass production (TSS) as function of influent COD in the calibration and two scenarios with lower organic matter content.

Moreover, Fig. 7.13 shows the relative proportion of each particulate component respect to the total biomass. The proportion of microalgae in microalgae/bacteria biomass increases with an influent with lower organic matter (from 65% to 90%). This result is in accordance with the results showed by Park and Craggs (2011b), where the proportion of microalgae in the microalgae/bacteria biomass of an HRAP operating at 4-days HRT with CO₂ addition (approximately the same of our pilot raceways HRT= 4.4 d) was around 80.5%. Moreover, microalgae production in our system (Delhi, California) (13.7 gTSS m⁻²d⁻¹ in average) is congruent with the values showed by Park and Craggs (2011b) obtained with an HRAP located at the Ruakura Research Centre, Hamilton, New Zealand (mean areal algal productivity = 16.7 ± 7.1 g m⁻²d⁻¹).

The increase of production in our systems respect to the production value obtained during the calibration is related with light attenuation as explained before. As can be observed in Fig. 7.14, an influent with less particulate organic matter slightly increases the light factor $f_L(I)$ promoting the growth

of microalgae, especially at days 3-4, where the light attenuation was the most limiting factor during the calibration.

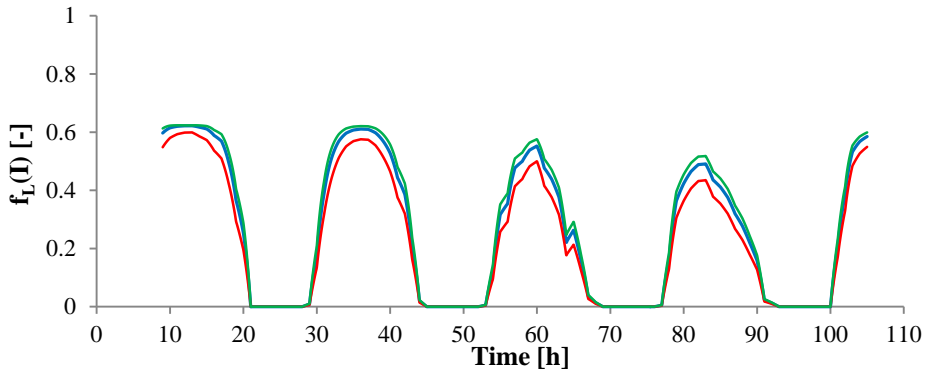


Figure 7.14 Comparison between light factor ($f_L(I)$) evolutions over the 4 days of the experiment as function of COD influent. Red line correspond to COD = 186 $\text{gO}_2 \text{m}^{-3}$ (calibration value), green line to COD = 93 $\text{gO}_2 \text{m}^{-3}$ and blue line to COD = 56 $\text{gO}_2 \text{m}^{-3}$.

7.6 Conclusion

In this paper the integral microalgae-bacteria model BIO_ALGAE for microalgae based wastewater treatment systems was presented. Biological processes, chemical and physical parameters affecting simultaneously microalgae and bacteria were implemented in COMSOL Multiphysics™ software.

Based on RWQM1 and ASM3, BIO_ALGAE model considers carbon limitation on the growth of microalgae and autotrophic bacteria, and factors to represent photosynthesis, photolimitation, light attenuation, photorespiration, temperature dependency and the hydrodynamics of the system.

The parameters selected for calibration were based on a global sensibility analysis and previous works: microalgae and heterotrophic bacteria specific growth rate, decay of heterotrophic bacteria and the 3 parameters related to the transfer of gases to the atmosphere. Calibration and validation were

conducted comparing simulated results and experimental data from triplicate pilot raceway ponds fed with facultative pond effluent for two different periods of four days. Results of the calibration and validation have indicated that the model was able to accurately reproduce total biomass concentrations, pH, dissolved oxygen and nutrient concentrations.

The developed model has demonstrated to be a useful tool to simulate the performance of microalgae-bacteria wastewater treatment, and in particular to inferring the relative proportion of microalgae and bacteria, and to make predictions on biomass production.

The next step in order to better understand microalgal-bacterial wastewater treatment would be to predict the production of microalgae and nutrient uptake using the model over a long period of time.

7.7 Appendix

Table A7.1 Mathematical description of the processes of the model (processes rates).

Processes	Process rate [M L ⁻³ T ⁻¹]
Microalgae (X_{ALG}) processes	
1a. Growth of X _{ALG} on S _{NH4}	$\rho_{1a} = \mu_{ALG} \cdot f_{T,FS}(T) \cdot \eta_{PS}(I, S_{O_2}) \cdot \frac{S_{CO_2} + S_{HCO_3}}{K_{C,ALG} + S_{CO_2} + S_{HCO_3} + \frac{S_{CO_2}^2}{I_{CO_2,ALG}}} \cdot \frac{S_{NH_3} + S_{NH_4}}{K_{N,ALG} + S_{NH_3} + S_{NH_4}} \cdot \frac{S_{PO_4}}{K_{P,ALG} + S_{PO_4}} \cdot X_{ALG}$
1b. Growth of X _{ALG} on S _{NO3}	$\rho_{1b} = \mu_{ALG} \cdot f_{T,FS}(T) \cdot \eta_{PS}(I, S_{O_2}) \cdot \frac{S_{CO_2} + S_{HCO_3}}{K_{C,ALG} + S_{CO_2} + S_{HCO_3} + \frac{S_{CO_2}^2}{I_{CO_2,ALG}}} \cdot \frac{S_{NO_3}}{K_{N,ALG} + S_{NO_3}} \cdot \frac{K_{N,ALG}}{K_{N,ALG} + S_{NH_3} + S_{NH_4}} \cdot \frac{S_{PO_4}}{K_{P,ALG} + S_{PO_4}} \cdot X_{ALG}$
2. Endogenous respiration of X _{ALG}	$\rho_2 = k_{resp,ALG} \cdot f_{T,FS}(T) \cdot \frac{S_{O_2}}{K_{O_2,ALG} + S_{O_2}} \cdot X_{ALG}$
3. Decay of X _{ALG}	$\rho_3 = k_{death,ALG} \cdot f_{T,FS}(T) \cdot X_{ALG}$
Heterotrophic bacteria (X_H) (aerobic and denitrifying activity)	
4a. Aerobic growth of X _H on S _{NH4}	$\rho_{4a} = \mu_H \cdot f_{T,MB}(T) \cdot \frac{S_s}{K_{S,H} + S_s} \cdot \frac{S_{O_2}}{K_{O_2,H} + S_{O_2}} \cdot \frac{S_{NH_4} + S_{NH_3}}{K_{N,H} + S_{NH_4} + S_{NH_3}} \cdot X_H$
4b. Aerobic growth of X _H on S _{NO3}	$\rho_{4b} = \mu_H \cdot f_{T,MB}(T) \cdot \frac{S_s}{K_{S,H} + S_s} \cdot \frac{S_{O_2}}{K_{O_2,H} + S_{O_2}} \cdot \frac{S_{NO_3}}{K_{N,H} + S_{NO_3}} \cdot X_H$
5. Anoxic growth of X _H on S _{NO2} (denitrification on S _{NO2})	$\rho_5 = \mu_H \cdot \eta_H \cdot f_{T,MB}(T) \cdot \frac{S_s}{K_{S,H} + S_s} \cdot \frac{K_{O_2,H}}{K_{O_2,H} + S_{O_2}} \cdot \frac{S_{NO_2}}{K_{NO_2,H,anox} + S_{NO_2}} \cdot X_H$

6. Anoxic growth of X_H on S_{NO_3} (denitrification on S_{NO_3})	$\rho_6 = \mu_H \cdot \eta_H \cdot f_{T,MB}(T) \cdot \frac{S_S}{K_{S,H} + S_S} \cdot \frac{K_{O_2,H}}{K_{O_2,H} + S_{O_2}} \cdot \frac{S_{NO_3}}{K_{NO_3,H,anox} + S_{NO_3}} \cdot X_H$
7. Aerobic endogenous respiration of X_H	$\rho_7 = k_{resp,H} \cdot f_{T,MB}(T) \cdot \frac{S_{O_2}}{K_{O_2,H} + S_{O_2}} \cdot X_H$
8. Anoxic endogenous respiration of X_H	$\rho_8 = k_{resp,H} \cdot \eta_H \cdot f_{T,MB}(T) \cdot \frac{K_{O_2,H}}{K_{O_2,H} + S_{O_2}} \cdot \frac{S_{NO_3} + S_{NO_2}}{K_{NO_3,H,anox} + S_{NO_2} + S_{NO_3}} \cdot X_H$
9. Decay of X_H	$\rho_9 = k_{death,H} \cdot f_{T,MB}(T) \cdot X_H$
Autotrophic bacteria (nitrifying activity)	
10. Growth of X_{AOB}	$\rho_{10} = \mu_{AOB} \cdot f_{T,MB}(T) \cdot \frac{S_{O_2}}{K_{O_2,AOB} + S_{O_2}} \cdot \frac{S_{NH_3} + S_{NH_4}}{K_{NH_4,AOB} + S_{NH_4} + S_{NH_3}} \cdot \frac{S_{CO_2} + S_{HCO_3}}{K_{C,AOB} + S_{CO_2} + S_{HCO_3}} \cdot X_{AOB}$
11. Growth of X_{NOB}	$\rho_{11} = \mu_{NOB} \cdot f_{T,MB}(T) \cdot \frac{S_{O_2}}{K_{O_2,NOB} + S_{O_2}} \cdot \frac{K_{I,NH_4}}{K_{I,NH_4} + S_{NH_4} + S_{NH_3}} \cdot \frac{S_{NO_2}}{K_{NO_2,NOB} + S_{NO_2}} \cdot \frac{S_{CO_2} + S_{HCO_3}}{K_{C,NOB} + S_{CO_2} + S_{HCO_3}} \cdot X_{NOB}$
12. Endogenous respiration of X_{AOB}	$\rho_{12} = k_{resp,AOB} \cdot f_{T,MB}(T) \cdot \frac{S_{O_2}}{K_{O_2,AOB} + S_{O_2}} \cdot X_{AOB}$
13. Endogenous respiration of X_{NOB}	$\rho_{13} = k_{resp,NOB} \cdot f_{T,MB}(T) \cdot \frac{S_{O_2}}{K_{O_2,NOB} + S_{O_2}} \cdot X_{NOB}$
14a. Decay of X_{AOB}	$\rho_{14a} = k_{death,AOB} \cdot f_{T,MB}(T) \cdot X_{AOB}$
14b. Decay of X_{NOB}	$\rho_{14b} = k_{death,NOB} \cdot f_{T,MB}(T) \cdot X_{NOB}$

Hydrolysis, Chemical equilibrium and Transfer of gases	
15. Hydrolysis	$\rho_{15} = k_{\text{HYD}} \cdot \frac{X_S/X_H}{Y_{\text{HYD}} + (X_S/X_H)} \cdot X_H$
16. Chemical equilibrium $\text{CO}_2 \leftrightarrow \text{HCO}_3^-$	$\rho_{16} = k_{\text{eq},1} \cdot (S_{\text{CO}_2} - S_H S_{\text{HCO}_3} / K_{\text{eq},1})$
17. Chemical equilibrium $\text{HCO}_3^- \leftrightarrow \text{CO}_3^{2-}$	$\rho_{17} = k_{\text{eq},2} \cdot (S_{\text{HCO}_3} - S_H S_{\text{CO}_3} / K_{\text{eq},2})$
18. Chemical equilibrium $\text{NH}_4^+ \leftrightarrow \text{NH}_3$	$\rho_{18} = k_{\text{eq},3} \cdot (S_{\text{NH}_4} - S_H S_{\text{NH}_3} / K_{\text{eq},3})$
19. Chemical equilibrium $\text{H}^+ \leftrightarrow \text{OH}^-$	$\rho_{19} = k_{\text{eq},w} \cdot (1 - S_H S_{\text{OH}} / K_{\text{eq},w})$
20. S_{O_2} transfer to the atmosphere	$\rho_{20} = k_{a,\text{O}_2} \cdot (S_{\text{O}_2}^{\text{WAT}} - S_{\text{O}_2})$
21. S_{CO_2} transfer to the atmosphere	$\rho_{21} = k_{a,\text{CO}_2} \cdot (S_{\text{CO}_2}^{\text{WAT}} - S_{\text{CO}_2})$
22. S_{NH_3} transfer to the atmosphere	$\rho_{22} = k_{a,\text{NH}_3} \cdot (-S_{\text{NH}_3})$

Table A7.2. Matrix of stoichiometric parameters that relates processes and components through stoichiometric coefficients A7.4

	S_{NH4}	S_{NH3}	S_{NO3}	S_{NO2}	S_{CO2}	S_{HCO3}	S_{CO3}	S_{PO4}	S_{O2}	S_H	S_{OH}	S_S	S_I	X_{AlG}	X_S	X_I	X_H	X_{AOB}	X_{NOB}
ρ_{1a}	$V_{1,1a}$				$V_{5,1a}$			$V_{8,1a}$	$V_{9,1a}$	$V_{10,1a}$				$V_{14,1a}$					
ρ_{1b}			$V_{3,1b}$		$V_{5,1b}$			$V_{8,1b}$	$V_{9,1b}$	$V_{10,1b}$				$V_{14,1b}$					
ρ_2	$V_{1,2}$				$V_{5,2}$			$V_{8,2}$	$V_{9,2}$	$V_{10,2}$				$V_{14,2}$		$V_{16,2}$			
ρ_3	$V_{1,3}$				$V_{5,3}$			$V_{8,3}$		$V_{10,3}$				$V_{14,3}$	$V_{15,3}$	$V_{16,3}$			
ρ_{4a}	$V_{1,4a}$				$V_{5,4a}$			$V_{8,4a}$	$V_{9,4a}$	$V_{10,4a}$		$V_{12,4a}$					$V_{17,4a}$		
ρ_{4b}			$V_{3,4b}$		$V_{5,4b}$			$V_{8,4b}$	$V_{9,4b}$	$V_{10,4b}$		$V_{12,4b}$					$V_{17,4b}$		
ρ_5				$V_{4,5}$	$V_{5,5}$			$V_{8,5}$		$V_{10,5}$		$V_{12,5}$						$V_{17,5}$	
ρ_6			$V_{3,6}$		$V_{5,6}$			$V_{8,6}$		$V_{10,6}$		$V_{12,6}$						$V_{17,6}$	
ρ_7	$V_{1,7}$				$V_{5,7}$			$V_{8,7}$	$V_{9,7}$	$V_{10,7}$						$V_{16,7}$	$V_{17,7}$		
ρ_8	$V_{1,8}$		$V_{3,8}$	$V_{4,8}$	$V_{5,8}$			$V_{8,8}$		$V_{10,8}$						$V_{16,8}$	$V_{17,8}$		
ρ_9															$V_{15,9}$	$V_{16,9}$	$V_{17,9}$		
ρ_{10}	$V_{1,10}$			$V_{4,10}$	$V_{5,10}$			$V_{8,10}$	$V_{9,10}$	$V_{10,10}$								$V_{18,10}$	
ρ_{11}			$V_{3,11}$	$V_{4,11}$	$V_{5,11}$			$V_{8,11}$	$V_{9,11}$	$V_{10,11}$									$V_{19,11}$
ρ_{12}	$V_{1,12}$				$V_{5,12}$			$V_{8,12}$	$V_{9,12}$	$V_{10,12}$						$V_{16,12}$		$V_{18,12}$	
ρ_{13}	$V_{1,13}$				$V_{5,13}$			$V_{8,13}$	$V_{9,13}$	$V_{10,13}$						$V_{16,13}$			$V_{19,13}$
ρ_{14a}															$V_{15,14a}$	$V_{16,14a}$		$V_{18,14a}$	
ρ_{14b}															$V_{15,14b}$	$V_{16,14b}$			$V_{19,14b}$
ρ_{15}	$V_{1,15}$				$V_{5,15}$			$V_{8,15}$		$V_{10,15}$		$V_{12,15}$	$V_{13,15}$		$V_{15,15}$				
ρ_{16}					$V_{5,16}$	$V_{6,16}$				$V_{10,16}$									
ρ_{17}						$V_{6,17}$	$V_{7,17}$			$V_{10,17}$									
ρ_{18}	$V_{1,18}$	$V_{2,18}$								$V_{10,18}$									
ρ_{19}										$V_{10,19}$	$V_{11,19}$								
ρ_{20}									$V_{9,20}$										
ρ_{21}					$V_{5,21}$														
ρ_{22}		$V_{2,22}$																	

Table A7.3 Values of biokinetic, chemical and physic parameters.

Parameters	Description	Value	Unit	Source
Microalgae (X_{ALG})				
μ_{ALG}	Maximum growth rate of X_{ALG}	1.5	d^{-1}	Calibrated
$k_{resp,ALG}$	Endogenous respiration constant	0.1	d^{-1}	Reichert et al., 2001
$k_{death,ALG}$	Decay constant	0.1	d^{-1}	Reichert et al., 2001
$K_{C,ALG}$	Saturation constant of X_{ALG} on S_{CO_2}	4E-3	$gC\ m^{-3}$	Novak and Brune, 1985
$I_{CO_2,ALG}$	Inhibition constant of X_{ALG} on S_{CO_2}	120	$gC\ m^{-3}$	Silva and Pirt, 1984
$K_{N,ALG}$	Saturation constant of X_{ALG} on nitrogen sp.	0.1	$gN\ m^{-3}$	Reichert et al., 2001
$K_{O_2,ALG}$	Saturation constant of X_{ALG} on S_{O_2}	0.2	$gO_2\ m^{-3}$	Reichert et al., 2001
$K_{P,ALG}$	Saturation constant of X_{ALG} for S_{HPO_4}	0.02	$gP\ m^{-3}$	Reichert et al., 2001
Heterotrophic bacteria (X_H)				
μ_H	Maximum growth rate of X_H	1.3	d^{-1}	Calibrated
η_H	Anoxic reduction factor for X_H	0.6	–	Gujer et al., 1999
$k_{resp,H}$	Endogenous respiration rate of X_H	0.3	d^{-1}	Reichert et al., 2001
$K_{O_2,H}$	Saturation constant of X_H for S_{O_2}	0.2	$gO_2\ m^{-3}$	Reichert et al., 2001
$K_{N,H}$	Saturation constant of X_H for S_N	0.2	$gN\ m^{-3}$	Reichert et al., 2001
$K_{S,H}$	Saturation constant of X_H for S_S	20	$gCOD\ m^{-3}$	Henze et al., 2000
$K_{NO_3,H,anox}$	Saturation constant of X_H for S_{NO_3}	0.5	$gN\ m^{-3}$	Reichert et al., 2001
$K_{NO_2,H,anox}$	Saturation constant of X_H for S_{NO_2}	0.2	$gN\ m^{-3}$	Reichert et al., 2001
$k_{death,H}$	Decay constant of X_H	0.3	d^{-1}	Calibrated
Autotrophic bacteria: ammonia oxidizing bacteria (X_{AOB}) and nitrite oxidizing bacteria (X_{NOB})				
μ_{AOB}	Maximum growth rate of X_{AOB}	0.63	d^{-1}	Gujer et al., 1999
μ_{NOB}	Maximum growth rate of X_{NOB}	1.1	d^{-1}	Gujer et al., 1999
$K_{O_2,AOB}/K_{O_2,NOB}$	Saturation constant of X_{AOB} / X_{NOB} for S_{O_2}	0.5	$gO_2\ m^{-3}$	Reichert et al., 2001
$K_{NH_4,AOB}$	Saturation constant of X_{AOB} on S_{NH_4}	0.5	$gN\ m^{-3}$	Reichert et al., 2001
K_{I,NH_4}	Ammonia inhibition constant of X_{NOB}	5.0	$gN\ m^{-3}$	Henze et al., 2000
$K_{NO_2,NOB}$	Saturation constant of X_{NOB} for S_{NO_2}	0.5	$gN\ m^{-3}$	Henze et al., 2000
$K_{C,AOB}/K_{C,NOB}$	Saturation constant of X_{AOB} / X_{NOB} for S_{HCO_3}	0.5	$gC\ m^{-3}$	Henze et al., 2000
$k_{resp,AOB}/k_{resp,NOB}$	Endogenous respiration rate of X_{AOB} / X_{NOB}	0.05	d^{-1}	Reichert et al., 2001
$k_{death,AOB}/k_{death,NOB}$	Decay constant of X_{AOB} and X_{NOB}	0.2	d^{-1}	Henze et al., 2000
Hydrolysis				
k_{HYD}	Hydrolysis rate constant	3.0	d^{-1}	Reichert et al., 2001
Photorespiration factor of microalgae				
K_{PR}	Inhibition constant of photorespiration	0.03	–	Solimeno et al., 2017b

τ	Excess of S_{O_2} coefficient	3.5	–	Fernández et al., 2014
$\zeta_{O_2}^{SAT}$	S_{O_2} air saturation	9.07	$gO_2 m^{-3}$	Fernández et al., 2014
Thermal factor of microalgae and bacteria				
T_{OPT}	Optimum temperature for X_{ALG} growth	25	$^{\circ}C$	Dauta et al., 1990
s	Normalized parameter	30	–	Dauta et al., 1990
θ	Temperature coefficient for X_H growth	1.07		Sperling, 2005
Light factor of microalgae				
α	Activation rate	1.9E-3	$(\mu E m^{-2})^{-1}$	Wu and Merchuk, 2001
β	Inhibition rate	5.7E-7	$(\mu E m^{-2})^{-1}$	Wu and Merchuk, 2001
γ	Production rate	0.14	s^{-1}	Wu and Merchuk, 2001
δ	Recovery rate	4.7E-4	s^{-1}	Wu and Merchuk, 2001
K_1	Biomass extinction coefficient	0.07	$m^2 g^{-1}$	Molina et al., 1994
Parameters		Equations		
Chemical equilibrium $CO_2 \leftrightarrow HCO_3^-$.		$K_{eq,1} = 10^{17.843 - \frac{3404.71}{273.15+T} - 0.032786(273.15+T)}$		
Chemical equilibrium $HCO_3^- \leftrightarrow CO_3^{2-}$		$K_{eq,2} = 10^{9.494 - \frac{2902.39}{273.15+T} - 0.02379(273.15+T)}$		
Chemical equilibrium $NH_4^+ \leftrightarrow NH_3$		$K_{eq,3} = 10^{2.891 - \frac{2727}{(273.15+T)}}$		
Chemical equilibrium $H^+ \leftrightarrow OH^-$		$K_{eq,w} = 10^{-\frac{4470.99}{273.15+T} + 12.0875 - 0.01706(273.15+T)}$		
Kinetics parameters				
$k_{eq,1}$	Dissociation constant of $CO_2 \leftrightarrow HCO_3^-$.	10000	d^{-1}	Reichert et al., 2001
$k_{eq,2}$	Dissociation constant of $HCO_3^- \leftrightarrow CO_3^{2-}$	1000	d^{-1}	Reichert et al., 2001
$k_{eq,3}$	Dissociation constant of $NH_4^+ \leftrightarrow NH_3$	1000	d^{-1}	Reichert et al., 2001
$k_{eq,w}$	Dissociation constant of $H^+ \leftrightarrow OH^-$	1000	$g m^{-1} d^{-1}$	Reichert et al., 2001
Transfer of gases to the atmosphere				
K_{a,O_2}	Mass transfer coefficient for S_{O_2}	0.16	h^{-1}	Calibrated
K_{a,CO_2}	Mass transfer coefficient for S_{CO_2}	0.14	h^{-1}	Calibrated
K_{a,NH_3}	Mass transfer coefficient for S_{NH_3}	0.14	h^{-1}	Calibrated

Table A7.4 Mathematical expressions of the stoichiometric coefficients of each process.

Stoichiometric coefficients	Unit
Growth of X_{ALG} on S_{NH4}	
$v_{1,1a} = -i_{N,ALG}$	gN gCOD ⁻¹
$v_{5,1a} = -i_{C,ALG}$	gC gCOD ⁻¹
$v_{8,1a} = -i_{P,ALG}$	gP gCOD ⁻¹
$v_{9,1a} = 8i_{C,ALG}/3 + 8i_{H,ALG} - i_{O,ALG} - 12i_{N,ALG}/7 + 40i_{P,ALG}/31$	gO ₂ gCOD ⁻¹
$v_{10,1a} = i_{N,ALG}/14 - 2i_{P,ALG}/31$	gH gCOD ⁻¹
$v_{14,1a} = 1$	gCOD gCOD ⁻¹
Growth of X_{ALG} on S_{NO3}	
$v_{3,1b} = -i_{N,ALG}$	gN gCOD ⁻¹
$v_{5,1b} = -i_{C,ALG}$	gC gCOD ⁻¹
$v_{8,1b} = -i_{P,ALG}$	gP gCOD ⁻¹
$v_{9,1b} = 8i_{C,ALG}/3 + 8i_{H,ALG} - i_{O,ALG} + 20i_{N,ALG}/7 + 40i_{P,ALG}/31$	gO ₂ gCOD ⁻¹
$v_{10,1b} = -i_{N,ALG}/14 - 2i_{P,ALG}/31$	gH gCOD ⁻¹
$v_{14,1b} = 1$	gCOD gCOD ⁻¹
Endogenous respiration of X_{ALG}	
$v_{1,2} = i_{N,ALG} - f_{ALG} i_{N,XI}$	gN gCOD ⁻¹
$v_{5,2} = i_{C,ALG} - f_{ALG} i_{C,XI}$	gC gCOD ⁻¹
$v_{8,2} = i_{P,ALG} - f_{ALG} i_{P,XI}$	gP gCOD ⁻¹
$v_{9,2} = (i_{O,ALG} - f_{ALG} i_{O,XI}) - 8(i_{H,ALG} - f_{ALG} i_{H,XI}) - 8/3(i_{C,ALG} - f_{ALG} i_{C,XI}) + 12/7(i_{N,ALG} - f_{ALG} i_{N,XI}) - 40/31(i_{P,ALG} - f_{ALG} i_{P,XI})$	gO ₂ gCOD ⁻¹
$v_{10,2} = -1/14(i_{N,ALG} - f_{ALG} i_{N,XI}) + 2/31(i_{P,ALG} - f_{ALG} i_{P,XI})$	gH gCOD ⁻¹
$v_{14,2} = -1$	gCOD gCOD ⁻¹
$v_{16,2} = f_{ALG}$	gCOD gCOD ⁻¹
Decay of X_{ALG}	
$v_{1,3} = i_{N,ALG} - (1 - f_{ALG})Y_{ALG} i_{N,XS} - f_{ALG} Y_{ALG} i_{N,ALG}$	gN gCOD ⁻¹
$v_{5,3} = i_{C,ALG} - (1 - f_{ALG})Y_{ALG} i_{C,XS} - f_{ALG} Y_{ALG} i_{C,ALG}$	gC gCOD ⁻¹
$v_{8,3} = i_{P,ALG} - (1 - f_{ALG})Y_{ALG} i_{P,XS} - f_{ALG} Y_{ALG} i_{P,ALG}$	gP gCOD ⁻¹
$v_{10,3} = -1/14(i_{N,ALG} (1 - f_{ALG})Y_{ALG} i_{N,XS} - f_{ALG} Y_{ALG} i_{N,XI}) + 2/31(i_{P,ALG} (1 - f_{ALG})Y_{ALG} i_{P,XS} - f_{ALG} Y_{ALG} i_{P,XI})$	gH gCOD ⁻¹
$v_{14,3} = -1$	gCOD gCOD ⁻¹
$v_{15,3} = (1 - f_{ALG})$	gCOD gCOD ⁻¹
$v_{16,3} = f_{ALG} Y_{ALG}$	gCOD gCOD ⁻¹
Aerobic growth of X_H on S_{NH4}	
$v_{1,4a} = i_{N,SS}/Y_H - i_{N,BM}$	gN gCOD ⁻¹
$v_{5,4a} = i_{C,SS}/Y_H - i_{C,BM}$	gC gCOD ⁻¹

$v_{8,4a} = i_{P,SS}/Y_H - i_{P,BM}$	gP gCOD ⁻¹
$v_{9,4a} = -(1 - Y_H)/Y_H$	gO ₂ gCOD ⁻¹
$v_{10,4a} = -1/14 (i_{N,SS}/Y_H - i_{N,BM}) + 2/31 (i_{P,SS}/Y_H - i_{P,BM})$	gH gCOD ⁻¹
$v_{12,4a} = -1/Y_H$	gCOD gCOD ⁻¹
$v_{17,4a} = 1$	gCOD gCOD ⁻¹
Aerobic growth of X_H on S_{NO3}	
$v_{3,4b} = i_{N,SS}/Y_H - i_{N,BM}$	gN gCOD ⁻¹
$v_{5,4b} = i_{C,SS}/Y_H - i_{C,BM}$	gC gCOD ⁻¹
$v_{8,4b} = (i_{P,SS}/Y_H - i_{P,BM})$	gP gCOD ⁻¹
$v_{9,4b} = -(1 - Y_H)/Y_H$	gO ₂ gCOD ⁻¹
$v_{10,4b} = -1/14 (i_{N,SS}/Y_H - i_{N,BM}) + 2/31 (i_{P,SS}/Y_H - i_{P,BM})$	gH gCOD ⁻¹
$v_{12,4b} = -1/Y_H$	gCOD gCOD ⁻¹
$v_{17,4b} = 1$	gCOD gCOD ⁻¹
Anoxic growth of X_H on S_{NO2}	
$v_{4,5} = -(1 - Y_{H,NO2})/(1.71Y_{H,NO2})$	gN gCOD ⁻¹
$v_{5,5} = (i_{C,SS}/Y_{H,NO2} - i_{C,BM})$	gC gCOD ⁻¹
$v_{8,5} = (i_{P,SS}/Y_{H,NO2} - i_{P,BM})$	gP gCOD ⁻¹
$v_{10,5} = 1/24 (i_{O,SS}/Y_{H,NO2} - i_{O,BM}) - 1/3 (i_{H,SS}/Y_{H,NO2} - i_{H,BM}) - 1/9 (i_{C,SS}/Y_{H,NO2} - i_{C,BM}) - 1/93 (i_{P,SS}/Y_{H,NO2} - i_{P,BM})$	gH gCOD ⁻¹
$v_{12,5} = -1/Y_{H,NO2}$	gCOD gCOD ⁻¹
$v_{17,5} = 1$	gCOD gCOD ⁻¹
Anoxic growth of X_H on S_{NO3}	
$v_{3,6} = -(1 - Y_{H,NO3})/(1.14Y_{H,NO3})$	gN gCOD ⁻¹
$v_{4,6} = (1 - Y_{H,NO3})/(1.14Y_{H,NO3})$	gN gCOD ⁻¹
$v_{5,6} = (i_{C,SS}/Y_{H,NO3} - i_{C,BM})$	gC gCOD ⁻¹
$v_{8,6} = (i_{P,SS}/Y_{H,NO3} - i_{P,BM})$	gP gCOD ⁻¹
$v_{10,6} = 1/14 (i_{N,SS}/Y_{H,NO3} - i_{N,BM}) + 2/31 (i_{P,SS}/Y_{H,NO3} - i_{P,BM})$	gH gCOD ⁻¹
$v_{12,6} = -1/Y_{H,NO3}$	gCOD gCOD ⁻¹
$v_{17,6} = 1$	gCOD gCOD ⁻¹
Aerobic endogenous respiration of X_H	
$v_{1,7} = i_{N,BM} - f_{XI} i_{N,XI}$	gN gCOD ⁻¹
$v_{5,7} = i_{C,BM} - f_{XI} i_{C,XI}$	gC gCOD ⁻¹
$v_{8,7} = i_{P,BM} - f_{XI} i_{P,XI}$	gP gCOD ⁻¹
$v_{9,7} = -(1 - f_{XI})$	gO ₂ gCOD ⁻¹
$v_{10,7} = -1/14 (i_{N,BM} - f_{XI} i_{N,XI}) + 2/31 (i_{P,BM} - f_{XI} i_{P,XI})$	gH gCOD ⁻¹
$v_{16,7} = f_{XI}$	gCOD gCOD ⁻¹
$v_{17,7} = -1$	gCOD gCOD ⁻¹

Anoxic endogenous respiration of X_H	
$v_{1,8} = i_{N,BM} - f_{XI} i_{N,XI}$	gN gCOD ⁻¹
$v_{3,8} = (f_{XI} - 1)/1.14$	gN gCOD ⁻¹
$v_{4,8} = (1 - f_{XI})/1.14$	gN gCOD ⁻¹
$v_{5,8} = i_{C,BM} - f_{XI} i_{C,XI}$	gC gCOD ⁻¹
$v_{8,8} = i_{P,BM} - f_{XI} i_{P,XI}$	gP gCOD ⁻¹
$v_{10,8} = 1/40 (i_{O,BM} - f_{XI} i_{O,XI}) - 1/5 (i_{H,BM} - f_{XI} i_{H,XI}) - 1/15 (i_{C,BM} - f_{XI} i_{C,XI}) + 1/35 (i_{N,BM} - f_{XI} i_{N,XI}) - 1/31 (i_{P,BM} - f_{XI} i_{P,XI})$	gH gCOD ⁻¹
$v_{16,8} = f_{XI}$	gCOD gCOD ⁻¹
$v_{17,8} = -1$	gCOD gCOD ⁻¹
Decay of X_H	
$v_{15,9} = (1 - f_{XI})$	gCOD gCOD ⁻¹
$v_{16,9} = f_{XI}$	gCOD gCOD ⁻¹
$v_{17,9} = -1$	gCOD gCOD ⁻¹
Growth of ammonia oxidizing bacteria (X_{AOB})	
$v_{1,10} = -1/Y_{AOB}$	gN gCOD ⁻¹
$v_{4,10} = 1/Y_{AOB} - i_{N,BM}$	gN gCOD ⁻¹
$v_{5,10} = -i_{C,BM}$	gC gCOD ⁻¹
$v_{8,10} = -i_{P,BM}$	gP gCOD ⁻¹
$v_{9,10} = 1 - 3.43/Y_{AOB}$	gO ₂ gCOD ⁻¹
$v_{10,10} = 2/14 Y_{AOB} - 1/14 (i_{N,BM}) - 2/31 (i_{P,BM})$	gH gCOD ⁻¹
$v_{18,10} = 1$	gCOD gCOD ⁻¹
Growth of nitrite oxidizing bacteria (X_{NOB})	
$v_{3,11} = 1/Y_{NOB} - i_{N,BM}$	gN gCOD ⁻¹
$v_{4,11} = -1/Y_{NOB}$	gN gCOD ⁻¹
$v_{5,11} = -i_{C,BM}$	gC gCOD ⁻¹
$v_{8,10} = -i_{P,BM}$	gP gCOD ⁻¹
$v_{9,11} = 1 - 1.14/Y_{NOB}$	gO ₂ gCOD ⁻¹
$v_{10,11} = -1/14 (i_{N,BM}) - 2/31 (i_{P,BM})$	gH gCOD ⁻¹
$v_{19,11} = 1$	gCOD gCOD ⁻¹
Endogenous respiration of X_{AOB}	
$v_{1,12} = i_{N,BM} - f_{XI} i_{N,XI}$	gN gCOD ⁻¹
$v_{5,12} = i_{C,BM} - f_{XI} i_{C,XI}$	gC gCOD ⁻¹
$v_{8,12} = i_{P,BM} - f_{XI} i_{P,XI}$	gP gCOD ⁻¹
$v_{9,12} = -(1 - f_{XI})$	gO ₂ gCOD ⁻¹
$v_{10,12} = -1/14 (i_{N,BM} - f_{XI} i_{N,XI}) + 2/31 (i_{P,BM} - f_{XI} i_{P,XI})$	gH gCOD ⁻¹
$v_{16,12} = f_{XI}$	gCOD gCOD ⁻¹

$v_{18,12} = -1$	gCOD gCOD ⁻¹
Endogenous respiration of X_{NOB}	
$v_{1,13} = i_{N,BM} - f_{XI} i_{N,XI}$	gN gCOD ⁻¹
$v_{5,13} = i_{C,BM} - f_{XI} i_{C,XI}$	gC gCOD ⁻¹
$v_{8,13} = i_{P,BM} - f_{XI} i_{P,XI}$	gP gCOD ⁻¹
$v_{9,13} = -(1 - f_{XI})$	gO ₂ gCOD ⁻¹
$v_{10,13} = -1/14 (i_{N,BM} - f_{XI} i_{N,XI}) + 2/31 (i_{P,BM} - f_{XI} i_{P,XI})$	gH gCOD ⁻¹
$v_{16,13} = f_{XI}$	gCOD gCOD ⁻¹
$v_{19,13} = -1$	gCOD gCOD ⁻¹
Decay of X_{AOB} and X_{NOB}	
$v_{15,14a} = (1 - f_{XI})$	gCOD gCOD ⁻¹
$v_{16,14a} = f_{XI}$	gCOD gCOD ⁻¹
$v_{18,14a} = -1$	gCOD gCOD ⁻¹
$v_{15,14b} = (1 - f_{XI})$	gCOD gCOD ⁻¹
$v_{16,14b} = f_{XI}$	gCOD gCOD ⁻¹
$v_{19,14b} = -1$	gCOD gCOD ⁻¹
Hydrolysis	
$v_{1,15} = -(1 - f_{SI})i_{N,SS} - f_{SI}i_{N,SI} + i_{N,XS}$	gN gCOD ⁻¹
$v_{5,15} = i_{C,XS} - (1 - f_{SI})Y_{HYD}i_{C,SS} - f_{SI}Y_{HYD}i_{C,SI}$	gC gCOD ⁻¹
$v_{8,15} = i_{P,XS} - (1 - f_{SI})Y_{HYD}i_{P,SS} - f_{SI}Y_{HYD}i_{P,SI}$	gP gCOD ⁻¹
$v_{10,15} = -1/14 (i_{N,XS} - (1 - f_{SI})Y_{HYD}i_{N,SS} - f_{SI}Y_{HYD}i_{N,SI}) + 2/31 (i_{P,XS} - (1 - f_{SI})Y_{HYD}i_{P,SS} - f_{SI}Y_{HYD}i_{P,SI})$	gH gCOD ⁻¹
$v_{12,15} = (1 - f_{SI})Y_{HYD}$	gCOD gCOD ⁻¹
$v_{13,15} = (f_{SI})Y_{HYD}$	gCOD gCOD ⁻¹
$v_{15,15} = -1$	gCOD gCOD ⁻¹
Chemical equilibria CO₂ ↔ HCO₃⁻	
$v_{5,16} = -1$	gC gC ⁻¹
$v_{6,16} = 1$	gC gC ⁻¹
$v_{10,16} = 1/12$	gH gC ⁻¹
Chemical equilibria HCO₃⁻ ↔ CO₃²⁻	
$v_{6,17} = -1$	gC gC ⁻¹
$v_{7,17} = 1$	gC gC ⁻¹
$v_{10,17} = 1/12$	gH gC ⁻¹
Chemical equilibria NH₄⁺ ↔ NH₃	
$v_{1,18} = -1$	gN gN ⁻¹
$v_{2,18} = 1$	gN gN ⁻¹
$v_{10,18} = 1/14$	gH gN ⁻¹

Chemical equilibria $H^+ \leftrightarrow OH^-$	
$v_{10,19} = 1$	gH gH ⁻¹
$v_{11,19} = 1$	gH gH ⁻¹
Oxygen transfer to the atmosphere	
$v_{9,20} = 1$	–
Carbon dioxide transfer to the atmosphere	
$v_{5,21} = 1$	–
Ammonia transfer to the atmosphere	
$v_{2,22} = 1$	–

Table A7.5 Values of fractions of carbon, hydrogen, oxygen and nitrogen in microalgae and bacteria biomass.

Parameters	Description	Value	Unit	Source
Fractions of microalgal biomass (X_{ALG})				
$i_{C,ALG}$	Fraction of carbon in microalgae	0.387	gC gCOD ⁻¹	Reichert et al., 2001
$i_{H,ALG}$	Fraction of hydrogen in microalgae	0.075	gH gCOD ⁻¹	Reichert et al., 2001
$i_{O,ALG}$	Fraction of oxygen in microalgae	0.538	gO gCOD ⁻¹	Reichert et al., 2001
$i_{N,ALG}$	Fraction of nitrogen in microalgae	0.065	gN gCOD ⁻¹	Reichert et al., 2001
$i_{P,ALG}$	Fraction of phosphorus in microalgae	0.01	gP gCOD ⁻¹	Reichert et al., 2001
Fractions of bacteria biomass (X_H, X_{AOB}, X_{NOB})				
$i_{C,BM}$	Fraction of carbon in bacteria	0.323	gC gCOD ⁻¹	Reichert et al., 2001
$i_{H,BM}$	Fraction of hydrogen in bacteria	0.060	gH gCOD ⁻¹	Reichert et al., 2001
$i_{O,BM}$	Fraction of oxygen in bacteria	0.155	gO gCOD ⁻¹	Reichert et al., 2001
$i_{N,BM}$	Fraction of nitrogen in bacteria	0.075	gN gCOD ⁻¹	Reichert et al., 2001
$i_{P,BM}$	Fraction of phosphorus in bacteria	0.018	gP gCOD ⁻¹	Reichert et al., 2001
Fractions of slowly biodegradable substrates (X_S)				
$i_{C,XS}$	Fraction of carbon in X_S	0.318	gC gCOD ⁻¹	Reichert et al., 2001
$i_{H,XS}$	Fraction of hydrogen in X_S	0.045	gH gCOD ⁻¹	Reichert et al., 2001
$i_{O,XS}$	Fraction of oxygen in X_S	0.156	gO gCOD ⁻¹	Reichert et al., 2001
$i_{N,XS}$	Fraction of nitrogen in X_S	0.034	gN gCOD ⁻¹	Reichert et al., 2001
$i_{P,XS}$	Fraction of phosphorus in X_S	0.005	gP gCOD ⁻¹	Reichert et al., 2001
Fractions of inert particulate organics (X_I)				
$i_{C,XI}$	Fraction of carbon in X_I	0.327	gC gCOD ⁻¹	Reichert et al., 2001
$i_{H,XI}$	Fraction of hydrogen in X_I	0.037	gH gCOD ⁻¹	Reichert et al., 2001
$i_{O,XI}$	Fraction of oxygen in X_I	0.150	gO gCOD ⁻¹	Reichert et al., 2001

$i_{N,XI}$	Fraction of nitrogen in X_I	0.016	$gN\ gCOD^{-1}$	Reichert et al., 2001
$i_{P,XI}$	Fraction of phosphorus in X_I	0.005	$gP\ gCOD^{-1}$	Reichert et al., 2001
Fractions of readily biodegradable substrates (S_S)				
$i_{C,SS}$	Fraction of carbon in S_S	0.318	$gC\ gCOD^{-1}$	Reichert et al., 2001
$i_{H,SS}$	Fraction of hydrogen in S_S	0.045	$gH\ gCOD^{-1}$	Reichert et al., 2001
$i_{O,SS}$	Fraction of oxygen in S_S	0.156	$gO\ gCOD^{-1}$	Reichert et al., 2001
$i_{N,SS}$	Fraction of nitrogen in S_S	0.034	$gN\ gCOD^{-1}$	Reichert et al., 2001
$i_{P,SS}$	Fraction of phosphorus in S_S	0.005	$gP\ gCOD^{-1}$	Reichert et al., 2001
Fractions of soluble inert organics (S_I)				
i_{C,S_I}	Fraction of carbon in S_I	0.327	$gC\ gCOD^{-1}$	Reichert et al., 2001
i_{H,S_I}	Fraction of hydrogen in S_I	0.037	$gH\ gCOD^{-1}$	Reichert et al., 2001
i_{O,S_I}	Fraction of oxygen in S_I	0.150	$gO\ gCOD^{-1}$	Reichert et al., 2001
i_{N,S_I}	Fraction of nitrogen in S_I	0.016	$gN\ gCOD^{-1}$	Reichert et al., 2001
i_{P,S_I}	Fraction of phosphorus in S_I	0.005	$gP\ gCOD^{-1}$	Reichert et al., 2001
Fractions of inert produced by biomass degradation				
f_{ALG}	Production of X_I in endogenous resp. of X_{ALG}	0.1	$gCOD\ gCOD^{-1}$	Sah et al., 2011
f_{XI}	Production of X_I in endogenous resp. of X_H	0.1	$gCOD\ gCOD^{-1}$	Sah et al., 2011
Yield of biomass				
Y_{ALG}	Yield of X_{ALG}	0.62	$gCOD\ gCOD^{-1}$	Reichert et al., 2001
Y_H	Yield of X_H on S_{O_2}	0.6	$gCOD\ gCOD^{-1}$	Reichert et al., 2001
Y_{H,NO_3}	Yield of X_H on S_{NO_3}	0.5	$gCOD\ gCOD^{-1}$	Reichert et al., 2001
Y_{H,NO_2}	Yield of X_H on S_{NO_2}	0.3	$gCOD\ gCOD^{-1}$	Reichert et al., 2001
Y_{AOB}	Yield of X_{AOB}	0.13	$gCOD\ gCOD^{-1}$	Reichert et al., 2001
Y_{NOB}	Yield of X_{NOB}	0.03	$gCOD\ gCOD^{-1}$	Reichert et al., 2001
Y_{HYD}	Hydrolysis saturation constant	1	$gCOD\ gCOD^{-1}$	Reichert et al., 2001

Uncertainty analysis

Following Morris's method an orientation Matrix is developed assuming $p = 4$, $\Delta = 2/3$ and $k = 3$. We analyse $k = 3$ uncertainty parameters: the maximum specific rate of microalgae growth (μ_{ALG}), and the maximum growth rate and the decay of heterotrophic bacteria (μ_H and $k_{death,H}$). These parameters may contain values in the set $\{0, 1/3, 2/3, 1\}$.

Assuming a random base value $\mathbf{x}^* = \{1/3, 0, 1/3\}$, we construct the matrices defined in the previously work (Solimeno et al., 2016):

$$\mathbf{B} = \begin{pmatrix} 0 & 0 & 0 \\ 1 & 0 & 0 \\ 1 & 1 & 0 \\ 1 & 1 & 1 \end{pmatrix} \quad (7.3)$$

$$\mathbf{J} = \begin{pmatrix} 1 & 1 & 1 \\ 1 & 1 & 1 \\ 1 & 1 & 1 \\ 1 & 1 & 1 \end{pmatrix} \quad (7.4)$$

$$\mathbf{D}^* = \begin{pmatrix} 1 & 0 & 0 \\ 0 & -1 & 0 \\ 0 & 0 & 1 \end{pmatrix} \quad (7.5)$$

$$\mathbf{P}^*_{(3,3)} = \begin{pmatrix} 1 & 0 & 0 \\ 0 & 0 & 1 \\ 0 & 1 & 0 \end{pmatrix} \quad (7.6)$$

The modified sampling matrix \mathbf{B}' is shown in below.

$$\left(\quad \quad \right)$$

$$\mathbf{B}'_{(3,3)} = \begin{pmatrix} 0 & 1/2 & 1/2 \\ 1/2 & 1 & 1/2 \\ 1/2 & 1/2 & 0 \end{pmatrix} \quad (7.7)$$

\mathbf{B}' is then multiplied by $\Delta = 2/3$, defined earlier, to create the following matrix:

$$\Delta \mathbf{B}'_{(5,4)} = \begin{pmatrix} 0 & 2/3 & 0 & 2/3 \\ 2/3 & 2/3 & 0 & 2/3 \\ 2/3 & 0 & 0 & 2/3 \\ 2/3 & 0 & 2/3 & 2/3 \\ 2/3 & 0 & 2/3 & 0 \end{pmatrix} \quad (7.8)$$

Matrices \mathbf{D}^* and \mathbf{P}^* define the orientation of trajectory (for $k = 3$, there are 2^3 different possibilities for \mathbf{D}^* , each one with probability $1/8$, and $3! = 6$ possibilities for \mathbf{P}^* each one with probability $1/6$). Then \mathbf{B}^* becomes:

$$\begin{aligned} (\mathbf{J}_{(4,1)} \mathbf{x}^* + \Delta \mathbf{B}')^* \mathbf{P}^* &= \left\{ \begin{pmatrix} 1/3 & 0 & 1/3 \\ 1/3 & 0 & 1/3 \\ 1/3 & 0 & 1/3 \end{pmatrix} + \begin{pmatrix} 0 & 1/3 & 1/3 \\ 1/3 & 2/3 & 1/3 \\ 1/3 & 1/3 & 1/3 \end{pmatrix} \right\} \cdot \begin{pmatrix} 1 & 0 & 0 \\ 0 & 0 & 1 \\ 0 & 1 & 0 \end{pmatrix} \\ &= \begin{pmatrix} 1/3 & 1/3 & 2/3 \\ 2/3 & 2/3 & 2/3 \\ 2/3 & 1/3 & 1/3 \end{pmatrix} \cdot \begin{pmatrix} 1 & 0 & 0 \\ 0 & 0 & 1 \\ 0 & 1 & 0 \end{pmatrix} \quad (7.9) \end{aligned}$$

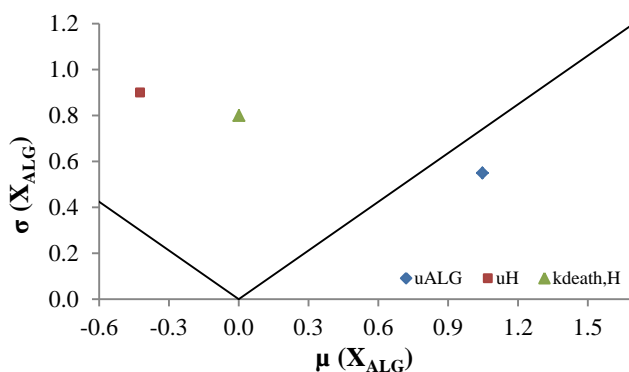
Finally, matrix \mathbf{B}^* becomes

$$\mathbf{B}^* = \begin{pmatrix} 1/3 & 2/3 & 1/3 \\ 2/3 & 2/3 & 2/3 \\ 2/3 & 2/3 & 1/3 \end{pmatrix} \quad (7.10)$$

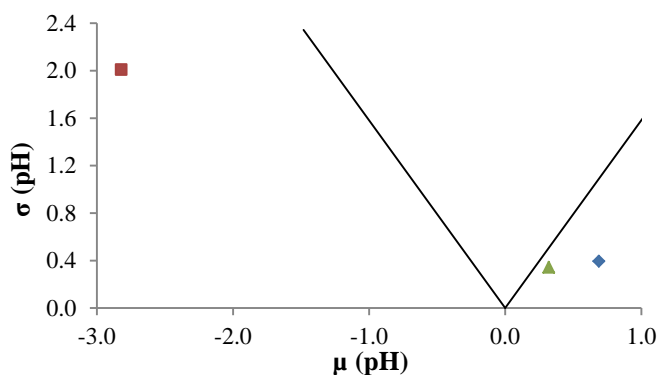
The Morris's method results were evaluated by comparing the means and standard deviations of the distribution function $F_{i,j}$ for each input. Means

and standard deviations of the 3 input parameters were plotted in Fig. S1 for the 4 output variables considered (X_{ALG} , pH, S_{O_2} and X_H). These variables were selected respect of the other outputs of the model because resulted to be the outputs more sensitive during the model simulations.

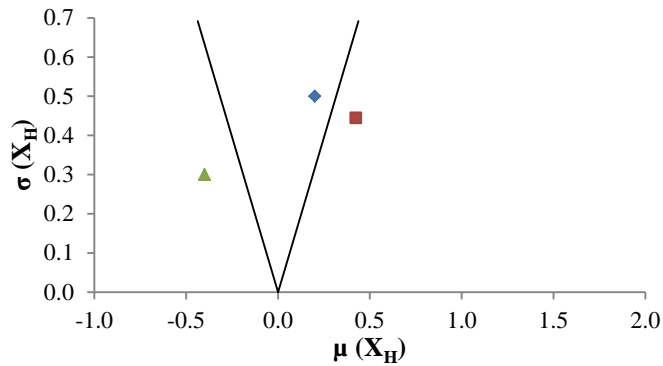
In Fig. A7.1 there are two lines corresponding to $\mu_{i,j} = \pm 2SEM_{i,j}$ to facilitate the interpretation of the results. Parameters that lie inside the wedge obtained by the two lines are deemed as non-influential or negligible. Otherwise, if the parameters lie outside the wedge, it indicates to have significant effect on the output (Sin et al., 2009; Morris, 1991).



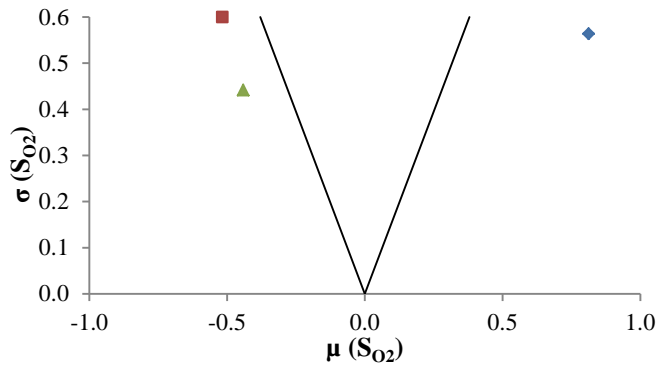
a)



b)



c)



d)

Fig. A7.1 Sensitivity measures of the distribution of elementary effects of the inputs on the model outputs a) X_{ALG} , b) pH, c) X_H , d) S_{O_2} . Lines correspond to $\mu_i = \pm 2SEM_i$. Figure legends for graphics shown in the bottom right graph (a).

From the graphical Morris approach it was clear that the maximum specific growth rate of microalgae (μ_{ALG}) and the maximum specific growth rate of heterotrophic bacteria (μ_H) had great influence on microalgae (X_{ALG}) and heterotrophic biomass (X_H), respectively (Fig. A7.1a-c). Likewise, the effect of growth (μ_{ALG} , μ_H) and decay rate ($k_{death,H}$) on pH (Fig. A7.1b) and dissolved oxygen (S_{O_2}) (Fig. A7.1d) outputs were mediated through the concentrations of microalgae and heterotrophic biomass (X_{ALG} , X_H). Microalgae biomass was not very sensitive to the maximum specific growth

rate and decay of heterotrophic bacteria ($\mu_H, k_{\text{death,H}}$), likewise heterotrophic biomass was not sensitive to the maximum specific growth rate of microalgae (μ_{ALG}). These parameters were distributed inside the wedge formed by $\mu_{ij} = \pm 2 SEM_{ij}$, indicating that their effects on model output were negligible (Fig. A7.1a-c).

8

Long-term BIO_ALGAE validation

This chapter is based on the article:

- ❖ A. Solimeno, J. García. (in preparation). Microalgae and bacteria dynamics in high rate algal ponds based on modelling results: long-term application of BIO_ALGAE model.

8.1 Introduction

High rate algal pond (HRAP) technology for municipal, industrial and agricultural wastewater treatment was developed in California by Oswald in the 1950s as an alternative to conventional waste stabilisation ponds (WPS) (Oswald and Gotaas, 1957). The lower footprint of HRAP systems coupled with the benefit of production of valuable products (e.g. biofuels, bioplastics) as by-products of microalgae feedstocks makes them more attractive over WPS (Faleschini et al., 2012, García et al., 2000c).

HRAPs are based on microalgae and bacteria interactions in wastewater exposed to light. Microalgae photosynthesis provides oxygen necessary for the degradation of organic compounds present in wastewater by aerobic bacteria. During bacterial organic matter oxidation, CO₂ is produced and it is available for both photosynthesis and nitrification (Oswald, 1988). Multiple reactions and processes that occur in microalgae-bacteria systems are quite difficult to control (Fuentes et al., 2016, Awuah, 2006; García et al., 2006). In fact, these reactions and processes depend on ever-changing environmental variables such as solar radiation and temperature.

Despite of these systems have been studied for many years, still today physical, chemical and biochemical reactions that occur in microalgae-bacteria systems are known at a much lower level in comparison to conventional technologies, such as activated sludge. In fact, it is very challenging to understand which are the main factors affecting microorganisms growth and production (i.e. microalgae and bacteria), and how changes the relatively proportion of microorganisms. Recently, variations of biomass production over a year in pilot-scale HRAPs were evaluated by Mehrabadi et al. (2016). These authors observed that changes in microalgae concentration were linked to seasonal fluctuations in temperature and light intensity in the absence of nutrient limitation. Moreover, HRAP operating conditions play an important role on biomass composition, and of course the efficiency for removing pollutants. In the study conducted by Park and Craggs (2011b), hydraulic retention time (HRT) clearly influenced microalgae proportion dynamics. Lower HRT (2 days) gave as result much more microalgae respect to bacteria (80% in average of total biomass), while

higher HRT (8 days) had less microalgae proportion (56% in average of total biomass). Authors estimated microalgae proportion indirect measurements through chlorophyll-a concentration. At present time is not trivial to have a direct measure of microalgae and bacteria proportion.

Mathematical models have proven to be useful tools to optimize and understand the inner functioning of biological wastewater treatment systems, including microalgae-bacteria systems (Zhou et al., 2014; Packer et al., 2011). Solimeno et al. (2017a) developed the mechanistic BIO_ALGAE model to understand the internal functioning of the complexity of microalgae-bacteria systems. The model predicts microbial biomass production, and therefore allows evaluation of the relative proportions of the microorganism considered (Solimeno et al., 2017a, 2017b, 2015).

The main sources of inspiration for building the model were the River Water Quality Model 1 (RWQM1) (Reichert et al., 2001) and the modify ASM3 model (Iacopozzi et al., 2007), both of the International Water Association (IWA). RWQM1 and ASM3 were selected to describe microalgae and bacteria processes, respectively. Inorganic carbon as a limiting substrate for the growth of microalgae is one of the major innovative features of BIO_ALGAE. Moreover, temperature, photorespiration, pH dynamics, solar radiation, light attenuation and transfer of gases to the atmosphere are considered main limiting factors for microalgae growth. BIO_ALGAE was implemented in the COMSOL Multiphysics™ software, which solves the problem equations using the finite elements method (FEM), and was previously calibrated and validated with high quality experimental data from triplicated pilot HRAPs receiving real wastewater (Solimeno et al., 2017a). Calibration was conducted adjusting 6 parameters selected after a Morris's sensitivity analysis: microalgae and heterotrophic bacteria specific growth rate, decay of heterotrophic bacteria and 3 parameters related to the transfer of gases to the atmosphere. These parameters were calibrated were carefully calibrated and validated in our previous work comparing experimental data over 4 intensive days of experiments in order to predict daily fluctuations of the components in the ponds, and the relative proportions of microalgae and bacteria in a short-time scale. A long-term validation is essential to demonstrate the usefulness of the model to predict seasonal variations of

microalgae and bacteria biomass, and the effect of different HRT operating strategies on the HRAP performance.

Therefore, the aim of the present study is to validate the BIO_ALGAE model with experimental data from a pilot HRAP gathered during two different seasons (summer and winter), and operating at different HRT (4 and 8 days). Moreover, the potential of the model is demonstrated by means of practical study cases in which microalgae production, the relative proportion of microalgae and bacteria and the ammonium removal efficiency were compared over a year cycle. HRAP performance were investigated operating with constant HRT (4 and 8 days) and changing the operating conditions of the ponds from April to September (HRT = 4 days) and from October to March (HRT = 8 days). Microalgae and bacteria interactions, the effect of different HRT operating strategies and variations of environmental conditions were studied in order to optimize biomass production and ammonium removal efficiency.

8.2 Material and methods

8.2.1 Experimental data

The data used for simulations were obtained from previous studies conducted by the authors in a pilot HRAP (García et al., 2000b; 2006). A detailed description of the system can be found in these studies. In brief, the pilot HRAP was installed outdoors on the roof of the Group of Environmental Engineering and Microbiology (GEMMA) building (Universitat Politècnica de Catalunya-BarcelonaTech, Barcelona, Spain, latitude: 41° 23' 24.7380" N; longitude: 2° 9' 14.4252" E). Monitoring of the pilot lasted approximately one year, although the data used in this paper were from July 1993 to October 1993 (Period I), and from November 1993 to February 1994 (Period II), corresponding to low and high hydraulic retention time (HRT, 4 and 8 days, referred as HRAP_{4d} and HRAP_{8d}) of the pilot, respectively. Note that low HRT was used in warmer periods (summer-autumn), and high HRT in colder periods (autumn-winter), as

usually is done in these systems to maintain contaminant removal efficiencies (García et al., 2006).

The pilot HRAP was a typical race track built in PVC with a water surface area of 1.54 m^2 and a water depth of 0.34 m , and a nominal volume of 0.47 m^3 (Fig. 8.1). A single paddlewheel was set to provide a rotational speed of 5 rpm , so that determined a mid-channel velocity of approximately 9 cm s^{-1} , avoiding biomass settling. HRAP received primary treated urban wastewater from the nearest street sewer, which was continuously pumped to the pond. Primary treatment was conducted in a 0.5 m^3 storage tank. Hydraulic retention time (HRT) of the HRAP was controlled by wastewater flow.

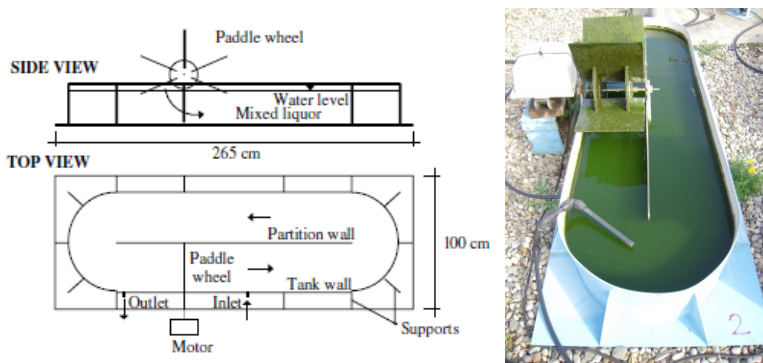


Figure 8.1 Diagram of top and side views of the pilot HRAP on the left and a picture on the right. The system was located roof of the Group of Environmental Engineering and Microbiology (GEMMA) building (Universitat Politècnica de Catalunya-BarcelonaTech, Barcelona, Spain).

Samples of HRAP influent, HRAP mixed liquor (identical to HRAPs effluent. because of almost perfect complete mixing) were taken once a week, at $2:00 \text{ PM} \pm 1 \text{ hour}$. Description of the methods used for analyses can be found in García et al. (2000b; 2002). Water temperature, pH and DO were taken weekly, at $9:00 \text{ AM} \pm 1$ and at $2:00 \text{ PM} \pm 1$ hour. Irradiance and air temperature were obtained from a nearby meteorological station.

8.2.2 Model implementation

Simulations were conducted using the BIO_ALGAE model. A detailed description of the components, the biokinetic processes, and the chemical and physical equations were presented in previous Chapters (Solimeno et al., 2015, 2017a, 2017b). To make easier here the understanding of the simulation results, Tables A8.1 and A8.2 in Appendix present the biokinetic processes and the matrix of stoichiometric parameters. Values of biokinetic, physical and chemical parameters are shown in Appendix, Tables A8.3-A8.4. Mathematical expressions of the stoichiometric coefficients of each process are shown Table A8.5.

The model was implemented in COMSOL Multiphysics™ v5.1 software. A simplified 1D domain was used to represent a single vertical section of the pilot HRAP. Assuming that each section behaves similarly due to perfect mixing of culture medium, this reasonable simplification allowed reducing computational cost. Hydrodynamics, transport of dissolved and particulate species and transfer of gases to the atmosphere take place along 0.47 m long of domain, which represents the nominal volume of the pilot HRAP distributed along one dimension.

Light attenuation was considered in the model, though pond depth was not incorporated into the domain design (1D). Using Beer-Lambert law irradiance decays exponentially as it penetrates into the almost perfectly homogeneous HRAP section due to microalgae, bacteria and other particulate fractions present in the mixed liquor. Assuming therefore culture medium in perfect mixing and isotropic respect of the light direction, an average irradiance I [MT^{-3}] was used to represent irradiance at any point of the pond (Solimeno et al., 2017a). The penetration pathway corresponded to the depth of the HRAP (0.3 m).

8.2.3 Validation procedure

BIO_ALGAE includes 93 parameters describing microalgae, bacteria, physical and chemical processes (Tables A8.3-A8.4, Appendix).

Influent HRAP average concentrations observed in each period were used as constant input values to run simulations (Table 8.1a). Influent concentration of nitrate and nitrite were lower than analytical method's detection limit and therefore considered to be zero in the input for the model. Ammonium nitrogen resulted almost to be 90% of dissolved Kjeldahl nitrogen, and therefore the concentration of organic nitrogen present in the influent wastewater was neglected in the model (García et al., 2000).

Fractions of influent COD were estimated from recommended values for primary effluents in Activated Sludge Model No1 (ASM1) (Henze et al., 2000). Accordingly, the proportion of each fraction was defined as: 22% S_S (readily biodegradable soluble organic matter), 50% X_S (slowly biodegradable particulate organic matter), 10% S_I (inert soluble organic matter), 8% X_I (inert particulate organic matter) and 10% X_H (heterotrophic bacteria). In the present work microalgae, bacteria biomass and soluble and inert organic matter are transformed from COD to TSS assuming a ratio COD/TSS= 0.80 (Sperling, 2007; Khorsandi et al., 2014) in order to compare experimental and simulation results. Note that the present work not follows the models of the International Water Association (IWA) (Sah et al., 2011; Reichert et al., 2001), where total suspended solids (TSS) and organic matter concentrations are expressed in g COD m⁻³. Maximum and minimum water temperature and irradiance recorded over the two periods investigated are shown in Table 8.1b.

Table 8.1 a) Average (and standard deviation) of influent HRAP water quality parameters during the two periods considered for validation (Period I: July 21st – October 14th, 1993; Period II: November 10th, 1993 – February 8th, 1994). These data were used as constant input values to run simulations. $n = 30$ for each period. b) Maximum and minimum water temperature and irradiance recorded.

a)

Parameters	Influent wastewater Period I	Influent wastewater Period II
pH	7.7 (0.8)	7.8 (0.6)
COD _{TOT} (g COD m ⁻³)	180 (84)	194 (50)
NH ₄ ⁺ -N (g m ⁻³)	39.8 (25)	43.7 (28)
PO ₄ -P (g m ⁻³)	6.0 (2.5)	6.0 (1.7)
Alkalinity (g CaCO ₃ m ⁻³)	388 (48)	421 (54)

Note: S_s, X_s, X_H, X_I, X_{AOB} and X_{NOB} influent concentrations were estimated from COD_{TOT} concentration.

b)

	Water temperature [°C]		Irradiance [μmol m ⁻² s ⁻¹]	
	Min	Max	Min	Max
Period I	11.1	29.7	0	1000
Period II	2.2	16.1	0	610

The concentrations of components in the mixed liquor of the HRAP measured at the beginning of the two experimental periods are shown and described in Table 8.2. The concentration of each particulate component (X_{ALG}, X_S, X_I, X_H, X_{AOB} and X_{NOB}) in the mixed liquor was not known. Therefore, an initial ratio of particulate components to estimate their concentrations was established from the initial TSS (assumed to be as the sum of X_{ALG}, X_S, X_I, X_H, X_{AOB} and X_{NOB}) value based on previous simulation tests in order to match the initial pattern trend of pH, dissolved oxygen, and nutrients (i.e. nitrogen and carbon) data. Validation was performed comparing measured data with simulation patterns using graphical representations of the two periods considered (with different HRT). Tested components during validation were: pH, dissolved oxygen (S_{O2}), bicarbonate (S_{HCO3}), ammonium (S_{NH4}), nitrate (S_{NO3}), nitrite (S_{NO2}) and TSS.

Table 8.2 Initial concentrations of components in the mixed liquor of the pilot HRAP used for simulations: Period I (corresponding exactly to July 21st, 1993) and Period II (corresponding exactly to November 10th, 1993). Data were recorded at 2:00 PM.

Components	Description	Concentrations		Units
		July 21 st , 1993	November 10 th , 1993	
S _{NH4}	Ammonium nitrogen	0.28	1	g N-NH ₄ m ⁻³
S _{NH3}	Ammonia nitrogen	0.20	0.017	g N-NH ₃ m ⁻³
S _{NO3}	Nitrate nitrogen	4.94	10	g N-NO ₃ m ⁻³
S _{NO2}	Nitrite nitrogen	8.46	0.90	g N-NO ₂ m ⁻³
S _{CO2}	Carbon dioxide	0.05	1.29	g C-CO ₂ m ⁻³
S _{HCO3}	Bicarbonate	40	20	g C-HCO ₃ m ⁻³
S _{CO3}	Carbonate	2.87	0.003	g C-CO ₃ m ⁻³
S _{PO4}	Phosphate phosphorus	0.12	0.12	g P-PO ₄ m ⁻³
S _{O2}	Dissolved oxygen	19.5	9	g O ₂ m ⁻³
S _H	Hydrogen ions	6.03 E-10	3.79 E-9	g H m ⁻³
S _{OH}	Hydroxide ions	1.28 E-5	1.17 E-2	g H-OH m ⁻³
S _S	Readily biodegradable soluble organic matter	0.8	6	g COD m ⁻³
X _{ALG}	Microalgae	240	64	g COD m ⁻³
X _H	Heterotrophic bacteria	56	16	g COD m ⁻³
X _{AOB}	Ammonium oxidizing bacteria	1.2	2	g COD m ⁻³
X _{NOB}	Nitrite oxidizing bacteria	0.04	0.08	g COD m ⁻³
X _S	Slowly biodegradable particulate organic matter	12	4	g COD m ⁻³
X _I	Inert particulate organic matter	24	16	g COD m ⁻³

Note: X_{ALG}, X_S, X_H, X_I, X_{AOB} and X_{NOB} concentrations were estimated from TSS concentration. S_S was estimated from previous simulation tests.

8.2.4 Case studies: relative proportion of microalgae and bacteria, and biomass production forecasting over a year cycle

Practical case studies were done to evaluate the variations in biomass production and the relative proportion of microalgae and bacteria over a year cycle (from January to December). In these studies we simulated the evolution of microalgae, bacteria and TSS concentrations starting from the initial mixed liquor concentration used for the validation of the model at the beginning of the month of February, and using the average influent wastewater concentration (Table 8.3), the. In addition, ammonium and ammonia concentration ($S_{\text{NH}_4} + S_{\text{NH}_3}$), as indicator of removal efficiency, were evaluated.

Three scenarios were evaluated: 1) the HRAP operating at 4-day ($\text{HRAP}_{4\text{d}}$) over the whole year; 2) the HRAP operating at 8-day ($\text{HRAP}_{8\text{d}}$) over the whole year and 3) the HRAP operating with different HRT, from April to September at 4-day HRT and from October to March at 8-day HRT ($\text{HRAP}_{8-4-8\text{d}}$).

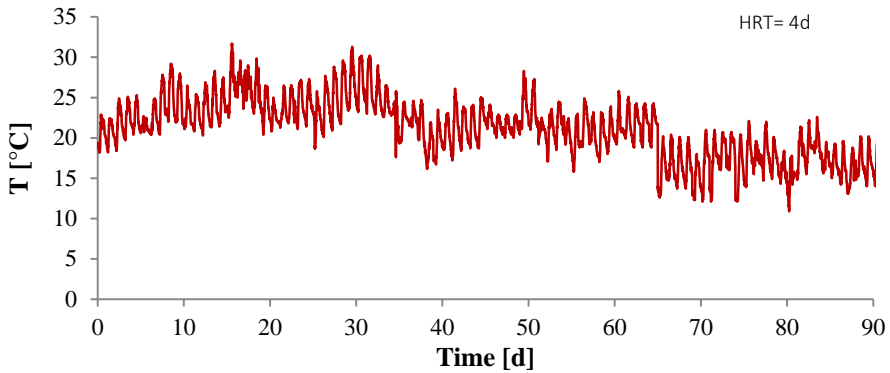
Water temperature data taken weekly at 9:00 AM ± 1 hour, and at 2:00 PM ± 1 hour measured over the one year monitoring period, and irradiance data from the nearby meteorological station were implemented to run simulations for study cases.

Table 8.3 Annual average (and standard deviation) of influent HRAP water quality parameters used for case studies. Ranges are shown. $n = 96$ (8 samples for each month).

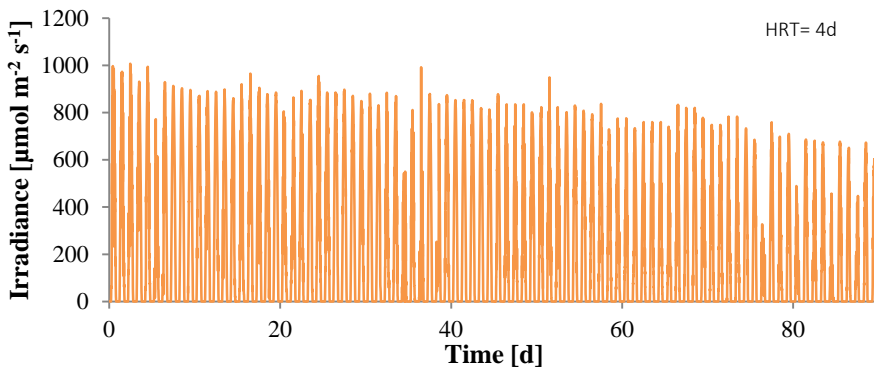
Parameters	Influent wastewater	Range
pH	7.68 (0.26)	7.18 – 8.13
COD_{TOT} (g COD m^{-3})	212 (62)	89 - 356
$\text{NH}_4^+ - \text{N}$ (g m^{-3})	49 (14.2)	18 – 76
$\text{PO}_4^{3-} - \text{P}$ (g m^{-3})	7.5 (1.2)	3.6 – 13
Alkalinity (g CaCO_3 m^{-3})	401 (56)	224 - 536

8.3 Results and discussion

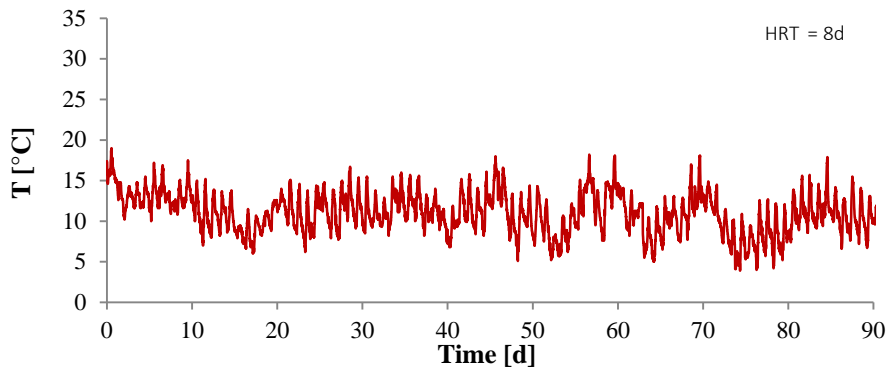
Fig. 8.2 shows the changes in air temperature and irradiance over the two periods considered for validation. As can be seen temperature and irradiance were greater in Period I than in Period II. Also in Period I the general trend of temperature and irradiance was to progressively decrease from July to October, while changes in Period II were more subtle.



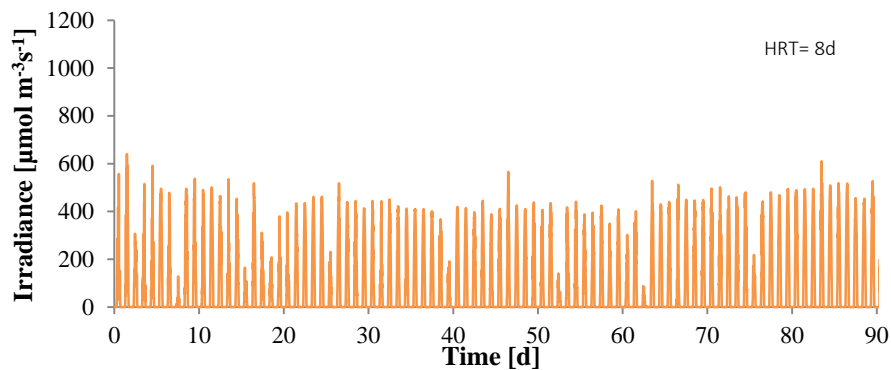
a)



b)



c)



d)

Figure 8.2 Changes in air temperature and irradiance in Barcelona over Period I (July 21st – October 14th, 1993, HRAP_{4d}) (a, b), and over Period II (November 10th, 1993 – February 8th, 1994, HRAP_{8d}) (c, d). HRT in each period also shown.

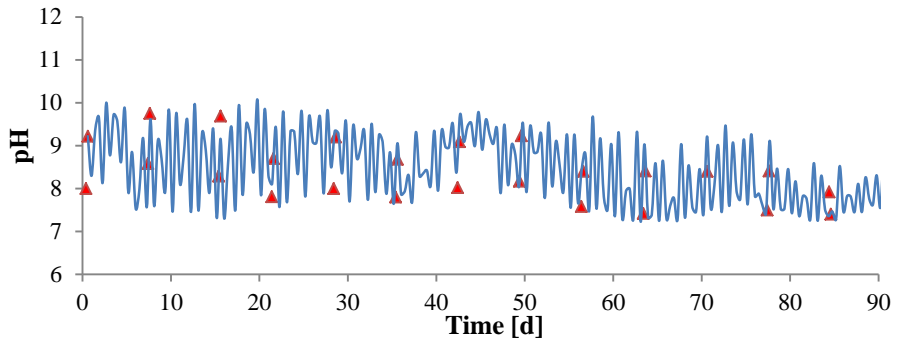
8.3.1 HRAP_{4d} validation (Period I)

Figs. 8.3 and 8.4 show the results of the validation in the HRAP_{4d} from July to October. Simulations were able to follow measured pH and dissolved oxygen (S_{O_2}) trends during the whole experimental period (Fig. 8.3a-b). As can be seen, both variables have a daily wavelike pattern due mostly to microalgae photosynthetic activity. This trend is in agreement with previous simulation results carried out during calibration conducted in previous Chapter (Solimeno et al., 2017a), and also with previous experimental studies (García et al., 2006b). Simulated daily minimum and maximum values were generally higher and lower than values measured at 9:00 AM and 2:00 PM,

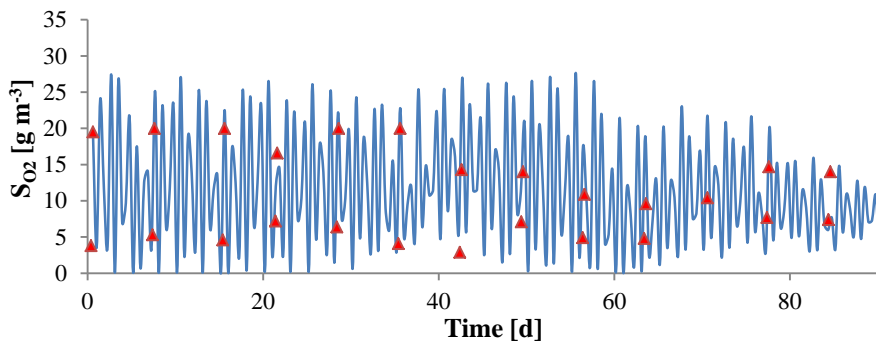
respectively, because the peaks of microalgae activity does not necessary coincide with these hours. From simulations, pH values ranged from 7.4 to 10.1, with an average of 8.5, while S_{O_2} concentration ranged from $0 \text{ gO}_2 \text{ m}^{-3}$ to $28.1 \text{ gO}_2 \text{ m}^{-3}$, with an average of $11.2 \text{ gO}_2 \text{ m}^{-3}$. It is possible to see how at the end of this period daily fluctuations of pH and S_{O_2} were slightly smoother than at the beginning of the study. At night S_{O_2} concentration decreased to be usually less than $5 \text{ gO}_2 \text{ m}^{-3}$, and even in some few cases almost 0 due to the lack of photosynthesis and the intense microbial respiration.

Simulations were able to follow with different degree of success the trend observed for measured bicarbonate (S_{HCO_3}), ammonium (S_{NH_4}), nitrate (S_{NO_3}) and nitrite (S_{NO_2}) (Fig. 8.3c-f). Simulated bicarbonate and ammonium curves matched quite well the experimental data and present a clear wavelike pattern mostly related to photosynthesis again, with lower values of both variables during daytime. Microalgae grow during daytime using bicarbonate as carbon source, and subsequently pH raises favoring conversion of ammonium to ammonia, and a part is lost through volatilization. Moreover, microalgae uptake also contributes to ammonium decrease during daytime. These trends are also in agreement with simulation results carried out during calibration in our previous study (Chapter 7; Solimeno et al., 2017a), and also with previous experimental studies (García et al., 2006). Daily fluctuations of bicarbonate and ammonium tended to soften towards the end of Period I (Fig. 8.3c-d), in connection with the same pattern observed for pH and dissolved oxygen. This is indicative of a lower photosynthetic activity due to decrease of incident irradiance and temperature.

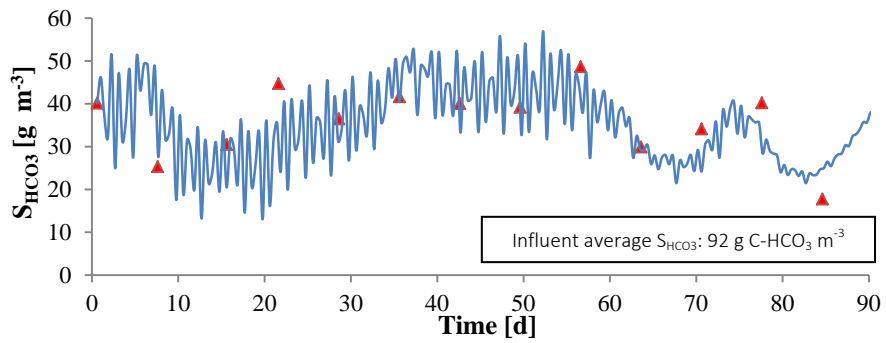
As can be seen in Fig. 8.3d ammonium simulated concentrations were relatively low and constant during July and August (the first 60 days), and increased from mid-September, in correspondence with the decrease in incident irradiance and temperature. This is in connection with the lower overall microalgae activity. Higher values of nitrate and nitrite were observed towards the end of the period, when ammonium was also higher. The model was able to simulate these trends described for nitrate and nitrite quite well, and it can be seen that photosynthesis is much less affecting these compounds due to the much lower daily wavelike trends.



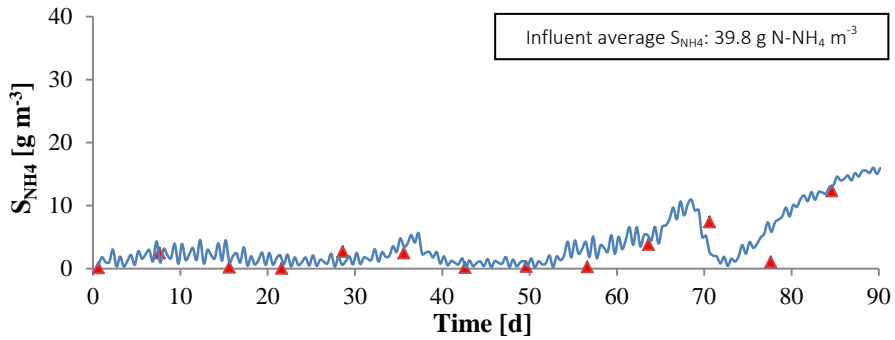
a)



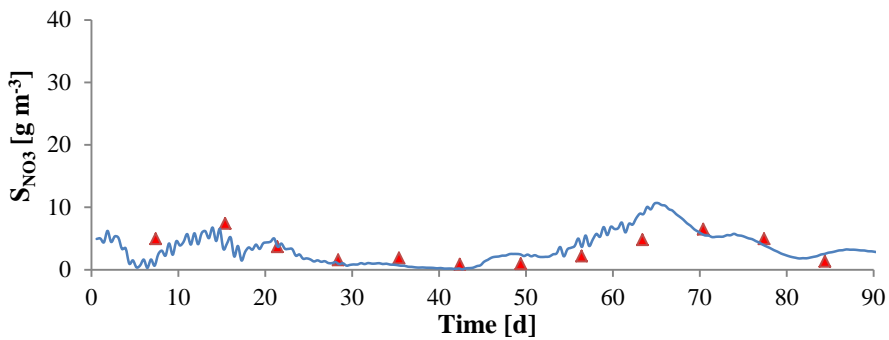
b)



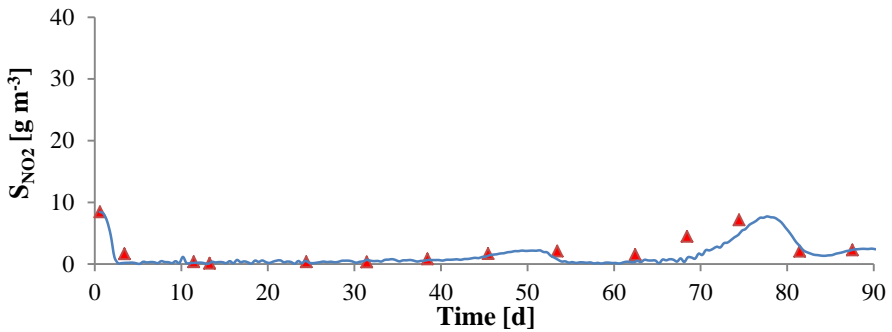
c)



d)



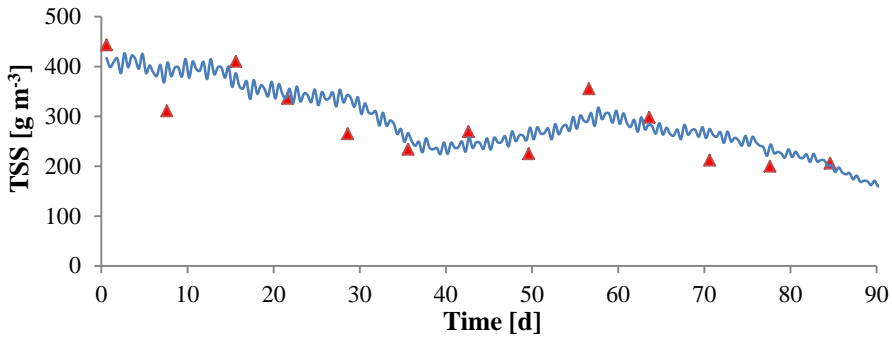
e)



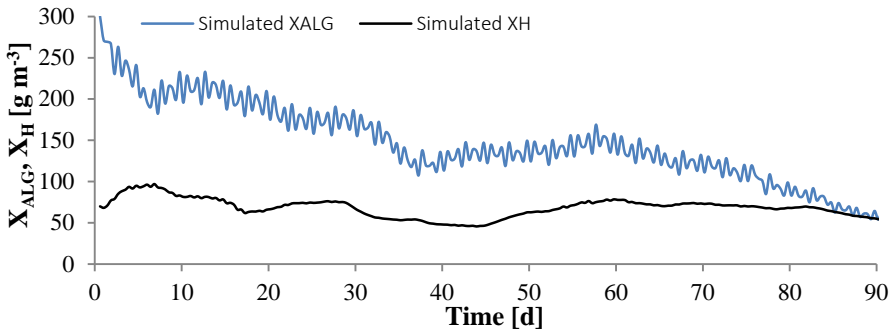
f)

Figure 8.3 Changes in experimental (red triangles) and simulated (blue line) a) pH, b) dissolved oxygen (S_{O_2}), c) bicarbonate (S_{HCO_3}), d) ammonium (S_{NH_4}), e) nitrate (S_{NO_3}) and f) nitrite (S_{NO_2}) concentrations over the Period I (July 21st – October 14th, 1993) in the HRAP_{4d}. Note that in a) and b) values measured at 9:00 AM \pm 1 hour and 2:00 PM \pm 1 hour are shown. All other values measured at 2:00 PM \pm 1 hour. Higher values of pH and dissolved oxygen observed at 2:00 PM \pm 1 hour. Nitrate and nitrite concentrations were not detected in influent wastewater.

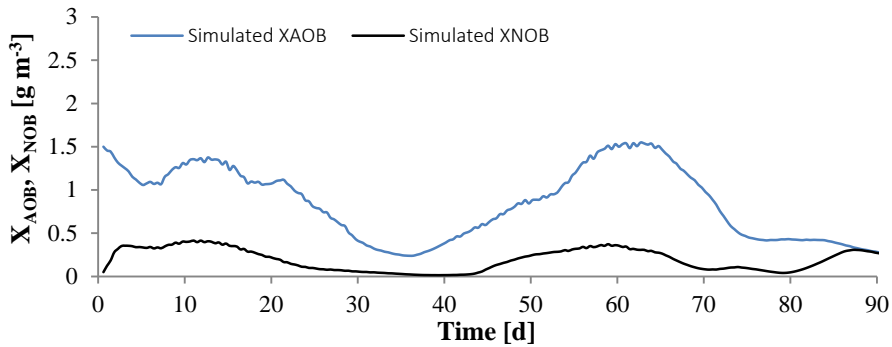
Simulated TSS concentration fits experimental data with a good degree of accuracy (Fig. 8.4a). In addition, the model is able to predict simulated curves of microalgal (X_{ALG}) and bacterial biomass concentrations (X_H , X_{AOB} and X_{NOB}) (Fig. 8.4b-c). Simulated microalgae concentration presents a wavelike trend, reflecting microalgae grow during daytime (crest) and decay at night (trough), while obviously simulated heterotrophic bacteria concentrations do not have this pattern. During the period, microalgae concentration gradually decreased towards the end, following the pattern of irradiance and temperature, while heterotrophic bacteria remained relatively constant. In July and August (the first 60 days) high irradiance and temperature produced a high photosynthetic activity which at the same time gave place to high daily peaks of dissolved oxygen (often greater than $25 \text{ gO}_2 \text{ m}^{-3}$). Subsequently these peaks seem to limit microalgae growth due to photorespiration as it is next explained.



a)



b)



c)

Figure 8.4 Changes in experimental (red triangles) and simulated (blue and black lines) a) Total suspended solids (TSS), b) microalgae (X_{ALG}) and heterotrophic bacteria (X_H), and c) nitrifying bacteria (X_{AOB} and X_{NOB}) over the Period I (July 21st – October 14th, 1993) in HRAP_{4d}. Experimental values measured at 2:00 PM ± 1 hour.

As can be seen in Fig. 8.5, the photorespiration factor ($f_{PR}(O_2)$) reduced many times microalgae growth from 20 to 40% (values of the factor from 0.8 to 0.6, respectively). Thus, excess of oxygen caused less microalgae production that could had been avoided with more oxygen transfer to the atmosphere. Also the drop in temperature from mid-September (day 65) had impact on microalgae, causing a reduction of growth from 10 to 20% through the thermic photosynthetic factor ($f_{T_{FS}}$) (Fig. 8.6).

Nitrifying bacteria concentration was very low in comparison to heterotrophic bacteria. This observation has already been reported in previous simulation studies, and even with other types of systems (Solimeno et al., 2017a; Samsó and García, 2013; Krasnits et al., 2009).

Altogether simulation results have demonstrated that much of the organic matter present in the mixed liquor corresponds to microalgae (55% in average of TSS) and heterotrophic bacteria (26% in average of TSS). Nitrifying bacteria are comparatively very low (0.35%), and the remaining solids are attributable to X_S (5.5%) and X_I (13.2%).

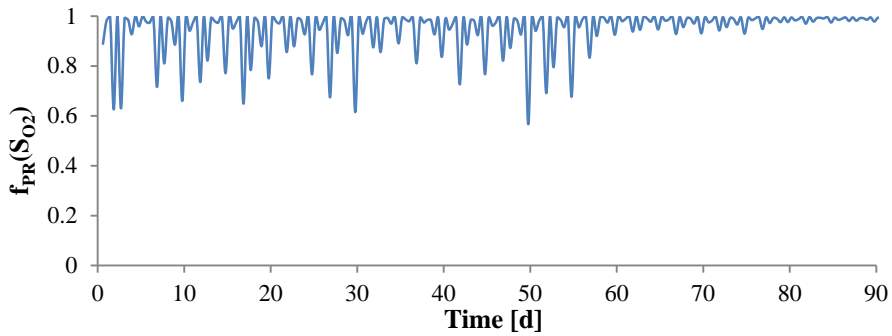


Figure 8.5 Changes in the values of photorespiration factor ($f_{PR}(S_{O_2})$) over Period I (July 21st – October 14th, 1993) in HRAP_{4d}.

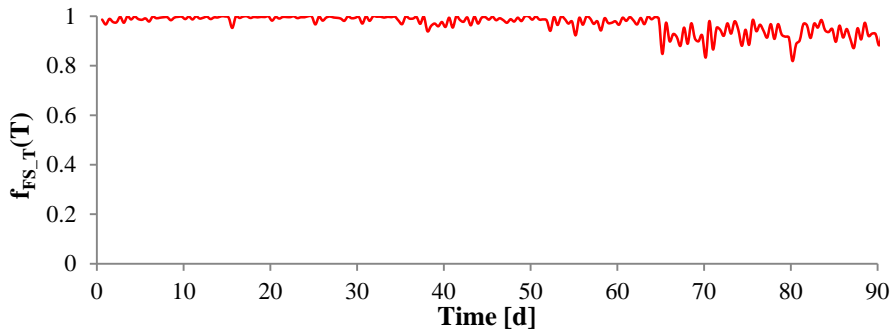


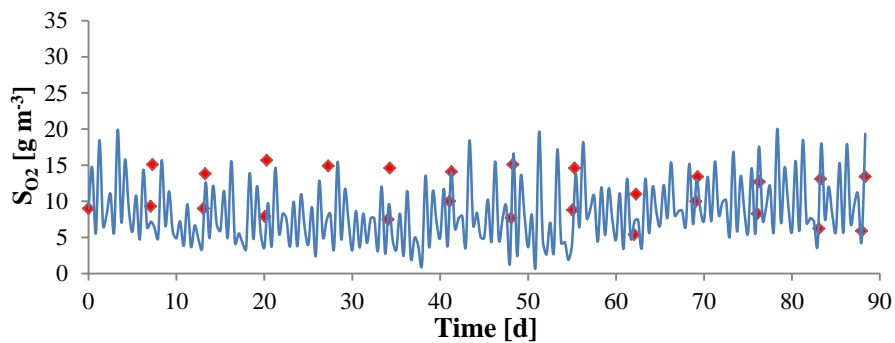
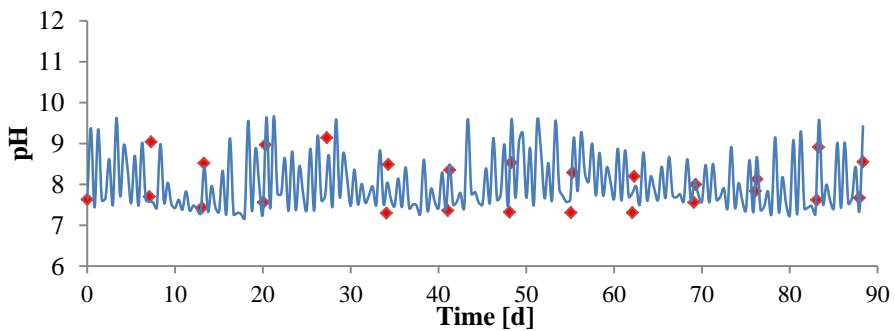
Figure 8.6. Changes in the values of thermic photosynthetic factor ($f_{FS,T}(T)$) over Period I (July 21st – October 14th, 1993) in HRAP_{4d}.

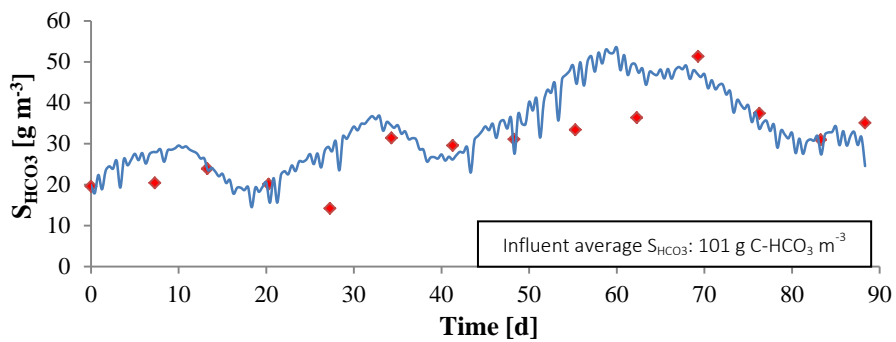
8.3.2 HRAP_{8d} validation (Period II)

Figs. 8.7 and 8.8 show the results of the validation in the HRAP_{8d} from November to February. Again, the model showed the wavelike trend for pH and S_{O_2} during the whole experimental period (Fig. 8.7a-b), with lower values in comparison to Period I. The fitting degree was slightly lower than in Period I. Simulation results indicated that pH values ranged from 7.2 to 9.6, with an average of 8.1, while S_{O_2} concentrations ranged from $0.9 \text{ gO}_2 \text{ m}^{-3}$ to $20 \text{ gO}_2 \text{ m}^{-3}$ with an average of $11 \text{ gO}_2 \text{ m}^{-3}$. Daily fluctuations of pH and S_{O_2} were shorter than in Period I. Respect to Period I, at night S_{O_2} concentration decreased rarely less than $5 \text{ gO}_2 \text{ m}^{-3}$ due to the lower overall

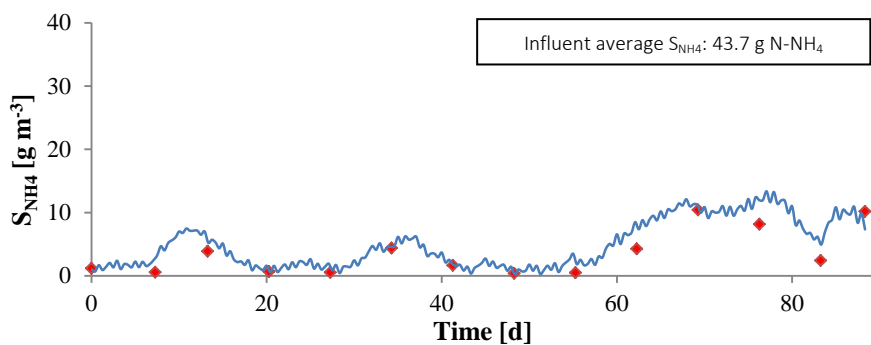
microbial respiration and lower temperature, which increased transference from the atmosphere to the mixed liquor.

Likewise the validation results of HRAP_{4d}, the model was able to reproduce quite successfully the trend of bicarbonate (S_{HCO_3}), ammonium (S_{NH_4}) and nitrite (S_{NO_2}) data. Conversely, simulated nitrate (S_{NO_3}) concentration did not match experimental data as good as in Period I. Simulated bicarbonate and ammonium had the wavelike pattern already mentioned in Period I, but with shorter daily fluctuations, similar to the last part of Period I (when irradiation and temperature decreased). This is indicative of a lower overall photosynthetic activity in comparison to Period I. Much higher values of nitrite were observed towards the end of Period II when ammonium concentration was higher.

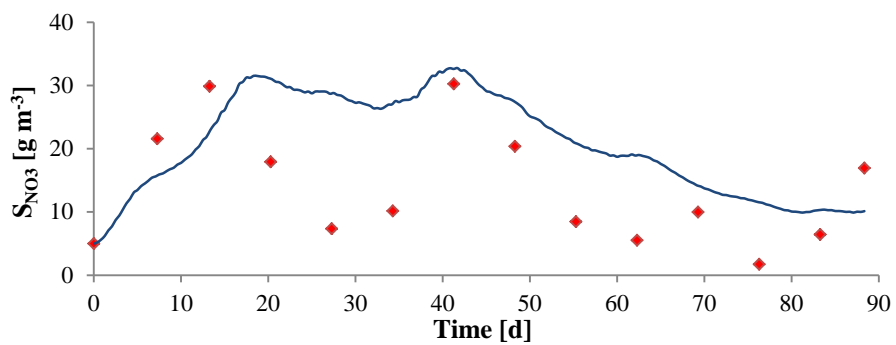




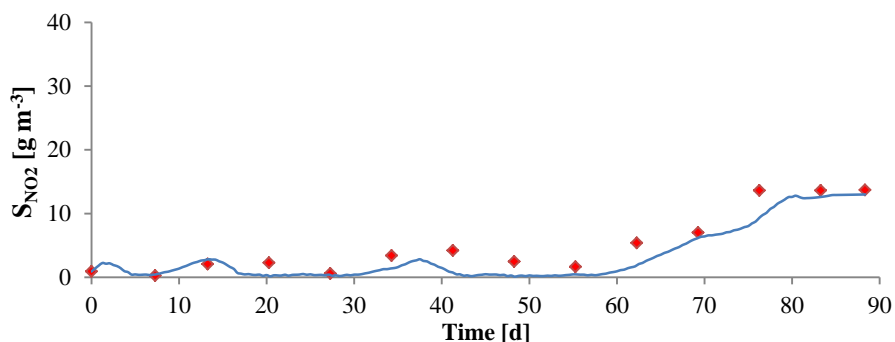
c)



d)



e)



f)

Figure 8.7 Changes in experimental (red diamonds) and simulated (blue line) a) pH, b) dissolved oxygen (S_{O_2}), c) bicarbonate (S_{HCO_3}), d) ammonium (S_{NH_4}), e) nitrate (S_{NO_3}) and f) nitrite (S_{NO_2}) concentrations over the Period II (November 10th, 1993 – February 8th, 1994) in the HRAP_{8d}. Note that in a) and b) values measured at 9:00 AM \pm 1 hour and 2:00 PM \pm 1 hour are shown. All other values measured at 2:00 PM \pm 1 hour. Higher values of pH and dissolved oxygen observed at 2:00 PM \pm 1 hour. Nitrate and nitrite concentrations were not detected in influent wastewater.

As can be seen in Fig. 8.8a, the model was able to simulate TSS concentration with a good degree of accuracy. Respect to HRAP_{4d}, TSS concentration, and microalgae and bacteria predicted concentrations were lower (although HRT was higher than in Period I). Lower microalgae concentrations were mostly due to the temperature (and to less extend to irradiance). Fig. 8.9 shows reduction of growth from 10 to 30% through the thermic photosynthetic factor ($f_{T_{FS}}$), and as can be seen was much lower in Period II than in Period I (compare with Fig. 8.6).

In average of TSS microalgae biomass concentration was higher (58%) than heterotrophic bacteria (22%). Nitrifying bacteria biomass is comparatively much lower (2.4%), but higher than the estimated in Period I. The remaining solids are attributable to X_s (6%) and X_I (11.6%).

Comparative evaluation indicates that increasing HRT from 4-day in Period I to 8-day in Period II caused a clear increase in nitrification activity. High HRT maximize nitrification performance because nitrifying bacteria growth slowly (Liu et al., 2004).

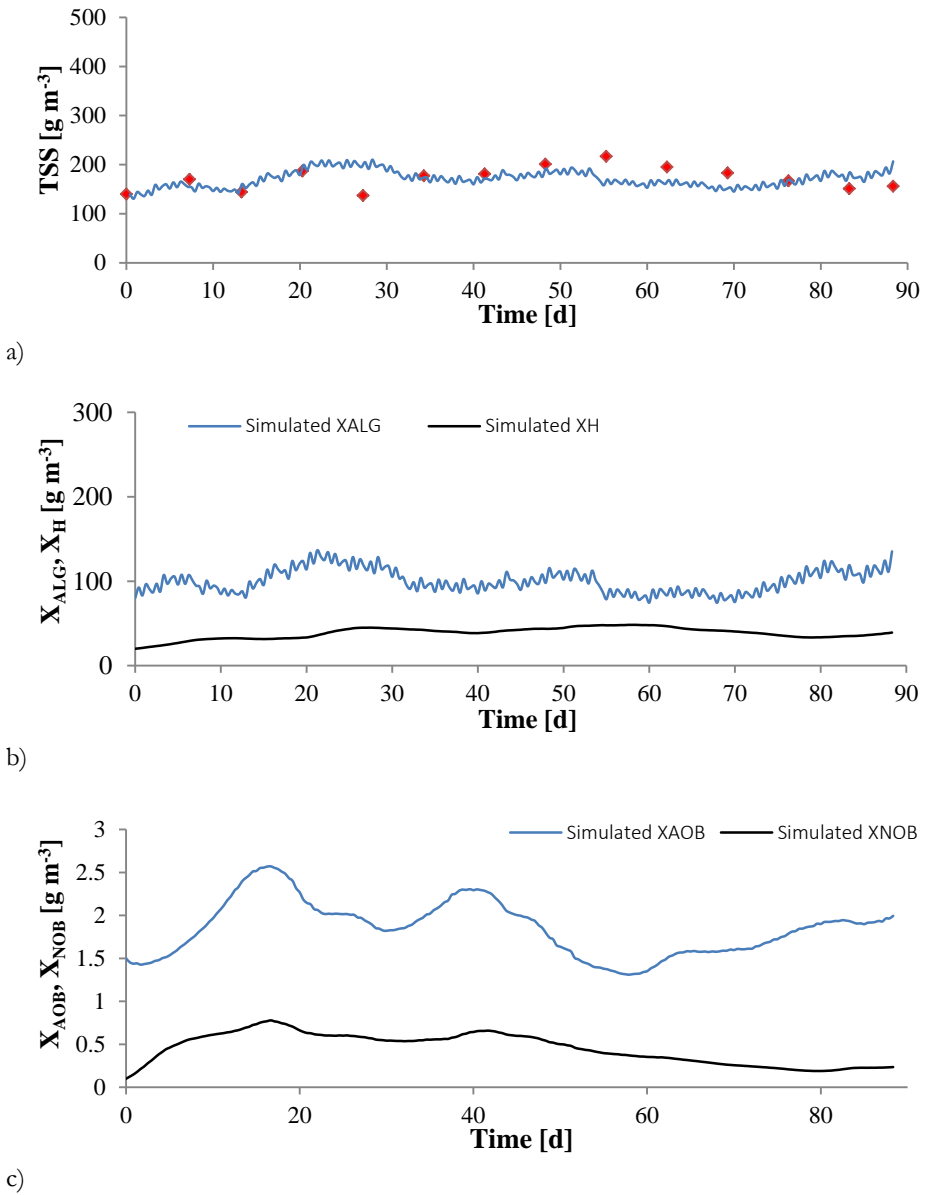


Figure 8.8 Changes in experimental (red diamonds) and simulated (blue and black lines) a) Total suspended solids (TSS), b) microalgae (X_{ALG}) and heterotrophic bacteria (X_H) and c) nitrifying bacteria (X_{AOB} and X_{NOB}) over the Period II (November 10th, 1993 – February 8th, 1994) in HRAP_{8d}. Experimental values measured at 2:00 PM \pm 1 hour.

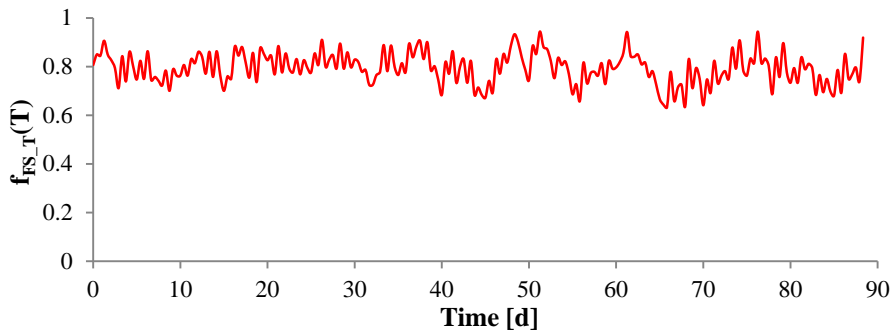


Figure 8.9 Changes in the values of thermic photosynthetic factor ($f_{FS-T}(T)$) over the Period II (November 21th, 1993 – February 8th, 1994) in HRAP_{8d}.

8.3.3 Study case: relative proportion of microalgae and bacteria, biomass production and ammonium removal efficiency of HRAP_{4d} over a year cycle

In this case study thanks to the BIO_ALGAE model the relative proportion of microalgae and bacteria, and the production of microalgae are predicted with the HRAP operating continuously with 4-day HRT. Fig. 8.10 presents simulations of microalgae, heterotrophic bacteria and TSS concentrations. Microalgae concentration changed over the year, being lower in colder months (from November to March) and higher in warmer months (from April to October). Photorespiration effect limited microalgae growth during the warmer months keeping the concentrations around 225 gTSS m^{-3} . Heterotrophic bacteria concentration was quite constant over the year due to the constant influent wastewater features. As can be seen from Fig. 8.11a, microalgae proportion with respect to bacteria increased from April to October up to 60-75% and dropped down to 27-33% from November to March. The trends suggested by these results are in accordance with the experimental studied by Park and Craggs (2011b), where the proportion of microalgae (estimated indirectly) in the microalgae/bacteria biomass of an HRAP operating at 4-days HRT with CO_2 addition in summer was estimated to be around 80%.

Microalgae and TSS production are compared in Fig. 8.11b. Predictions indicate that with a 4-day HRT it is possible to reach up to $20 \text{ gTSS m}^{-2}\text{d}^{-1}$ of

microalgae biomass production in warmer months. Although pH values in summer are very high (> 9 , Fig. 8.12), the model indicates that microalgae are not carbon limited (carbon Monod function = 0.99). Furthermore, dissolved oxygen in excess also lowers growth through photorespiration (average $f_{PR}(S_{O_2}) = 0.62$ in summer) (Fig. 8.12).

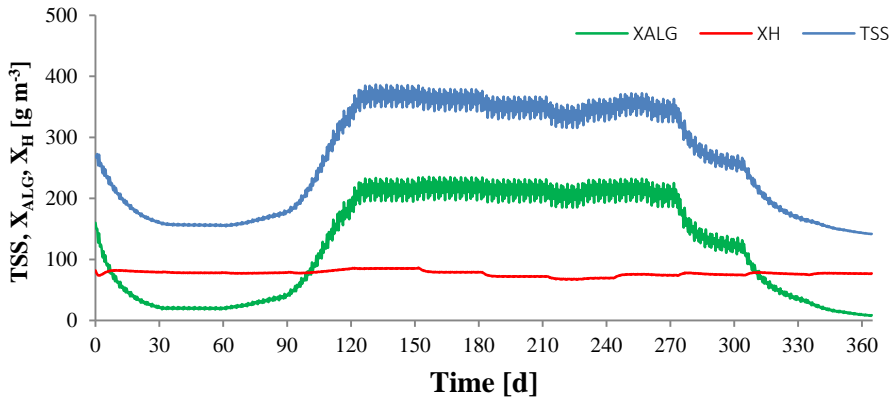
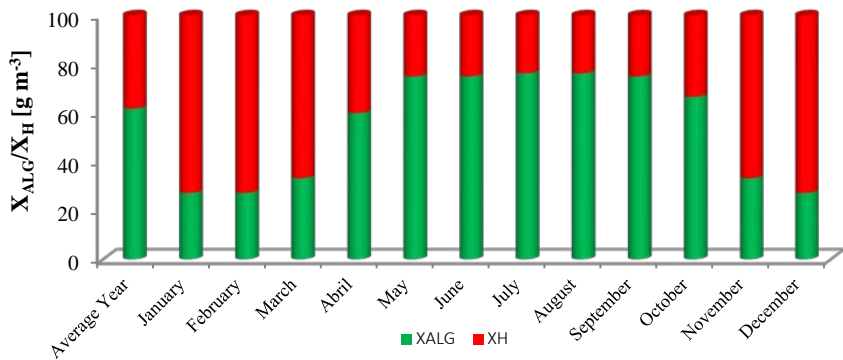
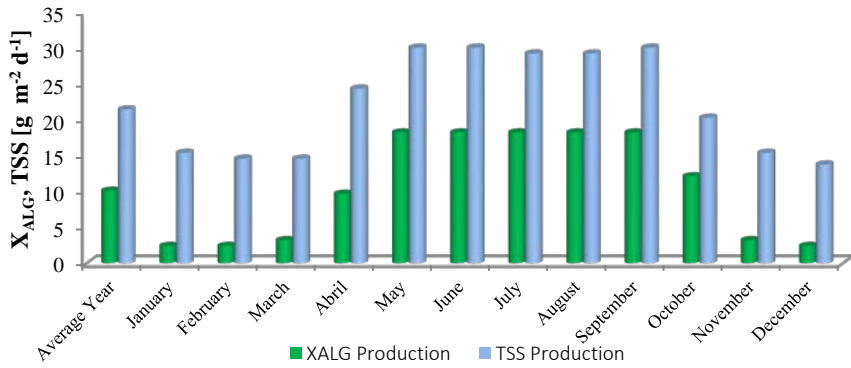


Figure 8.10 Simulated total suspended solids (TSS) (blue line), microalgae (X_{ALG}) (green line) and heterotrophic bacteria (X_H) (red line) concentration over a year (from January to December) in HRAP_{4d}.



a)



b)

Figure 8.11 Average annual and monthly a) microalgae (X_{ALG}) and heterotrophic bacteria (X_H) concentration proportion, and b) microalgae (X_{ALG}) and total suspended solids (TSS) in HRAP_{4d}.

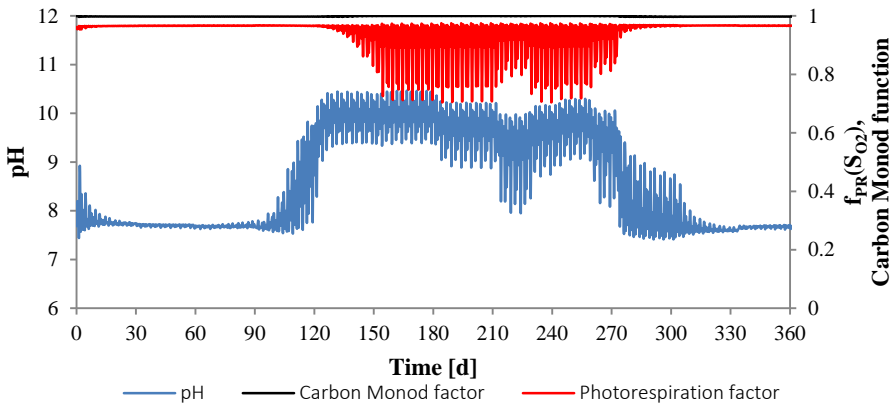


Figure 8.12 Changes of in pH, photorespiration factor $f_{PR}(S_{O_2})$ and carbon Monod function value over a year in HRAP_{4d}.

Ammoniacal nitrogen concentration (sum of ammonium plus ammonia $S_{NH_4} + S_{NH_3}$, from now on “ammonium” was used as indicator of efficiency of HRAP treatment wastewater. As can be seen in Fig. 8.13, ammonium concentration has a clear seasonal pattern. In colder months, approximately an average of 40% of the influent ($49 \text{ gN}_{NH_4} \text{ m}^{-3}$) is removed, while in warmer months average removal rate goes up to 90%.

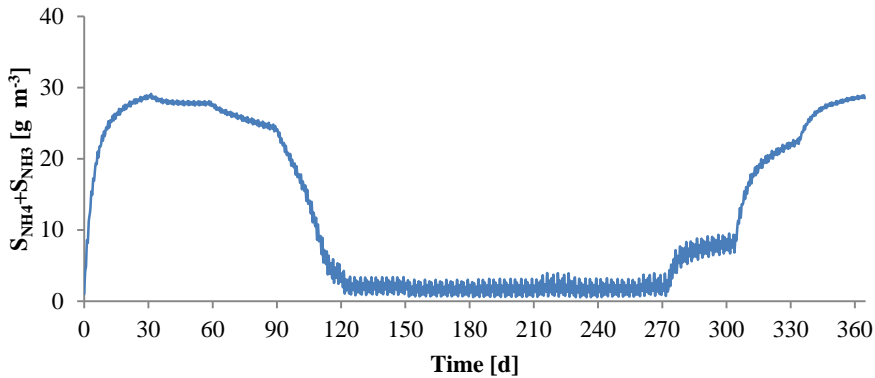


Figure 8.13 Changes of ammonium and ammonia ($S_{\text{NH}_4} + S_{\text{NH}_3}$) concentration and pH value over a year in HRAP_{4d}.

8.3.4 Study case: relative proportion of microalgae and bacteria, biomass production and ammonium removal efficiency of HRAP_{8d} over a year cycle

In this case study the HRAP is continuously operated with 8-day HRT. Fig. 8.14 presents simulations of microalgae, heterotrophic bacteria and TSS concentrations. Microalgae concentrations changed less over the year in comparison to the HRAP_{4d}. Heterotrophic bacteria concentrations were quite constant over the year, and had similar concentrations to HRAP_{4d}. As can be seen from Fig. 8.15a, microalgae proportion in comparison to bacteria from April to October up to 76-78%, and slightly dropped down to 65-68% from November to March. In this case study microalgae were more abundant than heterotrophic bacteria over the entire year. These trends are not in agreement with the experimental studied by Park and Craggs (2011b), where the proportion (microalgae was estimated indirectly) of an HRAP operating at 8-days HRT with CO₂ addition in summer was estimated to be around 55.6%, much lower than in a 4-day HRT. Park and Craggs (2011b) indicated that microalgae growth was limited due to low light availability in the pond. Irradiance was attenuated by the high biomass concentration up to 430 gVSS m⁻³, while in our numerical experiment the biomass concentration in term of TSS is maintained below of 400 gTSS m⁻³.

Microalgae and TSS production are compared in Fig. 8.15b. Predictions indicate that with an 8-day HRT it is possible to reach up to $10.6 \text{ gTSS m}^{-2}\text{d}^{-1}$ of microalgae biomass production in warmer months, which resulted 50% lower than microalgae production predicted in 4-day HRT. In this case study pH is also very high in summer (> 9 , Fig. 8.16), however the model indicates that microalgae are not carbon limited. Furthermore, dissolved oxygen in excess also lowers growth through photorespiration (average $f_{\text{PR}}(S_{\text{O}_2}) = 0.42$ in summer) (Fig. 8.17). Excess of dissolved oxygen concentration was much higher than $\text{HRAP}_{4\text{d}}$. With an 8-day HRT the influent organic matter concentration in the pond is reduced, therefore oxygen demand by heterotrophic bacteria to oxidize organic matter was lower than oxygen produced by microalgae during the photosynthesis due to the high concentration of microalgae (260 gTSS m^{-3} in summer). As can be seen in Fig. 8.18, the model prediction indicated that average ammonium removal rate goes up to 98% of the influent ($49 \text{ gN-NH}_4 \text{ m}^{-3}$) over the whole year.

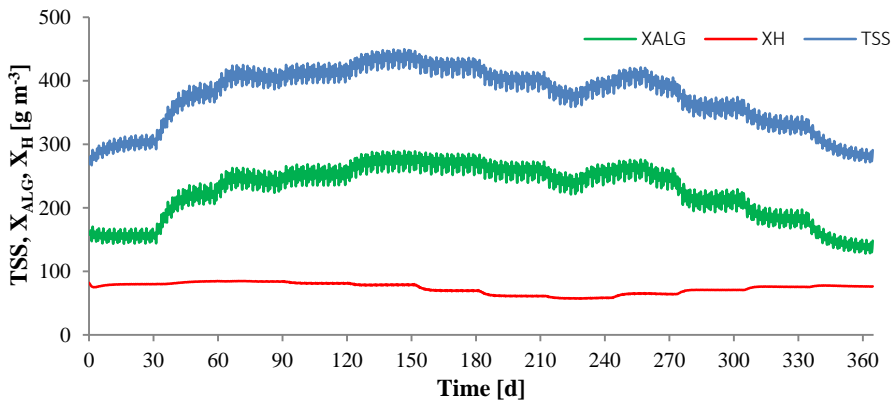
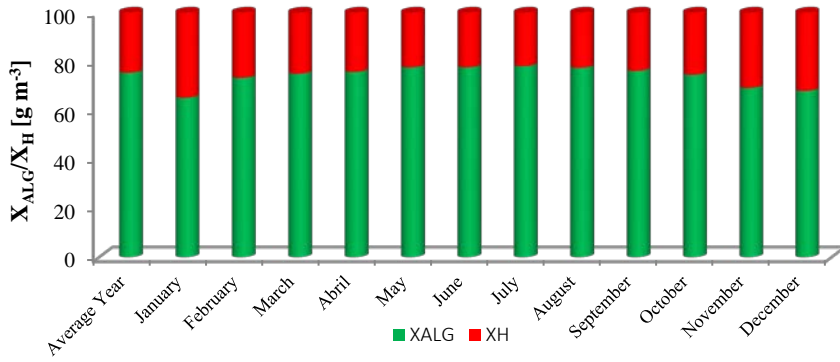
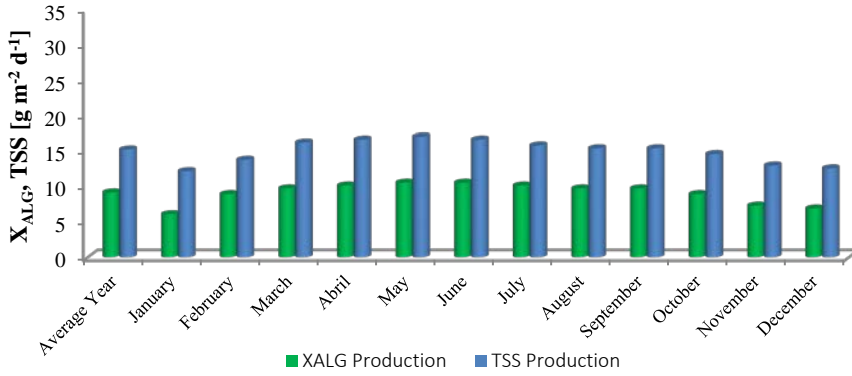


Figure 8.14 Simulated total suspended solids (TSS) (blue line), microalgae (X_{ALG}) (green line) and heterotrophic bacteria (X_{H}) (red line) concentration over a year (from January to December) in $\text{HRAP}_{8\text{d}}$.



a)



b)

Figure 8.15 Average annual and monthly a) microalgae (X_{ALG}) and heterotrophic bacteria (X_H) concentration proportion, and b) microalgae (X_{ALG}) and total suspended solids (TSS) in HRAP_{8d}.

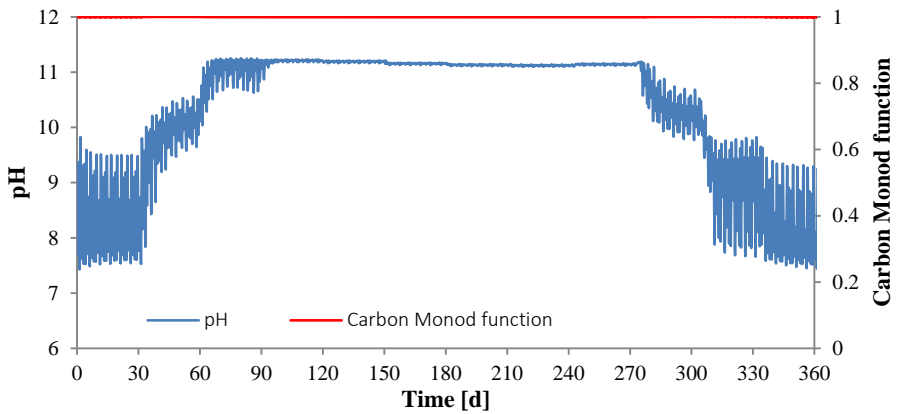


Figure 8.16 Changes of pH value and carbon Monod function over a year in HRAP_{8d}.

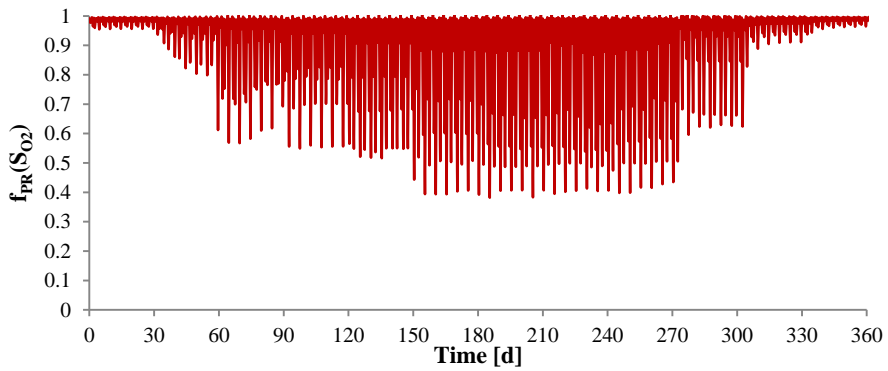


Figure 8.17 Changes in the values of photorespiration factor ($f_{PR}(S_{O_2})$) over a year in HRAP_{8d}.

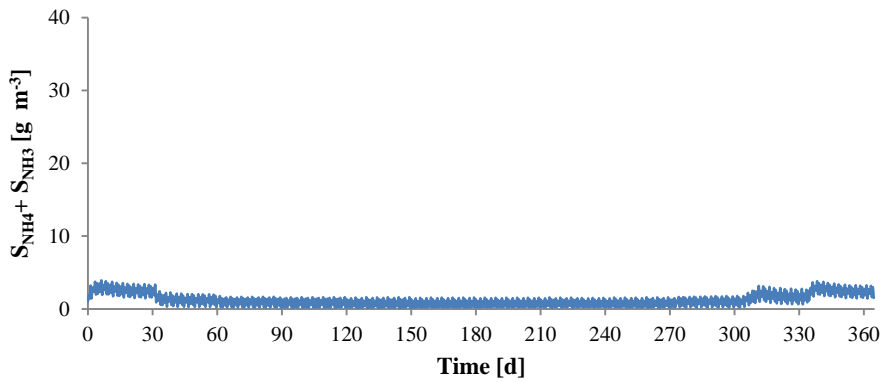


Figure 8.18 Changes of ammonium and ammonia ($S_{NH_4}+S_{NH_3}$) over a year in HRAP_{8d}.

8.3.5 Study case: optimization of microalgae production and ammonium removal efficiency over a year cycle

In this case study the HRAP is operate with changing HRT. Higher HRT (8-day) was used in the colder months (from October to March) and lower HRT (4-day) in the warmer months (from April to September) (HRAP_{8-4-8d}). This strategy was selected from results obtained in the previous case studies.

Fig. 8.19 presents simulations of microalgae, heterotrophic bacteria and TSS concentrations. Microalgae concentrations and microalgae/bacteria proportion (not shown, but can be deduced) changed slightly over the year in comparison to the other two case studies. Microalgae biomass production was also optimized (Fig. 8.20). With HRAP_{8-4-8d} the production increased of 30% and 35% respects to HRAP_{4d} and HRAP_{8d}, respectively.

As can be seen in Fig. 8.21 the model prediction indicated that average removal rate of ammonium goes up to 92% ($49 \text{ gN_NH}_4 \text{ m}^{-3}$) over the whole year.

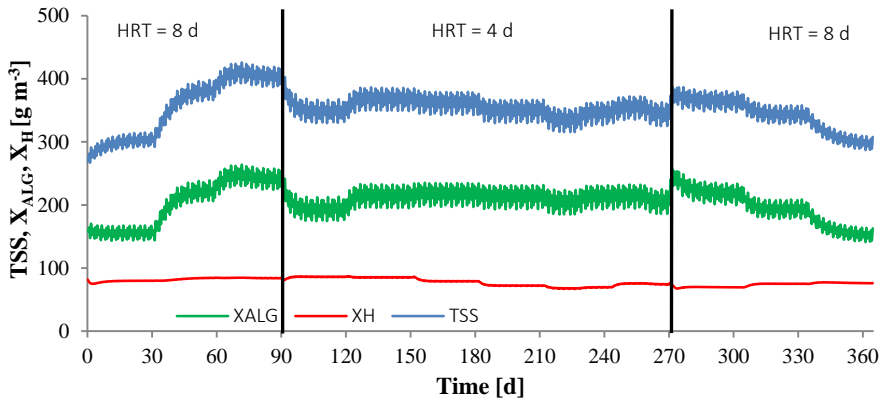


Figure 8.19 Simulated total suspended solid (TSS) (blue line), microalgae (X_{ALG}) (green line) and heterotrophic bacteria (X_H) (red line) concentration over a year (from January to December) in HRAP_{8-4-8d}. Vertical black lines indicate HRT change.

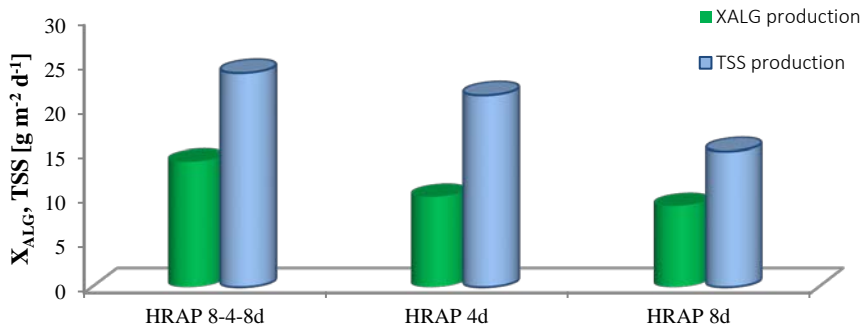


Figure 8.20 Comparison of average annual microalgae (X_{ALG}) and Total Suspended Solids (TSS) production over a year as function of different HRT operating strategies.

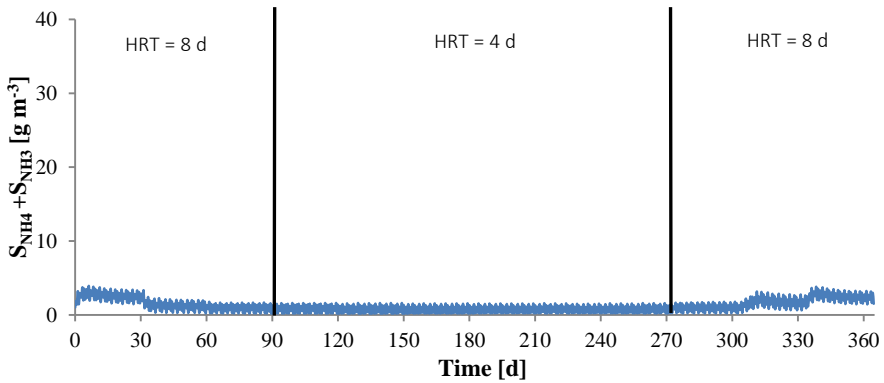


Figure 8.21 Changes of ammonium and ammonia ($S_{NH_4} + S_{NH_3}$) concentration over a year in HRAP_{8.4.8d}. Vertical black lines indicate the change of HRT.

8.4 Conclusion

In this work the BIO_ALGAE model was validated in a long-term period in a pilot HRAP operating at different HRT (4 and 8 days) corresponding at summer and winter season (respectively). The model matched quite accurately HRAP dynamics using the calibrated values of 6 parameters obtained in a previous work by the authors.

BIO_ALGAE has demonstrated by means of practical study cases to be a useful tool to understand microalgae and bacteria interactions in wastewater

treatment, and in particular to study the effect of different HRT operating strategies and variations of environmental conditions over a year cycle on the relative proportion of microalgae and bacteria and biomass production. Moreover thanks to the model was possible to optimize biomass production.

8.5 Appendix

Table A8.1 Mathematical description of the processes of the model (processes rates).

Processes	Process rate [M L ⁻³ T ⁻¹]
Microalgae (X_{ALG}) processes	
1a. Growth of X _{ALG} on S _{NH4}	$\rho_{1a} = \mu_{ALG} \cdot f_{T,FS}(T) \cdot \eta_{PS}(I, S_{O_2}) \cdot \frac{S_{CO_2} + S_{HCO_3}}{K_{C,ALG} + S_{CO_2} + S_{HCO_3} + \frac{S_{CO_2}^2}{I_{CO_2,ALG}}} \cdot \frac{S_{NH_3} + S_{NH_4}}{K_{N,ALG} + S_{NH_3} + S_{NH_4}} \cdot \frac{S_{PO_4}}{K_{P,ALG} + S_{PO_4}} \cdot X_{ALG}$
1b. Growth of X _{ALG} on S _{NO3}	$\rho_{1b} = \mu_{ALG} \cdot f_{T,FS}(T) \cdot \eta_{PS}(I, S_{O_2}) \cdot \frac{S_{CO_2} + S_{HCO_3}}{K_{C,ALG} + S_{CO_2} + S_{HCO_3} + \frac{S_{CO_2}^2}{I_{CO_2,ALG}}} \cdot \frac{S_{NO_3}}{K_{N,ALG} + S_{NO_3}} \cdot \frac{K_{N,ALG}}{K_{N,ALG} + S_{NH_3} + S_{NH_4}} \cdot \frac{S_{PO_4}}{K_{P,ALG} + S_{PO_4}} \cdot X_{ALG}$
2. Endogenous respiration of X _{ALG}	$\rho_2 = k_{resp,ALG} \cdot f_{T,FS}(T) \cdot \frac{S_{O_2}}{K_{O_2,ALG} + S_{O_2}} \cdot X_{ALG}$
3. Decay of X _{ALG}	$\rho_3 = k_{death,ALG} \cdot f_{T,FS}(T) \cdot X_{ALG}$
Heterotrophic bacteria (X_H) (aerobic and denitrifying activity)	
4a. Aerobic growth of X _H on S _{NH4}	$\rho_{4a} = \mu_H \cdot f_{T,MB}(T) \cdot \frac{S_s}{K_{S,H} + S_s} \cdot \frac{S_{O_2}}{K_{O_2,H} + S_{O_2}} \cdot \frac{S_{NH_4} + S_{NH_3}}{K_{N,H} + S_{NH_4} + S_{NH_3}} \cdot X_H$
4b. Aerobic growth of X _H on S _{NO3}	$\rho_{4b} = \mu_H \cdot f_{T,MB}(T) \cdot \frac{S_s}{K_{S,H} + S_s} \cdot \frac{S_{O_2}}{K_{O_2,H} + S_{O_2}} \cdot \frac{S_{NO_3}}{K_{N,H} + S_{NO_3}} \cdot X_H$
5. Anoxic growth of X _H on S _{NO2} (denitrification on S _{NO2})	$\rho_5 = \mu_H \cdot \eta_H \cdot f_{T,MB}(T) \cdot \frac{S_s}{K_{S,H} + S_s} \cdot \frac{K_{O_2,H}}{K_{O_2,H} + S_{O_2}} \cdot \frac{S_{NO_2}}{K_{NO_2,H,anox} + S_{NO_2}} \cdot X_H$

6. Anoxic growth of X_H on S_{NO_3} (denitrification on S_{NO_3})	$\rho_6 = \mu_H \cdot \eta_H \cdot f_{T,MB}(T) \cdot \frac{S_S}{K_{S,H} + S_S} \cdot \frac{K_{O_2,H}}{K_{O_2,H} + S_{O_2}} \cdot \frac{S_{NO_3}}{K_{NO_3,H,anox} + S_{NO_3}} \cdot X_H$
7. Aerobic endogenous respiration of X_H	$\rho_7 = k_{resp,H} \cdot f_{T,MB}(T) \cdot \frac{S_{O_2}}{K_{O_2,H} + S_{O_2}} \cdot X_H$
8. Anoxic endogenous respiration of X_H	$\rho_8 = k_{resp,H} \cdot \eta_H \cdot f_{T,MB}(T) \cdot \frac{K_{O_2,H}}{K_{O_2,H} + S_{O_2}} \cdot \frac{S_{NO_3} + S_{NO_2}}{K_{NO_3,H,anox} + S_{NO_2} + S_{NO_3}} \cdot X_H$
9. Decay of X_H	$\rho_9 = k_{death,H} \cdot f_{T,MB}(T) \cdot X_H$
Autotrophic bacteria (nitrifying activity)	
10. Growth of X_{AOB}	$\rho_{10} = \mu_{AOB} \cdot f_{T,MB}(T) \cdot \frac{S_{O_2}}{K_{O_2,AOB} + S_{O_2}} \cdot \frac{S_{NH_3} + S_{NH_4}}{K_{NH_4,AOB} + S_{NH_4} + S_{NH_3}} \cdot \frac{S_{CO_2} + S_{HCO_3}}{K_{C,AOB} + S_{CO_2} + S_{HCO_3}} \cdot X_{AOB}$
11. Growth of X_{NOB}	$\rho_{11} = \mu_{NOB} \cdot f_{T,MB}(T) \cdot \frac{S_{O_2}}{K_{O_2,NOB} + S_{O_2}} \cdot \frac{K_{I,NH_4}}{K_{I,NH_4} + S_{NH_4} + S_{NH_3}} \cdot \frac{S_{NO_2}}{K_{NO_2,NOB} + S_{NO_2}} \cdot \frac{S_{CO_2} + S_{HCO_3}}{K_{C,NOB} + S_{CO_2} + S_{HCO_3}} \cdot X_{NOB}$
12. Endogenous respiration of X_{AOB}	$\rho_{10} = k_{resp,AOB} \cdot f_{T,MB}(T) \cdot \frac{S_{O_2}}{K_{O_2,AOB} + S_{O_2}} \cdot X_{AOB}$
13. Endogenous respiration of X_{NOB}	$\rho_{13} = k_{resp,NOB} \cdot f_{T,MB}(T) \cdot \frac{S_{O_2}}{K_{O_2,NOB} + S_{O_2}} \cdot X_{NOB}$
14a. Decay of X_{AOB}	$\rho_{14a} = k_{death,AOB} \cdot f_{T,MB}(T) \cdot X_{AOB}$
14b. Decay of X_{NOB}	$\rho_{14b} = k_{death,NOB} \cdot f_{T,MB}(T) \cdot X_{NOB}$

Hydrolysis, Chemical equilibrium and Transfer of gases	
15. Hydrolysis	$\rho_{15} = k_{\text{HYD}} \cdot \frac{X_S/X_H}{Y_{\text{HYD}} + (X_S/X_H)} \cdot X_H$
16. Chemical equilibrium $\text{CO}_2 \leftrightarrow \text{HCO}_3^-$	$\rho_{16} = k_{\text{eq},1} \cdot (S_{\text{CO}_2} - S_H S_{\text{HCO}_3} / K_{\text{eq},1})$
17. Chemical equilibrium $\text{HCO}_3^- \leftrightarrow \text{CO}_3^{2-}$	$\rho_{17} = k_{\text{eq},2} \cdot (S_{\text{HCO}_3} - S_H S_{\text{CO}_3} / K_{\text{eq},2})$
18. Chemical equilibrium $\text{NH}_4^+ \leftrightarrow \text{NH}_3$	$\rho_{18} = k_{\text{eq},3} \cdot (S_{\text{NH}_4} - S_H S_{\text{NH}_3} / K_{\text{eq},3})$
19. Chemical equilibrium $\text{H}^+ \leftrightarrow \text{OH}^-$	$\rho_{19} = k_{\text{eq},w} \cdot (1 - S_H S_{\text{OH}} / K_{\text{eq},w})$
20. SO_2 transfer to the atmosphere	$\rho_{20} = k_{a,\text{O}_2} \cdot (S_{\text{O}_2}^{\text{WAT}} - S_{\text{O}_2})$
21. SCO_2 transfer to the atmosphere	$\rho_{21} = k_{a,\text{CO}_2} \cdot (S_{\text{CO}_2}^{\text{WAT}} - S_{\text{CO}_2})$
22. SNH_3 transfer to the atmosphere	$\rho_{22} = k_{a,\text{NH}_3} \cdot (-S_{\text{NH}_3})$

Table A8.2 Matrix of stoichiometric parameters that relates processes and components through stoichiometric coefficients A8.4

	S _{NH4}	S _{NH3}	S _{NO3}	S _{NO2}	S _{CO2}	S _{HCO3}	S _{CO3}	S _{PO4}	S _{O2}	S _H	S _{OH}	S _S	S _I	X _{ALG}	X _S	X _I	X _H	X _{NOB}	X _{NOB}
ρ _{1a}	V _{1,1a}				V _{5,1a}			V _{8,1a}	V _{9,1a}	V _{10,1a}				V _{14,1a}					
ρ _{1b}			V _{3,1b}		V _{5,1b}			V _{8,1b}	V _{9,1b}	V _{10,1b}				V _{14,1b}					
ρ ₂	V _{1,2}				V _{5,2}			V _{8,2}	V _{9,2}	V _{10,2}				V _{14,2}		V _{16,2}			
ρ ₃	V _{1,3}				V _{5,3}			V _{8,3}		V _{10,3}				V _{14,3}	V _{15,3}	V _{16,3}			
ρ _{4a}	V _{1,4a}				V _{5,4a}			V _{8,4a}	V _{9,4a}	V _{10,4a}		V _{12,4a}					V _{17,4a}		
ρ _{4b}			V _{3,4b}		V _{5,4b}			V _{8,4b}	V _{9,4b}	V _{10,4b}		V _{12,4b}					V _{17,4b}		
ρ ₅				V _{4,5}	V _{5,5}			V _{8,5}		V _{10,5}		V _{12,5}					V _{17,5}		
ρ ₆			V _{3,6}		V _{5,6}			V _{8,6}		V _{10,6}		V _{12,6}					V _{17,6}		
ρ ₇	V _{1,7}				V _{5,7}			V _{8,7}	V _{9,7}	V _{10,7}						V _{16,7}	V _{17,7}		
ρ ₈	V _{1,8}		V _{3,8}	V _{4,8}	V _{5,8}			V _{8,8}		V _{10,8}						V _{16,8}	V _{17,8}		
ρ ₉															V _{15,9}	V _{16,9}	V _{17,9}		
ρ ₁₀	V _{1,10}			V _{4,10}	V _{5,10}			V _{8,10}	V _{9,10}	V _{10,10}								V _{18,10}	
ρ ₁₁			V _{3,11}	V _{4,11}	V _{5,11}			V _{8,11}	V _{9,11}	V _{10,11}									V _{19,11}
ρ ₁₂	V _{1,12}				V _{5,12}			V _{8,12}	V _{9,12}	V _{10,12}						V _{16,12}		V _{18,12}	
ρ ₁₃	V _{1,13}				V _{5,13}			V _{8,13}	V _{9,13}	V _{10,13}						V _{16,13}			V _{19,13}
ρ _{14a}															V _{15,14a}	V _{16,14a}		V _{18,14a}	
ρ _{14b}															V _{15,14b}	V _{16,14b}			V _{19,14b}
ρ ₁₅	V _{1,15}				V _{5,15}			V _{8,15}		V _{10,15}		V _{12,15}	V _{13,15}		V _{15,15}				
ρ ₁₆					V _{5,16}	V _{6,16}				V _{10,16}									
ρ ₁₇						V _{6,17}	V _{7,17}			V _{10,17}									
ρ ₁₈	V _{1,18}	V _{2,18}								V _{10,18}									
ρ ₁₉										V _{10,19}	V _{11,19}								
ρ ₂₀									V _{9,20}										
ρ ₂₁					V _{5,21}														
ρ ₂₂		V _{2,22}																	

Table A8.3 Values of biokinetic, chemical and physic parameters.

Parameters	Description	Value	Unit	Source
Microalgae (X_{ALG})				
μ_{ALG}	Maximum growth rate of X_{ALG}	1.5	d^{-1}	Calibrated
$k_{resp,ALG}$	Endogenous respiration constant	0.1	d^{-1}	Reichert et al., 2001
$k_{death,ALG}$	Decay constant	0.1	d^{-1}	Reichert et al., 2001
$K_{C,ALG}$	Saturation constant of X_{ALG} on S_{CO_2}	4E-3	$gC\ m^{-3}$	Novak and Brune, 1985
$I_{CO_2,ALG}$	Inhibition constant of X_{ALG} on S_{CO_2}	120	$gC\ m^{-3}$	Silva and Pirt, 1984
$K_{N,ALG}$	Saturation constant of X_{ALG} on nitrogen sp.	0.1	$gN\ m^{-3}$	Reichert et al., 2001
$K_{O_2,ALG}$	Saturation constant of X_{ALG} on S_{O_2}	0.2	$gO_2\ m^{-3}$	Reichert et al., 2001
$K_{P,ALG}$	Saturation constant of X_{ALG} for S_{HPO_4}	0.02	$gP\ m^{-3}$	Reichert et al., 2001
Heterotrophic bacteria (X_H)				
μ_H	Maximum growth rate of X_H	1.3	d^{-1}	Calibrated
η_H	Anoxic reduction factor for X_H	0.6	–	Gujer et al., 1999
$k_{resp,H}$	Endogenous respiration rate of X_H	0.3	d^{-1}	Reichert et al., 2001
$K_{O_2,H}$	Saturation constant of X_H for S_{O_2}	0.2	$gO_2\ m^{-3}$	Reichert et al., 2001
$K_{N,H}$	Saturation constant of X_H for S_N	0.2	$gN\ m^{-3}$	Reichert et al., 2001
$K_{S,H}$	Saturation constant of X_H for S_S	20	$gCOD\ m^{-3}$	Henze et al., 2000
$K_{NO_3,H,anox}$	Saturation constant of X_H for S_{NO_3}	0.5	$gN\ m^{-3}$	Reichert et al., 2001
$K_{NO_2,H,anox}$	Saturation constant of X_H for S_{NO_2}	0.2	$gN\ m^{-3}$	Reichert et al., 2001
$k_{death,H}$	Decay constant of X_H	0.3	d^{-1}	Calibrated
Autotrophic bacteria: ammonia oxidizing bacteria (X_{AOB}) and nitrite oxidizing bacteria (X_{NOB})				
μ_{AOB}	Maximum growth rate of X_{AOB}	0.63	d^{-1}	Gujer et al., 1999
μ_{NOB}	Maximum growth rate of X_{NOB}	1.1	d^{-1}	Gujer et al., 1999
$K_{O_2,AOB}/K_{O_2,NOB}$	Saturation constant of X_{AOB} / X_{NOB} for S_{O_2}	0.5	$gO_2\ m^{-3}$	Reichert et al., 2001
$K_{NH_4,AOB}$	Saturation constant of X_{AOB} on S_{NH_4}	0.5	$gN\ m^{-3}$	Reichert et al., 2001
K_{I,NH_4}	Ammonia inhibition constant of X_{NOB}	5.0	$gN\ m^{-3}$	Henze et al., 2000
$K_{NO_2,NOB}$	Saturation constant of X_{NOB} for S_{NO_2}	0.5	$gN\ m^{-3}$	Henze et al., 2000
$K_{C,AOB}/K_{C,NOB}$	Saturation constant of X_{AOB} / X_{NOB} for S_{HCO_3}	0.5	$gC\ m^{-3}$	Henze et al., 2000
$k_{resp,AOB}/k_{resp,NOB}$	Endogenous respiration rate of X_{AOB} / X_{NOB}	0.05	d^{-1}	Reichert et al., 2001
$k_{death,AOB}/k_{death,NOB}$	Decay constant of X_{AOB} and X_{NOB}	0.2	d^{-1}	Henze et al., 2000
Hydrolysis				
k_{HYD}	Hydrolysis rate constant	3.0	d^{-1}	Reichert et al., 2001
Photorespiration factor of microalgae				
K_{PR}	Inhibition constant of photorespiration	0.03	–	Solimeno et al., 2017b
τ	Excess of S_{O_2} coefficient	3.5	–	Fernández et al., 2014

$c_{O_2}^{SAT}$	S_{O_2} air saturation	9.07	$gO_2 m^{-3}$	Fernández et al., 2014
Thermal factor of microalgae and bacteria				
T_{OPT}	Optimum temperature for X_{ALG} growth	25	°C	Dauta et al., 1990
s	Normalized parameter	30	–	Dauta et al., 1990
θ	Temperature coefficient for X_H growth	1.07		Sperling, 2005
Light factor of microalgae				
α	Activation rate	1.9E-3	$(\mu E m^{-2})^{-1}$	Wu and Merchuk, 2001
β	Inhibition rate	5.7E-7	$(\mu E m^{-2})^{-1}$	Wu and Merchuk, 2001
γ	Production rate	0.14	s^{-1}	Wu and Merchuk, 2001
δ	Recovery rate	4.7E-4	s^{-1}	Wu and Merchuk, 2001
K_I	Biomass extinction coefficient	0.07	$m^2 g^{-1}$	Molina et al., 1994
Parameters		Equations		
Chemical equilibrium $CO_2 \leftrightarrow HCO_3^-$.		$K_{eq,1} = 10^{17.843 - \frac{3404.71}{273.15+T} - 0.032786(273.15+T)}$		
Chemical equilibrium $HCO_3^- \leftrightarrow CO_3^{2-}$		$K_{eq,2} = 10^{9.494 - \frac{2902.39}{273.15+T} - 0.02379(273.15+T)}$		
Chemical equilibrium $NH_4^+ \leftrightarrow NH_3$		$K_{eq,3} = 10^{2.891 - \frac{2727}{(273.15+T)}}$		
Chemical equilibrium $H^+ \leftrightarrow OH^-$		$K_{eq,w} = 10^{-\frac{4470.99}{273.15+T} + 12.0875 - 0.01706(273.15+T)}$		
Kinetics parameters				
$k_{eq,1}$	Dissociation constant of $CO_2 \leftrightarrow HCO_3^-$.	10000	d^{-1}	Reichert et al., 2001
$k_{eq,2}$	Dissociation constant of $HCO_3^- \leftrightarrow CO_3^{2-}$	1000	d^{-1}	Reichert et al., 2001
$k_{eq,3}$	Dissociation constant of $NH_4^+ \leftrightarrow NH_3$	1000	d^{-1}	Reichert et al., 2001
$k_{eq,w}$	Dissociation constant of $H^+ \leftrightarrow OH^-$	1000	$g m^{-1} d^{-1}$	Reichert et al., 2001
Transfer of gases to the atmosphere				
K_{a,O_2}	Mass transfer coefficient for S_{O_2}	0.16	h^{-1}	Calibrated
K_{a,CO_2}	Mass transfer coefficient for S_{CO_2}	0.14	h^{-1}	Calibrated
K_{a,NH_3}	Mass transfer coefficient for S_{NH_3}	0.14	h^{-1}	Calibrated

Table A8.4 Mathematical expressions of the stoichiometric coefficients of each process.

Stoichiometric coefficients	Unit
Growth of X_{ALG} on S_{NH4}	
$v_{1,1a} = -i_{N,ALG}$	gN gCOD ⁻¹
$v_{5,1a} = -i_{C,ALG}$	gC gCOD ⁻¹
$v_{8,1a} = -i_{P,ALG}$	gP gCOD ⁻¹
$v_{9,1a} = 8i_{C,ALG}/3 + 8i_{H,ALG} - i_{O,ALG} - 12i_{N,ALG}/7 + 40i_{P,ALG}/31$	gO ₂ gCOD ⁻¹
$v_{10,1a} = i_{N,ALG}/14 - 2i_{P,ALG}/31$	gH gCOD ⁻¹
$v_{14,1a} = 1$	gCOD gCOD ⁻¹
Growth of X_{ALG} on S_{NO3}	
$v_{3,1b} = -i_{N,ALG}$	gN gCOD ⁻¹
$v_{5,1b} = -i_{C,ALG}$	gC gCOD ⁻¹
$v_{8,1b} = -i_{P,ALG}$	gP gCOD ⁻¹
$v_{9,1b} = 8i_{C,ALG}/3 + 8i_{H,ALG} - i_{O,ALG} + 20i_{N,ALG}/7 + 40i_{P,ALG}/31$	gO ₂ gCOD ⁻¹
$v_{10,1b} = -i_{N,ALG}/14 - 2i_{P,ALG}/31$	gH gCOD ⁻¹
$v_{14,1b} = 1$	gCOD gCOD ⁻¹
Endogenous respiration of X_{ALG}	
$v_{1,2} = i_{N,ALG} - f_{ALG} i_{N,XI}$	gN gCOD ⁻¹
$v_{5,2} = i_{C,ALG} - f_{ALG} i_{C,XI}$	gC gCOD ⁻¹
$v_{8,2} = i_{P,ALG} - f_{ALG} i_{P,XI}$	gP gCOD ⁻¹
$v_{9,2} = (i_{O,ALG} - f_{ALG} i_{O,XI}) - 8(i_{H,ALG} - f_{ALG} i_{H,XI}) - 8/3(i_{C,ALG} - f_{ALG} i_{C,XI}) + 12/7(i_{N,ALG} - f_{ALG} i_{N,XI}) - 40/31(i_{P,ALG} - f_{ALG} i_{P,XI})$	gO ₂ gCOD ⁻¹
$v_{10,2} = -1/14(i_{N,ALG} - f_{ALG} i_{N,XI}) + 2/31(i_{P,ALG} - f_{ALG} i_{P,XI})$	gH gCOD ⁻¹
$v_{14,2} = -1$	gCOD gCOD ⁻¹
$v_{16,2} = f_{ALG}$	gCOD gCOD ⁻¹
Decay of X_{ALG}	
$v_{1,3} = i_{N,ALG} - (1 - f_{ALG})Y_{ALG} i_{N,XS} - f_{ALG} Y_{ALG} i_{N,ALG}$	gN gCOD ⁻¹
$v_{5,3} = i_{C,ALG} - (1 - f_{ALG})Y_{ALG} i_{C,XS} - f_{ALG} Y_{ALG} i_{C,ALG}$	gC gCOD ⁻¹
$v_{8,3} = i_{P,ALG} - (1 - f_{ALG})Y_{ALG} i_{P,XS} - f_{ALG} Y_{ALG} i_{P,ALG}$	gP gCOD ⁻¹
$v_{10,3} = -1/14(i_{N,ALG} (1 - f_{ALG})Y_{ALG} i_{N,XS} - f_{ALG} Y_{ALG} i_{N,XI}) + 2/31(i_{P,ALG} (1 - f_{ALG})Y_{ALG} i_{P,XS} - f_{ALG} Y_{ALG} i_{P,XI})$	gH gCOD ⁻¹
$v_{14,3} = -1$	gCOD gCOD ⁻¹
$v_{15,3} = (1 - f_{ALG})$	gCOD gCOD ⁻¹
$v_{16,3} = f_{ALG} Y_{ALG}$	gCOD gCOD ⁻¹
Aerobic growth of X_H on S_{NH4}	
$v_{1,4a} = i_{N,SS}/Y_H - i_{N,BM}$	gN gCOD ⁻¹
$v_{5,4a} = i_{C,SS}/Y_H - i_{C,BM}$	gC gCOD ⁻¹

$v_{8,4a} = i_{P,SS}/Y_H - i_{P,BM}$	gP gCOD ⁻¹
$v_{9,4a} = -(1 - Y_H)/Y_H$	gO ₂ gCOD ⁻¹
$v_{10,4a} = -1/14 (i_{N,SS}/Y_H - i_{N,BM}) + 2/31 (i_{P,SS}/Y_H - i_{P,BM})$	gH gCOD ⁻¹
$v_{12,4a} = -1/Y_H$	gCOD gCOD ⁻¹
$v_{17,4a} = 1$	gCOD gCOD ⁻¹
Aerobic growth of X_H on S_{NO3}	
$v_{3,4b} = i_{N,SS}/Y_H - i_{N,BM}$	gN gCOD ⁻¹
$v_{5,4b} = i_{C,SS}/Y_H - i_{C,BM}$	gC gCOD ⁻¹
$v_{8,4b} = (i_{P,SS}/Y_H - i_{P,BM})$	gP gCOD ⁻¹
$v_{9,4b} = -(1 - Y_H)/Y_H$	gO ₂ gCOD ⁻¹
$v_{10,4b} = -1/14 (i_{N,SS}/Y_H - i_{N,BM}) + 2/31 (i_{P,SS}/Y_H - i_{P,BM})$	gH gCOD ⁻¹
$v_{12,4b} = -1/Y_H$	gCOD gCOD ⁻¹
$v_{17,4b} = 1$	gCOD gCOD ⁻¹
Anoxic growth of X_H on S_{NO2}	
$v_{4,5} = -(1 - Y_{H,NO2})/(1.71Y_{H,NO2})$	gN gCOD ⁻¹
$v_{5,5} = (i_{C,SS}/Y_{H,NO2} - i_{C,BM})$	gC gCOD ⁻¹
$v_{8,5} = (i_{P,SS}/Y_{H,NO2} - i_{P,BM})$	gP gCOD ⁻¹
$v_{10,5} = 1/24 (i_{O,SS}/Y_{H,NO2} - i_{O,BM}) - 1/3 (i_{H,SS}/Y_{H,NO2} - i_{H,BM}) - 1/9 (i_{C,SS}/Y_{H,NO2} - i_{C,BM}) - 1/93 (i_{P,SS}/Y_{H,NO2} - i_{P,BM})$	gH gCOD ⁻¹
$v_{12,5} = -1/Y_{H,NO2}$	gCOD gCOD ⁻¹
$v_{17,5} = 1$	gCOD gCOD ⁻¹
Anoxic growth of X_H on S_{NO3}	
$v_{3,6} = -(1 - Y_{H,NO3})/(1.14Y_{H,NO3})$	gN gCOD ⁻¹
$v_{4,6} = (1 - Y_{H,NO3})/(1.14Y_{H,NO3})$	gN gCOD ⁻¹
$v_{5,6} = (i_{C,SS}/Y_{H,NO3} - i_{C,BM})$	gC gCOD ⁻¹
$v_{8,6} = (i_{P,SS}/Y_{H,NO3} - i_{P,BM})$	gP gCOD ⁻¹
$v_{10,6} = 1/14 (i_{N,SS}/Y_{H,NO3} - i_{N,BM}) + 2/31 (i_{P,SS}/Y_{H,NO3} - i_{P,BM})$	gH gCOD ⁻¹
$v_{12,6} = -1/Y_{H,NO3}$	gCOD gCOD ⁻¹
$v_{17,6} = 1$	gCOD gCOD ⁻¹
Aerobic endogenous respiration of X_H	
$v_{1,7} = i_{N,BM} - f_{XI} i_{N,XI}$	gN gCOD ⁻¹
$v_{5,7} = i_{C,BM} - f_{XI} i_{C,XI}$	gC gCOD ⁻¹
$v_{8,7} = i_{P,BM} - f_{XI} i_{P,XI}$	gP gCOD ⁻¹
$v_{9,7} = -(1 - f_{XI})$	gO ₂ gCOD ⁻¹
$v_{10,7} = -1/14 (i_{N,BM} - f_{XI} i_{N,XI}) + 2/31 (i_{P,BM} - f_{XI} i_{P,XI})$	gH gCOD ⁻¹
$v_{16,7} = f_{XI}$	gCOD gCOD ⁻¹
$v_{17,7} = -1$	gCOD gCOD ⁻¹

Anoxic endogenous respiration of X_H	
$v_{1,8} = i_{N,BM} - f_{XI} i_{N,XI}$	gN gCOD ⁻¹
$v_{3,8} = (f_{XI} - 1)/1.14$	gN gCOD ⁻¹
$v_{4,8} = (1 - f_{XI})/1.14$	gN gCOD ⁻¹
$v_{5,8} = i_{C,BM} - f_{XI} i_{C,XI}$	gC gCOD ⁻¹
$v_{8,8} = i_{P,BM} - f_{XI} i_{P,XI}$	gP gCOD ⁻¹
$v_{10,8} = 1/40 (i_{O,BM} - f_{XI} i_{O,XI}) - 1/5 (i_{H,BM} - f_{XI} i_{H,XI}) - 1/15 (i_{C,BM} - f_{XI} i_{C,XI}) + 1/35 (i_{N,BM} - f_{XI} i_{N,XI}) - 1/31 (i_{P,BM} - f_{XI} i_{P,XI})$	gH gCOD ⁻¹
$v_{16,8} = f_{XI}$	gCOD gCOD ⁻¹
$v_{17,8} = -1$	gCOD gCOD ⁻¹
Decay of X_H	
$v_{15,9} = (1 - f_{XI})$	gCOD gCOD ⁻¹
$v_{16,9} = f_{XI}$	gCOD gCOD ⁻¹
$v_{17,9} = -1$	gCOD gCOD ⁻¹
Growth of ammonia oxidizing bacteria (X_{AOB})	
$v_{1,10} = -1/Y_{AOB}$	gN gCOD ⁻¹
$v_{4,10} = 1/Y_{AOB} - i_{N,BM}$	gN gCOD ⁻¹
$v_{5,10} = -i_{C,BM}$	gC gCOD ⁻¹
$v_{8,10} = -i_{P,BM}$	gP gCOD ⁻¹
$v_{9,10} = 1 - 3.43/Y_{AOB}$	gO ₂ gCOD ⁻¹
$v_{10,10} = 2/14 Y_{AOB} - 1/14 (i_{N,BM}) - 2/31 (i_{P,BM})$	gH gCOD ⁻¹
$v_{18,10} = 1$	gCOD gCOD ⁻¹
Growth of nitrite oxidizing bacteria (X_{NOB})	
$v_{3,11} = 1/Y_{NOB} - i_{N,BM}$	gN gCOD ⁻¹
$v_{4,11} = -1/Y_{NOB}$	gN gCOD ⁻¹
$v_{5,11} = -i_{C,BM}$	gC gCOD ⁻¹
$v_{8,10} = -i_{P,BM}$	gP gCOD ⁻¹
$v_{9,11} = 1 - 1.14/Y_{NOB}$	gO ₂ gCOD ⁻¹
$v_{10,11} = -1/14 (i_{N,BM}) - 2/31 (i_{P,BM})$	gH gCOD ⁻¹
$v_{19,11} = 1$	gCOD gCOD ⁻¹
Endogenous respiration of X_{AOB}	
$v_{1,12} = i_{N,BM} - f_{XI} i_{N,XI}$	gN gCOD ⁻¹
$v_{5,12} = i_{C,BM} - f_{XI} i_{C,XI}$	gC gCOD ⁻¹
$v_{8,12} = i_{P,BM} - f_{XI} i_{P,XI}$	gP gCOD ⁻¹
$v_{9,12} = -(1 - f_{XI})$	gO ₂ gCOD ⁻¹
$v_{10,12} = -1/14 (i_{N,BM} - f_{XI} i_{N,XI}) + 2/31 (i_{P,BM} - f_{XI} i_{P,XI})$	gH gCOD ⁻¹
$v_{16,12} = f_{XI}$	gCOD gCOD ⁻¹

$v_{18,12} = -1$	gCOD gCOD ⁻¹
Endogenous respiration of X_{NOB}	
$v_{1,13} = i_{N,BM} - f_{XI} i_{N,XI}$	gN gCOD ⁻¹
$v_{5,13} = i_{C,BM} - f_{XI} i_{C,XI}$	gC gCOD ⁻¹
$v_{8,13} = i_{P,BM} - f_{XI} i_{P,XI}$	gP gCOD ⁻¹
$v_{9,13} = -(1 - f_{XI})$	gO ₂ gCOD ⁻¹
$v_{10,13} = -1/14 (i_{N,BM} - f_{XI} i_{N,XI}) + 2/31 (i_{P,BM} - f_{XI} i_{P,XI})$	gH gCOD ⁻¹
$v_{16,13} = f_{XI}$	gCOD gCOD ⁻¹
$v_{19,13} = -1$	gCOD gCOD ⁻¹
Decay of X_{AOB} and X_{NOB}	
$v_{15,14a} = (1 - f_{XI})$	gCOD gCOD ⁻¹
$v_{16,14a} = f_{XI}$	gCOD gCOD ⁻¹
$v_{18,14a} = -1$	gCOD gCOD ⁻¹
$v_{15,14b} = (1 - f_{XI})$	gCOD gCOD ⁻¹
$v_{16,14b} = f_{XI}$	gCOD gCOD ⁻¹
$v_{19,14b} = -1$	gCOD gCOD ⁻¹
Hydrolysis	
$v_{1,15} = -(1 - f_{SI})i_{N,SS} - f_{SI}i_{N,SI} + i_{N,XS}$	gN gCOD ⁻¹
$v_{5,15} = i_{C,XS} - (1 - f_{SI})Y_{HYD}i_{C,SS} - f_{SI}Y_{HYD}i_{C,SI}$	gC gCOD ⁻¹
$v_{8,15} = i_{P,XS} - (1 - f_{SI})Y_{HYD}i_{P,SS} - f_{SI}Y_{HYD}i_{P,SI}$	gP gCOD ⁻¹
$v_{10,15} = -1/14 (i_{N,XS} - (1 - f_{SI})Y_{HYD}i_{N,SS} - f_{SI}Y_{HYD}i_{N,SI}) + 2/31 (i_{P,XS} - (1 - f_{SI})Y_{HYD}i_{P,SS} - f_{SI}Y_{HYD}i_{P,SI})$	gH gCOD ⁻¹
$v_{12,15} = (1 - f_{SI})Y_{HYD}$	gCOD gCOD ⁻¹
$v_{13,15} = (f_{SI})Y_{HYD}$	gCOD gCOD ⁻¹
$v_{15,15} = -1$	gCOD gCOD ⁻¹
Chemical equilibria CO₂ ↔ HCO₃⁻	
$v_{5,16} = -1$	gC gC ⁻¹
$v_{6,16} = 1$	gC gC ⁻¹
$v_{10,16} = 1/12$	gH gC ⁻¹
Chemical equilibria HCO₃⁻ ↔ CO₃²⁻	
$v_{6,17} = -1$	gC gC ⁻¹
$v_{7,17} = 1$	gC gC ⁻¹
$v_{10,17} = 1/12$	gH gC ⁻¹
Chemical equilibria NH₄⁺ ↔ NH₃	
$v_{1,18} = -1$	gN gN ⁻¹
$v_{2,18} = 1$	gN gN ⁻¹
$v_{10,18} = 1/14$	gH gN ⁻¹

Chemical equilibria $H^+ \leftrightarrow OH^-$	
$v_{10,19} = 1$	gH gH ⁻¹
$v_{11,19} = 1$	gH gH ⁻¹
Oxygen transfer to the atmosphere	
$v_{9,20} = 1$	–
Carbon dioxide transfer to the atmosphere	
$v_{5,21} = 1$	–
Ammonia transfer to the atmosphere	
$v_{2,22} = 1$	–

Table A8.5 Values of fractions of carbon, hydrogen, oxygen and nitrogen in microalgae and bacteria biomass.

Parameters	Description	Value	Unit	Source
Fractions of microalgal biomass (X_{ALG})				
$i_{C,ALG}$	Fraction of carbon in microalgae	0.387	gC gCOD ⁻¹	Reichert et al., 2001
$i_{H,ALG}$	Fraction of hydrogen in microalgae	0.075	gH gCOD ⁻¹	Reichert et al., 2001
$i_{O,ALG}$	Fraction of oxygen in microalgae	0.538	gO gCOD ⁻¹	Reichert et al., 2001
$i_{N,ALG}$	Fraction of nitrogen in microalgae	0.065	gN gCOD ⁻¹	Reichert et al., 2001
$i_{P,ALG}$	Fraction of phosphorus in microalgae	0.01	gP gCOD ⁻¹	Reichert et al., 2001
Fractions of bacteria biomass (X_H, X_{AOB}, X_{NOB})				
$i_{C,BM}$	Fraction of carbon in bacteria	0.323	gC gCOD ⁻¹	Reichert et al., 2001
$i_{H,BM}$	Fraction of hydrogen in bacteria	0.060	gH gCOD ⁻¹	Reichert et al., 2001
$i_{O,BM}$	Fraction of oxygen in bacteria	0.155	gO gCOD ⁻¹	Reichert et al., 2001
$i_{N,BM}$	Fraction of nitrogen in bacteria	0.075	gN gCOD ⁻¹	Reichert et al., 2001
$i_{P,BM}$	Fraction of phosphorus in bacteria	0.018	gP gCOD ⁻¹	Reichert et al., 2001
Fractions of slowly biodegradable substrates (X_S)				
$i_{C,XS}$	Fraction of carbon in X_S	0.318	gC gCOD ⁻¹	Reichert et al., 2001
$i_{H,XS}$	Fraction of hydrogen in X_S	0.045	gH gCOD ⁻¹	Reichert et al., 2001
$i_{O,XS}$	Fraction of oxygen in X_S	0.156	gO gCOD ⁻¹	Reichert et al., 2001
$i_{N,XS}$	Fraction of nitrogen in X_S	0.034	gN gCOD ⁻¹	Reichert et al., 2001
$i_{P,XS}$	Fraction of phosphorus in X_S	0.005	gP gCOD ⁻¹	Reichert et al., 2001
Fractions of inert particulate organics (X_I)				
$i_{C,XI}$	Fraction of carbon in X_I	0.327	gC gCOD ⁻¹	Reichert et al., 2001
$i_{H,XI}$	Fraction of hydrogen in X_I	0.037	gH gCOD ⁻¹	Reichert et al., 2001
$i_{O,XI}$	Fraction of oxygen in X_I	0.150	gO gCOD ⁻¹	Reichert et al., 2001

$i_{N,XI}$	Fraction of nitrogen in X_I	0.016	$gN\ gCOD^{-1}$	Reichert et al., 2001
$i_{P,XI}$	Fraction of phosphorus in X_I	0.005	$gP\ gCOD^{-1}$	Reichert et al., 2001
Fractions of readily biodegradable substrates (S_S)				
$i_{C,SS}$	Fraction of carbon in S_S	0.318	$gC\ gCOD^{-1}$	Reichert et al., 2001
$i_{H,SS}$	Fraction of hydrogen in S_S	0.045	$gH\ gCOD^{-1}$	Reichert et al., 2001
$i_{O,SS}$	Fraction of oxygen in S_S	0.156	$gO\ gCOD^{-1}$	Reichert et al., 2001
$i_{N,SS}$	Fraction of nitrogen in S_S	0.034	$gN\ gCOD^{-1}$	Reichert et al., 2001
$i_{P,SS}$	Fraction of phosphorus in S_S	0.005	$gP\ gCOD^{-1}$	Reichert et al., 2001
Fractions of soluble inert organics (S_I)				
i_{C,S_I}	Fraction of carbon in S_I	0.327	$gC\ gCOD^{-1}$	Reichert et al., 2001
i_{H,S_I}	Fraction of hydrogen in S_I	0.037	$gH\ gCOD^{-1}$	Reichert et al., 2001
i_{O,S_I}	Fraction of oxygen in S_I	0.150	$gO\ gCOD^{-1}$	Reichert et al., 2001
i_{N,S_I}	Fraction of nitrogen in S_I	0.016	$gN\ gCOD^{-1}$	Reichert et al., 2001
i_{P,S_I}	Fraction of phosphorus in S_I	0.005	$gP\ gCOD^{-1}$	Reichert et al., 2001
Fractions of inert produced by biomass degradation				
f_{ALG}	Production of X_I in endogenous resp. of X_{ALG}	0.1	$gCOD\ gCOD^{-1}$	Sah et al., 2011
f_{XI}	Production of X_I in endogenous resp. of X_H	0.1	$gCOD\ gCOD^{-1}$	Sah et al., 2011
Yield of biomass				
Y_{ALG}	Yield of X_{ALG}	0.62	$gCOD\ gCOD^{-1}$	Reichert et al., 2001
Y_H	Yield of X_H on S_{O_2}	0.6	$gCOD\ gCOD^{-1}$	Reichert et al., 2001
Y_{H,NO_3}	Yield of X_H on S_{NO_3}	0.5	$gCOD\ gCOD^{-1}$	Reichert et al., 2001
Y_{H,NO_2}	Yield of X_H on S_{NO_2}	0.3	$gCOD\ gCOD^{-1}$	Reichert et al., 2001
Y_{AOB}	Yield of X_{AOB}	0.13	$gCOD\ gCOD^{-1}$	Reichert et al., 2001
Y_{NOB}	Yield of X_{NOB}	0.03	$gCOD\ gCOD^{-1}$	Reichert et al., 2001
Y_{HYD}	Hydrolysis saturation constant	1	$gCOD\ gCOD^{-1}$	Reichert et al., 2001

9

Conclusions

The overall objective of this research was to develop a fundamentally based modelling approach for microalgae biomass prediction that integrates biokinetic, chemical and physical processes that occur in microalgae systems in order to advance the understanding of microalgae and bacteria interactions in wastewater treatment systems. To accomplish the general objective of this PhD, a new integral mechanistic model was developed to simulate microalgae-based wastewater treatment systems.

The following conclusions can be drawn from the specific objectives presented in the first part of this thesis.

- A new mechanistic microalgae model was presented and calibrated. The model was built in COMSOL MultiphysicsTM. The model considers the growth of microalgae as a function of light intensity and temperature, as well as availability of nitrogen and other nutrients. Simulation results showed the potential of the model to predict microalgae growth and production, nutrient uptake, and the influence of temperature, light intensity and pH on microalgae biokinetic processes. Regarding model outputs, the maximum specific growth rate of microalgae (μ_{ALG}) and the transfer of the gases to the atmosphere (K_{a,O_2} , K_{a,CO_2} and K_{a,NH_3}) were the parameters that need to be calibrated properly. Temperature and irradiance demonstrated to be the main limiting factors in microalgae systems.
- A global sensitivity analysis was applied to evaluate the sensitivity of model outputs with respect to a subset of key input parameters. The Morris method of Elementary Effects (EEs) confirmed that the maximum specific growth rate of microalgae (μ_{ALG}) was the parameter with the greatest impact on simulation outputs. Small perturbations of +/- 60% on the optimal range values of the parameters related to transfer of gases to the atmosphere had negligible effect on model outputs.
- The microalgae model was able to reproduce the hydrodynamic behaviour and the light attenuation effect on microalgae growth in both vertical and horizontal closed photobioreactors. Parameters related to the transfer of gases to the atmosphere in each type of reactor were

calibrated due to the different design and volume of the open body. Dissolved oxygen accumulation represented the main limiting factor on microalgae growth in the closed reactors. By the implementation of a photorespiration factor $f_{PR}(S_{O_2})$, the model has allowed to reproduce the dissolved oxygen accumulation profile throughout the reactor loop configuration and to optimize their design in order to prevent microalgae inhibition. Moreover, microalgae production was predicted over a long-term period of time as function of temperature and irradiance. High temperatures during summer limited the microalgae growth, therefore cooling water strategies could help optimize the production.

- BIO_ALGAE is the integral mechanistic model describing the complex interactions in mixed algal-bacterial systems built in the COMSOL MultiphysicsTM software. The model includes crucial physical, chemical and biokinetic processes of microalgae as well as bacteria in wastewater. The Morris's sensitivity analysis results showed that microalgae and heterotrophic bacteria specific growth rates, decay of heterotrophic bacteria and 3 parameters related to the transfer of gases to the atmosphere were the parameters with the greatest influence on the model outputs. BIO_ALGAE model was calibrated and validated in a short-time scale (4 days) with high quality experimental data from triplicated pilot HRAPs receiving real wastewater. Results of the calibration and validation have indicated that the model was able to accurately reproduce the daily fluctuations of different components in the ponds, and the relative proportion of microalgae and bacteria. Model prediction indicated that much of the average biomass corresponds to microalgae (65% in average of TSS) and heterotrophic bacteria (21% in average). Furthermore, the model was used to investigate the relative effect of the factors that affect microalgae growth and the effect of different influent organic matter concentration on total biomass production. Light attenuation was the most limiting factor that reduced microalgae growth up to 60% due to the high concentration of particulate components in the pond. When reducing influent organic matter, microalgae production was increased from 8.7 g TSS m⁻²d⁻¹ to

13.5 g TSS m⁻²d⁻¹ and also microalgae/bacteria proportion changed (microalgae changed from 65% to 90%).

- The BIO_ALGAE model was validated in a long-term period (summer and winter) in a pilot high rate algal pond (HRAP). The model was able to simulate with a good degree of accuracy the dynamics of different components in the pond, including the total biomass, during two different seasons (summer and winter), as well as the operation at different hydraulic retention time (HRT, 4 and 8 days). By means of practical study cases, the influence of different HRT operating strategies and the seasonal variations of temperature and irradiance were investigated in respect to the relative proportion of microalgae and bacteria, and biomass production over a year cycle. Model predictions showed that the proportion of microalgae in the microalgal/bacterial biomass is quite constant in warmer months in HRAPs with 8-day HRT (76-78%) and 4-day HRT (60-75%). In colder months microalgae proportion in comparison to bacteria slightly dropped down in HRAPs with 8-day HRT (65-68%) and is strongly reduced with 4-day HRT (27-33%). Moreover, thanks to the model it was possible to optimize the overall microalgae production and ammonium removal efficiency. By operating with lower HRT (4 days) in warmer months and higher HRT (8 days) average annual microalgae production increased up to 14.1 g TSS m⁻²d⁻¹, as compared to 10.2 g TSS m⁻²d⁻¹ and 9.2 g TSS m⁻²d⁻¹ operating with constant HRT (4 and 8 days, respectively) over a year cycle. The average removal efficiency of ammonium was further controlled through this suitable HRT operating strategy; it was reduced to less than 5 g N-NH₄ m⁻³ over the whole year. BIO_ALGAE has demonstrated to be a useful tool to understand microalgae and bacteria interactions in wastewater treatment, and in particular to study the effect of different HRT operating strategies and variations of environmental conditions over a year cycle on the relative proportion of microalgae and bacteria and biomass production.

References

- Abdel-Raouf, N., Al-Homaidan, A.A., Ibraheem, I.B. 2012. Microalgae and wastewater treatment. Saudi J.Biol Sci 19, 257-275.
- Acién, F., Fernández Sevilla, J.M., Molina Grima, E. 2013. Photobioreactors for the production of microalgae. Reviews in Environmental Science and Bio/Technology ,Volume 12, Issue 2, pp 131-151.
- Acién, F.G., García Camacho, F., Sánchez Pérez, J.A., Fernández Sevilla, J., Molina Grima, E., 1998. Modelling of biomass productivity in tubular photobioreactors for microalgal cultures. Effects of dilution rate, tube diameter and solar irradiance. Biotechnol. Bioeng. 58, 605–611.
- Aiba, S. 1982. Growth kinetics of photosynthetic microorganisms. Adv. Biochem. Eng. 23, 85–156.
- Alam, F.M., McNaught, K.R., Ringrose, T.J. 2004. Using Morris' randomized OAT design as a factor screening method for developing simulation metamodels. Proceedings of the 2004 Winter Simulation Conference R .G. Ingalls, M. D. Rossetti, J. S. Smith, and B. A. Peters, eds.
- Al-Rawahi, N.Z., Zurigat, Y.H., Al-Azri N.A. 2011. Prediction of Hourly Solar Radiation on Horizontal and Inclined Surfaces for Muscat/Oma. The Journal of Engineering Research Vol 8 No 2, 19-31.
- Andrade, M.R.; Costa, J.A.V. Mixotrophic cultivation of microalga *Spirulina platensis* using molasses as organic substrate. Aquaculture 2007, 264, 130–134.
- Anesio, A.M., Tranvik, L.J., Granéli, W. 1999. Production of Inorganic Carbon from Aquatic Macrophytes by Solar Radiation. Ecology Vol. 80, No. 6 (Sep., 1999), pp. 1852-1859.

- Anning, T., MacIntyre, H., Pratt, S., Sammes, P., Gibb, S., Geider, R. 2000. Photoacclimation in the marine diatom *Skeletonema costatum*, *Limnol. Oceanogr.* 45 (8) 1807–1817.
- APHA-AWWA-WPCF (2001). APHA-AWWA-WPCF Standard Methods for the Examination of Water and Wastewater (twentieth ed.) American Public Health Association, Washington DC.
- Aslan, S., Kapdan, I. 2006. Batch kinetics of nitrogen and phosphorus removal from synthetic wastewater by algae. *Ecological Engineering*, 28(1), 64-70.
- Avoz, Y., Goldman, J.C. 1982. Free ammonia inhibition of algal photosynthesis in intensive culture. *APPL Environ Microbiol.* 43, 735-739.
- Awuah, E. 2006. Pathogen removal mechanisms in macrophyte and algal waste stabilization ponds, Taylor & Francis.
- Awuah, E., 2006. Pathogen removal mechanisms in waste stabilisation ponds. PhD thesis, Wageningen University/UNESCO-IHE Institute for Water Education, The Netherlands.
- Baldizon, M.E, Dolmus, R., Quintana, J., Navarro, Y., Donze, M., 2002. Comparison of conventional and macrophyte-based systems for the treatment of domestic wastewater. *Water Science and Technology* 45, 111–116.
- Banat, I., Puskas, K., Esen, I., Daher, R.A., 1990. Wastewater treatment and algal productivity in an integrated ponding system. *Biological Wastes* 32, 265– 275.
- Barbato, F., Simbolotti, G., 2009. Tecniche di colture di microalghe. Technology Information from ENEA, ENEA 2009 TB04.
- Béchet, Q., Shilton, A., Guieysse, B., 2013. Modelling the effects of light and temperature on algae growth: State of the art and critical assessment for productivity prediction during outdoor cultivation. *Biotechnology Advances* 31, 1648-1663.

- Benedetti, L., Meirlaen, J., Sforzi, F., Facchi, A., Gandolfi, C., Vanrolleghem, P.A. 2007. Dynamic integrated water quality modelling: A case study of the Lambro River, northern Italy. *Water SA* Vol. 33 No. 5 October 2007.
- Benemann, J.R., 1986. *Microalgae biotechnology: Products, processes and opportunities*, vol. 1. OMEC International Inc.
- Beran, B. and Kargi, F., 2005. A dynamic mathematical model for wastewater stabilization ponds. *Ecological Modelling*, 181(1), pp.39-57.
- Bernard, O., Mairet, F., Chachuat, B. 2016. *Modelling of Microalgae Culture Systems with Applications to Control and Optimization*. *Adv. Biochem. Eng. Biotechnol.* 153: 59-87
- Bernard, O. 2011. Hurdles and challenges for modelling and control of microalgae for CO₂ mitigation and biofuel production. *Journal of Process Control* 21 1378– 1389.
- Bernard, O., Masci, P., Sciandra, A. 2009. A photobioreactor model in nitrogen limited conditions. In: *Proceedings of the sixth conference on mathematical modelling*, Vienna.
- Bitog, J.P., Lee, I.-B., Lee, C.-G., Kim, K.-S., Hwang, H.-S., Hong, S.-W., Seo, I.-H., Kwon, K.-S., Mostafa, E. 2011. Application of computational fluid dynamics for modelling and designing photobioreactors for microalgae production: A review. *Computers and Electronics in Agriculture* 76(2), 131–147.
- Bonachela, J.A., Raghiv, M., Levin, S.A. 2011. Dynamic model of flexible phytoplankton nutrient uptake. *Proc. Natl. Acad. Sci. U.S.A.* 108, 20633-200638.
- Borowitzka, M.A., Moheimani, N.R. 2013. *Open pond culture systems. Algae for biofuels energy*. Springer, New York, pp. 133-152.
- Bordel, S., Guieysse, B., Muñoz, R. 2009. Mechanistic model for the reclamation of industrial wastewaters using algal-bacterial photobioreactors. *Environ Sci Technol*; 43(9): 3200–3207.

- Boussiba, S., Shadler, T., Karamanos, T. Y., Mollion, J., Morva, H., Verdus, D., Christiaen, M.C. 1988. *Anabaena azollae* as a nitrogen biofertilizer. *Algal biotechnology* 169-178.
- Bouterfas, R., Belkoura, M., Dauta, A. 2002. Light and temperature effects on the growth rate of three freshwater [2pt] algae isolated from a eutrophic lake, *Hydrobiologia* 489 207–217.
- Brennan, L., Owende, P., 2010. Biofuels from microalgae- A review of technologies for production, processing, and extractions of biofuels and co-products. *Renew. Sustain. Energy Rev.* 14, 557-577.
- Brown L.C., Barnwell T.O. 1987. The enhanced stream water quality models QUAL2E and QUAL2E-UNCAS: Documentation and User Manual, Report EPA/600/3-87/007, U.S. EPA, Athens, GA, USA.
- Buhr, H.O., Miller, S.B. 1983. A dynamic model of the high-rate algal bacterial wastewater treatment pond. *Water Res* 17:29-37.
- Camacho Rubio F., García Camacho, F., Fernández Sevilla, J.M., Chisti, Y., Molina Grima, E. 2003. A mechanistic model of photosynthesis in microalgae. *Biotechnol Bioeng*;81(4): 459–73.
- Camacho Rubio F., Acien Fernández, F.G., García Camacho, F., Sánchez Pérez, J.A., Molina Grima, E., 1999. Prediction of dissolved oxygen and carbon dioxide concentration profiles in tubular photo- bioreactors for microalgal culture. *Biotechnology and bioengineering* 62, 71–86.
- Campolongo, F., Saltelli, A., Cariboni, J. 2011. From screening to quantitative sensitivity analysis. A unified approach. *Computer Physics Communications* 182 (2011) 978–988.
- Campolongo, F., Cariboni, J., Saltelli, A. 2007. An effective screening design for sensitivity analysis of large models *Environmental Modelling & Software* 22 1509e151.
- Campolongo, F., Tarantola, S., Saltelli, A., 1999. Tackling quantitatively large dimensionality problems. *Computer Physics Communications* 117, 75e85.

- Campolongo, F., Braddock, R., 1999. The use of graph theory in the sensitivity analysis of the model output: a second order screening method. *Reliability Engineering and System Safety* 64 1–12.
- Cherif, M., Loreau, M. 2010. Towards a more biologically realistic use of Droop's equations to model growth under multiple nutrient limitation. *Oikos* 119: 897–907.
- Chisti, Y., 2007. Biodiesel from microalgae. *Biotechnology Advances* 25, 294-306.
- Correll, D.L. 1999. Phosphorus: A Rate Limiting Nutrient in Surface Waters. *Poultry Science* 78:674–682.
- Costache T. A, Ación Fernández F.G., Morales M., Fernández Sevilla J.M., Stamatini, I., Molina, E., 2013 Comprehensive model of microalgae photosynthesis rate. *Appl Microbiol Biotechnol.*, 17:7627-37.
- Craggs, R., Lundquist, T.J., Benemann, J.R. 2013. Wastewater treatment and algal biofuel production. In: Borowitzka, M.A. Moheimani, N.R (eds) *Algae for biofuels and energy*. Springer, New York, pp. 153-163.
- Craggs, R.J., Heubeck, S., Lundquist, T.J., Benemann, J.R. 2011. Algae biofuel from wastewater treatment high rate algal ponds. *Water Sci. Technol.* 63(4), 660-665.
- Crill, P.A., 1977. The photosynthesis-light curve: a simple analogy model. *J. Theor. Biol.*, 6: 506-516.
- Christenson, L.B., Sims, R.C. (2012). Rotating algal biofilm reactor and spool harvester for wastewater treatment with biofuels by-products. *Biotechnology and Bioengineering* Volume 109, Issue 7, pages 1674–1684.
- Cromar, N.J., Fallowfield, H.J., Martin, N.J., 1996. Influence of environmental parameters on biomass production and nutrient removal in high rate algal pond operated by continuous culture. *Water Science and Technology* 34, 133– 140.

- Dalrymple O.K., Halfhide T, Udom I, Gilles B, Wolan J, Zhang Q, Ergas S. 2013. Wastewater use in algae production for generation of renewable resources: a review and preliminary results. *Aquat Biosyst.* Jan 5; 9(1):2.
- Dauta, A., Devaux, J., Piquemal, F., Boumnic, L. 1990. Growth rate of four freshwater algae in relation to light and temperatura. *Hydrobiologia* 207, 221-226.
- Dekissa, T., Meirlaen, J., Ashton, P.J., Vanrolleghem, P.A. 2004. Symplifying dynamic riverwater quality modelling: A case study of inorganic nitrogen dynamics in the Crocodile River (South Africa). *Water, Air, and Soil Pollution* **155**: 303–320.
- Deltares Delft 3D manual, 2006. <http://delftsoftware.wldelft.nl/>
- DHI, 1992. MIKE11. User Manual. Danish Hydraulic Institute, Denmark.
- Diehl, J.M., Sciences, T.U.o.N.C.a.C.H.E., Engineering. 2007. The Effect of Urea-ammonium-nitrate Fertilizer Amended with Urease and Nitrification Inhibitors on Nitrogen Cycling in Highly Organic Agricultural Soil. University of North Carolina at Chapel Hill.
- Doty Energy. 2010. <http://www.dotyenergy.com/Markets/Micro-algae>
- Droop, M.R., 1974. The nutrient status of algal cells in batch culture. *J. Mar. Biol. Assoc. U.K.* 54, 825-855.
- Droop, M.R. 1968. Vitamin B2 and marine ecology. IV. The kinetics of uptake, growth and inhibition in *Monochrysis lutheri*'. *J. Mar. Biol. Ass. U.K.* 48, 689-733.
- Eykhoff, P. 1974. *System Identification: Parameter and State Estimation*, Wiley & Sons.
- Eilers, P.H.C., Peters, J.C.H., 1988. A model for the relationship between light intensity and the rate of photosynthesis in phytoplankton. *Ecological Modeling* 42, 199-215.
- EIA. 2017. <http://www.eia.gov/petroleum/gasdiesel>

- Enzing, C., Ploeg, M., Barbosa, M., Sijtsma, L., 2014. Microalgae-based products for the food and feed sector: an outlook for Europe. European Commission EUR 26255 - Joint Research Centre - Institute for Prospective Technological Studies. EUR - Scientific and Technical Research series - ISSN 1831-9424.
- Faleschini, M., Esteves, J.L., Valero, M.C., 2012. The effects of hydraulic and organic loadings on the performance of a full scale facultative pond in a temperate climate region (Argentine Patagonia). *Water Air Soil Pollut.* 223 (5), 2483-2493.
- Fernández, I. Ación, F.G., Berenguel, M., Guzmán J.L., Andrade, G.A., Pagano, D.J. 2014. A Lumped parameter chemical-physical model for tubular photobioreactors. *Chemical Engineering Science* 112, 116-129.
- Fernández, I., Ación, F.G., Fernández, J.M., Guzmán, J.L., Magán, J.J., Berenguel, M. 2012. Dynamic model of microalgal production in tubular photobioreactor. *Biosource Technology* 126, 172-181.
- Franz, A., Lehr, F., Posten, C., Schaub, G., 2012. Modeling microalgae cultivation productivities in different geographic locations - estimation method for idealized photobioreactors. *Biotechnology Journal* 7(4), 546–557.
- Fuentes, J.L., Inés Garbayo, I., Cuaresma, M., Montero, Z., González-del-Valle, M., Vílchez, C. 2016. Impact of Microalgae-Bacteria Interactions on the Production of Algal Biomass and Associated Compounds. *Mar. Drugs*, 14, 100.
- García, J., Green, B.F., Lundquist, T., Mujeriego, R. Hernández-Mariné, M., Oswald, W.J. 2006. Long term diurnal variations in contaminant removal in high rate ponds treating urban wastewater. *Bioresource Technology* 97: 1709–1715.
- García, J., Hernández-Mariné, M., and Mujeriego, R. 2002. Analysis of key variables controlling phosphorus removal in high rate oxidation ponds provided with clarifiers. *Water SA* 28, 1-8.

- García, J., Mujeriego, R., Bourrouet, A., Peñuelas, G. Freixes, A. 2000a. Wastewater treatment by pond systems: experiences in Catalonia, Spain. *Water Science and Technology* 42(10-11), 35-42.
- García, J., Mujeriego, R., Hernández-Mariné, M. 2000b. High rate algal pond operating strategies for urban wastewater nitrogen removal. *Journal of Applied Phycology* 12, 331-339.
- García, J., Hernández-Mariné, M., Mujeriego, R., 2000c. Influence of phytoplankton composition on biomass removal from high-rate oxidation lagoons by means of sedimentation and spontaneous flocculation. *Water Environ. Res.* 72, 230–237.
- García, J., Hernández-Mariné, M., Mujeriego, R., 1998. Tratamiento de aguas residuales urbanas mediante lagunas de alta carga: evaluación experimental. *Tratamiento de Aguas Residuales Urbanas* 5, 35–50.
- Gaudes et al., 2011. Microalgae as source of high-added value compounds. A brief review of recent work. *Biotechnology Progress* Volume 27, Issue 3, pages 597–613.
- Gernaey, K.V., Van Loosdrecht, M.C.M., Henze, M., Lind, M., Jørgensen, S.B. 2004. Activated sludge wastewater treatment plant modelling and simulation: state of the art. *Environmental Modelling & Software* 19, 763-783.
- Geider, R.J., La Roche, J. 2002. Redfield revisited: variability of C:N:P in marine microalgae and its biochemical basis. *Eur. J. Phycol.* 37 (01), 1-17.
- Geider, RJ, MacIntyre, H.L., Kana, TM. 1998. A dynamic regulatory model of phytoplanktonic acclimation to light, nutrients, and temperature. *Limnol Oceanogr*;43: 679–94.
- Gehring, T., Silva, J. D., Kehl, O., Castilhos, A. B., Costa, R. H. R., Uhlenhut, F., Alex, J., Horn, H. and Wichern, M. 2010. Modelling waste stabilisation ponds with an extended version of ASM3, *Water Science and Technology*, 61(3), 713-720.

- Gordillo, F.J.L., Goutx, M., Figueroa, F.L., Niell, F.X. Effects of light intensity, CO₂ and nitrogen supply on lipid class composition of *Dunaliella viridis*. 1998 *J. Appl. Phycol.* 10, 135–144.
- Guillard, R.R.L., Lorenzen, C.J., 1972. Yellow-green algae with chlorophyllide. *J. Phycol.* 8 (1), 10-14.
- Gujer, W., Henze, M., Mino, T., Van Loosdrecht, M. 1999. Activated Sludge Model No. 3. *Water Science and Technology* Vol 39 No 1 pp 183–193.
- Hach Company. 1992. Hach water analysis handbook. Hach Company.
- Halfhide, T., Dalrymple, O., Wilkie, A., Trimmer, J., Gillie, B., Udom, I., Zhang, Q., Ergas, S.J. 2015. Growth of an Indigenous Algal Consortium on Anaerobically Digested Municipal Sludge Centrate: Photobioreactor Performance and Modeling. *BioEnergy Research* 8, 249-258.
- Hase, R., Oikawa, H., Sasao, C., Morita, M., Watanabe, Y., 2000. Photosynthetic production of microalgal biomass in a raceway system under greenhouse conditions in Sendai city. *J. Biosci. Bioeng.* 89 (2), 157–163.
- He, L., Venkat R. Subramanian, Yinjie J. Tang. 2012. Experimental analysis and model-based optimization of microalgae growth in photobioreactors using flue gas. *Biomass and Bioenergy* 41, 131-138.
- Henze, M., et al., 2011. *Biological Wastewater Treatment: Principles, Modelling and Design*. London: IWA Publishing.
- Henze, M., Gujer, W., Mino, T., van Loosdrecht, M. 2000. Activated sludge models ASM1, ASM2, ASM2d and ASM3.
- Henze, M., Gujer, W., Mino, T., Matsuo, T., Wentzel, M.C., Gerrit. v., Marais, R., Van Loosdrecht M.C.M. 1999. 'Activated Sludge Model No. 2D, ASM2D, *Wat. Sci. Tech.* Vol. 39, n 1, pp 165-182.
- Henze, M., Gujer, W., Mino, T., Matsuo, T., Wentzel, M. C. and Marais, G. v. R. 1995. 'Activated Sludge Model No. 2. Activated Sludge Model No. 2', IAWQ Scientific and Technical Report, IAWQ, London.

- Henze, M., Grady, C. P. L., Gujer, W., Marasi, G. v. R., Matsuo, T. 1987. Activated Sludge Model No. 1, IAWQ, London.
- Hiatt, W. C., Leslie Grady, Jr. C. P. 2008. An Updated Process Model for Carbon Oxidation, Nitrification, and Denitrification Water Environment Research Vol. 80, No. 11, pp. 2145-2156.
- Huisman, J. Population dynamics of light-limited phytoplankton: microcosm experiments. Ecology 1999; 80 202–10.
- Hulatt, C.J., Thomas, D.N., 2011. Productivity, carbon dioxide uptake and net energy return of microalgal bubble column photobioreactors. Biosour. Technol. 102, 5775-5787.
- Iacopozzi, I., Innocenti, V., Marsili-Libelli, S., Giusti, E. (2007). A modified Activated Sludge Model No. 3 (ASM3) with two-step nitrification–denitrification. Environmental Modelling & Software 22, 847-861.
- Jeppsson, U. 1997. A General Description of the IAWQ Activated Sludge Model No. 1. IEA, Lund, Sweden.
- Kang, R., Wang, J., Shi, D., Cong, W., Cai, Z., Ouyang, F. 2004. Interactions between organic and inorganic carbon sources during mixotrophic cultivation of *Synechococcus* sp. Biotechnol Lett 26:1429–1432.
- King, D.M., Perera, B.J.C. 2013. Morris method of sensitivity analysis applied to assess the importance of input variables on urban water supply yield – A case study. Journal of Hydrology 477, 17-23.
- Khorsandi, H., Alizadeh, R., Tosinejad, h., Porghaffar, H. 2014. Analysis of nitrogenous and algal oxygen demand in effluent from a system of aerated lagoons followed by polishing pond. Water Science & Technology 70.1 – 95.
- Kong, Q.X., Li, L., Martinez, B., Chen, P., Ruan, R., (2010). Culture of microalgae *Chlamydomonas reinhardtii* in wastewater for biomass feedstock production. Applied biochem. and Biotechnol. 160, 9–18.
- Korner, H. and Zumft, W.G. 1986. Expression of denitrification enzymes in response to the dissolved oxygen level and respiratory substrate in

- continuous culture of *Pseudomonas stutzeri*. *Appl Environ Microbiol.* 1989 Jul; 55(7):1670-6.
- Krasnits E, Friedler E, Sabbah I, Beliavski M, Tarre S, Green M. Spatial distribution of major microbial groups in a well-established constructed wetland treating municipal wastewater. 2009. *Ecological Engineering* Volume 35, Issue 7, Pages 1085–1089.
- Kurano, N., Miyachi, S. 2005. Selection of microalgal growth model for describing specific growth rate-light response using extended information criterion. *Journal of Bioscience and Bioengineering* 100(4), 403–408.
- Langergraber, G., Rousseau, D., García, J., Mena, J., 2009. CWM1: a general model to describe biokinetic processes in subsurface flow constructed wetlands. *Water science and technology: a journal of the International Association on Water Pollution Research* 59(9), 1687–97.
- Larsdotter, K. 2006. Wastewater treatment with microalgae-a literature review, *Vatten.* 31–38.
- Laws, E.A., Taguchi, S., Hirata, J., Pang, L., 1988. Optimization of microalgal production in a shallow outdoor flume. *Biotechnology and Bioengineering* 32, 140–147.
- Liang, Z., Liu, Y., Ge, F., Xu, Y., Tao, N., Peng, F., Wong, M. 2013. Efficiency assessment and pH effect in removing nitrogen and phosphorus by algae-bacteria combined system of *Chlorella vulgaris* and *Bacillus licheniformis*. *Chemosphere* 92, 1383-1389.
- Liu, Y., Yang, S.H., Tay, J.H. 2004. Improved stability of aerobic granules by selecting slow-growing nitrifying bacteria. *Journal of Biotechnology* Volume 108, Issue 2, Pages 161–169.
- Lundquist T. 2009. The Links between algal biofuels and wastewater treatment. In: *Proceedings to algae biomass summit.* San Diego.

- Mehrabadi, A. Farida, M. M., Craggs, R. 2016. Variation of biomass energy yield in wastewater treatment high rate algal ponds. *Algal Research* Vol. 15, Pages 143–151
- Meisner A., 2007. Contributo al 7th European Workshop on Biotechnology of Microalgae. June 11-13, 2007, Nuthetal, Germany.
- Mairet, F., Bernard, O., Masci, P., Lacour, T., Sciandra, A. 2011. Modelling neutral lipid production by the microalga *Isochrysis affinis galbana* under nitrogen limitation. *Biores. Technol.* 102:142–149.
- Mairet, F., Moisan, M., and Bernard, O. 2010. Interval observer-based estimator of specific growth rate in bioreactors. *Journal Européen des Systèmes Automatisés* 44(4-5), 493–507.
- Marsollier, L., Stinear, T., Aubry, J., Saint Andre, J.P., R. Robert, P. Legras, A.L.Manceau, C. Audrain, S. Bourdon, H. Kouakou, B. Carbonnelle, Aquatic plants stimulate the growth of and biofilm formation by *Mycobacterium ulcerans* in axenic culture and harbor these bacteria in the environment, *Appl. Environ. Microbiol.* 70 (2004) 1097–1103.
- Martínez, M.E., Camacho, F., Jiménez, J.M., Espínola, J.B. 1997. Influence of lught intensity on the kinetic and yeld parameters of *Chlorella pyrenoidosa* mixotrophic growth. *Process Biochem*; 32 (2):93-8.
- Mata, T.M., Martins, A.A., Caetano, N.S. 2010. Microalgae for biodiesel production and other applications: a review. *Renew. Sustain. Energy Rev.* 14, 217-232.
- Myers, J. 1948. Observations on a Texas Sewage Lagoon. Bureau of Sanitary Engineering Pubs., Texas State Department of Health. Texas. 23 pp.
- Metting, F. 1996. Biodiversity and application of microalgae. *Journal of Industrial Microbiology&Biotechnology*, 17, 477–489.
- Milano, J., Ong, H. C., Masjuki, H.H., Chong, W.T., Man Kee Lam, Ping Kwan Loh, Vellayan, V. 2016. Microalgae biofuels as an alternative to fossil fuel for power generation. *Renewable and Sustainable Energy Reviews*, Volume 58, May 2016, Pages 180-197.

- Molina Grima, E., Fernández, J., Acien Fernández, G., Chisti, Y., 2001. Tubular photobioreactor design for algae cultures. *Journal of biotechnology* 92, 113–131.
- Molina Grima, E., Fernandez Sevilla, J.M., Sanchez Perez, J.A., Garcia Camacho, F. 1996. A study on simultaneous photolimitation and photoinhibition in dense microalgal cultures taking into account incident and averaged irradiances. *J. Biotechnol.* 45, 59–69.
- Molina Grima, E., García Camacho, F., Sánchez Pérez, J.A., Fernández Sevilla, J., Acien Fernández, F.G., Contreras Gómez, A. 1994. A mathematical model of microalgal growth in light limited chemostat cultures. *J. Chem. Technol. Biotechnol.* 61, 167–173.
- Monod, J. The growth of bacterial cultures. Pasteur Institute, Paris, France, 1949.
- Moreno-Grau, S., García-Sánchez, A., Moreno-Clavel, J., Serrano-Aniorte, J. and Moreno-Grau, M.D. 1996. A mathematical model for waste water stabilization ponds with macrophytes and microphytes. *Ecological Modelling*, 91(1-3), pp.77–103.
- Morris, M.D. 1991. Factorial Sampling Plans for Preliminary Computational Experiments. *Technometrics*, Vol. 33, No. 2. pp. 161-174.
- Mostert, E.S., Grobbelaar, J.H. 1987. The Influence of Nitrogen and Phosphorus on Algal Growth and Quality in Outdoor Mass Algal Cultures. *Biomass* 13 (1987) 219-233.
- Moya, M. J. Sanchez-Guardamino, M. L. Vilavella, A. Barberá, E. 1997. Growth of *Haematococcus lacustris*: A Contribution to Kinetic Modelling. *J. Chem. Tech. Biotechnol.* 1997, 68, 303-309.
- Novak, J.T., Brune, D.E. 1985. Inorganic carbon limited growth kinetics of some freshwater algae. *Water Res.* 19, 215-225.
- Nurdogan, Y., Oswald, W.J. 1995. Enhanced nutrient removal in high rate ponds. *Wat. Sci. Tech.* 31: 33-44.

- Oswald, W.J. 1998. Micro-algae and waste-water treatment. In Borowitzka MA, Borowitzka LJ. (eds) *Micro-algal Biotechnology*. Cambridge U.P., Cambridge, 305-328.
- Oswald, W.J., 1987. Sewage treatment in tropical high rate ponds. In: National Conference on Environmental Engineering, Lake Buena Vista.
- Oswald, W.J., Golouke, C.G. 1960. Biological transformation of solar energy. *Adv Appl Microbiol.* 1960;2:223-62.
- Oswald, W.J., Gotaas, H.B. 1957. Photosynthesis in sewage treatment. *Trans. Am. Soc. Civ. Eng.* 122 73-105.
- Oswald, W.J., Gotaas, H.B., Golouke, C.G., Kellen, W.R. 1957. Algae in waste treatment. *Sewage Ind. Wastes* 29 437-457.
- Packer, A., Li, Y., Andersen, T., Hu, Q., Kuang, Y., Sommerfeld, M. 2011. Growth and neutral lipid synthesis in green microalgae: a mathematical model. *Bioresour. Technol.*, 102:111–7.
- Park, K.C.; Whitney, C.; McNichol, J.C.; Dickinson, K.E.; MacQuarrie, S.; Skrupski, B.P.; Zou, J.; Wilson, K.E.; O’Leary, S.J.B.; McGinn, P.J. 2012. Mixotrophic and photoautotrophic cultivation of 14 microalgae isolates from Saskatchewan, Canada: Potential applications for wastewater remediation for biofuel production. *J. Appl. Phycol.*24, 339–348.
- Park, J.B.K., Craggs, R.J., Shilton, A.N., 2011. Wastewater treatment high rate algal ponds for biofuel production. *Bioresource Technology*, 102(1), 35–42.
- Park, J. B. K., Craggs, R. J. 2011a. Algal production in wastewater treatment high rate algal ponds for potential biofuel use. *Water Sci. Technol.*, 63(10), 2403-2410.
- Park, J. B. K., Craggs, R. J. 2011b. Nutrient removal in wastewater treatment high rate algal ponds with carbon dioxide addition. *Water Sci. Technol.*, 63(8), 1758-1764.

- Pawlowski, L. 2004. Modélisation de l'incorporation du carbone photosynthétique en environnement marin contrôlé par ordinateur. PhD thesis, Université Pierre et Marie Curie, Paris VI.
- Powell, N., Shilton, A., Chisti, Y. & Pratt, S. 2009. Towards luxury uptake process via microalgae - Defining the polyphosphate dynamics. *Water Research* 43 (17), 4207–4213.
- Powell E.E., Mapiour, M.L., Evitts, R.W., Hill, G.A. 2009. Growth kinetics of *Chlorella vulgaris* and its use as a cathodic half cell. *Bioresour Technol*;100(1): 269-74.
- Quinn, J., de Winter, L., Bradley, T. 2011. Microalgae bulk growth model with application to industrial scale systems. *Biosource Technology* 102, 5083-5092.
- Rawat, I., Ranjith Kumar, R., Mutanda, T., Bux, F., 2011. Due role of microalgae: Phycoremediation of domestic wastewater and biomass production for sustainable biofuels production. *Appl. Energ.* 88 (10), 3411-3424.
- Reichert, P., Vanrolleghem. P., 2001. Identifiability and uncertainty analysis of the River Water Quality Model No. 1 (RWQM1). *Water Science and Technology* Vol 43 No 7, pp 329-338.
- Reichert, P., Borchardt, D., Henze, M., Rauch, W., Shanahan, P., Somlyódy, L., Vanrolleghem, P. 2001. River Water Quality Model no. 1 (RWQM1): II. Biochemical process equations. *Water science and technology: a journal of the International Association on Water Pollution Research* 43(5), 11–30.
- Reichert. P. 1998. AQUASIM 2.0 User Manual. Swiss Federal Institute for Environmental Science and Technology (EAWAG).
- Richmond, Amos. 2004. Handbook of Microalgal Culture: Biotechnology and Applied Phycology. Blackwell Publishing Ltd., 2004. eBook Collection (EBSCOhost), EBSCOhost (accessed February 23, 2012).

- Richmond, A., Cheng-Wu, Z., Zarmi, Y., 2003. Efficient use of strong light for high photosynthetic productivity: interrelationships between the optical path, the optimal population density and cell-growth inhibition. *Biomolecular Engineering* 20, 229–236.
- Ruano, M.V., Ribes, J., Ferrer, J., Sin, G. 2011. Application of the Morris method for screening the influential parameters of fuzzy controllers applied to wastewater treatment plants. *Water Science & Technology* 63.10.
- Ruiz-Marin, A., Mendoza-Espinosa, L.G., Stephenson, T. Growth and nutrient removal in free and immobilized green algae in batch and semi-continuous cultures treating real wastewater, *Bioresour. Technol.* 101 (2010) 58–64.
- Sah, L., Rousseau, D., Hooijmans, C.M., Lens, P. 2011. 3D model for a secondary facultative pond. *Ecological Modelling* 222(9), 1592–1603.
- Saltelli, A., Tarantola, S., Campolongo, F. 2000. Sensitivity analysis as an ingredient of modelling, *Statistical Science*, 15(4): 377-395.
- Sanchez, J.F., Fernández-Sevilla, J.M., Acien, F.G., Ceron, M.C., Perez-Parra, J. & Molina-Grima, E., 2008. Biomass and lutein productivity of *Scenedesmus almeriensis*: influence of irradiance, dilution rate and temperature. *Appl. Microbiol. Biotechnol.*, 79, 719–729.
- Santiago, J., Corre, B., Claeys-Bruno, M., Sergent, M. 2012. Improved sensitivity through Morris extension. *Chemometrics and Intelligent Laboratory Systems* 113 52–57.
- Samsó R., García J. 2013. Bacteria distribution and dynamics in constructed wetlands based on modelling results. *Science of The Total Environment* Volumes 461–462, 1, Pages 430–440.
- Sayed, M. Abdoa, S.A. Abo El-Eninb, K.M. El-Khatibb, M.I. El-Galadb, S.Z. Wahbaa, G. El Diwanib, Gamila H. Alia. 2016. Preliminary economic assessment of biofuel production from microalgae. *Renewable and Sustainable Energy Reviews* Volume 55, pp.1147–1153.

- Seibert, M., 2009. Applied photosynthesis for biofuels production. National Renewable Energy Laboratory, Golden, CO 80401.
- Serodes, J. B., Walsh, E., Goulet, O., De la Node, J. & Lescelleur, C. (1991). Tertiary treatment of municipal wastewater using bioflocculating microalgae. *Can. J. Civ. Eng.*, 18, 940-944.
- Sheehan, J., Dunahay, T., Benemann, J., Roessler, P., 1998. A Look Back at the U.S. Department of Energy's Aquatic Species Program – Biodiesel from Algae. National Renewable Energy Laboratory, NREL/TP-580-24190.
- Shelef, G., 1982. High rate algal ponds for wastewater treatment and protein production. *Water Science and Technology* 14, 439–452.
- Shilton, A.N., Mara, D.D., 2005. CFD (computational fluid dynamics) modelling of baffles for optimizing tropical waste stabilization pond system. *Water Science and Technology* 51, 103–106.
- Shrestha, N.K., Leta, O.T., Bauwens, W. 2016. Development of RWQM1-based integrated water quality model in OpenMI with application to the River Zenne, Belgium. *Hydrological Sciences Journal*, pp 1-25.
- Silva, H.J., Pirt, J. 1984. Carbon dioxide inhibition of photosynthetic growth of chlorella. *Journal of General Microbiology*, 130, 2833-2838.
- Silyn-Roberts G, Lewis G. In situ analysis of Nitrosomonas spp. In wastewater treatment wetland biofilms. *Water Res* 2001;35:2731-9
- Sin, G., Gernaey, K.V. 2009. Improving the Morris method for sensitivity analysis by scaling elementary effects. 19th European Symposium on Computer Aided Process Engineering – ESCAPE19 J. Jezowski and J. Thullie (Editors).
- Sin, G., Gernaey, K.V., Neumann, M.B., van Loosdrecht, M.C.M., Gujer, W., 2009. Uncertainty analysis in WWTP model applications: a critical discussion using an example from design. *Water Res.* 43 (11), 2894–2906.

- Smith, R. C. 2014. Uncertainty Quantification Theory, Implementation, and Applications. SIAM - Computational Science and Engineering Series, CS12, 2014.
- Smit, A. J. 2002. Nitrogen Uptake by *Gracilaria gracilis* (Rhodophyta): Adaptations to a Temporally Variable Nitrogen Environment. *Botanica Marina*, 45(2), 196-209.
- Solimeno, A., Parker, L., Lundquist, T., García, J. 2017a. Integral microalgae-bacteria model (BIO_ALGAE): application to wastewater high rate algal ponds. *Water Research* (In preparation.).
- Solimeno, A., Acien, F.G., García, J. 2017b. Mechanistic model for design, analysis, operation and control of microalgae cultures: Calibration and application to tubular photobioreactors. *Algal Research* 21, 236-246.
- Solimeno, A., Samsó, R., García, J. 2016. Parameter sensitivity analysis of a mechanistic model to simulate microalgae growth. *Algal Research* 15, 217-223.
- Solimeno, A., Samsó, R., Uggetti, E., Sialve, B., Steyer, J.P., Gabarró, A., García, J. 2015. New mechanistic model to simulate microalgae growth. *Algal Research* 12, 350-358.
- Sommer, U. 2011. A comparison of the Droop and the Monod models of nutrient limited growth applied to natural populations of phytoplankton. *British Ecology Society*, 5(4), 535-544.
- Sommer, U. 1991. A comparison of the Droop and the Monod models of nutrient limited growth applied to natural populations of phytoplankton. *Functional Ecology*, 5, 535-544.
- Sperling, M. V. 2007. Waste stabilization ponds. IWA Publishing, London, Uk.
- Spolaore, P., Joannis-Cassan, C., Duran, E., Isambert, A. Commercial Applications of Microalgae. *Journal of bioscience and bioengineering* 2006, 101, 87-96.

- Steele, J.II. 1962. Environmental control of photosynthesis in the sea. *Limnol. Oceanogr.* 7: 137-150.
- Steen, P.v.d., Rahsilawati, K., Rada-Ariza, A.M., Lopez-Vazquez, C.M., Lens, P.N.L. 2015. A new photoactivated sludge system for nitrification by an algal-bacterial consortium in a photo-bioreactor with biomass recycle. *Water Science & Technology*, 443-450.
- Sterner, R. W., Grover, J. P. 1998. Algal growth in warm temperature reservoirs: Kinetic examination of nitrogen, temperature, light and other nutrients. *Science*, 32(12).
- Stewart, W. D. P. 1974. *Algal physiology and biochemistry*, Blackwell Scientific Publications, Oxford, 989 pp.
- Stokes, G. 1851. On the Effect of the Internal Friction of Fluids on the Motion of Pendulums. *Transactions of the Cambridge Philosophical Society* 9: 8–106.
- Suganyaa, T., Varmana, M., Masjukia, H.H., Renganathanb, S. 2016. Macroalgae and microalgae as a potential source for commercial applications along with biofuels production: A biorefinery approach. *Renewable and Sustainable Energy Reviews*, Volume 55, Pages 909–941.
- Sumner, T., Shephard, E., Bogle, I.D.L., 2012. A methodology for global-sensitivity analysis of time-dependent outputs in systems biology modelling. *J. R. Soc. Interface* 9, 2156–2166.
- Sutherland, D., Turnbull, M., Matthew, H. Broady, P. Craggs, R.J. 2014. Effects of two different nutrient loads on microalgal production, nutrient removal and photosynthetic efficiency in pilot-scale wastewater high rate algal ponds. *Water Research*; 66C, 53-62.
- Syrett, P.J. 1981. Nitrogen metabolism of microalgae. In *Physiological bases of phytoplankton ecology* (T. Platt, ed.). *Canadian Bulletin of Fisheries and Aquatic Sciences* 210:182-210.

- Tang, D., Han, W., Li, P., Miao, X., and Zhong, J. 2011. CO₂ biofixation and fatty acid composition of *Scenedesmus obliquus* and *Chlorella pyrenoidosa* in response to different CO₂ levels. *Bioresource technology*, Elsevier Ltd, 102(3), 3071-3076.
- Tredici, M.R., Materassi, R. 1992. From open ponds to vertical alveolar panels: the Italian experience in the development of reactor for the mass cultivation of phototrophic microorganism. *J. appl. Phycol.* 4; 221-231.
- Tricolici, O., Bumbaca, C., Postolacheb, C. 2014. Microalgae–Bacteria System for Biological Wastewater Treatment. *Journal of Environmental Protection and Ecology* 15, No 1, 268–276.
- Trinh Anh Duc, G. Vachaud, M.P.Bonnet, N. Prieur, Vu Duc Loi, Le Lan Anh. 2007. Experimental investigation and modelling approach of the impact of urban wastewater on a tropical river; a case study of the Nhue River, Hanoi, Vietnam. *Journal of Hydrology* 334, 347-358.
- Ugwu, C.U., Aoyagi, H., Uchiyama, H. 2008. Photobioreactors for mass cultivation of algae. *Bioresour. Technol.*, 99: 4021-4028.
- Vanhooren, H., Meirlaen, J., Amerlinck, Y., Claeys, F., Vangheluwe, H. and Vanrolleghem, P. A. 2002. ‘WEST: Modelling biological wastewater treatment’, *J. Hydroinformatics* 5, 27–50.
- Van Loosdrecht, M.C.M., Ekama, G.A., Wentzel, M.C., Hooijmans, C.M., Lopez-Vazquez, C.M., Meijer, S.C.F., Brdanovic, D. 2015. Introduction to modelling of activated sludge processes *Applications of Activated Sludge Models*. IWA Publishing, London, UK, pp. 1-68.
- Van Loosdrecht M.C.M., Henze M. 1999. Maintenance, endogeneous respiration, lysis, decay and predation. *Water Sci Technol* 39:107-117.
- Wagner, D. S., Borja Valverde-Perez, Mariann Sæbø, Marta Bregua de la Sotilla, Jonathan Van Wagenen, Barth F. Smets, Benedek Gy. Plosz. 2016. Towards a consensus-based biokinetic model for green microalgae- The ASM-A. *Water Research* 103. 485-499.

- Wang, J., Yang, H., Wang, F. 2014. Mixotrophic cultivation of microalgae for biodiesel production: status and prospects. *Appl Biochem Biotechnol* 172:3307–3329.
- Wang, B., Lan, Q., Horsman, M., 2012. Closed photobioreactors for production of microalgal biomasses. *Biotechnology Advances* 30 904–912.
- WPCF. 1990. Operation of Municipal Wastewater Treatment Plants. Manual of practice 11. WPCF. Alexandria. 1234 PP.
- Weissmand, J.C., Goebel, R.P. 1987. Design and Analysis of Microalgal Open Pond Systems for the Purpose of Producing Fuels. SERI/STR-231-2840.
- Wolf, G., Picioreanu, C., van Loosdrecht, M.C.M., 2007. Kinetic modeling of phototrophic biofilms: the PHOBIA model. *Biotechnol. Bioeng.* 97 (5), 1064–1079.
- Wu, X., Merchuk, J. 2001. A model integrating fluid dynamics in photosynthesis and photoinhibition processes. *Chemical Engineering Science* 56, 3527–3538.
- Wu, Y.-H., Li, X., Yu, Y., Hu, H.-Y., Zhang, T.-Y. and Li, F.-M. 2013. An integrated microalgal growth model and its application to optimize the biomass production of *Scenedesmus* sp. LX1 in open pond under the nutrient level of domestic secondary effluent. *Bioresource technology*, 144, pp.445-451.
- Xu, A. 2010. The development, validation, and applications of an improved activated sludge model, Ph. D. Thesis, University of Regina, Regina, Saskatchewan, Canada.
- Yang, A. 2011. Modeling and Evaluation of CO₂ Supply and Utilization in Algal Ponds. *Industrial & Engineering Chemistry Research*, 50(19).
- Yuan, S., Zhou, X., Chen, R., Song, B. 2014. Study on modelling microalgae growth in nitrogen-limited culture system for estimating biomass productivity. *Renewable and Sustainable Energy Reviews* 34, 525–535.

- Zambrano, J., Krustok, I., Nehrenheim, E., Carlsson, B. 2016. A simple model for algae-bacteria interaction in pho-bioreactors. *Algal Research*, 19, 155-161.
- Zonneveld, C., 1998. Light-limited microalgae growth: a comparison of modelling approaches. *Ecological Modelling* 113 41-54.
- Zhou, X., Yuan, S., Chen, R., Song, B., 2014. Modelling microalgae growth in nitrogen-limited continuous culture. *Energy* 73; 575-580.

Curriculum vitae

Alessandro Solimeno was born in Foggia (Italy), in 1987. He obtained his undergraduate degree in Civil Engineering specialized in Hydraulic Engineering at the Politecnico di Bari (Italy) in 2012. In 2013, he started his PhD research at the GEMMA (Group of Environmental Engineering and Microbiology) in the Universitat Politècnica de Catalunya-BarcelonaTech.

Articles in referred journals

- A. Solimeno, J. García. (in preparation). Microalgae-bacteria models evolution: from microalgae steady-state models to integrated microalgae-bacteria wastewater treatment models – a comparative review.
- A. Solimeno, J. García. (in preparation). Microalgae and bacteria dynamics in high rate algal ponds based on modelling results: long-term application of BIO_ALGAE model.
- A. Solimeno, L. Parker, T. Lundquist, J. García. (submitted). Integral microalgae-bacteria model (BIO_ALGAE): application to wastewater high rate algal ponds.
- S. Gargallo, A. Solimeno, M. Martín. (submitted). Which are the most sensitive parameters for suspended solids modelling in constructed wetlands?
- A. Solimeno, F. G. Acién, J. García. 2017. Mechanistic model for design, analysis, operation and control of microalgae cultures: calibration and application to tubular photobioreactors. Algal research.
- A. Solimeno, R. Samsó, E. Uggetti, B. Sialve, J.P. Steyer, A. Gabarró, J. García. 2015. New mechanistic model to simulate microalgae growth. Algal Research, 12:350-358.
- A. Solimeno, R. Samsó, J. García. 2015. Parameter sensitivity analysis of a mathematical model to simulate microalgae growth. Algal Research, 15:217–223.

Conference contributions

Oral communications

- A. Solimeno, J. García. (6-7 Abril 2017). Mechanistic model for design, analysis, operation and control of microalgae cultures: calibration and application to tubular photobioreactors. FITEMI 2017. Palermo, Italy.
- A. Solimeno, T. Lundquist, J. García. (16-17 March 2017). Integral microalgae-bacteria model (BIO_ALGAE): application to wastewater high rate algal ponds. 1st IWA Conference on Algal Technologies for Wastewater Treatment and Resource Recovery. Delft, The Netherlands.
- A. Solimeno, J. García. (26-29 June 2016). New mechanistic model to simulate microalgae growth. 6th International Conference of Algal Biomass, Biofuels&Bioproducts 2016. San Diego. California.
- A. Solimeno, J. García. (17-19 September 2014). Calibration of a biokinetic model to simulate microalgae growth. COMSOL Conference 2014, Cambridge, United Kingdom.

Posters

- *A. Solimeno*, J. García. (3-5 Abril 2014). Bio-kinetic model for complex algae and bacteria systems. Young Algaeneers Sysposium 2014, Narbonne-Montpellier, France.
- *A. Solimeno*, J. García. (23-25 October 2013). Bio-kinetic model for complex algae and bacteria systems. COMSOL Conference 2013, Rotterdam, The Netherlands.

Participation in R+D projects

- Production and digestion of algal biomass in wastewater treatment systems (DIPROBIO, CTM2012-37860) (2013-2016), financed by the Spanish Ministry of Science and Innovation, coordinated by the Group of Environmental Engineering and Microbiology (GEMMA-UPC).
- Biogas production from microalgae-bacteria grown in closed photobioreactors for wastewater treatment (FOTOBIOGAS, CTQ2014-57293-C3-3-R) (2015-2017), financed by the Spanish Ministry of Science and Innovation, coordinated by the Group of Environmental Engineering and Microbiology (GEMMA-UPC).
- Biotechnologies for urban wastewater treatment in Badajoz, Spain; financed by Quarq Enterprise S.A, coordinated by the Group of Environmental Engineering and Microbiology (GEMMA-UPC).

Courses

- WINTER SCHOOL (11-14 February 2014) – INSA, Applied Science National Institute of Toulouse, France.

Stays in foreign recognized research institutions

- Department of Civil and Environmental Engineering at California Polytechnic State University, San Luis Obispo, California. 6 months, from March to August 2016.
- Department of Civil and Environmental Engineering at Universitat Politècnica de Catalunya-BarcelonaTech, Barcelona, Spain. 10 months, from September 2011 to June 2012.